The Simulation of Sampling Disturbance and Its Effects on the Deformation Behaviour of Clays

by

AHMED RAMEZ HAJJ

B.Eng.(American University of Beirut, Lebanon)
M.Sc.(Eng) (University of Birmingham, England)

A thesis submitted to
The University of Sheffield
Department of Civil and Structural Engineering
for the Degree of Doctor of Philosophy

November 1990

To the memory of my father

RAMEZ MUHAMMAD EL-HAJJ
(1929-1989)

Contents

AKNOWLEDGEMENTS

The author is indebted to his supervisor Dr C.C. Hird for his guidance, supervision, assistance and constructive criticism throughout the whole period of this research.

The author wishes to express his gratitude to the Head of Civil and Structural Engineering Department, Professor T.H. Hanna for his encouragement and help. He would also like to thank members of the Geotechnics staff in the Department, Dr. W.F. Anderson, Dr I.C. Pyrah and Dr S. Wheeler for their cooperation and readiness to help.

Thanks are due to the technical and secretarial staff in the Department, in particular D. Thompson, P.L. Osborne, P.J. Oldfield, T. Robinson, M. Foster and Jeanne Cheetham for their assistance.

The author would like to thank the Hariri Foundation and their representatives in London for their financial and moral support throughout the duration of this work. Thanks are also due to Ove Arup and Partners.

Finally, the author wishes to express his gratitude and love to his mother, Imtissal, and brothers, Muhammad, Ghassan and Adnan and to his girlfriend, Miss Kim Clarke, for their support, encouragement and companionship which were crucial to the completion of this work.

SUMMARY

The importance of studying the behaviour of soil at small strain levels (< 0.1 %) has been increasingly recognised in recent years. In the laboratory, tests are usually conducted on tube samples retrieved from the ground, which inevitably suffer from disturbance.

This thesis describes an investigation of the effects of sampling disturbance on the small strain behaviour of one-dimensionally consolidated kaolin. Following the suggestion of Baligh (1985), tube sampling disturbance was simulated by applying a strain cycle in the triaxial cell. Comparative tests on 'disturbed' and 'undisturbed' specimens were conducted in a specially designed 100 mm hydraulic triaxial apparatus. Tests were also carried out in a 38 mm triaxial cell to study the effects of loading rate and overconsolidation ratio on the small strain deformation behaviour of isotropically consolidated kaolin.

In the 100 mm cell the local axial and radial strains were measured using proximity transducers mounted on adjustable fittings, enabling small strains to be measured accurately at any stage of a test. The axial strain was also measured between the end caps and externally. Comparisons of these three axial strain measurements showed that, under favourable conditions when bedding errors are negligible, end cap or external strains may be considered satisfactory. Bedding errors are reduced by consolidating the specimen to a high stress level and providing a rigid connection to the top cap. External strains must be corrected for equipment compliance.

Tests for the effects of sampling disturbance indicated that reconsolidating disturbed specimens to their initial stress conditions results in an adequate recov-

ery of the small strain stiffness, but yields a higher stiffness at larger strains. The recovery of the small strain stiffness was better in compression tests than in extension tests and further work is required to understand this finding. Specimens were observed to approach failure during the simulation of sampling disturbance.

For isotropically consolidated specimens, the relationships between normalised small strain stiffness at a given strain level and both overconsolidation ratio and rate of shearing were linear on a semi-logarithmic scale. This is in agreement with expectation on the basis of most previous research, but the effect of overconsolidation ratio requires further study using one-dimensionally consolidated specimens.

The experimental results were compared with the predictions from theoretical models based on critical state soil mechanics. These comparisons showed that the behaviour of kaolin under monotonic loading can be adequately predicted, even at small strains. Encouraging predictions were also made for behaviour during the loading cycle, as sampling disturbance was simulated. However, futher theoretical developments are needed to take into account the rate of shearing. The critical state parameters derived from the present tests and used in the model predictions showed close agreement with those obtained by other researchers.

LIST OF SYMBOLS

Alphabetical Letters

a Lower bellofram seal area

A Upper bellofram seal area

A_c Cross-sectional area of triaxial specimen

A_r Tube sampler area ratio

b Function in Al-Tabbaa's model

b_{max} Maximum value of b

B Skempton's pore water pressure coefficient

B_s Average tube sampler diamater

B_i Inside diameter of tube sampler

B_o Outside diameter of tube sampler

C Constant used in Wroth's stiffness-OCR relationship

c' Drained shear strength

C_1 Constant relating increments of stiffness and rest period

c_u Undrained shear strength

D Degree of disturbance

D_s Specimen diameter

E Young's modulus

E_{us} Undrained secant stiffness

E_{ut} Undrained tangent stiffness

f Step number during the application of isotropic consolidation pressure

F Flow rule function

F_d Deviator force

G Shear modulus

G' Drained shear modulus

h Hardening function in Al-Tabbaa's model ($= H + h_0$)

h_0 Hardening function in Al-Tabbaa's model

H Hardening function

k Inward movement of radial strain target

K' Drained bulk modulus

K_0 At rest pressure coefficient (normally consolidated soils)

K_{0u} At rest pressure coefficient (overconsolidated soils)

l inward movement of radial strain target

L Specimen height

L_0 Specimen height before consolidation

L_c Consolidated specimen height

L_g Specimen gauge length

L_{gc} Consolidated specimen gauge length

m Parameter used in the evaluation of K_{0u}

m_0 Parameter used in the evaluation of K_{0u}

M Slope of the critical state line in q, p' space

n Polynomial degree

n_g Number of points in each set of data used for tangent stiffness evaluation

n_i Number of points defining increment size during tangent stiffness evaluation

nn Number of steps for the application of isotropic consolidation pressure

N Specific volume at $p' = 1$ kPa (isotropic consolidation)

N_0 Specific volume at $p' = 1$ kPa (anisotropic consolidation)

OCR Overconsolidation ratio $(= \sigma'_{1max}/\sigma'_1)$

OCR_p Overconsolidation ratio $(= p'_{max}/p')$

p Mean total pressure

p' Mean effective pressure $(= \frac{\sigma'_1+2\sigma'_3}{3})$

p'_0 Mean effective pressure prior to loading

p_{1d} Mean effective pressure after one-dimensional consolidation

p_j Mean effective pressure after isotropic consolidation

p'_a Mean effective pressure after sampling

p'_b Mean effective pressure before sampling

p_c' Mean effective pressure after consolidation

p_{cs}' Mean effective pressure at critical state for a given v

p_i' Mean effective pressure prior to consolidation

p_{max}' Maximum mean effective pressure applied to a soil specimen

p_α' Coordinate of the centre of inner surface in Al-Tabbaa's model

r Inside radius of the 100 mm cell steel ring

R Ratio of sizes of inner and state boundary surfaces in Al-Tabbaa's model

R_1 Rate of axial stress application

R_3 Rate of radial stress application

R_s Specimen radius

S Scalar quantity in Al-Tabbaa's model

t Time

t_s Wall thickess of tube sampler

t_r Thickness of triaxial cell steel ring

u Pore water pressure

u_{avg} Average pore water pressure

q Deviator stress $(= \sigma_1 - \sigma_3)$

q_α Coordinate of the centre of inner surface in Al-Tabbaa's model

v Specific volume

V Lower chamber volume in the triaxial cell

v_κ Specific volume at $p' = 1$ kPa (overconsolidated soils)

x Upper proximity transducer target displacement

X Coefficient for M in Pender's model

y Lower proximity transducer target displacement

z Submersible LVDT armature displacement

W Weight of moving parts in the Bishop Wesley triaxial cell

Greek Symbols

α Exponent of OCR for the determination of K_{0u}

β Output reading from a proximity transducer

β_1 Parameter used for the evaluation of K_{0u}

β_t Output reading from a proximity transducer when no target placed opposite to it

ϵ_ℓ Average local axial strain

ϵ_{max} Maximum axial strain during tube sampling

ϵ_v Volumetric strain

ϵ_s Shear strain

ϵ_v^e Elastic volumetric strain

ϵ_s^e Elastic shear strain

ϵ_a Axial strain

ϵ_r Average radial strain

ϵ_{ec} Average end cap axial strain

ϵ_{ex} Average external axial strain

ϵ_t Tangential strain in the 100 mm cell steel ring

η Stress ratio q/p'

η_0 Stress ratio q/p' during one-dimensional consolidation

ϕ' Effective angle of friction

Γ Specific volume at critical state with $p' = 1$ kPa

κ Slope of the swelling line in $v, \ln p'$ space

κ^* Initial slope of the swelling line in $\ln v, \ln p'$ space

λ Slope of normal consolidation line in $v, \ln p'$ space

λ^* Slope of the normal consolidation line in $\ln v, \ln p'$ space

ν Poisson's ratio

ν' Effective or drained Poisson's ratio

ψ Exponent of the hardening function in Al-Tabbaa's model

σ_1 Vertical pressure

σ_3 Radial pressure

σ_1' Vertical effective pressure

σ_3' Radial effective pressure

σ_{1c}' In-situ vertical preconsolidation pressure

σ_{tc} Lower chamber pressure

σ_{3i} Initial radial pressure prior to consolidation

σ_t Tangential stress in the 100 mm cell steel ring

Subscripts

cs Critical state

nc Normally consolidated

f Final

i Initial

c Current

1 Strain on one side

Abbreviations

$^{\circ}C$ Degree Celcius

LVDT Linear variable differential transformer

hr Hour

m Meter

kN Kilonewton

μ**m** Micron

% Percentage

mm Millimeter

N Newton

|| Absolute value

ln Natural logarithm

log Logarithm base 10

LIST OF FIGURES

Chapter 1

Chapter 2

Chapter 3

Chapter 6

LIST OF PLATES

Chapter 3

LIST OF TABLES

Chapter 2

Chapter 3

Chapter 4

Chapter 5

Chapter 6

Chapter 1

INTRODUCTION

1.1 Determination of Stiffness Parameters

Geotechnical engineering design may involve calculations relating to both collapse and serviceability. Solutions for the collapse of soil structures can be provided by calculating the upper and lower bounds of loading using the theory of plasticity where the soil is assumed to behave in a rigid-perfectly plastic manner. However, this does not provide any information about the deformations taking place prior to collapse. The parameters required for such analyses are either c_u , the undrained shear strength, or c' and ϕ', the effective cohesion and effective angle of internal friction respectively. These are ususally determined with satisfactory accuracy on site (e.g. shear vane test) or in the laboratory (e.g. triaxial test)

On the other hand, solutions for the serviceability of soil structures generally prove more difficult due to the complexity of the deformation behaviour of soils. In stiff clays, settlements below footings and movements around excavations are usually

overestimated (Burland et al (1979) and Jardine et al (1986)). Before attempting to evaluate the magnitude of ground movements, it is therefore important to define appropriate stiffness parameters and to assess the factors controlling them.

1.1.1 Definition of Soil Stiffness

Stiffness is usually defined as the ratio of stress to strain increments at a certain stress or strain level. The main disadvantage of such a definition is that it does not distinguish between elastic and plastic components of deformation. As shown in Figure 1.1, there are two ways of defining stiffness, namely as a tangent and as a secant to a point on the stress strain curve. Tangent stiffness is more difficult to evaluate from test data since it requires the use of curve fitting techniques. By comparison with the secant stiffness, it is less affected by bedding errors. Strains corresponding to peak and ultimate strength can be more clearly identified by the tangent stiffness as shown in Figure 1.2 (Atkinson et al (1986)). Tangent stiffness is generally more suitable for numerical analyses of stress-strain behaviour, where loading is usually assumed to be applied in small increments.

1.1.2 Field and Laboratory Testing

Three main approaches may be taken for the evaluation of the required soil parameters : in-situ testing, laboratory testing and observation, measurement and back-analysis of full scale construction. Each of these approaches has its strengths and limitations. For example, boundary conditions during in-situ testing are usually poorly defined. Strain and drainage control are very difficult if not impossible to achieve. In contrast, laboratory tests involve well defined boundary conditions. In

addition, the accuracy of laboratory instrumentation is likely to be better than that of in-situ equipment because of the more favourable working environment. However, it has been realised for a long time (e.g. Cooling (1949)) that the validity of investigations carried out in the laboratory depends on the quality of samples and on how far they are representative of the stratum from which they are taken. Therefore, laboratory testing has two main disadvantages. The first is related to the volume of soil tested, which is relatively small compared to that involved in in-situ tests, and the second is associated with sampling disturbance. Sampling effects on laboratory specimens have been extensively investigated with some degree of success (Section 2.2). In general, in-situ tests also involve disturbance the size of which is very difficult to assess, except in the case of self-boring pressuremeter tests (e.g. Clarke and Wroth (1985), Fhaye and Randolph (1985), Sayed and Hamed (1988)).

The back-analysis of field observations can be relatively expensive and sometimes requires complicated soil modelling and computing. Nevertheless, back-analyses of foundations and retaining walls have been used by Burland et al (1979) and Jardine et al (1986) to determine stiffness parameters. The results showed good agreement with those from carefully conducted and specially instrumented triaxial tests and proved that such tests could be more reliable than plate load or pressuremeter tests. Such observations have demonstrated the importance of measuring the small strain behaviour of the soil accurately, especially when the stiffness parameter is being used in the design of geotechnical structures undergoing relatively small movements under working conditions.

Generally, comparisons between the results from conventional triaxial tests, plate load tests, and back-analysis have shown large discrepancies for the stiffness parameters of stiff clays. Marsland (1973) concluded that stiffnesses from laboratory tests are both variable and difficult to interpret and that plate load tests give the

highest and most reproducible stiffness values. St John (1975) similarly reported that conventional laboratory tests on London clay give lower values of stiffness than in-situ tests.

The explanations advanced for the discrepancies referred to above include :

1.1.2.1 The existence of fissures

In terms of fabric, the representativity of a laboratory specimen could be poor. Marsland (1971a) noted that for fissured London clay, the stiffness values from 38 mm triaxial specimens were larger than those from 100 mm ones. He concluded that the size of the specimen should be large enough to contain the soil fabric. However, Costa Filho (1980) reported that, if the fissures are closed, the effects on the stiffness are minimal. In glacial tills other factors such as the existence of boulders could be significant (Anderson and McKinlay (1975)).

1.1.2.2 Differences of stress history and applied loading

Stress paths during in situ testing are generally different from those in the laboratory (Parry (1979), Atkinson (1984)). It is not always possible to define the stress path being followed during in-situ tests.

In a triaxial test different values of stiffness will be obtained from compression and extension tests (Hight et al (1985)). Jardine et al (1985) reported that, for reconstituted London clay, the extension stiffness could be as low as 50% of the compression stiffness. Atkinson et al (1989) also investigated the stress-path dependency of stiffness for clay soil. In particular, they found that a large increase in stiffness

takes place upon any change in the effective stress path direction. Richardson (1988) argued that the stiffness is not only dependent on the stress path direction, but also on the size and timing of the stress increments. Ballasubramanian (1969) showed that increasing the stress increment with the same overall loading rate results in an increase in stiffness. Gens (1983) and Richardson (1988) found similarly that when a specimen of clay is left for a certain period of time under constant effective pressure, the subsequent stiffness can be expected to be higher.

The stress history prior to sampling and testing is another factor which could have important implications as far as the stiffness is concerned. Several researchers (e.g. Gens (1983) and Atkinson et al (1986)) have investigated the effects of consolidation path on the subsequent stiffness response. Natural soils are usually deposited under K_0-conditions (no lateral strain) while, for simplicity and to reduce the time taken, laboratory consolidations are usually carried out isotropically. For heavily overconsolidated London clay, Costa Filho (1980) reported that during the early stages of his tests the stiffness of anisotropically consolidated specimens was about 10% to 15% larger than that of isotropically consolidated ones.

Of particular relevence to the research described in this thesis is the stress history associated with sampling disturbance. During sampling, clay specimens follow complicated stress and strain paths (Baligh et al (1987) and Hight et al (1985)). The process of tube sampling and specimen preparation in the laboratory is likely to have a significant effect on the stress-strain response of the soil. This is discussed more fully in Chapter 2.

1.1.2.3 Non-linearity of stress-strain behaviour

For triaxial specimens, research at Imperial College (Costa Filho (1980) and Burland and Symes (1982)) revealed that conventional techniques (Bishop and Henkel (1962) and Bishop and Wesley (1975)) were not suitable for measuring small strains of up to 0.1%. The research demonstrated the need to carry out local axial strain measurements by mounting instrumentation directly on the specimen. It was also shown that the behaviour of clay soils was non-linear, even at small strains. Costa Filho (1980) concluded that the strain levels associated with the values previously quoted for laboratory stiffness had often been higher than those experienced in the field. Consequently, the laboratory stiffness had appeared too low.

The introduction of new strain measurement techniques has had a significant impact on the importance of laboratory testing relative to in-situ testing. Another significant factor has been the development of the Bishop and Wesley (1975) triaxial apparatus. Stresses are applied hydraulically making it relatively easy to apply any (axially symmetric) stress path. The development of this apparatus followed the introduction of the Stress Path Method by Lambe (1967) and Lambe and Whitman (1967). This method recognises the dependence of soil behaviour on the stress history and the stress path followed during applied loading. However, certain procedures have to be adopted to minimise the effects of sampling disturbance. One of them consists of restoring the initial effective stress conditions before sampling (Bjerrum (1973)). Another involves consolidating the specimen to a vertical effective pressure which exceeds 1.5 to 2 times the estimated in-situ preconsolidation pressure, σ'_{1c}, after which it is allowed to swell to the estimated overconsolidation ratio (OCR) (the SHANSEP approach advocated by Ladd and Foott (1974)).

1.2 Mathematical Models for Soil Deformation Behaviour

Mathematical models make use of physical theories relating to soil in order to describe its state and predict its response to loading. Ideally a model should be general enough to cater for any soil and loading conditions. However, this can only be achieved by increasing the complexity of the model and hence the number of input parameters. Researchers, therefore, have always tried to reach a compromise between complexity and generality.

In this section, some existing models will be briefly presented, with attention focussed on those which will be used in Chapter 7 for comparison with experimental data. The models are discussed in the context of axial symmetry (as in the triaxial cell).

1.2.1 Elastic Models

The most straightforward model used for predicting soil deformations is the linear elastic model. For an isotropic material, the linear elastic model predicts that :

$$\delta\epsilon_s^e = \frac{1}{3G'}\delta q \tag{1.1}$$

$$\delta\epsilon_v^e = \frac{1}{K'}\delta p' \tag{1.2}$$

where $\delta\epsilon_s$, $\delta\epsilon_v$, δq, and $\delta p'$ are the infinitessimal increments of shear strain, volumetric strain, deviator stress , and mean effective pressure respectively. G' is the shear modulus and K' is the bulk modulus.

Alternatively and more realistically, the values of G' and K' may vary with stress or strain. resulting in a non-linear elastic model. This version of the model has been used to predict the ground movements around excavations in London clay, as reported by Burland et al (1979) and Simpson et al (1979). However, it was reported that the computed distributions of strain were not always satisfactory. Furthermore, progressive movement was noticed behind walls in large excavations, indicating some inelastic behaviour. Simpson et al (1979) showed that a more complicated model which takes into account plastic behaviour would give more satisfactory results (see below). The elastic models may be modified to incorporate anisotropy at the expense of additional complexity (e.g. Costa Filho 1980).

1.2.2 Elasto-Plastic Models

Triaxial tests carried out on natural soils have revealed that only a limited amount elastic behaviour takes place initially during shearing (e.g. Atkinson (1973) and Ballasubramanian (1969)). Therefore, a model which caters for the initially elastic and subsequently plastic behaviour appears more suitable. Elasto-plastic models have been presented by, for example, Zienkiewicz (1977) and Atkinson (1981). The models can be represented by the following equations:

$$\delta\epsilon_s = \left(FH + \frac{1}{3G'}\right)\delta q + H\delta p' \tag{1.3}$$

$$\delta\epsilon_v = H\delta q + \left(\frac{H}{F} + \frac{1}{K'}\right)\delta p' \tag{1.4}$$

where F and H are the flow and hardening parameters respectively.

One of the successful versions of the elasto-plastic model is Model L.C. developed by Simpson et al (1979). This model takes also into consideration the initial high stiffness associated with recent stress history effects. The stress-strain curve is

divided into three parts, namely elastic, intermediate, and plastic. Applications of the model are given by Simpson et al (1979) and Burland et al (1979). However, with Model L C, predictions for normally consolidated clays are not likely to be very satisfactory due to plastic strains observed during the early stages of shearing. The family of elasto-plastic models includes the critical state models described in the next section. These are better suited to normally consolidated and lightly overconsolidated soils.

1.2.3 Critical State Models

Critical state soil mechanics makes use of a state boundary surface in q, p', v space to describe the state of a soil where v is the specific volume of the specimen. Soils falling below this surface, shown in Figure 1.3, are supposed to behave in an isotropic elastic manner. The critical state line represents states where distortion can take place indefinitely without any change in effective stress or specific volume. This is sometimes described as an ultimate state. Descriptions of the Cam-clay and Modified Cam-clay models are given by Schofield and Wroth (1968) and Roscoe and Burland (1968) respectively. For triaxial compression, the principal equations connected with the Modified Cam-clay model are as follows (Similar equations may be developed for triaxial extension):

Critical State Line

$$q = Mp' \tag{1.5}$$

$$v = \Gamma - \lambda ln p' \tag{1.6}$$

Normal Consolidation Line

$$v = N - \lambda ln p' \tag{1.7}$$

Swelling Line

$$v = v_\kappa - \kappa ln p' \tag{1.8}$$

State Boundary Surface :

$$q = Mp' \left[2exp\left(\frac{\Gamma - v - \lambda ln p'}{\lambda - \kappa} \right) - 1 \right]^{1/2} \tag{1.9}$$

where

M : slope of the critical state line in $q - p'$ space.

Γ : specific volume of soil at the critical state with $p' = 1.0$ kPa

λ : slope of the normal consolidation line

N : specific volume of soil consolidated isotropically to $p' = 1.0$ kPa

v_κ : value of specific volume for overconsolidated soils at $p' = 1.0$ kPa

κ : slope of the swelling line

Critical state models have been succesfully used for predicting the behaviour of isotropically and normally consolidated soils at fairly large strains. However, problems were encountered with overconsolidated soils in two respects. Roscoe and Burland (1968) reported that plastic deformation does take place along stress paths beneath the the state boundary surface and provided a method for the calculation of this additional component of strain. The second problem encountered with overconsolidated clays is that deformation is usually non-uniform as failure is approached whereas the models assume that strains are uniform.

Alternative models to the original Cam-clay model and the Modified Cam-clay model have been developed. These include :

1.2.3.1 Atkinson's model

Atkinson et al (1987) extended the modified Cam-clay model to make it applicable for anisotropically normally consolidated soils by assuming that the shearing stress path lies on the state boundary surface. Starting from Equation 1.9, the state boundary surface for K_0-consolidated soils was developed as :

$$\eta - \eta_0 = (XM - \eta_0)\left[2exp\left(\frac{\Gamma - v - \lambda ln p'}{\lambda - \kappa}\right) - 1\right]^{1/2} \tag{1.10}$$

where

η is the ratio of q/p'

η_0 is the initial value of η at the beginning of undrained loading

X is $+1$ for compression loading, and -1 for extension loading.

For overconsolidated clays the model suffers from the same limitations as the original models.

Thevanayagam and Prapaharan (1988) argued that the assumption that the stress path for normally consolidated specimens during shearing lies on the state boundary surface is not always true. Using Dafalias's (1987) version of the Modified Cam-clay which takes into account the anisotropic behaviour of clays, they introduced another equation for the state boundary surface. They also reported that the critical state lines are symmetrical about the p'-axis.

1.2.3.2 Pender's model

Pender (1977,1978) developed a model which allows plastic strains to occur below the state boundary surface and which can be used for overconsolidated as well as

normally consolidated soils. The generalised undrained stress path is given by :

$$\left(\frac{\eta-\eta_0}{XM-\eta_0}\right)^2 = \frac{p'_{cs}}{p'}\left\{\frac{1-p'/p'_0}{1-p'_0/p'_{cs}}\right\} \tag{1.11}$$

p'_0 and p'_{cs} are the initial mean effective pressures at the start of loading and on the critical state line at the current value of v respectively.

Strains are calculated by dividing them into elastic and plastic components. The elastic shear strain, ϵ^e_s, is assumed to be zero while the elastic volumetric strain, ϵ^e_v is calculated from equation 1.2. Plastic strains are calculated from the following equations :

$$\delta\epsilon^p_s = \frac{2\kappa\left(p'_0/p'_{cs}\right)(\eta-\eta_0)\,\delta\eta}{(XM)^2\,v\left(2p'_0/p'-1\right)\left[(AM-\eta_0)-(\eta-\eta_0)\,p'/p'_{cs}\right]} \tag{1.12}$$

$$\delta\epsilon^p_v = \frac{2\kappa\left(p'_0/p'_{cs}-1\right)\left(p'/p'_{cs}\right)(\eta-\eta_0)\,\delta\eta}{(XM-\eta_0)\,v\left(2p'_0/p'-1\right)} \tag{1.13}$$

The advantages of this model include its applicability to both anisotropically and isotropically consolidated soils. Its applicability to heavily overconsolidated soils makes it more relevant for many geotechnical engineering problems, although it does not take into account the inhomogeneous deformations that develop in such soils. In addition, the model can be used to predict stress paths and progressive deformations during cyclic loading.

1.2.3.3 Al-Tabbaa's model

Pender's model provides for both elastic and plastic strain componenents to be evaluated but does not identify elastic and plastic regions in q, p', v space. Al Tabbaa (1987) extended the modified Cam-clay model to take into account the limited elastic behaviour displayed by clays. She introduced within the state boundary surface a

second yield surface inside which the behaviour is isotropic, elastic and non-linear. The extra or revised parameters required for this model are :

λ^* : the slope of the normal consolidation line in $lnv - lnp'$ space

κ^* : the initial slope of the swelling lines in $lnv - lnp'$ space

M : the slope of the critical state line in $q - p'$ space

R : the ratio of the size of the inner yield surface to the state boundary surface.

ψ : exponent of the hardening function H

ν' : the effective or drained Poisson's ratio.

The state boundary surface is given by :

$$\left(p' - p_0'\right)^2 + \frac{q}{M^2} = p_0'^2 \tag{1.14}$$

and the inner yield surface by :

$$\left(p' - p_\alpha'\right)^2 - \frac{(q - q_\alpha)}{M^2} = R^2 p_0'^2 \tag{1.15}$$

where p_α and q_α are the coordinates of the centre of the inner ellipse as shown in Figure 1.4. Changes in the yield surface are governed by two rules concerning its translation and size within the state boundary surface. The translation rule is given by the following equations:

$$\delta p_\alpha' = \frac{\delta p_0'}{p_0'} p_\alpha' + S\left[\frac{\left(p' - p_\alpha'\right)}{R} - \left(p' - p_0'\right)\right] \tag{1.16}$$

$$\delta q_\alpha = \frac{\delta p_0'}{p_0'} q_\alpha + S\left[\frac{(q - q_\alpha)}{R} - q\right] \tag{1.17}$$

where the scalar quantity S is given by :

$$S = \frac{\left(p' - p_\alpha'\right)\left[\delta p' - \frac{\delta p_0'}{p_0'} p'\right] + \frac{(q - q_\alpha)}{M^2}\left[\delta q - \frac{\delta p_0'}{p_0'} q\right]}{\left(p' - p_\alpha'\right)\left[\frac{\left(p' - p_\alpha'\right)}{R} - \left(p' - p_\alpha'\right) + \frac{(q - q_\alpha)}{M^2}\left[\frac{(q - q_\alpha)}{M^2} - q\right]\right]} \tag{1.18}$$

Al-Tabbaa assumed that the size of the yield locus changes proportionally with that of the state boundary surface so that the ratio R is constant.

The elastic volumetric strain, ϵ_v^e inside the inner yield locus is given by equation 1.2. By introducing a hardening quantity h which is the sum of two components h_0 and H defined by the following equations :

$$h_0 = \frac{\left(p' - p'_\alpha\right)}{(\lambda^* - \kappa^*)} \left[p' \left(p' - p'_\alpha\right) + \frac{q\,(q - q_\alpha)}{M^2} \right] \tag{1.19}$$

$$H = [1/(\lambda^* - \kappa^*)] \left(\frac{b}{b_{max}} \right)^{\psi} p_0'^3 \tag{1.20}$$

where b and b_{max} are evaluated from :

$$b = \frac{1}{R p'_0} \left[\left(p' - p'_\alpha\right) \left[\frac{p' - p'_\alpha}{R} - \left(p' - p'_0\right) \right] + \frac{q - q_\alpha}{M^2} \left[\frac{q - q_\alpha}{R} - q \right] \right] \tag{1.21}$$

the plastic components of strain are given by :

$$\delta\epsilon_v^p = \frac{1}{h} \left[\left(p' - p'_\alpha\right)^2 + \left(p' - p'_\alpha\right) \frac{q - q_\alpha}{M^2} \right] \delta p' \tag{1.22}$$

$$\delta\epsilon_s^p = \frac{1}{h} \left[\left(p' - p'_\alpha\right) \frac{q - q_\alpha}{M^2} + \left[\frac{q - q_\alpha}{M^2} \right]^2 \right] \delta q \tag{1.23}$$

It can be easily shown that the model reduces to the Modified Cam-clay model for monotonic yielding loading conditions (when $H = 0$).

Al-Tabbaa's model applies to both isotropically and anisotropically consolidated soils and is suitable for cyclic loading applications. However, as recognised by Al-Tabbaa, the change from elastic to elasto-plastic behaviour is sometimes too abrupt by comparison with experimental data.

1.3 Research Objectives

As was made clear in Section 1.1, the triaxial testing of soil and associated measurement techniques have undergone appreciable developments over the past decade. However, sampling disturbance is still an issue of major concern. Although its effects

have been realised since the 1940's (e.g. Terzaghi (1941), Hvorslev (1949)), research in this field (reviewed in Chapter 2) has often dealt with stress relief and storage effects and has ignored the mechanical disturbance associated with tube sampling and specimen preparation. This is mainly due to the complicated stress and strain paths followed during such stages. Recently, an important advance was made by Baligh (1985) who introduced the Strain Path Method for deep foundation problems and used it to predict the strain suffered by the soil during tube sampling.

Research carried out by Hight et al (1985) and Baligh et al (1987) concentrated mainly on the investigation of tube sampling effects on the strength and large strain stiffness and the possible methods of reducing them. As will be seen in Chapter 2, the effect of tube penetration on the behaviour of normally consolidated clays is very significant. As the overconsolidation ratio increases, the strength and stiffness parameters are less affected (Hight et al (1985)).

In the present research, the main and overall objective was to use state-of -the-art triaxial testing techniques to simulate the sampling process and to compare the small strain behaviour of 'disturbed' and 'undisturbed' clays. Disturbance of a specimen was simulated by applying a strain cycle followed by a release of deviator stress. The specimen was then reconsolidated to its initial stress condition, before being sheared. The effects on small strain behaviour of other factors such as rate of shearing, initial overconsolidation ratio, and consolidation stress-path, were also investigated.

Hight et al (1985) and Baligh et al (1987) concentrated their investigations on undrained behaviour. In this work also only undrained shearing has been investigated since test durations could be minimised and a more extensive data base is available for comparison purposes.

The material used in this research was Speswhite kaolin. This had the advantage of avoiding the specimen non-uniformities usually encountered with natural soils. Specimens were prepared to a specified consolidation pressure before being set up in the cell, thereby producing specimens with identical stress histories and improving the repeatability of test results. The availability of a considerable amount of previous data, especially from tests in the triaxial cell, was a further advantage. Details of the testing programme are presented in Chapter 6.

Before the research could be carried out, it was necessary to undertake considerable development work in relation to the test equipment in the light of previous experience (Yung (1987)). Therefore the initial objectives were :

- To design and manufacture a Bishop and Wesley type triaxial apparatus for 100 mm diameter specimens, hereafter referred to as the 100 mm apparatus or cell, with special features required for the current tests (see Section 3.3)
- To improve the existing radial and axial small strain measurement techniques.
- To develop new and improved computer software to control the tests and log data.

In order to provide additional data which could be used to support the results from tests on the 100 mm diameter specimens, a number of tests were carried out on an existing stress path apparatus for 38mm diameter specimens, which will be referred to as the 38 mm apparatus or cell. The equipment had to be modified in order to measure axial strains inside the cell, so that strain data would be accurate enough to be compared with data from the larger cell. In these supporting tests, because of time constraints, only 'undisturbed' isotropically consolidated and swollen specimens were tested.

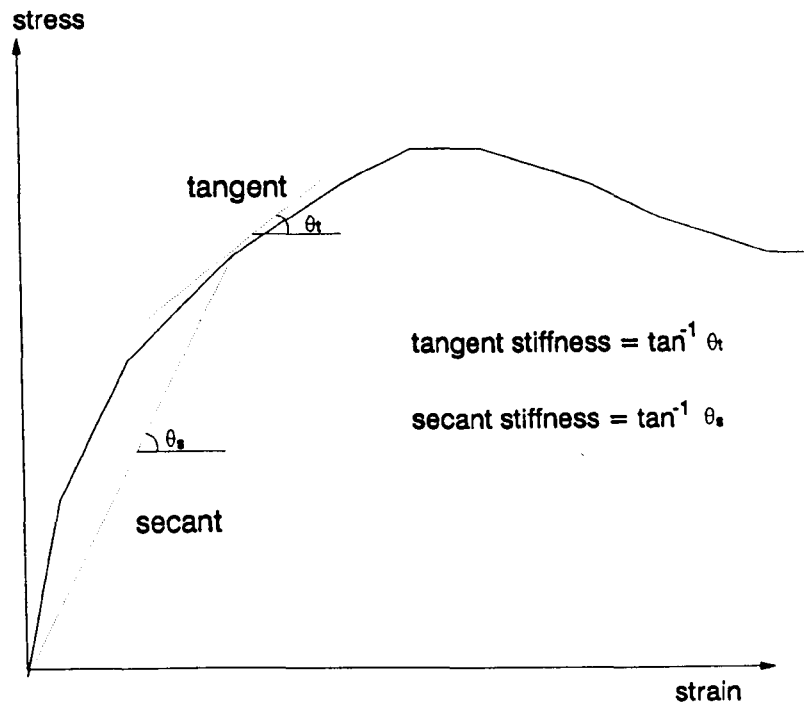

Fig 1.1 Definitions of stiffnesses

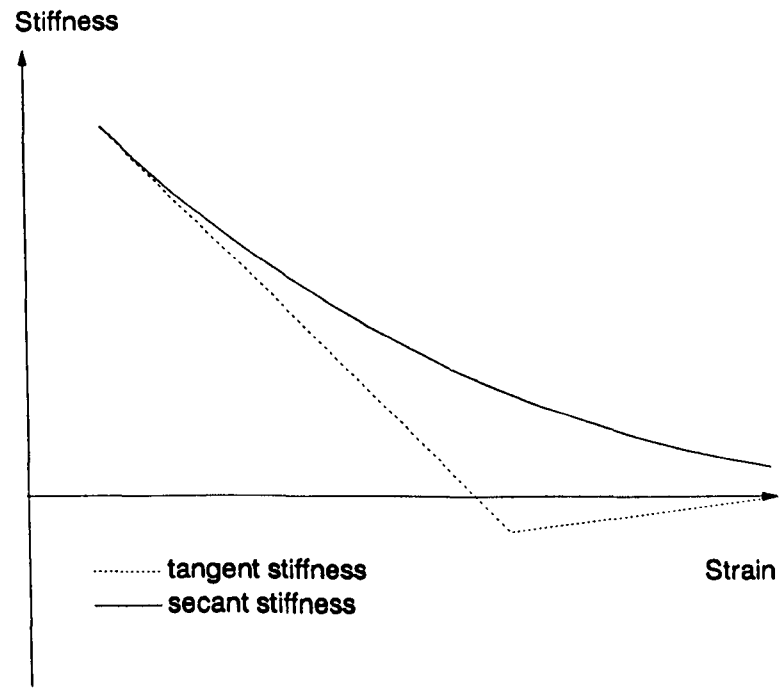

Fig 1.2 Comparison of variation of tangent and secant stiffnesses with strain

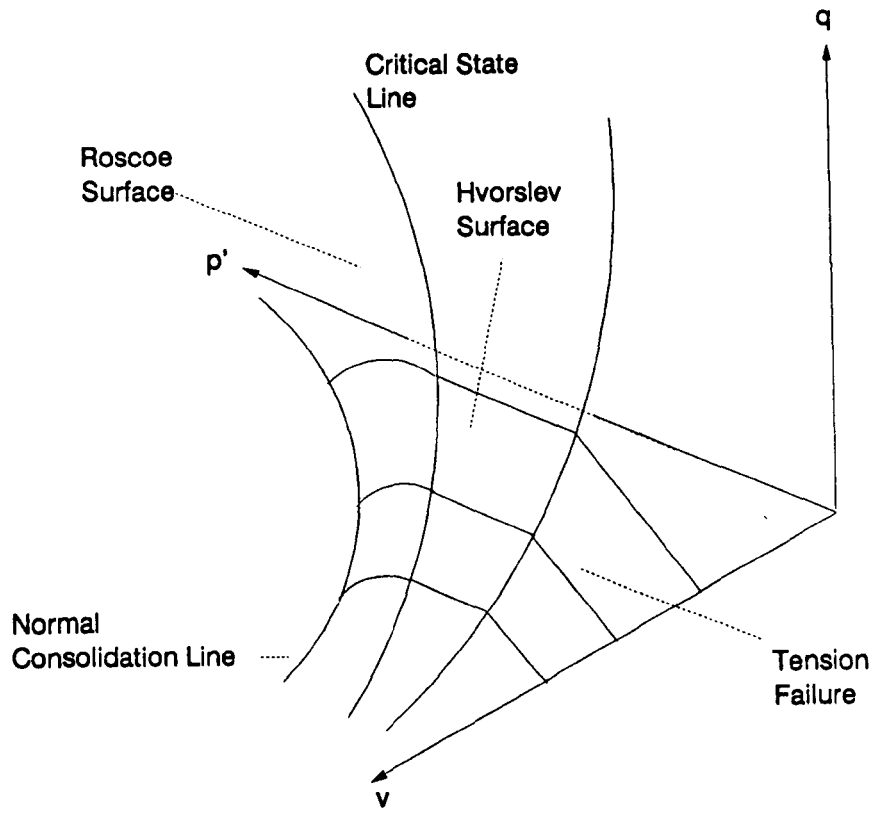

Fig 1.3 Critical state model - State Boundary Surface
(Isotropic Compression)

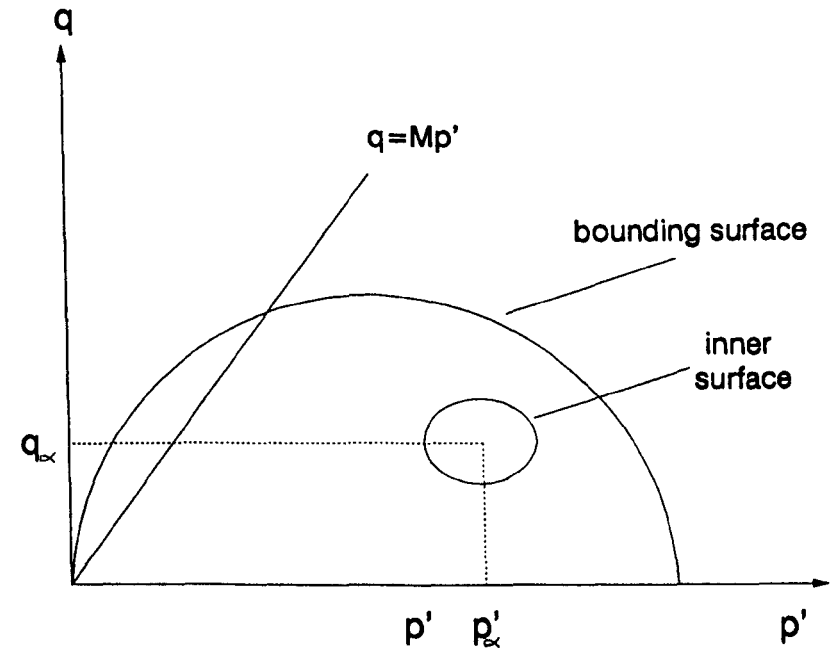

Fig 1.4 Yield and bounding surfaces in Al-Tabbaa's model

Chapter 2

LITERATURE REVIEW ON SAMPLING AND TESTING OF SOILS

2.1 Introduction

It has long been appreciated that measurements of soil parameters may be affected by the technique of sampling and testing in the laboratory. As pointed out in Chapter 1, both field and laboratory testing usually involve sampling disturbance of soil. While the evaluation of the disturbance effects in the field is very difficult if not impossible, recent research on tube sampling (Baligh et al (1987)) allows a better prediction of its effects on the behaviour of laboratory specimens. The first part of this Chapter deals with soil sampling and its effects in relation to triaxial testing. Other factors such as loading rate and OCR will also be considered. The remainder is concerned with improvements in testing techniques. Attention is focussed on

the Bishop and Wesley stress path apparatus and recent developments in strain measurement.

2.2 Sources and Effects of Sampling Disturbance

Table 2.1 presents a summary of the different possible sources of disturbance which can take place before, during, and after sampling. It can be seen that there are three principal categories of disturbance, namely disturbance due to stress relief, mechanical disturbance and disturbance due to water flow or chemical changes. These are not necessarily independent. Some sources of disturbance can be eliminated or reduced to negligible levels (e.g. freezing and piping) while others are less easily avoided. Under perfect conditions where mechanical and chemical disturbance are non-existant, the only source of disturbance would be the stress relief. This is usually called perfect sampling.

Irrespective of the method of sampling, no soil specimen can be considered totally undisturbed. The seriousness of the disturbance depends on the soil type and the parameters to be evaluated. Block sampling is usually used to minimise mechanical disturbance of the specimen. However, stress relief could still result in alteration of the stress-strain properties, depending on the type of soil and its stress history (see Section 2.3). Tube sampling is widely used for both research and commercial purposes due to its convenience. It is also used in offshore site investigations where block sampling is virtually impossible. Nevertheless, it has always been realised that the mechanical disturbance imposed on a tube sample is much larger than that associated with a block sample.

One of the most important sources of mechanical disturbance for tube samples

is the sampler penetration. There are two aspects of disturbance due to sampler penetration. Firstly, friction on the inside sampler wall can cause significant local distortion of the micro-structure of the soil which is noticeable when the specimen is split up and its fabric exposed, as reported by Hight et al (1985). Broms (1980) reported that large variations in friction forces occur in clays; the general trend is for friction to increase with decreasing rate of penetration, increasing surface roughness, and increasing plasticity. In normally consolidated clays, disturbance of the outer zone of the sample causes a significant increase in pore water pressure relative to that at the centre. This means that, under conditions of no overall water content change, water migrates from the outer disturbed zone to the inner (relatively undisturbed) one causing it to swell (Schjetne (1971)). Although friction forces are unavoidable, they can be minimised by increasing the rate of penetration and making sure that the sampler walls are as smooth as possible.

The second and more serious aspect of disturbance during tube penetration is the forced displacement of soil, which is a function of the geometry of the sampler. Hvorslev (1949) proposed the use of the area ratio defined in the following equation as an indicator of the extent of disturbance due to soil displacement :

$$A_r = (B_o^2 - B_i^2)/B_i^2 \tag{2.1}$$

where A_r is the area ratio and B_o and B_i are the outside and inside diameters of the sampler respectively (Figure 2.1). The larger the area ratio, the greater the disturbance caused to the soil sample. Hvorslev found that for equal area ratios and similar types of soil, the disturbance increases with increasing diameter of sampler and depth below ground level. Soft clays tend to suffer more disturbance than stiff clays or cohesionless soils. Hvorslev concluded that the value of the area ratio required for obtaining 'undisturbed' specimens depends on the design and method of operation of the sampler as well as its diameter. The current British Standard

Code of Practice on Site Investigation (B.S. 5930) suggests the use of an area ratio of around 30 %. An additional criterion suggested by Hvorslev was that the inside clearance ratio (ICR) given by :

$$ICR = \frac{B_s - B_i}{B_i} \tag{2.2}$$

where B_s is defined in Figure 2.1, should lie between 0.75 % and 1.5 % under normal conditions. He also recommended that for 'properly designed and operated' drive samplers of 50 mm to 70 mm inside diameter, ratios of specimen length to diameter can be increased to between 5 and 10 for cohesionless soils and between 10 and 20 for cohesive soils.

The most useful analysis of the effects of sampler geometry on the soil was presented by Baligh (1985) who developed the Strain Path Method and used it to evaluate the nature and extent of the mechanical disturbance along the centreline of the sample. As shown in Figure 2.2, elements of soil along the centreline of the sampler undergo axial compression followed by axial extension before finally experiencing zero net axial strain. The soil is assumed to remain undrained. This strain cycle represents the minimum disturbance that must take place during sampler penetration and is a function of the aspect ratio B_s/t_s, where t_s is the wall thickness of the sampler. The following important features were noticed by Baligh et al (1987)

- Even with very high aspect ratios (e.g. $B_s/t_s > 40$), elements along the sampler centerline may undergo failure even before entering the sampler.
- With normally consolidated and lightly overconsolidated clays the disturbance significantly changes their stress and strain history and has a considerable influence on their subsequent behaviour.
- With heavily overconsolidated clays the disturbance affects the subsequent

behaviour but to a much lesser extent than in the case of normally consolidated clays.

In the hypothetical situation where the ratio B_s/t_s tends to infinity, tube sampling disturbance would reduce to perfect sampling where the only source of disturbance would be the total stress relief.

Skempton and Sowa (1963) examined the effects of perfect sampling by monitoring the pore pressure in a K_0-consolidated triaxial specimen after total stress relief. They found that a reduction in the mean effective pressure of up to 20% could take place. No significant changes in the undrained shear strength were noticed after isotropic reconsolidation of the specimen, even though the stress paths followed in the tests were different. Tests carried out by Kirkpatrick and Rennie (1975) and by Hanzawa (1977) indicated similar results. Atkinson and Kubba (1981) found that normally K_0-consolidated specimens which were subjected to perfect sampling and reconsolidated back to the initial stresses did not exhibit similar values of stiffness to those of 'virgin' samples. However, they found that both samples had similar normalised effective stress paths.

Kirkpatrick and Khan (1984) and Kirkpatrick et al (1986) carried out triaxial tests on K_0-consolidated specimens to investigate the perfect sampling effects on kaolin and illite. They found that in both cases there were significant reductions in effective pressure and subsequently in unconsolidated undrained shear strength. They also reported that the reduction in undrained strength decreased with increasing overconsolidation ratio (OCR) and increased with the age of the specimen. These features are in agreement with those reported by Hight et al (1985). As shown in Figure 2.3, the effective stress history of the specimen is changed by the total stress relief. Subsequent reductions in both the peak undrained shear strength

and stiffness were noticed in Hight et al's unconsolidated undrained tests, especially in the case of normally consolidated soils. However, there was relatively little effect on the ultimate shear strength (Figure 2.3). Kirkpatrick et al (1986) concluded that for perfect samples, the degree of disturbance depends on the extent of the change in total stresses. The stress changes involved in the tests carried out by Skempton and Sowa (1963) did not exceed 100 kPa and therefore, according to Kirkpatrick et al (1986), were not large enough to change the soil structure significantly.

The above discussion indicates that stress relief effects on the undrained shear strength can be significant. The effects on stiffness do not seem to have been as extensively investigated as those on strength and, except in Hight et al (1985), apply for fairly large strains

In practice, stress relief is usually followed by a storage period, the length of which could have important consequences for the subsequent stress-strain behaviour of the soil. Hvorslev (1949) realised that, if soil specimens were not stored properly, their properties could be radically altered. Changes in water content during transport and storage can take place if the ends of the sampling tube are not well sealed. Different methods of storage have been proposed, some of which have been successful in preventing any significant change in water content (Holden (1971)). Ideally, soil specimens should be stored under the same stresses as existed in-situ, but this is not generally feasible.

Bjerrum (1973) found that the effects of storage on 'quick' clays were very significant, resulting in a reduction of 15% in the unconsolidated undrained shear strength after 3 days. He also reported that low plasticity clays tend to exhibit larger changes in undrained shear strength than high plasticity ones. Meyerhof and Murdock (1953) reported that the undrained shear strength of stiff fissured London

clay decreased with increasing storage period. Skempton and Henkel (1957), on the other hand, did not notice such a trend. This could be due to a superior method of sealing and storing the specimens. Tests carried out by Brown and Chow (1988) on normally consolidated kaolin showed that significant changes took place in specimens sealed with wax and stored without the application of estimated in-situ stresses. As shown in Table 2.2, the effects were more severe on stiffness than on strength. It can also be seen that storage under pressure substantially reduced the detrimental storage effects.

Broms (1980) and Kirkpatrick and Khan (1984) reported that the reduction in undrained shear strength during storage is the result of a decrease in the residual pore water pressure with time. They also noticed that the drop in the residual pore pressure could take place at constant water content. They were unable to explain this phenomenon, but noted that one reason could be cavitation taking place in the specimen during storage. This again suggests that, if storage effects are to be avoided, the specimen should not only be sealed well but also stored under the in-situ pressure condition .

Graham et al (1988) showed that strain dependent parameters such as the undrained stiffness are most affected by the storage stage. They studied the effects of 'drained' storage, where the specimen is allowed to change water content, and 'undrained storage', where no water content alterations were allowed, and found that undrained storage did not affect the undrained shear strength, while the stiffness showed a significant reduction. Samples with free access to water showed large changes in nearly all the soil parameters even after reconsolidation. Changes in the strain-dependent parameters were blamed on time-dependent micro-structural changes in the soil and not simply on the changes in the water content.

Other phenomena that could take place during storage, namely bacterial and chemical changes (Jerbo et al (1961)) and temperature variations (Kallestenius (1963)), have been found to be of no practical significance providing proper procedures are adhered to.

2.3 Methods of Evaluating and Correcting Sampling Disturbance

As seen in the previous section, the sampling disturbance of soil can be a complicated process and different sources of disturbance can act simultaneously. Researchers have generally attempted to simplify the sampling process by considering each source of disturbance separately, so as to make it easier to evaluate the effects of each one in terms of certain soil properties. Analytical evaluation has proved difficult if not impossible because sampling involves operator dependent effects and complex changes of stress and strain. This has resulted in reliance on qualitative descriptions for assessing the extent of disturbance. Table 2.3 shows a qualitative summary of the research concerning the methods of evaluating sampling disturbance effects.

Okumara (1971) and Nelson et al (1971) proposed the use of the residual effective stress to express the degree of disturbance quantitatively :

$$D = 1 - p_a^{'}/p_b^{'} \tag{2.3}$$

where D, $p_b^{'}$ and $p_a^{'}$ are the degree of disturbance, the mean effective pressure before sampling and the mean effective pressure after sampling respectively. Thus a totally undisturbed specimen would have a D-value equal to 0, while a highly disturbed specimen would have a D-value close to 1. Typical values of D are shown in Table

2.3. This approach was successfully used by Okumara (1971) to express the extent of disturbance in the case of block sampling. Atkinson and Kubba (1981) found that tube-sampled normally consolidated specimens have a larger value of D than perfect samples, reflecting the additional drop in the mean effective pressure due to mechanical disturbance. This approach can also be used to evaluate the disturbance due to storage by monitoring the residual pore pressure over the storage period.

Berre (1986) suggested the use of the volumetric strain undergone by the specimen during reconsolidation to the initial effective stresses as an indicator of the sample quality. He suggested 1.5% as the maximum allowable volumetric strain if the specimen is to be to considered of good quality. However, this was found to be difficult to achieve, especially in the case of soft clays. A better assessment of the maximum allowable volumetric strain is achieved when considered in conjunction with OCR and depth below ground level (Lacasse (1985)), as shown in Figure 2.4.

In numerical studies, Alonso et al (1981) showed that tube penetration disturbance is a strain controlled rather than a stress-controlled process. Subsequently, Baligh (1985) introduced the Strain Path Method (referred to in Section 2.2) for deep foundation problems. Using this method, the concept of an ideal sample was developed (Baligh et al (1987)) incorporating both stress relief and tube sampling effects. As mentioned above, the stress relief effects can be evaluated by calculating the value of D. The tube sampling effect is expressed in terms of the maximum axial strain undergone by a soil element along the centreline of the sampler (Figure 2.2) :

$$|\epsilon_{max}| = 0.385(t_s/B_s) \tag{2.4}$$

where $|\epsilon_{max}|$ is the absolute value of the maximum axial strain. The above equation represents an ideal (lower) limit to the mechanical disturbance that takes place during tube penetration. However, Baligh's approach only considers the mechanical

disturbance taking place along the centreline of the sampler. It does not consider the disturbance near the periphery where strain paths are known to be more complicated. As noted in Section 2.2, distortion along the specimen's periphery does not only affect soil in that zone but also the soil near the centreline because of water content redistribution.

The significance of ideal sampling is illustrated in Figure 2.5 where a comparison of the unconsolidated undrained behaviour of an undisturbed triaxial specimen, a perfect specimen, an ideally sampled specimen, and a good quality tube specimen is presented for normally consolidated Boston Blue clay (Baligh et al (1987). Although both perfect and ideal specimens have an undrained shear strength and stiffness higher than those of the good quality tube specimen, the overestimation associated with ideal sampling is far less than that of perfect sampling. The discrepancies between the strength and stiffness parameters from an ideal sample and those from a good quality tube sample can be attributed to the additional mechanical disturbance caused by friction along the periphery of the latter and increased during the preparation and setting up of the specimen in the triaxial cell. Figure 2.5 indicates that, even after perfect sampling, the undrained shear strength of an unconsolidated specimen is significantly reduced (Section 2.2).

Correction of sampling disturbance has been carried out through reconsolidation of the disturbed specimen to a predetermined effective pressure. The methods of reconsolidating clay specimens have been investigated by many authors. Hight et al (1985) reported that the stress path followed during reconsolidation to the initial stresses after sampling is very important as far as the stiffness response is concerned, especially during the early stages of shearing. For example, if the sampling process ended with unloading then the stiffest response would be noticed in tests that recompress the sample. Atkinson et al (1989) carried out a detailed study

on the effects of the recent stress history on the stiffness of clays and found that the stiffness is influenced by a change in the direction of the stress path, as shown in Figure 2.6. The small strain stiffness was found to vary by an order of magnitude with different rotations of the stress path. It was also reported that the effects of the recent stress history depend on the plasticity index, tending to be less marked for low plasticity clays.

Skempton and Sowa (1963) carried out isotropic reconsolidation and reported full recovery of the undrained shear strength. However, Kirkpatrick and Khan (1984) used different reconsolidation methods and found that isotropically consolidated specimens tended to either overestimate or underestimate the undrained shear strength depending on the ratio of p_c'/p_i' where p_i' and p_c' are the mean effective stresses initially and after reconsolidation respectively. Graham et al (1988) found that isotropic reconsolidation of normally consolidated clays to $p_c' = 0.6\sigma_{1c}'$ would give similar results to those from in-situ tests. In addition, they found that anisotropic reconsolidation to the original stresses gave a stress-strain response close to that of the in-situ soil, with a slight overestimation of the undrained shear strength. Reconsolidation after ideal sampling was studied by Baligh et al (1987). They found that recompression of Boston Blue clay to initial estimated in-situ stresses results in an approximate recovery of the undisturbed soil parameters. However, reconsolidation according to the SHANSEP approach (Ladd and Foott (1974)) was found to give a superior response, as shown in Figure 2.7. Previously, Hight et al (1985) had reported that reconsolidation to the initial in-situ stresses does not fully recover the stress-strain behaviour at small and intermediate strains but allows it to be 'bracketed'. Lacasse and Berre (1987) carried out tests similar to Baligh's on a different material, Drammen clay. They found that for normally consolidated and lightly overconsolidated clays tested in compression, the peak shear strength is

not affected by disturbance but the initial modulus is much lower for the disturbed specimens. Extension tests revealed that large strain shear strength and stiffness are higher for the disturbed specimens. The finding regarding peak shear strength in the compression tests seems to contradict that reported by Hight et al (1985) where the peak shear strength of the disturbed specimen was higher than that of the undisturbed specimen. An explanation for this cannot be provided since Lacasse and Berre (1987) do not indicate the method of reconsolidation, which may have a considerable effect on the subsequent stress-strain behaviour (see also Section 7.3.3).

From the above review it will be seen that data concerning the small strain response of soil after tube sampling is very limited. The effects on the small strain stiffness of mechanical disturbance, stress relief and subsequent recompression to initial stresses have not been fully investigated. This requires high quality testing making use of the developments described in Section 2.5.

2.4 Other Factors Affecting Deformation Behaviour

In addition to the effects of sampling disturbance on the stress-strain response of soils, other factors with significant effects have been considered by researchers. These include the rate of loading, the consolidation history and the overconsolidation ratio. Other factors such as temperature and ageing are also thought to have considerable influence. The discussion in this section will centre on the first three factors only. The rest have been covered in detail by Richardson (1988).

2.4.1 Rate of Loading

Previous studies of loading rate effects on the stress-strain behaviour of clays have mainly concentrated on the undrained strength rather than stiffness. Even when the relationship between stiffness and rate of loading has been looked into, the conclusions have been mainly qualitative and related to large strains only. However, the research has indicated that stiffness increases with increasing stress or strain rate in the same manner as strength, for which an increase of about 10 to 20 % for a tenfold increase in strain rate has been reported (Graham et al (1983)). Similar trends were also reported by Hight (1983). On the other hand, Richardson (1988) reported that, provided uniformity of the pore pressure during loading is ensured, the rate of loading may not be significant. In this case suitable loading rates may be calculated from the method suggested by Bishop and Henkel (1962). The review of the research in this field showed a lack of quantitative description of the stiffness-loading rate relationship.

2.4.2 Overconsolidation Ratio

By assuming that the 'pre-peak' stress-strain curves are closely linear, Wroth et al (1979) suggested a linear relationship between the normalised shear modulus, G/p_0', and $ln(OCR)$, which takes the form

$$\frac{G}{p_0'} = \left(\frac{G}{p_0'}\right)_{n.c.} [1 + C \times ln(OCR)] \tag{2.5}$$

where $(G/p_0')_{n.c.}$ is the normalised shear modulus for a normally consolidated specimens. Wroth et al did not have experimental evidence for the above relationship but there was experimental evidence for a similar relationship with c_u replacing p_0' as the normalising parameter (e.g. Ladd and Edgers (1972)).

Tests carried out by Gens (1983) on Lower Cromer Till and summarised in Figure 2.8 indicated that isotropically consolidated soils exhibit a linear relationship between normalised stiffness and $ln(OCR)$ while anisotropically consolidated specimens display a non-linear relationship. A maximum normalised stiffness can be noticed to take place at an OCR of around 2 to 4. It should be mentioned that the normalising parameter in the case of Gens's data is the initial vertical consolidation pressure (σ'_{ac}).

As mentioned above, Equation 2.5 has been developed by assuming a linear stress-strain relationship during the early stages of loading. Jardine et al (1984) reported that for one-dimensionally consolidated soils the relationship between E_{us}/c_u and $ln(OCR)$ is non-linear and depends on the strain level. For reconstituted specimens, E_{us}/c_u was a maximum at an OCR of about 2. No particular trend could be identified in the case of natural tube specimens. Richardson (1985) reported similar results for reconstituted one-dimensionally consolidated London clay and kaolin, but for isotropically consolidated specimens he reported a linear relationship between G/p'_0 and $ln(OCR)$. A similar trend was found by Atkinson and Little (1988) for a glacial till soil.

2.4.3 Consolidation History

Tests carried out by different researchers (e.g. Lewin (1970) and Koutsoftas (1980)) indicated that the stiffness of the soil increased with increasing slope of the consolidation stress path, η'_0. This effect was strongest in the case of compression tests on normally consolidated and overconsolidated clays.

As indicated in Figure 2.8, an anisotropically consolidated specimen exhibits a

higher normalised stiffness than a corresponding isotropically consolidated specimen. Similar results were reported by other researchers (e.g. Richardson (1988) and Graham et al (1988)) from tests on London clay and kaolin but the differences were significantly lower.

2.5 Stress Path Testing : Recent Improvements

In addition to the limitations of stress state that can be applied to the specimen, as discussed in detail by Baldi et al (1988), the standard triaxial tests described by Bishop and Henkel (1962) suffer from two main disadvantages. The first concerns the method of consolidating and shearing the specimens. The second relates to the strain measurement technique.

Figure 2.9a shows a conventional triaxial cell where the axial strain is measured by monitoring the loading ram movement and shearing is applied by increasing the axial stress while keeping the radial stress constant. This 'conventional' method of shearing is represented by a stress path with a slope of 3 in q, p space, which may not be similar to the stress path applied in the field. In addition, conventional triaxial testing involves isotropic consolidation of the specimen which is not a true representation of the natural anisotropic process.

The desire to test soils in the laboratory under conditions similar to those in-situ resulted in the introduction of a hydraulic stress path cell described by Bishop and Wesley (1975). This is shown in Figure 2.9b. Although loading is still axially symmetric, by changing the hydraulic pressures in the lower chamber and the cell, stress paths in any direction in q, p space can be followed relatively easily. The axial strain can be measured externally, by mounting cross-arms on the loading

ram supporting two vertical rods passing through clearance holes in the cell which deflect the displacement transducers. Alternatively, it can be evaluated from the lower chamber volume change as follows :

$$\epsilon_a = (\Delta V / a L_c) \times 100 \tag{2.6}$$

where ϵ_a is the axial strain, ΔV is the lower chamber volume change, a is the bellofram area, and L_c is the consolidated length of the specimen.

Costa Filho (1980) carried out tests on London clay to compare axial strains measured externally with those measured locally by mounting linear variable differential transformers (LVDTs) on the middle third of the specimen. As noted in Chapter 1, he reported that strains measured locally were much smaller than those measured externally. Similar results were reported by Burland and Symes (1982). The conclusion was that conventional strain measurements involve errors arising from a number of different sources.

2.5.1 Sources of Error in External Strain Measurements

Figure 2.10 illustrates some of the errors that can be included in a conventional strain measurement. Costa Filho (1985) showed that in certain cases the errors could be so large that the initial stress-strain behaviour would be completely masked. The errors fall generally into the following categories :

- Bedding errors : these occur whenever the specimen has irregular end surfaces or there is an initial lack of fit between the specimen top cap and the load cell. Stress-strain curves from tests with considerable bedding errors show a concave upwards shape in their initial part, as illustrated in Figure 2.11. The

traditional approach is to extend the linear portion and shift the origin for axial strain to the point of intersection. Of course, this procedure is unsatisfactory when small strain behaviour is being measured. The error due to irregular end surfaces depends on the type and extent of consolidation before shearing. If the specimen is brought to a fairly high consolidation pressure, the irregularities at the specimen ends may be supressed and most of the bedding between the specimen and the top cap removed (Atkinson and Evans (1985)). If the consolidation is anisotropic, then other types of bedding errors such as the lack of fit at the top cap connection would be effectively eliminated. However, if the soil specimen is very stiff, the supression of the irregularities could be incomplete. Atkinson and Evans (1985) suggested raising the stress level in the cell prior to shearing to eliminate the bedding errors. This method could prove to be effective in the case of soft clays, but in tests involving unloading recovery of the surface irregularities could take place as shown by Daramola (1978) in tests on sands and by Costa Filho (1980) and Gens (1983) in tests on London clay and Lower Cromer Till respectively.

- Misalignment of the specimen : as shown in Figure 2.12a the end surfaces of the triaxial specimen after trimming could be non-parallel. They also could be non-perpendicular to the vertical axis of symmetry of the specimen.

- Misalignment of the apparatus : the specimen should be loaded along its vertical axis of symmetry. Any misalignment, as shown in Figure 2.12b, could cause significant tilting of the specimen top cap and make the strain measurement inaccurate.

- Compressibilty of the cell components : the components shown in Figures 2.10 and 2.12 (e.g load cell, top cap) undergo compression during deviator stress application. Theoretically, it should be possible to determine their stiffness

and allow for the compression in the calculation of axial strain. However, the process would not be free from errors and could prove difficult, especially when certain components have non-linear stress-strain relationships (Jardine et al (1985)).

One of the common assumptions in triaxial strain measurement is the idealized right cylinder behaviour shown in Figure 2.13. End restraints on the specimen prevent such behaviour and instead the deformed shape shown in the same figure tends to develop. This would not only affect the axial strain measurement but also the radial strain measurement and, in turn, the determination of the Poisson's ratio (Moore (1966)). The problem of end restraint on the specimen has been realised since the 1940's (e.g. Taylor (1941)) but for convenience the majority of triaxial testing is still conducted with frictional ends.

Germaine and Ladd (1988) compared the behaviour of normally consolidated and overconsolidated clay specimens with frictional and frictionless ends and found that tests with frictional ends tend to involve water migration between the ends and the middle of the specimen. The migration was found to increase with increasing OCR and becomes substantial for highly dilatant soils. However, they concluded that the error in strain measurement due to end restraint for soft clays is relatively small. End friction effects were also found to be strain-rate dependent; some fast undrained tests did not allow water migration to take place. For samples with an OCR greater than 6, Germaine and Ladd concluded that lubricated ends should be used for tests where large strains (i.e $> 1.5\%$) need to be measured accurately and where pore water pressure measurement is required.

Many other studies have been made of the end restraint problem. For example, Sarsby et al (1980) reported that lubrication of the specimen ends could reduce

the small strain measurement accuracy by introducing an additional compressible component into the system. Maguire (1975) carried out a numerical analysis of end restraint effects and found that they were a function of the specimen height to diameter ratio and Poisson's ratio ν. Costa Filho (1980) used another numerical approach and reported similar results. He also found that, during the early stages of shearing, the difference between the apparent and true stiffness is modest. The results of a number of studies are presented in Figure 2.14 which shows that for a soil specimen with ν equal to 0.5, the stiffness would only be overestimated by about 10%. The above investigations indicate that the assumption of right cylinder behaviour over the middle part of the specimen and during the early stages of shearing is justified.

2.5.2 Strain Measurement Techniques

The deficiencies of external measurements have led to the introduction of a variety of techniques to measure axial strains along the middle portion of the specimen. As shown in Table 2.4, these techniques can be divided into two main categories, namely, optical and electronic.

Kirkpatrick and Belshaw (1968) used radiographic techniques to measure small strains in sand specimens, while Balasubramanian (1976), Roscoe et al (1973) and Arthur and Phillips (1975) used the same method for clay specimens. Although this technique has a relatively good accuracy, it can only be used for reconstituted specimens since it requires the installation of lead shot inside the specimen. Freeser (1984) modified the technique of optographic trace recording for use in triaxial testing. This involves the use of luminous points attached to the specimen and of a camera recording their position during the test. Although this method provides

information about the progressive failure mechanism of the specimen, its accuracy is rather limited.

Electronic transducers have been used by several researchers for both axial and radial strain measurement. LVDT's were used by Brown and Snaith (1974), Brown et al (1980), and Costa Filho (1980). Their accuracy has been shown to be satisfactory but the mounting methods, one of which is shown in Figure 2.15, are only suitable for small strain measurement as jamming, or even damage, of the transducers may take place at large strain or during failure. Burland and Symes (1982) developed an axial displacement gauge which employs electrolevel transducers. The principle is that a hinged arrangement, shown in Figure 2.16, converts the displacement between two footings mounted on the sample into a rotation of the transducer capsule from which the axial movement is calculated. Jardine (1985) introduced some changes to the configuration of these transducers to improve their resolution. The mounting is simpler than that of the LVDTs and the specimen can be brought to failure without difficulty. When using some of these transducers stiffer membranes or balancing weights have to be used in order to keep full contact between the specimen and the membrane during setting up and testing.

Clayton and Khatrush (1986) introduced a device for measuring axial strains which makes use of the Hall effect. The overall accuracy of these transducers did not appear to be better than that of the electrolevel gauges. Clayton and Khatrush also reported some unspecified problems during isotropic consolidation. In addition, the transducers have a small range (2.5 mm) which makes them unsuitable for use with soft soils which undergo large changes in dimensions during consolidation.

Proximity transducers have been used by some researchers, mainly for radial strain measurement. These devices respond to the presence of a metallic target in

their vicinity and the change in inductance brought about by eddy currents in the target. The magnitude of this change is related to the distance between the target and the transducer (Seippel (1983)). The main advantage of using such transducers is the fact that they can detect changes in the target position without any physical contact, although only over a limited range. Initially, proximity transducers were used to monitor radial strain during K_0-consolidation (Khan and Hoag (1979)) . However, Yung (1987) used them to measure axial as well as radial strains in tests on Cowden Till, as shown in Figure 2.17. Details of the method of mounting are presented in Section 3.3. Although the transducers proved to be sufficiently accurate, strains could only be measured during the early stages of the test and collapsible targets had to be mounted in order to avoid restraint or damage at larger strains. The particular transducers used by Yung had very stiff cables which made their mounting procedure difficult. Furthermore, the output from the transducers was non-linear resulting in a more complicated analysis of the calibration data. When proximity transducers are used in tests on stiff clays, such as Cowden Till, it is not too difficult to set the targets so that they remain in range during the saturation and consolidation stages of a test because the specimens undergo relatively small changes in height and diameter. The use of transducers with a 6 mm range proved satisfactory. However, initially soft clay specimens subjected to large consolidation pressures undergo relatively large changes in dimensions. A mechanism must therefore be provided which allows the position of the transducers to be changed during the test so as to keep them in range at all times. With such a mechanism, it is possible to deploy smaller range transducers. This is advantageous since the smaller the range, the higher the sensitivity. The type of the targets depends on the type of transducer employed and on the effect that the targets could have on the soil specimen. As will be described in Section 3.3, tests carried out by Yung (1987) and the Author have shown that the most sensitive and stable response is achieved by

using magnetic stainless steel targets. However, both Brown et al (1980) and Symes et al (1983) used aluminum foil targets which are flexible and much lighter than the magnetic stainless steel plates. They found that the stiffness of the soil specimen was unaffected by the attachment of these targets.

Although it is important to deploy highly accurate transducers, the errors in axial strain measurement can be much larger than those calculated from the transducer characteristics. Costa Filho (1985) blamed some of the additional errors on the following :

- Transducer and target mounting. The errors clearly depend on the transducer type and the method of mounting. For example, if proximity transducers are used, it is important to make sure that the target and transducer faces are parallel . During consolidation and shearing, some departure from this parallelism could take place, thus affecting the displacement measurement.

- Barrelling during shearing. As mentioned in Section 2.5.1, the soil specimen does not deform in a right cylinder manner. The rotation of targets mounted on the surface of the specimen may adversly affect the readings taken by a transducer.

- Tilting of the specimen during shearing. Axial displacements measured on two diametrically opposite sides of the specimen usually do not yield equal strains because of tilting of the specimen or the existence of non-homogeneities within the soil. For fairly homogeneous specimens, symmetry may be assumed without introducing significant uncertainties (Daramola (1978) and Burland and Symes (1982)).

Hird and Yung (1989) presented a detailed assessment of some of the errors

associated with their proximity transducer measurements. The predicted errors were as shown in Table 2.5. Two approaches were adopted in evaluating the errors in the system. The first incorporated both systematic and random errors while the second dealt with the random errors only. However, the scatter noticed on the stress-strain curves from shearing tests indicated much larger random errors than those calculated. Fluctuations in the pressure system, errors in load measurement, and time dependent strains were blamed. It was concluded that the achievement of accurate strain measurement is not sufficient if the soil stiffness is to be evaluated accurately; attention should also be given to the application and measurement of load.

2.5.3 Some Other Developments in Triaxial Testing

In addition to the introduction of the Bishop and Wesley apparatus and the developments in the strain measurement referred to above, other new techniques have been introduced that provide a better quality of control and more reliable data.

The introduction of microcomputer control (e.g. Atkinson et al (1985)) has permitted complicated tests to be carried out with relative ease and without the use of complicated mechanical equipment. Independent automatic control of axial stress, radial stress, and drainage rate means that effective stress paths in any direction in q, p' space can be followed.

For standard tests, Atkinson et al (1985) introduced a method of shearing whereby the specimen undergoes a constant rate of loading up to a certain level where the rate of axial strain is high enough to cause non-uniformity of pore water pressure in the specimen. At this point, the control is switched over to a constant

rate of axial straining. This hybrid method of shearing has been mainly introduced to avoid excessive rates of straining during the early stages of the test while preventing abrupt failure of the specimen. However, Jardine at al (1985) argued that the use of sufficiently low strain rates would suffice and would not involve switching between strain and stress control.

Electronic transducers and equipment have also been developed or improved to facilitate automatic data logging and test control. Important examples are :

- The mid-height pore water pressure transducer. A full description of this miniature pressure transducer is given by Hight (1982) and Baldi et al (1988). Uniformity of the pore pressure in the soil specimen can be checked by recording its value at the top and bottom of the specimen as well as at mid-height. Measurement at mid-height has the advantage of avoiding the zones affected by end restraint.

- The differential pressure transducer. In certain tests, for example liquefaction tests (Castro (1969)) or tests involving small effective stresses, it is more accurate to measure the effective confining pressure directly by using a differential pressure transducer.

- Volume change units. Alva-Hurtato and Selig(1981) presented a review of the available techniques for measuring specimen volume change. Automated volume change units, such as the one described by Tatsuoka (1981) which makes use of a differential pressure transducer or the unit developed at Imperial College and described in Section 3.3, have proved to be appropriate for back pressured saturated specimens. Unsaturated soils required more sophisticated volume change units.

Before sampling	During sampling	After sampling
Stress relief	Stress relief	Stress relief
Swelling	Remoulding	Migration of water within the sample
Compaction	Displacement	Loss of moisture
Displacement	Shattering stones at the cutting shoe	Freezing
Base Heave	Mixing or segregation	Overheating
Piping	Failure to recover	Vibration
Caving		Chemical changes
		Disturbance during extrusion and setting up

Table 2.1 Sources of soil sample disturbance
(after Clayton et al (1982))

Sample type	Average c kPa	Average E kPa
Not unloaded	111.4 (1.4)	11200 (1700)
Unloaded but not stored	66.2 (3.0)	6890 (210)
Unloaded, sealed with wax and stored	39.6 (3.7)	1720 (130)
Unloaded and stored in compressor		
(1)	55.0 (5.6)	5580 (280)
(2)	62.5 (0.9)	6980 (190)
(3)	63.6 (2.2)	6990 (180)

Note : Numbers in brackets represent standard deviation

Table 2.2 Effect of storage method on the strengh and stiffness
(after Brown and Chow (1988))

Authors	Change in vertical pressure (kPa)	$D = 1-p_o'/p_h'$	Effect before reconsolidation		Method of reconsolidation	Effect after reconsolidation	
			E	Cu		E	Cu
Skempton and Sowa (1963)	120	0.2 (p.s.)	—	—	Isotropic	—	RE
Atkinson and Kubba (1981)	276	0.18-0.3 (p.s.) 0.4-0.6 (t.s.)	CR	CR	Anisotropic to initial stresses	CR (50%)	—
Kirkpatrick et al (1986)	552	0.15 (p.s.)	CR	CR	Anisotropic to initial stresses	CR (50%)	RE
Hight et al (1986)	400	0.28 (p.s.) 0.43 (t.s.)	CR	CR (20%)	Anisotropic to initial stresses	SI	SR
Baligh et al (1987)	—	0.1 (p.s) 0.6 (t.s.)	FR (17%)	CR (75%)	Aniso. to init. stresses SHANSEP	SI RE	SI (10%) RE
Graham et al (1988)	160	0.15 (p.s.)	CR	CR	Anisotropic isotropic to σ_v' isotropic to 0.6 σ_v'	CR CR CR	RE SR SI

Notes D=0 Undisturbed
D=1 Completely Disturbed
RE Full recovery
CR Considerable reduction
SI slight increase
SR Slight reduction
FR Fair reduction
p.s. Perfect sampling
t.s. Tube samplimg

Table 2.3 Summary of recent research into sampling disturbance

Reference	Method	Strain measurement
Costa Filho (1980)	Linear variable differential transducers attached to studs or collars around the specimen	vertical
Burland & Symes (1982)	Electrolytic levels as horizontal inclenometers	ditto
Clayton & Katrush (1986)	Hall effect semiconductor mounted vertically along the side of the specimen	ditto
Hird & Yung (1989)	Proximity transducers mounted around the specimen to which metal targets are attached	vertical & horizontal
Roscoe et al (1963)	X-ray radiographs from a grid of columns of X-ray opaque particles within the specimen	ditto
Freeser (1984)	Optographic trace recording of luminous points mounted around the specimen	ditto
Menzies (1976)	Circular calliper fitted with LVDTs. Based on device suggested by Bishop and Henkel	horizontal
El-Ruwayih (1976)	Radial strain gauged rings attached to studs or directly to specimen	ditto

Table 2.4 Summary of local strain measurement techniques

Axial strain %	maximum error %	maximum fractional error	largest probable error %	largest probable fractional error
0.01	$8.01 * 10^{-3}$	0.801	$2.83 * 10^{-3}$	0.283
0.05	$8.06 * 10^{-3}$	0.161	$2.83 * 10^{-3}$	0.057
0.10	$8.12 * 10^{-3}$	0.081	$2.83 * 10^{-3}$	0.028

Table 2.5 Overall errors in axial strain measurement (after Hird and Yung (1989))

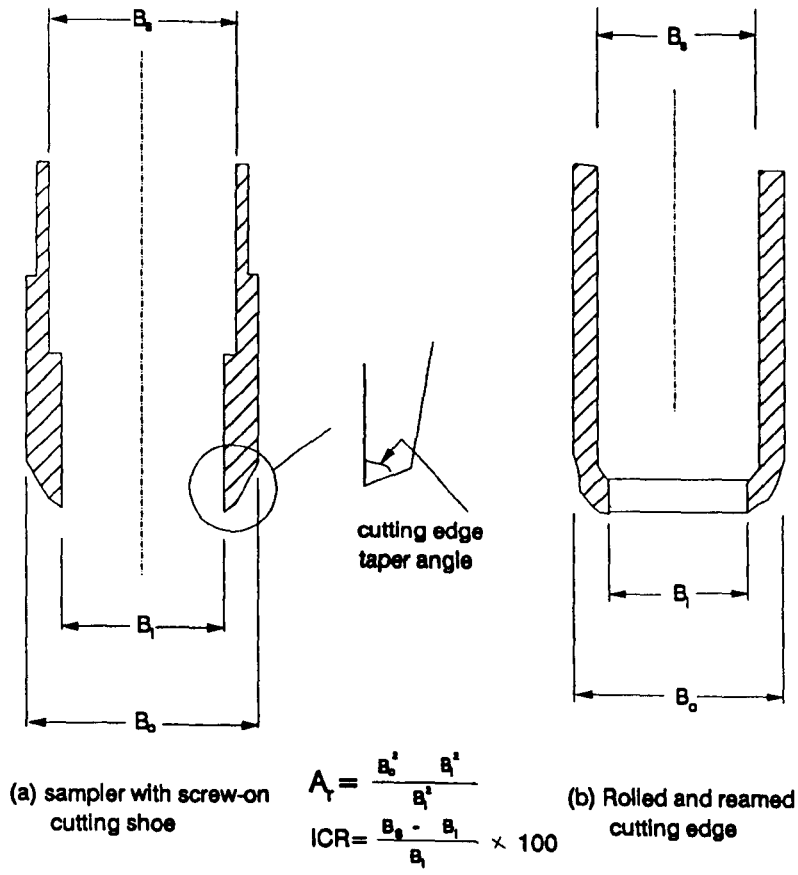

Fig 2.1 Definitions of Area ratio and Inside Clearance ratio

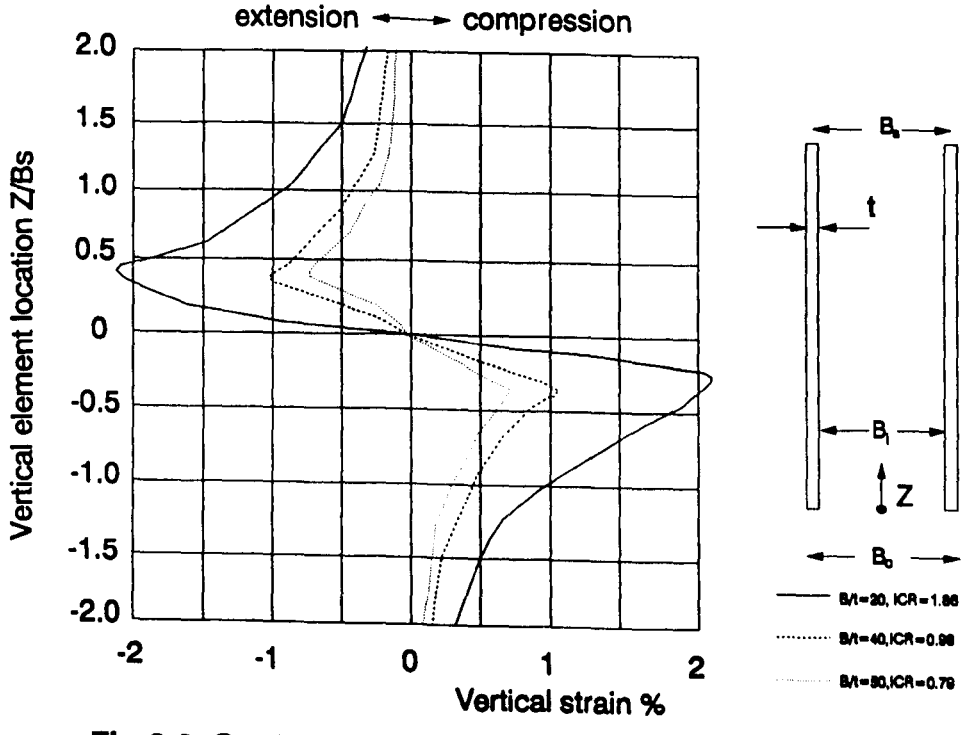

Fig 2.2 Straining history at centreline of simple sampler (after Baligh et al (1985))

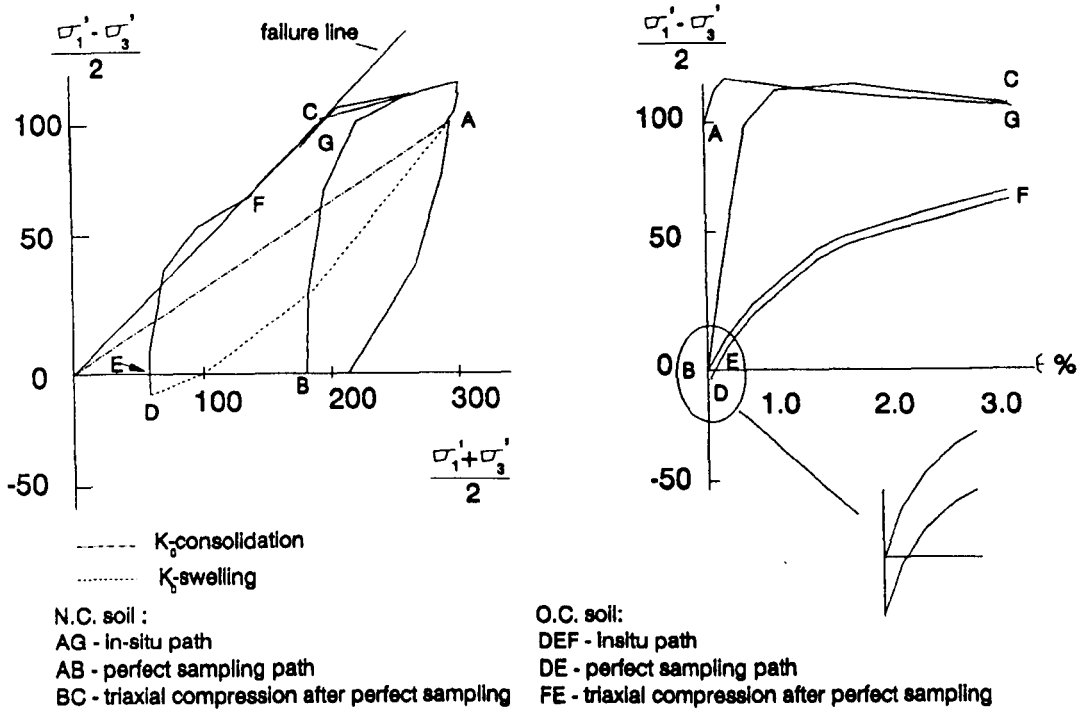

Fig 2.3 Perfect sampling of normally consolidated and heavily overconsolidated soil
(after Hight et al (1985))

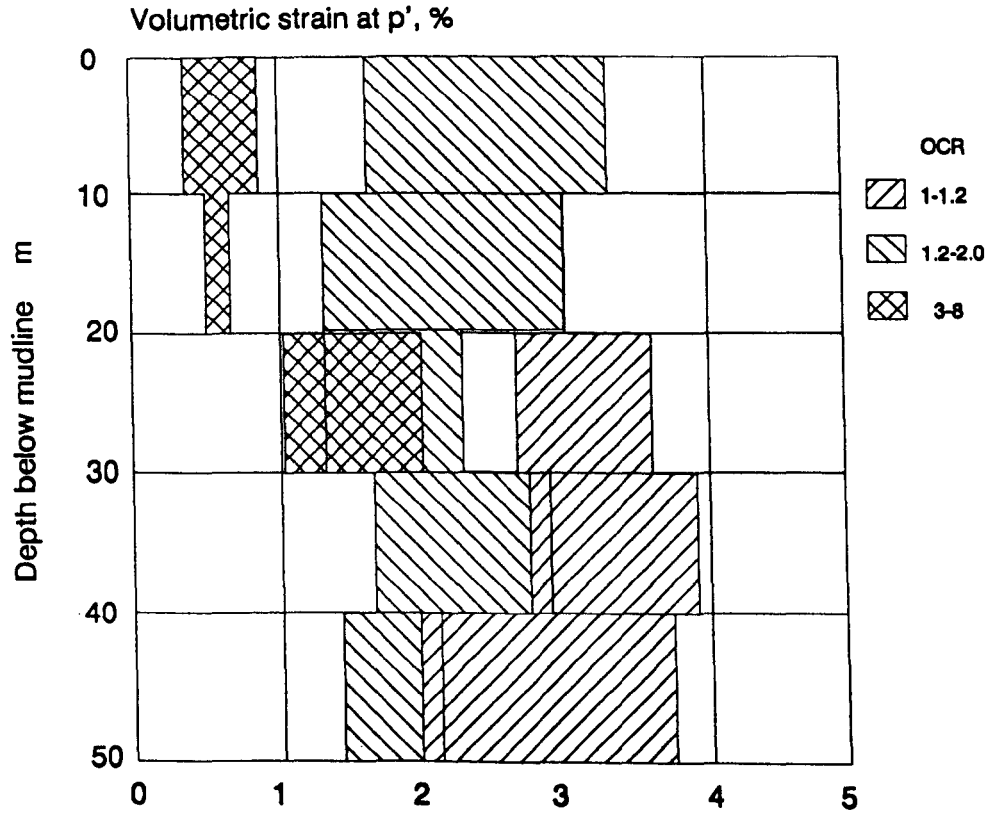

Fig 2.4 Strain at in-situ overburden stress from oedometer tests on high quality clay samples
(after Lacasse (1985))

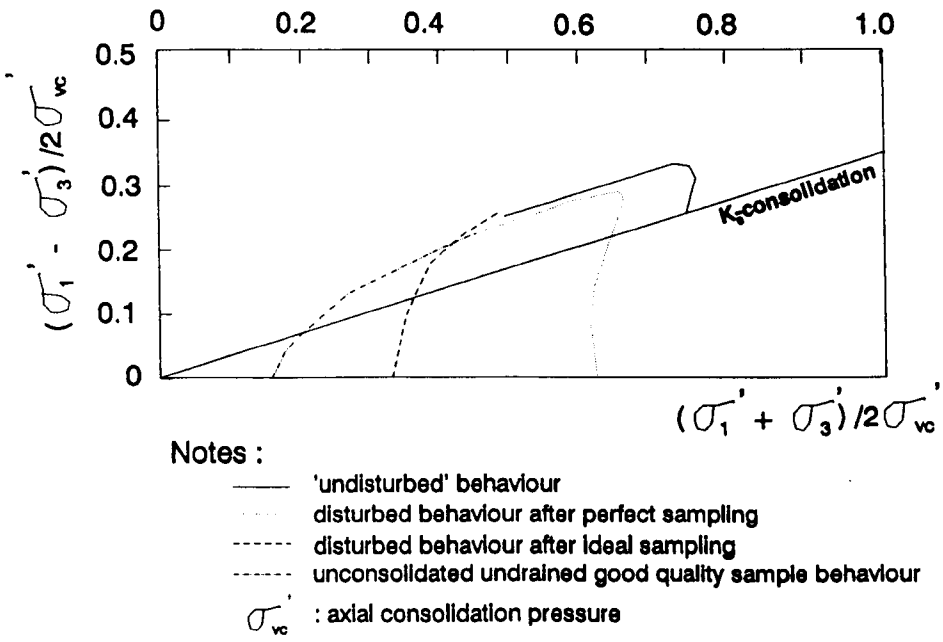

Fig 2.5 Comparison of ideal and perfect sampling disturbance effects on undrained behaviour of normally consolidated Boston Blue clay
(after Baligh et al (1987))

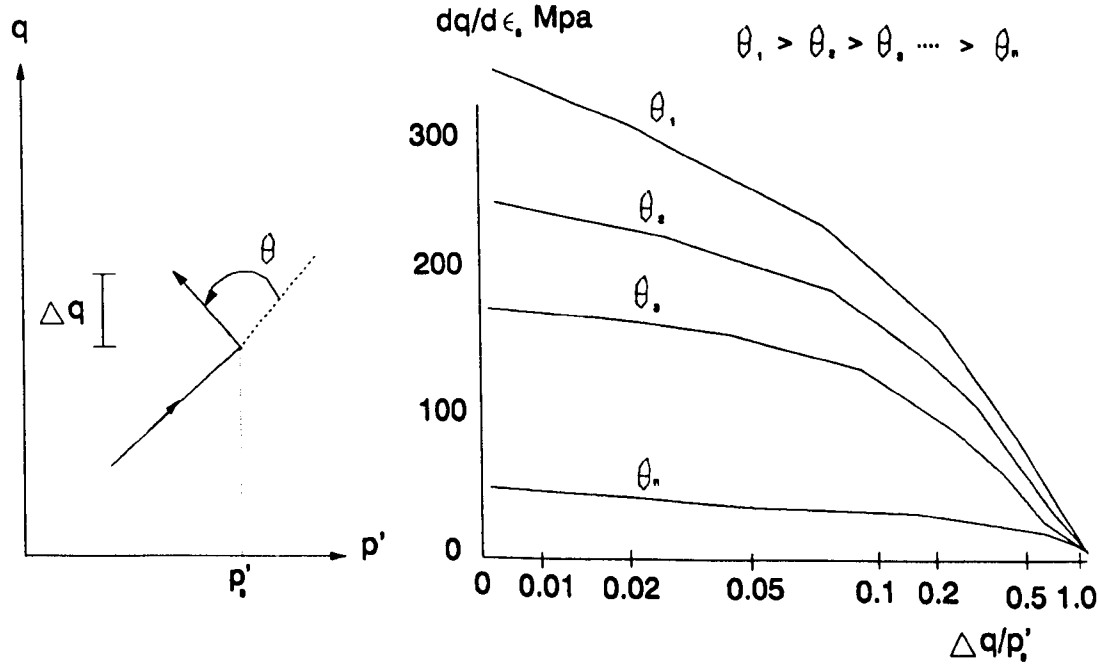

Fig 2.6 Effects of change in stress path direction on stiffness
(after Atkinson et al (1989))

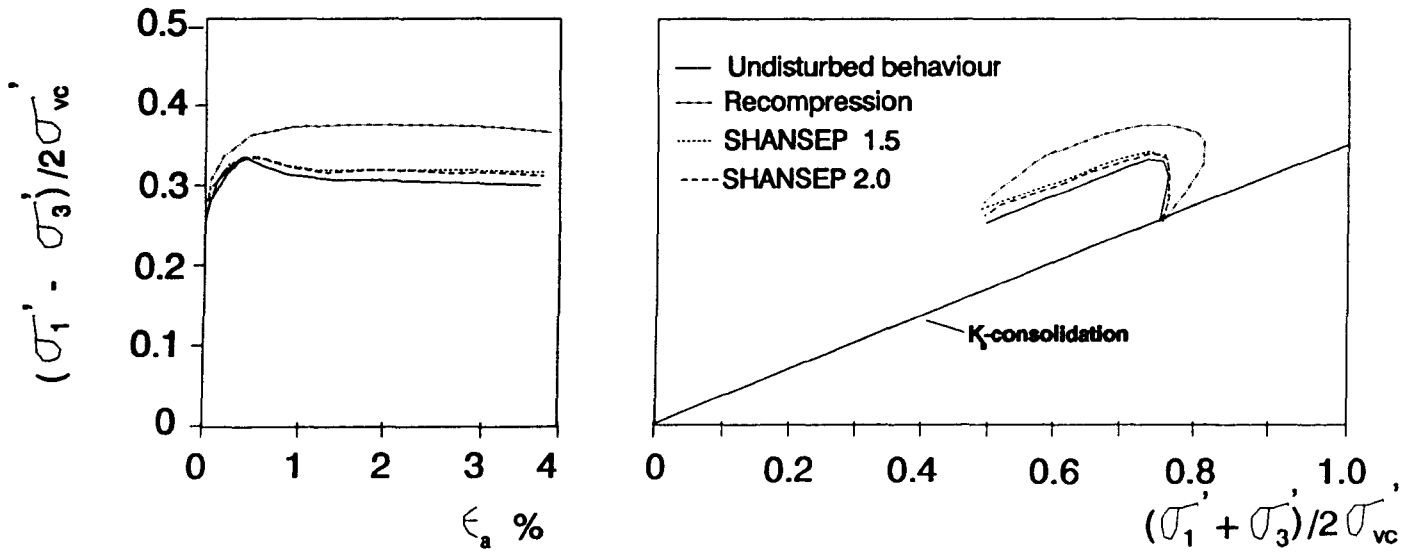

Fig 2.7 Reconsolidation effects on ideal sampling disturbance of normally consolidated Boston Blue clay

(after Baligh et al (1987))

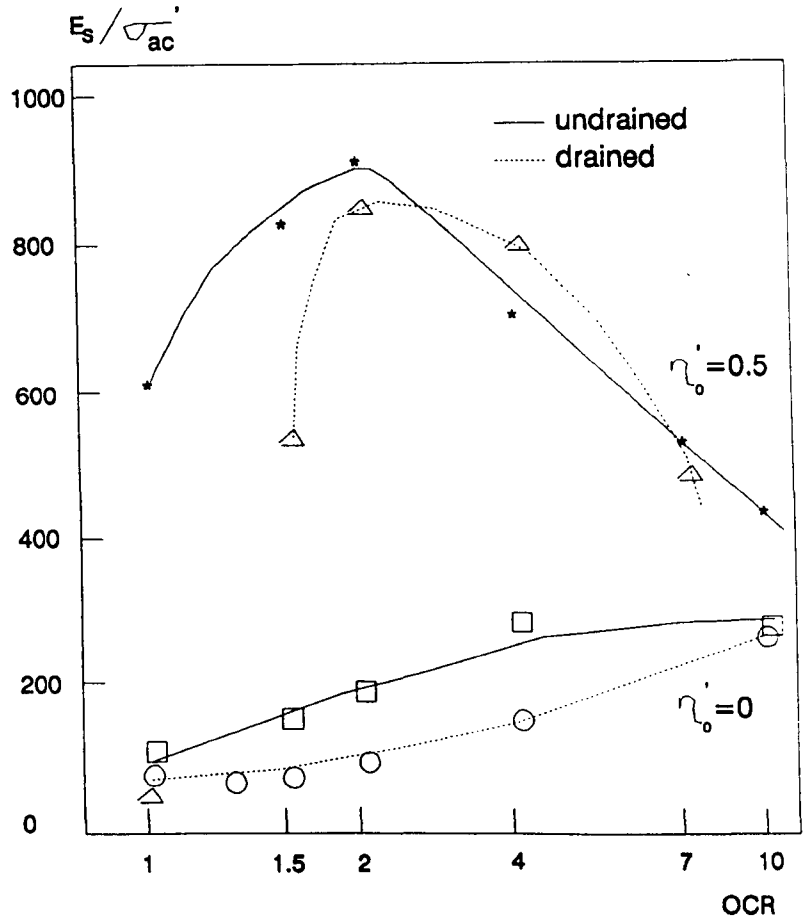

σ_{ac}' : axial consolidation pressure

Fig 2. 8 Variation of normalised stiffness for drained and undrained tests on Lower Cromer till
(after Gens (1982))

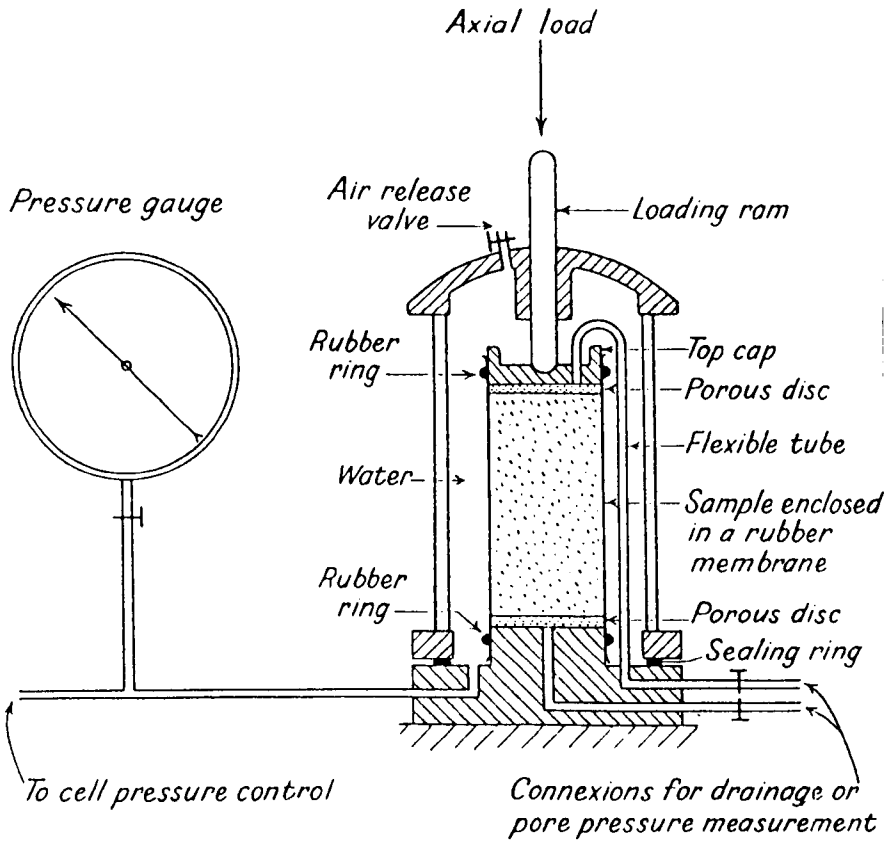

(a) Bishop & Henkel (1962)

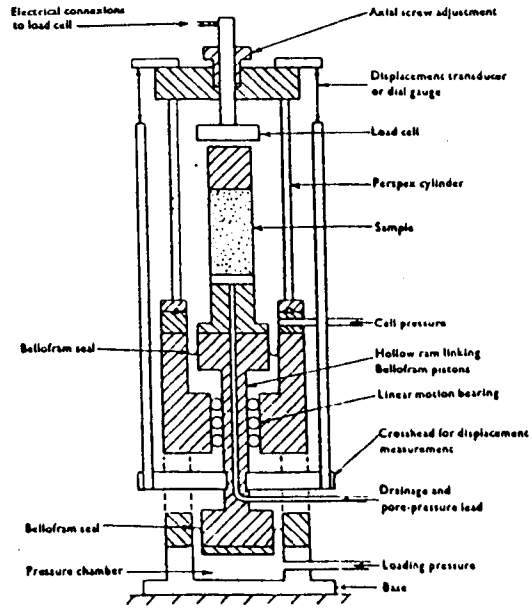

(b) Bishop & Wesley (1975)

Fig 2.9 Diagrammatic layout of the conventional and hydraulic triaxial cells

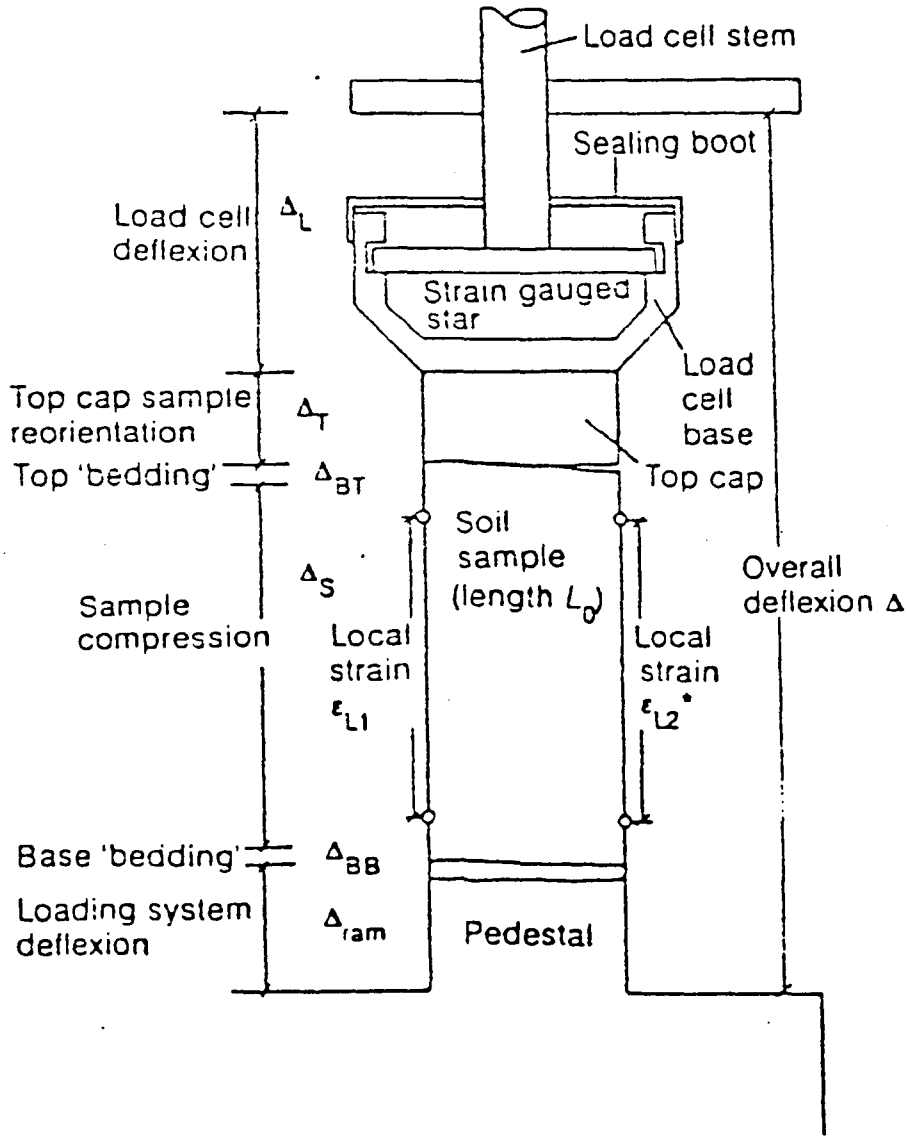

Fig 2.10 Sources of error in external strain measurement
(after Jardine et al (1984))

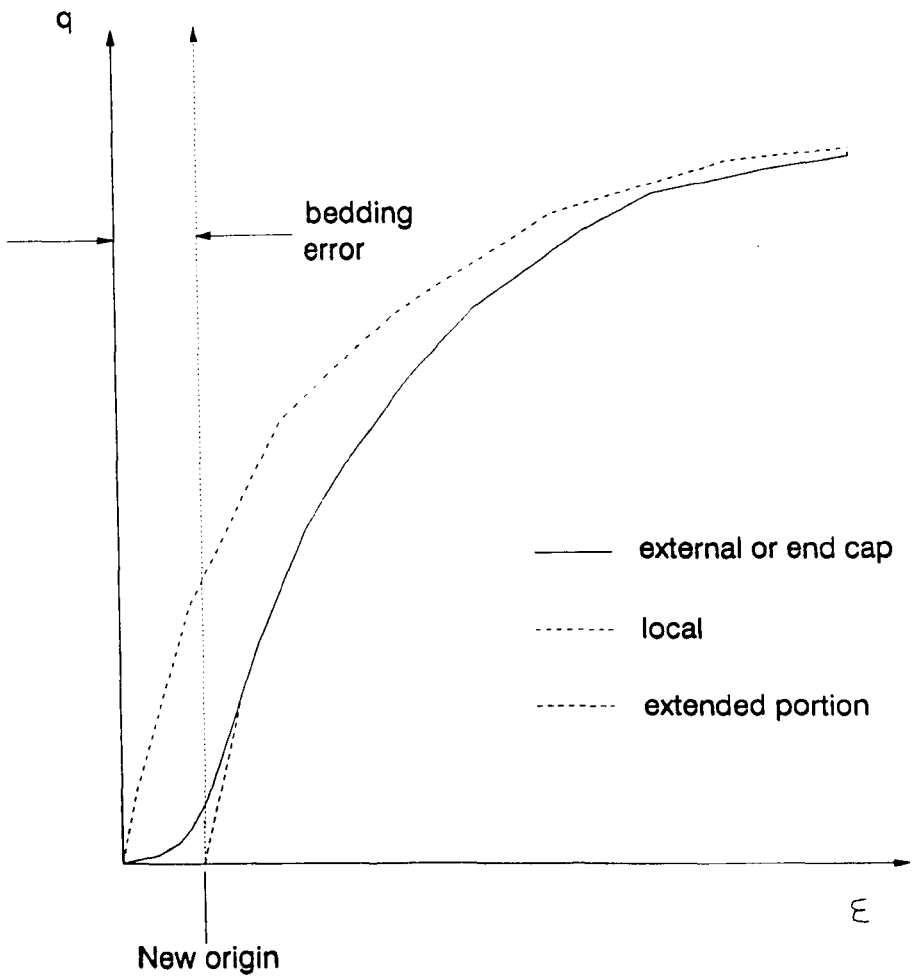

Fig 2.11 Effect of bedding errors on the shape of the stress-strain curve

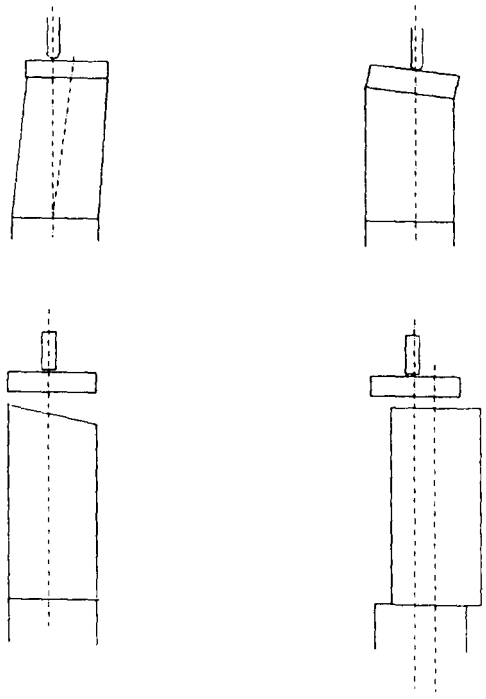

(a) due to specimen

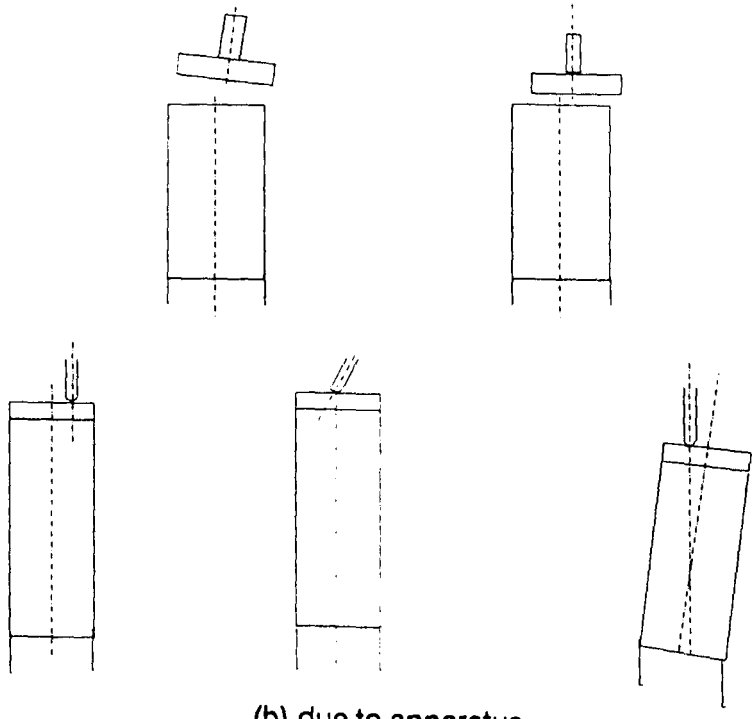

(b) due to apparatus

Fig 2.12 Misalignment in the triaxial cell
(after Baldi et al (1988))

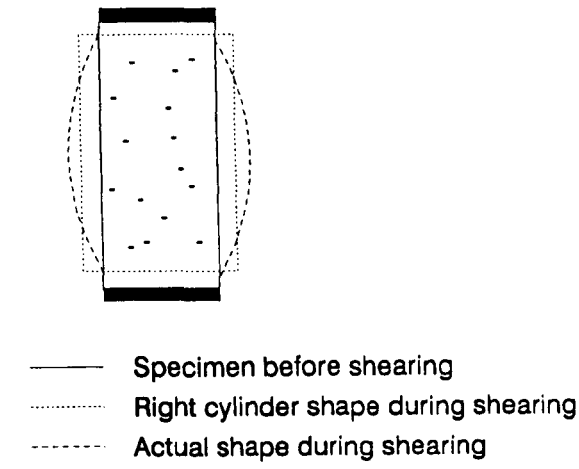

Fig 2.13 Right cylinder assumption and actual deformation of a triaxial specimen

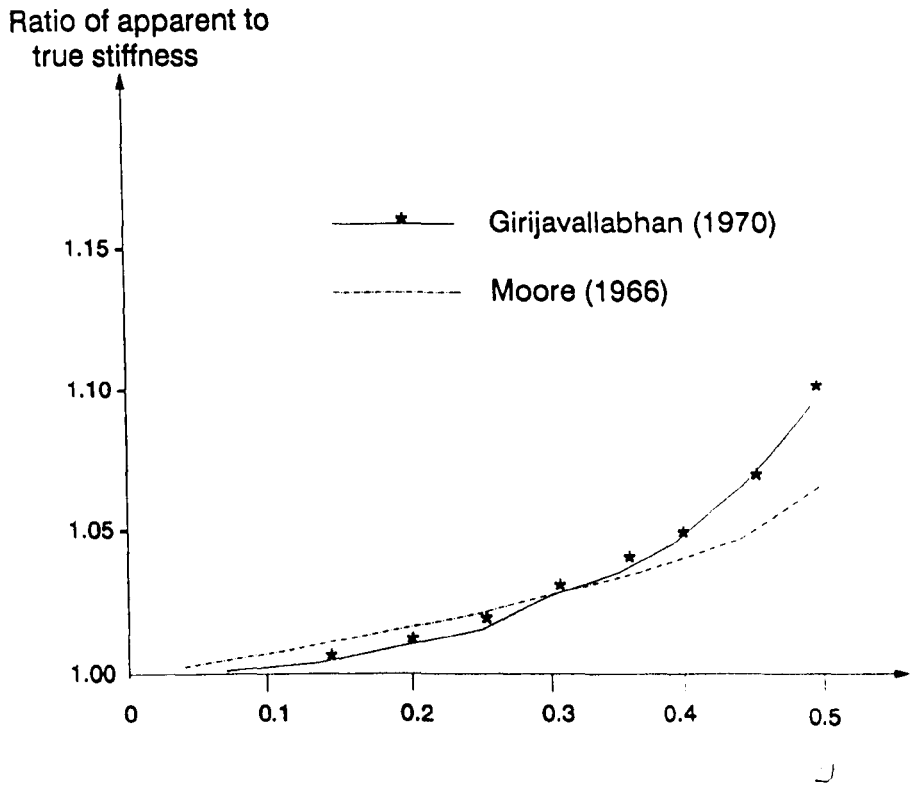

Fig 2.14 Effect of end restraint on stiffness in the triaxial cell (after Maguire (1975))

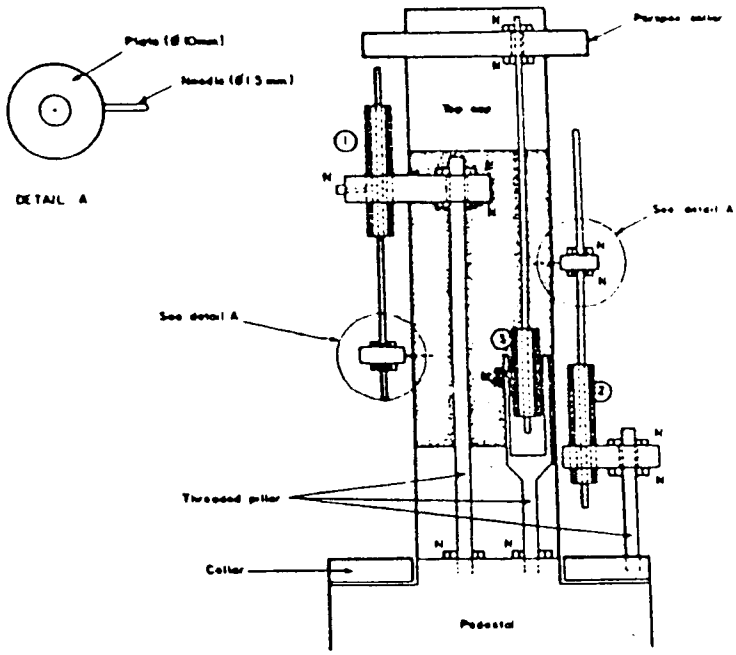

1 Bottom internal displacement transducer

2 Top internal displacement transducer

3 Overall displacement transducer

Obs 1: Not to scale

2: N = nut

Fig 2.15 The use of LVDTs for local axial strain measurement
(after Costa Filho (1985))

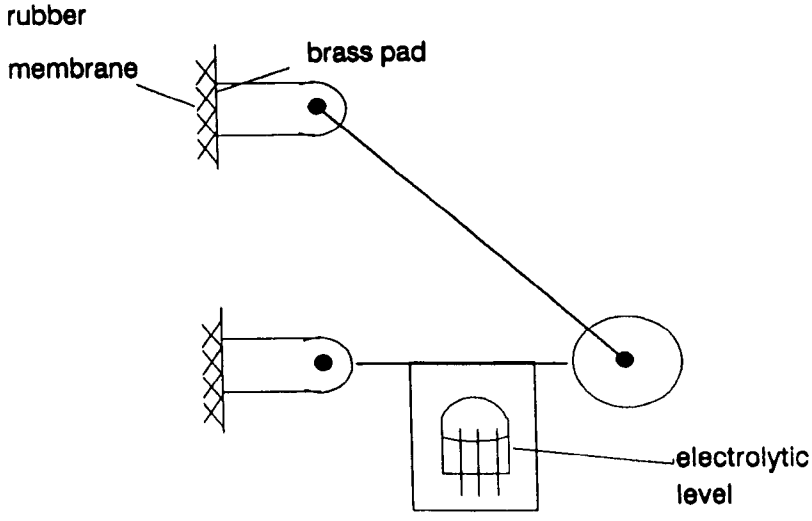

Fig 2.16 The use of electrolytic levels for local axial strain measurement
(after Burland & Symes (1982))

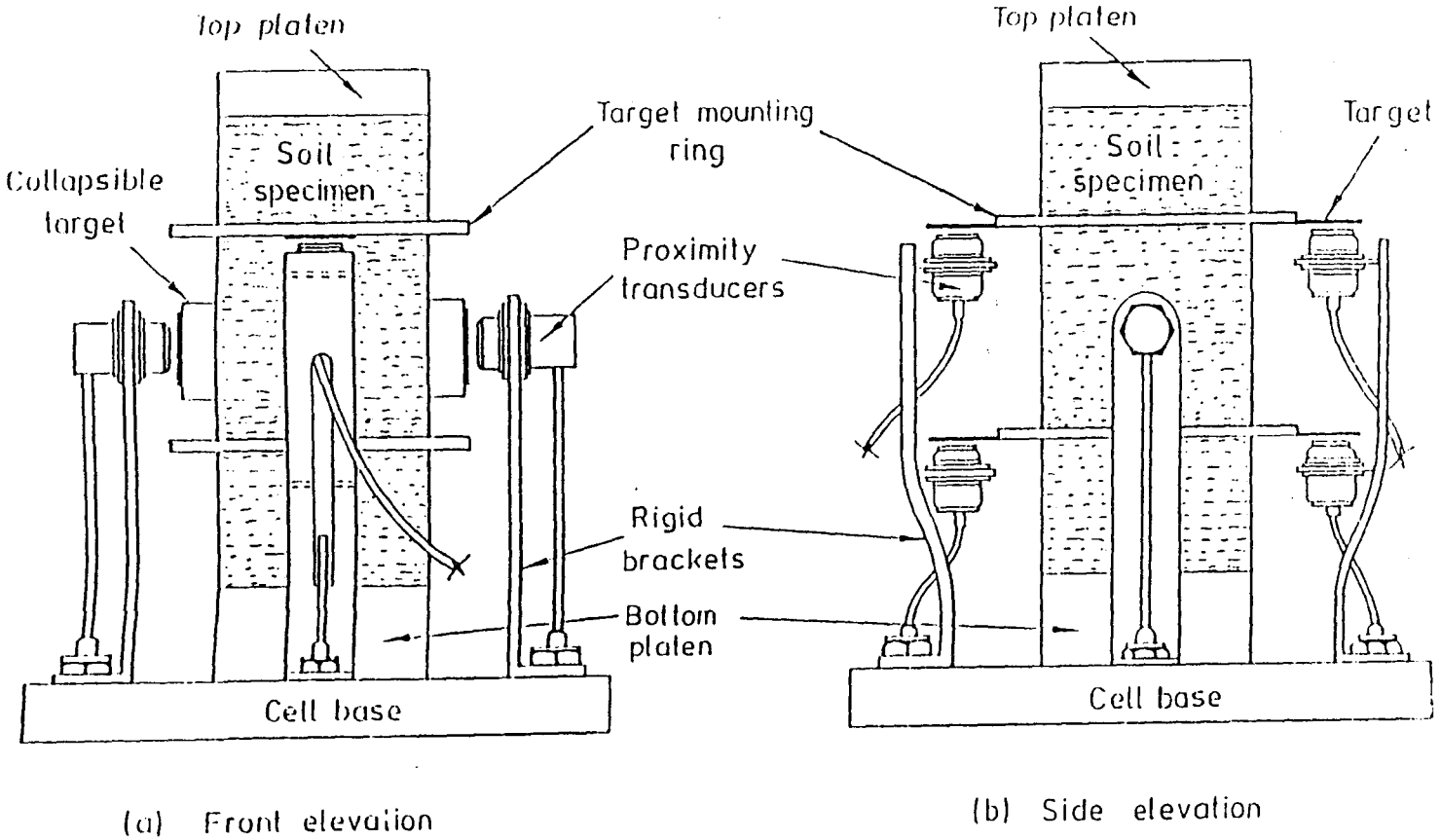

Fig 2.17 The use of proximity transducers for local axial and radial strain measurement (after Hird & Yung (1989))

Chapter 3

EQUIPMENT AND EXPERIMENTAL TECHNIQUES

3.1 Introduction

In Chapter 1, it was explained that the laboratory work would focus on the effects of sampling disturbance on the undrained small strain behaviour of kaolin. In order to carry out the experimental study outlined in Chapter 1, a special 100 mm triaxial stress path apparatus was designed and manufactured. Certain alterations were also made to an existing 38 mm cell. The first part of this chapter contains a brief review of the existing pieces of equipment in the research laboratory, along with their limitations. The second section describes the newly manufactured cell and associated instrumentation, together with the additional features introduced into the 38 mm apparatus. Finally, the third part of the chapter summarises the testing

procedures used, with particular reference to the problems associated with stress control and strain measurement.

3.2 Review of Existing Equipment

One 100 mm triaxial cell and one 38 mm cell were available at the beginning of the research. The 38 mm cell was used by Ilyas (1983) to investigate the behaviour of kaolinitic pottery clay. The larger cell was used by Yung (1987) to investigate the small strain behaviour of Cowden Till. Both cells operate on the principle described by Bishop and Wesley (1975) and were initially purchased from commercial manufacturers. However some alterations had to be carried out on them to rectify faults and provide more reliable data. Details of these alterations are given by Yung and Ilyas. Nevertheless, certain limitations remained.

3.2.1 Limitations of the 100 mm Apparatus

3.2.1.1 Bellofram area ratio

The cross-sectional area sealed by the lower chamber bellofram is unduly large. The area ratio (a/A), defined in Figure 3.1, is equal to 6.25. Although such a design has the advantage of permitting a large axial stress to be applied, the sensitivity of the system is lost. One step of the stepper motor controlling the lower chamber pressure would result in a change of 0.4 kPa in the lower chamber pressure and hence approximately 2.4 kPa in the deviator stress on the specimen. This causes an unnecessary additional difficulty in retrieving small strain data, which is especially serious in the case of soft soils. Furthermore, as will be discussed in Section 5.4.3,

during K_0-consolidation and K_0-swelling axial and radial stresses have to be applied incrementally and, in order to avoid large radial strains, the increments of axial stress should be as small as possible.

3.2.1.2 Top cap-load cell connection

The top cap has a flat surface at the contact point with the load cell, Figure 3.2b, instead of the usual curved recess shown in Figure 3.2a. This arrangement was adopted by Yung because, after isotropic consolidation, the load cell and the centre of the top cap were not perfectly aligned. With the traditional design, at the start of axial loading some horizontal movement of the top cap would take place which would result in stress and strain non-uniformities, especially during the early stages of shearing. In addition, some vertical movement of the whole specimen would occur, thus moving the targets mounted for the proximity transducers (see below) out of the most suitable range. On the other hand, with the design adopted, the specimen may not be loaded along its centreline. Consequently non-uniformities of stress and strain may still take place and the top cap is more likely to tilt, as found by Yung. In addition, with this type of connection, extension loading is not possible and the range of stress paths that can be applied is therefore restricted. At present there is not enough space around the top cap to change the connection into one which allows extension loading.

3.2.1.3 Arrangement of proximity transducers

Figure 2.17 shows the general arrangement of the instrumentation devised by Yung to measure local strains. Axial strain is measured on both sides of the specimen to

cater for tilt, and lateral strain is measured across one diameter. This arrangement has a major drawback. Since all the transducers are mounted on brackets bolted to the cell middle plate, their position cannot be changed once the test starts (i.e. the cell top is lowered over the specimen). This means that the initial separation of each target and transducer should be suitably within the working range. Saturation and consolidation of the soil specimens causes movement of the targets. If the soil is stiff (e.g. the Cowden Till tested by Yung), then the movements of the targets are small and the targets remain within range of the proximity transducers. Soft soils, however, undergo large movements during consolidation and such an arrangement is not then satisfactory. Even with stiff specimens, only strains during the early stages of shearing can be measured since the targets soon move out of range upon shearing. Finally, in order to bring the specimens to failure, a collapsible mounting arrangement for the targets has to be introduced to avoid jamming or damage to the equipment (Hird and Yung (1989)).

3.2.1.4 Access to cell parts

Because the proximity transducers used by Yung had very stiff leads, once they were mounted they were left in place and hence access to some parts of the cell and to the specimen was restricted. Also, to allow the local instrumentation to be installed, a 50 mm high aluminium spacing ring had to be fitted on top of the perspex of the cell top. This had the unfortunate result of hiding the top half of the specimen, including the contact point between the top cap and the load cell as well as the end cap strain instrumentation which will be described in Section 3.4.5.

3.2.2 Limitations of the 38 mm Apparatus

3.2.2.1 Pressure fluctuations

The GDS pressure controllers used in conjunction with the cell are supposed to maintain a constant pressure to a specified accuracy of ± 2kPa. However, fluctuations of up to ±5 kPa were observed by Ilyas. To overcome this problem, attenuators were fitted in the connecting lines but the fluctuations were still noticeable.

3.2.2.2 Axial strain measurement

Axial strains can be calculated from the volume change in the lower chamber. Another method consists of mounting two diametrically opposite vertical rods on cross-arms connected to the loading ram. The rods pass through holes in the cell base and terminate under dial gauges mounted on the cell top. At larger strains a comparison between the two methods showed acceptable percentage differences not exceeding 2%. However, as discussed in Chapter 2, external axial strain measurement has been found to be erroneous at small strain levels. Thus in the existing apparatus there was no way of accurately measuring small strains.

3.2.3 Limitations Common to Both Cells

Each cell, along with its peripheral equipment, was controlled by an Apple 2 Plus microcomputer, programmed in the BASIC language. Because of this, the speed of control and data collection were rather limited. Furthermore, because of the small memory of the computer, Yung had to insert a new floppy disk several times during

a test to store his data and the data could not be stored in both raw and processed forms. Back-up copies had to be made using a separate similar computer. Finally, data could not be processed directly using commercially available statistical and graphics packages (e.g. Lotus 123) because they were stored with a different format. This meant that another program had to be written to transform the data before it could be analysed using these packages.

3.3 Description of New and Modified Equipment

In view of the limitations discussed in the previous section, it was decided to develop another 100 mm triaxial apparatus for use in the investigation of sampling disturbance and also to modify the 38 mm cell so that it could be used to investigate soil behaviour at small strains.

Two options were available as far as the 100 mm cell was concerned. The first was to design and manufacture a cell in-house and the second was to purchase one from a commercial manufacturer. The main advantage of the first option was that the new apparatus would incorporate the special features required for the proposed testing programme. For example, enough space would be provided for the proximity transducers which would be on externally adjustable mountings. Significant modifications to a purchased cell would have been needed, which could have proved difficult, if not impossible. Another advantage was that the cost would be lower. Therefore, it was decided to adopt the first option. However, it was realised that the design, manufacture and assembly of the cell in-house would require a longer period of time.

3.3.1 Components of the New 100 mm Apparatus

Figure 3.3 shows a schematic representation of the apparatus. The main components are :

3.3.1.1 The triaxial cell

A cross section of the new cell is presented in Figure 3.4, while Plate 3.1 shows the cell assembled ready for use. The following features were introduced in order to overcome the limitations encountered with the existing 100 mm cell referred to in Section 3.2.1 :

- The bellofram area ratio (Figure 3.1) is now 2.25. With this area ratio an axial stress of 1000 kPa can be achieved in about 1100 steps and the axial stress increment on the specimen does not exceed 0.9 kPa. For a relatively high cell pressure of 700 kPa, the maximum deviator stress that can be applied is about 1100 kPa which is large enough to bring most soil specimens to failure.
- As shown in Plate 3.2, there is a steel ring at approximately the mid-height of the specimen on which the radial strain proximity transducers are mounted. This method of mounting has the benefit of permitting external adjustment of the proximity transducers, as will be described in Section 3.4.6. During a test, any change in the cell pressure results in a change in the stresses in the steel ring and causes it to deform. This has the potential to cause strain measurement errors. An analysis was therefore carried out to check on the deflection of the steel ring under radial pressure. This is presented in Appendix A and indicates that for a ring of 40 mm wall thickness, the deflection has a negligible effect on the radial strain measurement.

- The top cap is connected to the load cell by a vacuum connection. Figure 3.5 shows the components of the connection. A circular plate (A) is screwed onto the load cell (B). Through this plate there is a hole which is connected by a 2 mm diameter flexible pipe either to atmospheric pressure or to the cell pressure line. A rubber seal (C) fits onto the top cap (D) connected to the specimen. After the flexible pipe has been connected to the cell pressure line, the load cell and the plate are lowered into the rubber seal until the plate and the top cap are in contact. Any trapped water is squeezed out through the flexible pipe back into the cell. This operation involved maximum changes in deviator stress of ± 3 kPa and very small strains in the specimen. At this stage the flexible pipe is disconnected from the cell pressure line and opened to atmospheric pressure. Full contact is ensured by the difference between the pressures on each side of the rubber seal. For high extension loading a vacuum may be applied in the flexible pipe to increase the tensile capacity of the connection. However, this was unnecessary in the present research.

- Access to the specimen and proximity transducers has been made easier by providing more space around the bottom pedestal. The height and diameter of the cell top have been increased in order to allow more space for the vacuum top cap connection and the end cap axial strain instrumentation.

- As indicated in Figure 3.4, the moving cylinder in the lower chamber is guided by a plain bushing rather than a roller bearing in the lower chamber to minimize tilting and to ease manufacture. Modest friction losses in the bearing are not a problem since the axial stress is calculated from the load cell and cell pressure readings.

3.3.1.2 The stepper motors

These are precision pressure controllers (manufactured by Watson Smith ,Leeds, England) which can be operated either manually or by computer. The maximum number of steps that can be applied is 2000 so that if the limiting pressure from the air compressor is 800 kPa, each step will correspond to approximately 0.4 kPa. The three stepper motors are each connected to an air-liquid interface (one air-oil for the lower chamber and two air-water for the cell and back pressures). As illustrated in Figure 3.3, along each pressure line, a pressure gauge (manufactured by Budenburg Gauge Co. Ltd, Cheshire, England) is mounted to give a visual indication of the pressure levels.

3.3.1.3 The microcomputer

The computer is a 640K 16 bit IBM compatible PC with one 20 MB hard disc drive, one double sided 40 track floppy disc drive, a monochrome video monitor, an IBM printer, and an HP7475A plotter.

3.3.1.4 Interfaces for data logging

Two types of transducer-computer interface systems are used. The first, 'System 16' (manufactured by Sangamo, West Sussex, England), is used to convert analogue readings from the AC proximity transducers into digital signals accepted by the computer. The second, an "Analogue Input Unit" (AIU) type 2014 (manufactured by MC - Computers, Berkshire, England), is used to perform analogue to digital conversions for all the DC transducers. Two AC submersible LVDTs used for end cap axial strain measurement (see Section 3.4.5) are connected to type OD3 signal conditioning units (manufactured by Sangamo) before being connected to the AIU. They could not be interfaced via

the System 16 because the gain setting required for the proximity transducers differed from that needed for the submersible LVDTs.

3.3.2 Components of the Modified 38 mm Apparatus

The configuration of this system is presented in Figure 3.6. Its basic components are :

3.3.2.1 The microcomputer

A BBC Master microcomputer with two floppy disk drives, a monochrome video monitor and an Epson printer are used. Although this system is much less powerful and versatile than the one used in conjunction with the 100 mm cell, it was felt to be adequate for the proposed tests (see Section 6.2). The data analysis can still be carried out on an IBM compatible machine thus limiting the use of the BBC microcomputer to the control of tests and logging of data.

3.3.2.2 Interfaces for data logging

An Analogue Input Unit (AIU) similar to the one described in Section 3.3.1 is used. Again, two submersible LVDTs used for end cap axial strain measurement (see Section 3.4) were first connected to type OD3 signal conditioning units.

3.3.2.3 The pressure control systems

The lower chamber and cell pressures are controlled by two GDS controllers (manufactured by Geotechnical Systems Ltd, Walton-on-Thames, England). Each controller can perform the following actions : firstly, achieve a specified volume change or maintain a specified pressure and, secondly, read the volume change and pressure and provide information about the status of the controller (i.e. whether under automatic or manual control). More information about the behaviour of the controllers is provided by Ilyas(1983). In this research, the GDS controllers were used only to achieve target pressures set by the computer so as to follow a certain stress path. The back pressure was applied by a manually controlled manostat connected to a Budenberg pressure gauge, Figure 3.6.

3.3.2.4 The triaxial cell

Details of this cell and its characteristics have been presented by Bishop and Wesley (1975). Additional fittings have been mounted to permit end cap axial strain measurement as will be discussed below (Section 3.4.5).

3.4 The Instrumentation

In the previous section, reference has been made to load cells, pressure and displacement transducers, and proximity transducers. The calibration methods and performance of these devices will be discussed in Chapter 5. Here, the characteristics of the transducers and their methods of use will be briefly described.

3.4.1 The Load Cells

An Imperial College load cell was used in each of the triaxial cells to measure deviator forces. The principle of these cells has been described by El-Ruwayih (1975) and later by Hight (1983). They have a capacity of 350 kgf and are unaffected by horizontal forces or eccentricity of loading. Temperature effects are also thought to be minimal.

3.4.2 The Pressure Transducers

The cell, lower chamber, and pore water pressures at top and bottom of the specimen were measured in the 100 mm cell using transducers (manufactured by Bell and Howell, type 4-306-O1190-01MO) with a range of 0 to 700 kPa. A miniature transducer (manufactured by Druck, type PCDR81) was used to measure the mid-height pore water pressure following the method described by Hight (1983). In the 38 mm cell, the cell and lower chamber pressure were recorded by the GDS controllers. Another miniature transducer was installed in the bottom pedestal to measure pore water pressure.

3.4.3 The Volume Change Units

Imperial College units were deployed for measuring the volume changes of the specimens in both cells. Their maximum range is about 100 cc. Although this proved sufficient for the 38 mm specimens, a reversing valve had to be connected to the unit when it was used for the larger volume changes of the 100 mm specimens. De-airing is essential before use and checks on air in the unit or the pipes connected to it were

carried out frequently.

3.4.4 External Axial Strain Measurement

This is a conventional type of measurement where two LVDTs are mounted diametrically opposite to each other on cross-arms, as shown in Figure 3.7. In the 100 mm cell, the middle plate serves as a reference and the transducers deployed have a maximum travel of 50 mm. The external axial strain in the 38 mm cell was simply calculated from the volume change in the lower chamber, as recorded by the GDS controller.

Although the accuracies of the external measurements are inadequate at small strain levels (see Section 2.5), at large strains the percentage errors become relatively small and the external measurements become useful. The results at large strains can be cross checked against other types of measurement to give increased confidence in the data.

3.4.5 End-cap Axial Strain Measurement

The arrangement of the transducers in the 100 mm cell is presented in Figure 3.8. The bottom pedestal has an extension on which two diametrically opposite metal brackets of the shape shown in Figure 3.8a are bolted. Four stainless steel rods are mounted on these brackets on top of which a perspex ring is fixed. Two diametrically opposite cross-arms mounted on this ring hold the submersible LVDTs, Figure 3.8b. The armatures of the LVDTs rest under their own weight on two rectangular stainless steel targets connected to the top cap. Extensions for the armatures may

be attached to cater for axial movement during consolidation and to make sure that the transducers are in range during shearing. The above mounting arrangement was adopted because it was thought to be more rigid than the one used by Yung (1987). It also provided more space for the top cap-load cell connection described in Section 3.3.1 and for bulging of the specimen as it approached failure.

Because of the potential errors involved in external strain measurement discussed in Section 2.5.1, the measurement of axial strains in the 38 mm cell had to be improved if the data were to be compared with the high quality data from the 100 mm cell. Due to the limited space available in the 38 mm cell, the use of local instrumentation (proximity transducers or Imperial College electrolevel gauges) was ruled out and an alternative method had to be developed. It was decided to make use of some available submersible LVDTs and to measure axial strains between the specimen end caps. The arrangement finally adopted is presented in Figure 3.9. The two LVDTs are mounted on opposite sides of the loading ram inside the cell. An elliptical stainless steel plate is mounted on top of the specimen top cap with a 10 mm diameter hole in the middle (Figure 3.9b) to allow the load cell to touch the top cap in the normal way. On each side of the plate (Figure 3.9a), a fishing line is connected from which the LVDT armature is suspended. The armature and its connection to the fishing line have a weight large enough to cause the line to be fully stretched but small enough to avoid significant creep. This arrangement proved satisfactory, except that after isotropic consolidation the top cap could not be guaranteed to be horizontal and correctly aligned with the pin of the load cell. This caused eccentric loading, tilting of the top cap and sometimes complete masking of the true axial strain. As noted in Section 3.2.1, Yung (1987) used a flat surfaced top cap and assumed that a certain eccentricity in the loading could be tolerated. However, some of his end cap strain measurements still proved erroneous, since the

point of loading did not fall on the horizontal line passing through the two measurement points (Figure 3.10) and tilting of the top cap took place. To avoid such problems, a stainless steel tube was attached to the top cap in the manner shown in Figure 3.11. Immediately after the cell had been assembled, the load cell pin was lowered into the tube until full contact with the specimen top cap was achieved. In order to avoid excessive friction between the pin and the inside wall of the tube, silicon grease was spread over the inner surface of the pin. Air and grease could escape during penetration through a hole in the top of the pin. Trial tests indicated that some negative deviator stress (up to 20 kPa) took place during isotropic consolidation. This was the result of the still significant friction between the load cell pin and the stainless steel tube which opposed the downward movement of the top cap as the specimen reduced in volume. Similar problems were encountered during isotropic swelling. The problem was solved by getting the computer to monitor the deviator stress every 5 seconds. If the computer detected a value of deviator stress larger than ± 3 kPa, it adjusted the lower chamber pressure to bring the deviator stress back within the specified range.

3.4.6 Local Strain Measurement

As mentioned in Section 2.5.2, a number of different techniques have been introduced to measure the axial strain locally over the central part of the specimen. At Sheffield University, Yung (1987) developed a system based on the use of proximity transducers to measure both axial and radial strains. For the new 100 mm apparatus it was necessary to look for transducers with more flexible cables than those used by Yung and to find a method of mounting them so that their position could be changed from outside the cell during a test. In this way the problems related to

the limit on the range of transducer (see section 3.2.1) could be avoided.

A survey of the commercially available proximity transducers was carried out and three types from different manufacturers were tested in the laboratory. The SMP type manufactured by Sangamo was finally selected. The main advantages of this type, as compared to the one used by Yung, were much smaller size and weight, significantly higher sensitivity and much lower cost. The fact that the transducers have a range of only 2 mm, compared with 6 mm for those used by Yung was not seen as a problem since the transducers were to have externally adjustable mountings. However, this type of transducer was not intended to be immersed in water and some form of protection had to be developed.

A detailed investigation into the behaviour of the new transducers was carried out to evaluate their response with different target materials. The results showed that the best target material was magnetic stainless steel which, in addition to providing the most sensitive response, does not react with the cell water. Similar findings were reported by Yung.

A detailed drawing of the mounting unit is shown in Figure 3.12. Plate 3.3 shows a photograph of the unit. The proximity transducer is fitted into a stainless steel housing. This housing has a threaded end which screws into a stainless steel tube through which the cable of the proximity transducer is passed. To provide an effective seal between the housing unit and this tube, a groove is drilled in the flat part of the housing where an O-ring is placed. The tube is fitted in a brass tube which has two internal O-rings to prevent cell water from escaping between the two tubes. The outer brass tube is in a fixed position at all times while the inner tube holding the transducer is manoeuverable. The outer end of the inner tube is threaded where a nut is placed. By turning this nut, the position of the

proximity transducer can be altered. The whole mounting is attached to the cell by four screws entering threaded holes in a brass unit. An O-ring is provided at the surface of contact to prevent cell water from escaping. Adjustment of the position of the proximity transducer is carried out so that the inner tube is always moving towards the target. If the proximity transducer has to be moved away from the target, it is moved a larger distance than necessary and then brought back towards the target into the required position. This procedure eliminates slackness in the threads between the inner tube and the adjusting nut.

Sealing of the transducer housing was carried out using medical fingercots (type X200-906 manufactured by Regent, England). As shown in Plate 3.3, the housing has grooves for two O-rings. To increase the chances of proper sealing two fingercots, similar to the one shown in Plate 3.3, were used for each transducer. The first was rolled around the housing and an O-ring was placed in the groove. Then another fingercot was placed on top of the first one and sealed by the second O-ring.

In principle, the instrumentation arrangement for axial strain measurement is similar to that shown in Figure 2.17. Two pairs of proximity transducers are mounted on opposite sides of the specimen. The target movements are not generally equal and therefore separate adjustable mountings for each transducer had to be provided. Four holes were drilled in the cell middle plate, as shown in Plate 3.4. into which the mounting units were inserted. Since the target movements had to be monitored in a vertical plane passing through the vertical axis of symmetry of the specimen, the proximity transducers had to be positioned accordingly and also had to be equidistant from the axis of symmetry. The arms holding the axial strain transducers consisted of three brass tubes welded together as shown in Figure 3.13 and Plate 3.5. The rods were connected together and screwed to the housing in a way that allowed the flexible cable of the transducer to pass through them. Opposite

each transducer, a 30 mm × 30 mm × 1 mm stainless steel target is mounted on 6 mm thick perspex rings around the specimen, Figure 3.14. The rings have two pairs of diametrically opposite holes through which brass rods pass . On one end of each rod there is a small bearing pad of the same curvature as the specimen and, on the other, a V-shaped fitting. A rubber band passing over the V-shaped fitting is used to hold the perspex ring onto the specimen without causing the bearing pads to penetrate the membrane or deform the specimen locally. This method of mounting the targets was developed by Yung (1987).

Radial strain measurement was carried out in two perpendicular directions by symmetrically mounting four proximity transducers on straight stainless steel tubes which pass into adjustable mountings in the stainless steel ring described in Section 3.3.1, as shown in Figure 3.15 and Plate 3.2. Rectangular (45 mm × 15 mm × 1mm) magnetic stainless steel targets were attached to the membrane at about midheight of the specimen, each target being opposite a proximity transducer. Attachment of the targets to the rubber membrane was carried out by spreading silicon rubber gel over a roughly 5 mm diameter circular area in the middle of the target, Figure 3.16, and sticking it to the membrane. Support was needed for the first half hour until the silicon rubber set. The contact area between the target and the membrane was kept to a minimum to avoid restraining the specimen (see Section 5.4.2).

3.5 Specimen Preparation

3.5.1 Test Material

As mentioned in Chapter 1, the clay used in this research was Speswhite kaolin. This soil has been tested by many other researchers. Index and Cam-clay model parameters derived from previous studies (e.g Pang (1987) and Richardson (1988)) are presented in Tables 3.1 and 3.2 respectively. These were used to plan the specimen preparation procedure. The soil was prepared in the form of a slurry and consolidated one-dimensionally to form a cake from which triaxial specimens could be extracted. A similar technique was used previously by Pang (1987).

3.5.1.1 Slurry preparation

De-aired de-ionised water was first poured into the mechanical mixer which was then set in motion. Speswhite kaolin was sprinkled in to form a slurry of a water content equal to about 1.5 times the liquid limit. Although some researchers have suggested the use of a mixing water content of twice the liquid limit to ensure full homogeneity (e.g Sheeran and Krizek (1971)), a factor of 1.5 was adopted in this research since it allowed an entire batch to be mixed in one operation. A similar value was adopted by Kirkpatrick et al (1986). The mixing took place for about two hours after which the slurry was placed in the consolidation pot.

3.5.2 Consolidation

The consolidation pot had three main components, namely a bottom plate, a cylindrical body and a rubber bellows assembly, Figure 3.17. The body consisted of a number of chromium plated steel rings, each 153 mm high and 400 mm in diameter. Sealing between the rings was achieved by using O-rings. Steel tie rods were used to ensure that the rings were tightly clamped together between the bottom plate and the top plate of the bellows assembly during consolidation. The bellows assembly consisted of a steel top plate, a central piston, a rubber bellows, and a steel consolidation plate. It was filled with water which was pressurised by an air-water system. As settlement of the clay took place, the central piston, which was connected to the consolidation plate, moved downward. Porous plastic drainage layers were provided at the top and bottom of the sample. Drainage from the top of the sample was allowed by connecting a nylon tube passing inside the bellows assembly to the upper drainage layer. Two holes in the bottom plate allowed drainage from the base.

Before the pot was filled with slurry, silicon grease was applied to the internal wall of the pot to minimise friction between the consolidating slurry and the wall and to allow easier removal of the rings at the end of consolidation (see Section 3.5.3). The drainage disc was placed on the bottom plate under 100 mm of de-aired water. The slurry was poured into the consolidation pot under this de-aired water to make sure that no air was trapped in the clay. The top drainage disc was then placed on top of the slurry and the bellows assembly lowered, thereby displacing the water on top of the porous disc. The top and bottom plates were then clamped together by means of the tie rods. The consolidation pressure was applied in steps indicated in Table 3.3 up to a maximum of 150 kPa. Application of pressure increments was carried out after ensuring that no significant volume change was taking place after

the previous pressure increment (i.e.volume change of less than 0.1 litre in 24 hours). The final vertical effective pressure (150 kPa) was applied for a period of about 10 days to allow some secondary compression to occur.

During consolidation the volume of water squeezed out of the clay and the settlement of the piston were monitored regularly. The results for the two cakes (1 and 2) prepared for the present work are presented in Figure 3.18. The results indicate that there is a very good correspondence between volume change and piston settlement. This implies that the amount of air in the slurry was negligible. There is also a good agreement between the results for cakes 1 and 2. The modest divergence between the results noticed during the initial stage of loading, could be due to a difference in the amount of water left on top of the slurry before lowering the bellows assembly.

3.5.3 Triaxial Specimen Preparation

After consolidation, the pressure applied by the bellows assembly was released slowly and the rings forming the consolidation pot were removed by sliding them vertically upwards. The top drainage disc was then removed quickly to prevent water from being sucked back into the clay. Because the sampling process described below usually took about a day, a small amount of water was probably drawn back into the specimen from the bottom drainage disc which had to be left in place.

Sampling was carried out by using tubes with the maximum possible aspect ratio to minimise disturbance (see Section 2.3). The samplers were prepared from aluminium tubing and had the geometry shown in Figure 3.19. Silicon grease was applied on both the inside and outside of the tubes which were then driven by hand

using the guiding equipment shown in Figure 3.20 to ensure that penetration was taking place in a constant vertical direction. Seven 100 mm diameter tubes were pushed in first followed by twelve 38 mm diameter tubes in the top half of the cake, as shown in Figure 3.21. With the aid of a metal wire, the tubes were cut out of the cake before another set of 38 mm diameter samplers were driven into the bottom half of the cakle. The sample ends were cleaned up and waxed, and then closely wrapped in thin plastic sheeting (cling film). All the samplers were placed in polythene bags which were then sealed and placed in a temperature and moisture controlled room.

According to Baligh et al (1987), the maximum axial strain that takes place during tube penetration is given by Equation 2.4. This equation indicates that the maximum axial strains that occurred during the above sampling operation were about 0.7% and 1.0% for the 100 mm and the 38 mm specimens respectively. However, since the specimens were subsequently subjected to a high consolidation pressure, at least 2.3 times larger than that used in the consolidation pot, the effects of such disturbance could be assumed to be largely eliminated (Baligh et al 1987, Hight et al 1985, Graham et al 1988, and Ladd and Foott 1974). For the same reason and because of the care taken in sealing the specimens, storage effects, including the different times of storage for different specimens, could also be assumed minimal.

During the sampling operation, water content specimens were taken from various positions in the cake corresponding to the top and bottom of the sampling tubes. No systematic variation of water content in any direction was detected, although the average water content at the bottom might have been expected to be less than that at the top due to friction on the sides of the consolidation pot. Water sucked from the bottom drainage disc, if any, would not have reached the position of the bottom of the samplers and therefore would not have affected the water content measurements. The water contents were found to be 52.0 $\pm$ 1.6% and 53.0 $\pm$ 2.2

% for cakes 1 and 2 respectively. Both the variations of the water contents within each cake and the difference between the average values were considered acceptable since they amounted to less than 5% of the plasticity index of the clay.

3.5.4 Specimen Extrusion and Setting up

Before the specimen was extruded from the aluminum sampling tube, some preparations were made on both cells. Firsly, the pressure transducers were thoroughly de-aired and kept saturated prior to testing. The top and bottom porous stones were cleaned from soil particles in an ultrasonic bath and then left to saturate in boiling water for about 20 minutes. Checks on the rubber membrane and the fingercots (used to seal the proximity transducers) were carried out to find any possible defects which could result in leakage of water into the specimen or into the proximity transducers respectively.

Standard techniques were followed in the extrusion and setting up of the 38 mm diameter specimens. However, extra care had to be taken when placing the top cap to which the two strings holding the submersible LVDT armatures were attached.

In the case of the 100 mm specimens, the setting up was more complicated. A 100 mm diameter tube sampler was taken out of the storage room and placed in a vertical frame for extrusion using a hydraulic jack. The soil specimen was driven out of the tube into a specially manufactured 200 mm high split tube. The specimen was then trimmed and a water content specimen taken near both ends. The specimen was weighed and placed on the bottom pedestal of the triaxial cell on top of a saturated porous stone. The split tube was removed and measurements

of the specimen's height and diameter were taken by digital vernier (average of six measurements each).

The rubber membrane was then placed around the specimen using a standard membrane stretcher and two O-rings were placed around the bottom cap. A thin layer of silicon grease had previously been applied to the grooves on the top and bottom caps to ensure effective sealing of the membrane. The four proximity transducers used for the axial strain measurement were then sealed and the two perspex rings holding the targets for the local axial strain measurement were placed around the specimen, with their bearing pads placed on positions previously marked on the membrane. Silicon rubber adhesive beneath the pads was used as insurance against failure of the rubber band holding the pads onto the membrane (see Figure 3.14). The top cap, with the two rectangular targets for end cap strain measurement attached to it, was then placed over a porous disc on top of the specimen, while making sure that no air was trapped by opening the back pressure valve and letting water flow while the connection was taking place. It was important to make sure that the two end cap strain targets on which the LVDT armatures rested were in the same vertical plane as the local axial strain targets, so that all the axial strain readings were made in the same vertical plane. The rubber membrane was then rolled onto the top cap and sealed with two O-rings. The two submersible LVDTs were positioned so that, after the intermediate test stages, they would be in range at the start of shearing. The targets for local radial strain measurement were attached to the rubber membrane opposite the corresponding proximity transducers (see Section 3.4.6). At approximately mid-height of the specimen, a hole of about 2mm in diameter was opened in the rubber membrane. A rubber fitting used to attach the miniature pore pressure transducer to the specimen was glued using silicon rubber on the membrane over the hole, as shown in Figure 3.22. The transducer was then

pushed into the fitting and sealed on the outside with two O-rings.

The cell top was lifted by a pulley system, because of its heavy weight, and lowered slowly over the specimen. While the cell was being lowered, the flexible pipe from the load cell-top cap connection (see Section 3.3.1) was connected to a hole in the cell middle plate. Initially tap water was used to fill the cell, but because of the long duration of each test, algal growth occurred during trial tests. Therefore, de-ionised water, which showed very little algal growth, was used in all the main tests.

3.6 Test Stages

Tests in the 38 mm apparatus followed standard procedures as described by Bishop and Henkel (1962). All the consolidation and swelling stages were performed isotropically and the cell pressure increment was applied in one step only. Tests in the 100 mm apparatus were performed as follows :

3.6.1 Saturation

After the cell had been filled with water, the cell and lower chamber pressure valves were opened resulting in the application of an all round pressure of 13 kPa. This was the minimum pressure that could be applied under automated control. A period of about two hours was then allowed for pore water pressures in the specimen to equalise. Saturation was achieved in a conventional manner by increasing the cell pressure in increments of 50 kPa and recording Skempton's B-value ($= \Delta u/\Delta\sigma_3$ where Δu and $\Delta\sigma_3$ are the increments of pore water pressure and cell pressure

respectively). After applying the cell pressure, a period of about one hour was required to obtain comparable pore pressure readings at the mid-height and ends of the specimen. If the B-value was less than 0.98, the back pressure was increased to a value equal to the cell pressure minus 7 kPa and water was allowed to enter the specimen. Trial tests indicated that four increments of cell pressure, i.e. a total increase of 200 kPa, could achieve full saturation of the specimen. The time required for this stage was about 25 hours.

3.6.2 K_0-Consolidation

The specimen was required to follow a stress path such that the radial strain would not deviate from zero. One way of achieving this is to use trial and error, i.e. to try different stress paths and to find the one that leads to the smallest radial strain. For normal consolidation the value of K_0 has been found to be constant. A number of different methods predicting K_0 have been suggested with the most widely used being that of Jaky (1948)

$$K_0 = 1 - sin(\phi') \tag{3.1}$$

where ϕ' is the angle of friction of the soil. Hence, it has been relatively easy to carry out normal consolidation stages without causing any significant radial strains (e.g. Gens (1983)).

A second approach is to apply small increments of axial and radial stress and to check on the radial strain to make sure that it does not exceed a certain limit. If this limit is exceeded, stresses are changed to bring the strain back within the specified range. This method is potentially more accurate but requires radial strain measurement. In this research the proximity transducers were available to monitor the radial strain during consolidation and therefore the second method was used.

If the average of the two measurements exceeded ±0.005%, a correction was made to the axial or radial stress. On the other hand, if the excess pore water pressure measured at mid-height exceeded 10 kPa, pressure application was halted until the excess pore pressure decreased to a value less than 5 kPa.

On average, the K_0-consolidation stage bringing the specimens to a maximum effective pressure, σ_1', of 350 kPa took 10 days. A period of 40 hours was also allowed for secondary compression to take place.

3.6.3 K_0-Swelling

In order to prepare overconsolidated specimens, it was necessary for specimens to undergo swelling under K_0 conditions. Researchers have found that the determination of the stress path for K_0-swelling is much more difficult than that for normal consolidation because the value of K_0 is not constant. Gens (1983) found that using trial and error to determine the stress path in this case was time consuming. He nonetheless tried a limited number of stress paths and used the one that involved the minimum radial strain.

In the present research, the same method could be used as for normal consolidation. As before, the average radial strain was not allowed to exceed ±0.005% and the maximum excess pore water pressure was kept below 10 kPa. However, as will be shown in Chapter 6, control of the stress path during swelling was more difficult since the allowance of ±0.005% radial strain resulted in larger pressure changes than during normal consolidation.

At the end of swelling the specimen was allowed to stand for a period of 40 hours to reduce creep effects.

3.6.4 Sampling Disturbance, Deviator Stress Relief and Reconsolidation

Sampling disturbance was simulated in the tests by applying a strain cycle to the specimen. The size of the strain cycle was determined by referring to Figure 2.2, remembering that this figure applies to a soil element along the vertical axis of symmetry of the sampler and does not take into account friction effects along the sides of the tube. A strain cycle of 1% amplitude was chosen, corresponding to the disturbance imposed by a sampler with an aspect ratio (B_s/t_s) of 40. This was achieved by keeping the radial stress constant and varying the axial stress under undrained conditions

Immediately after the strain path was completed, the deviator stress was released to simulate the stress relief that takes place during sampling. Since the pore water pressure in the specimen was by now different from the back pressure previously applied, the axial and radial stresses were released (keeping the deviator stress equal to zero) until the average pore water pressure was equal to the back pressure, at which time the drainage valves were opened. The remaining total pressure was not released to avoid cavitation in the specimen or the drainage pipes.

Reconsolidation to the initial conditions (before disturbance) was carried out by following an effective stress path which led to a point on the consolidation or swelling stress path and then followed the original path back to the initial condition, Figure 3.23. In this way, the 'disturbed' and 'undisturbed' specimens had similar effective stress paths shortly before undrained shearing was started and recent stress history effects (Stallebrass (1990)) were avoided. As for the 'undisturbed' specimens, a period of about 40 hours after reconsolidation was given to the 'dis-

turbed' specimens for creep to occur.

3.6.5 Undrained Shearing

Although any total stress path could have been followed, for simplicity a conventional total stress path with a gradient $\Delta q/\Delta p = 3$ was adopted. The axial stress was changed at a rate of 2 kPa/hr. This proved to be slow enough for the equalisation of pore water pressure in the specimen (see Chapter 5).

At the end of shearing, the lower chamber pressure and cell pressure were slowly and simultaneously released under manual control. This ensured that no further significant deformation took place. Water was then drained out of the cell as soon as possible and the specimen was weighed and cut into six pieces to check the water content distribution with height.

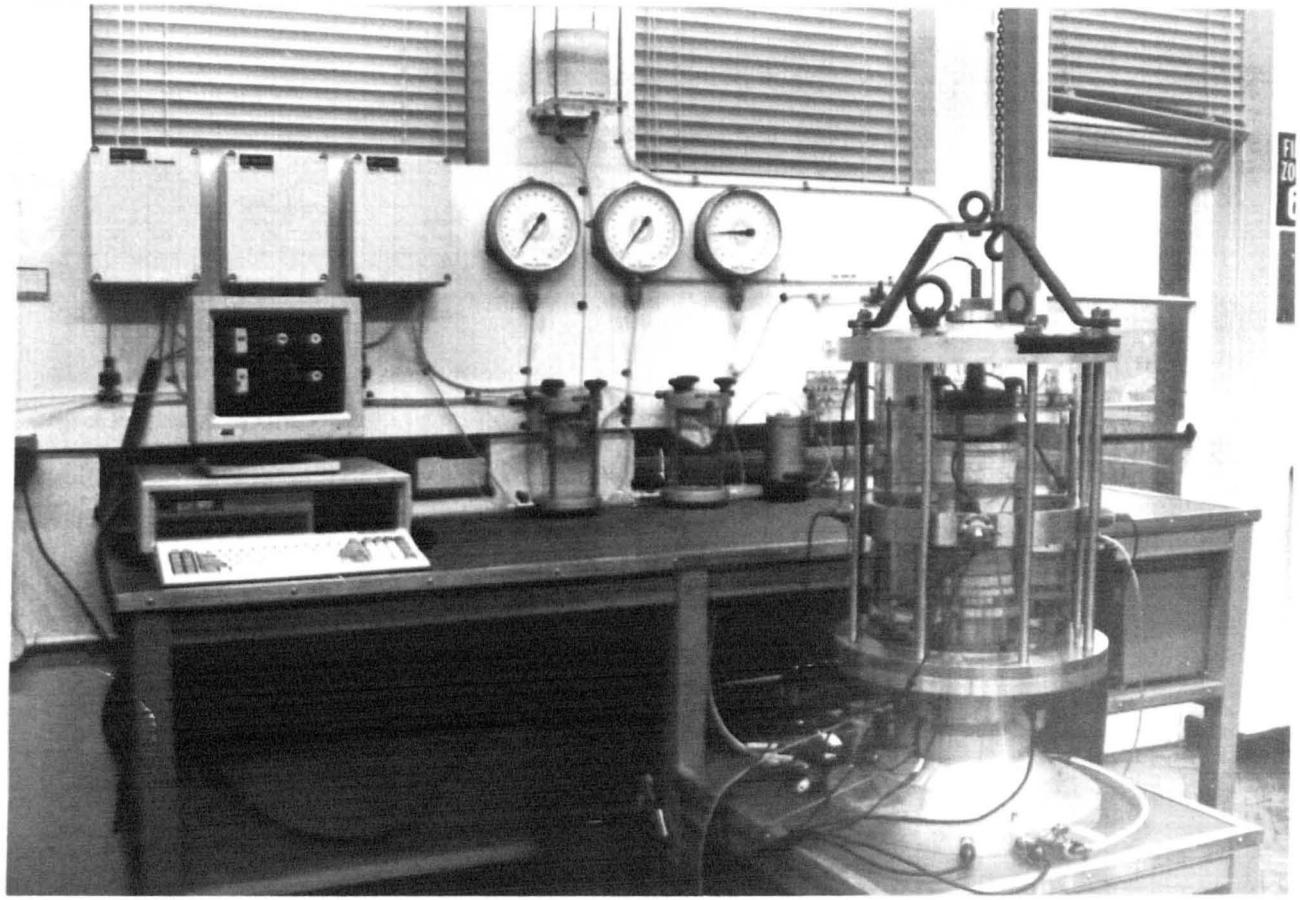

Plate 3.1 The 100 mm triaxial apparatus and associated equipment

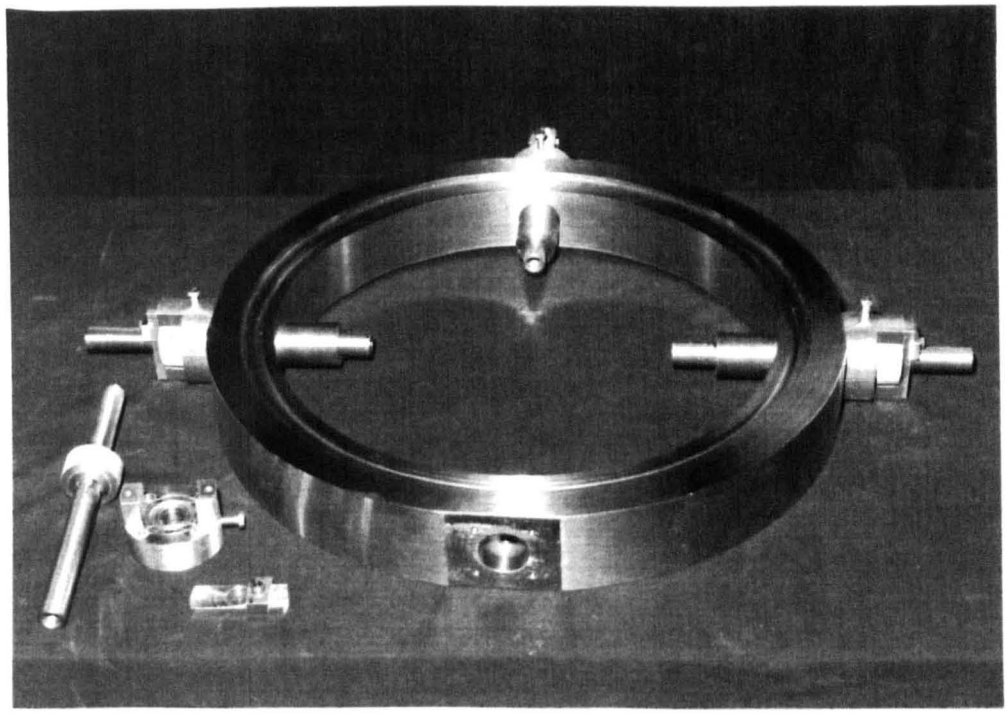

Plate 3.2 Arrangement for the mid-height steel ring in the 100 mm cell

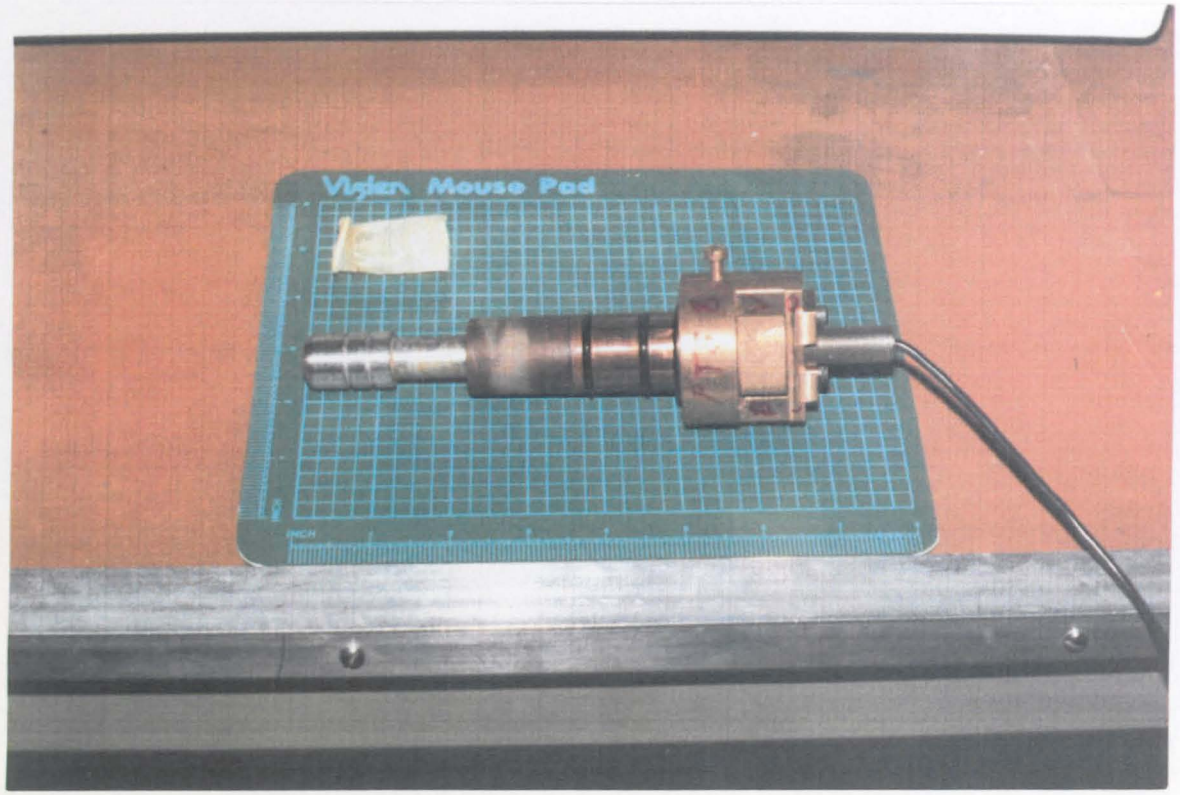

Plate 3.3 Mounting unit for the proximity transducer

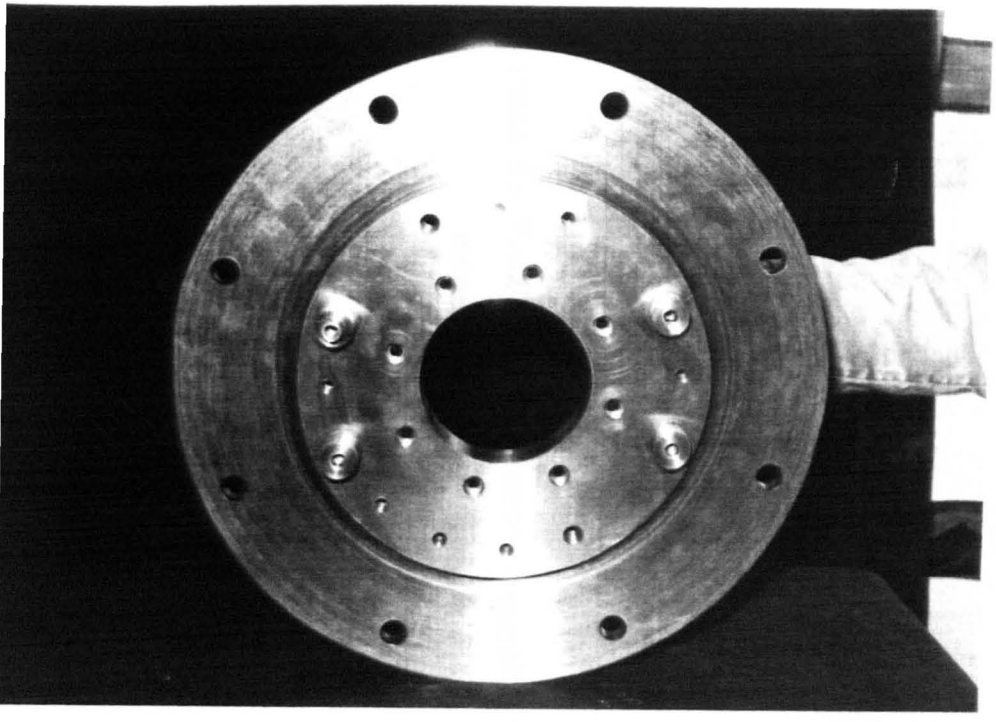

Top view

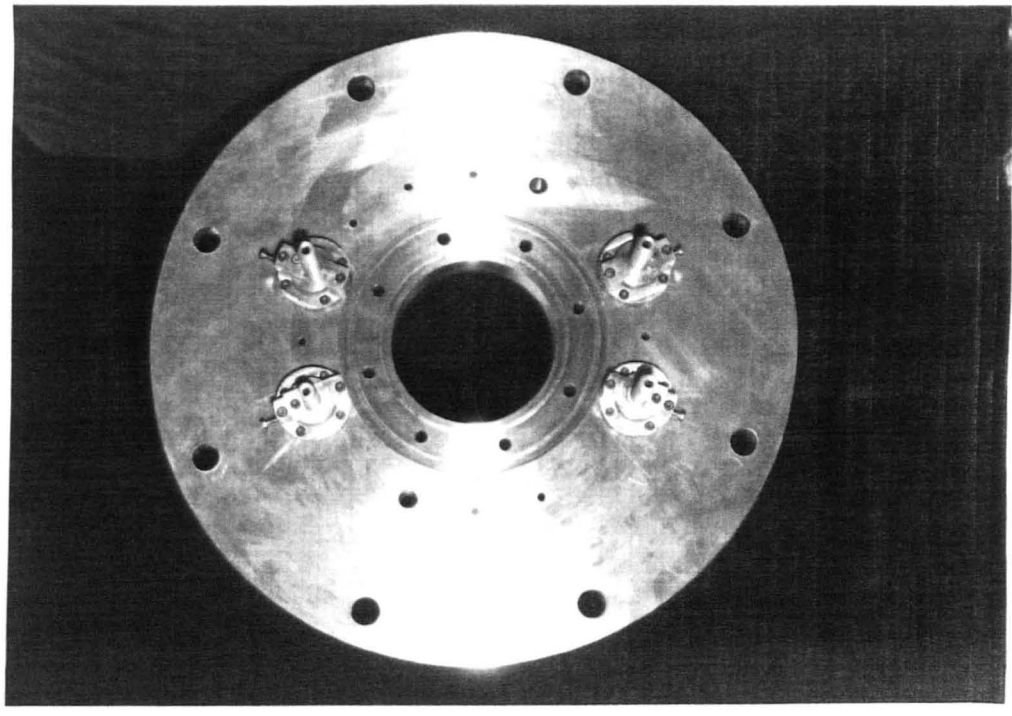

Bottom view

Plate 3.4 The 100 mm cell middle plate

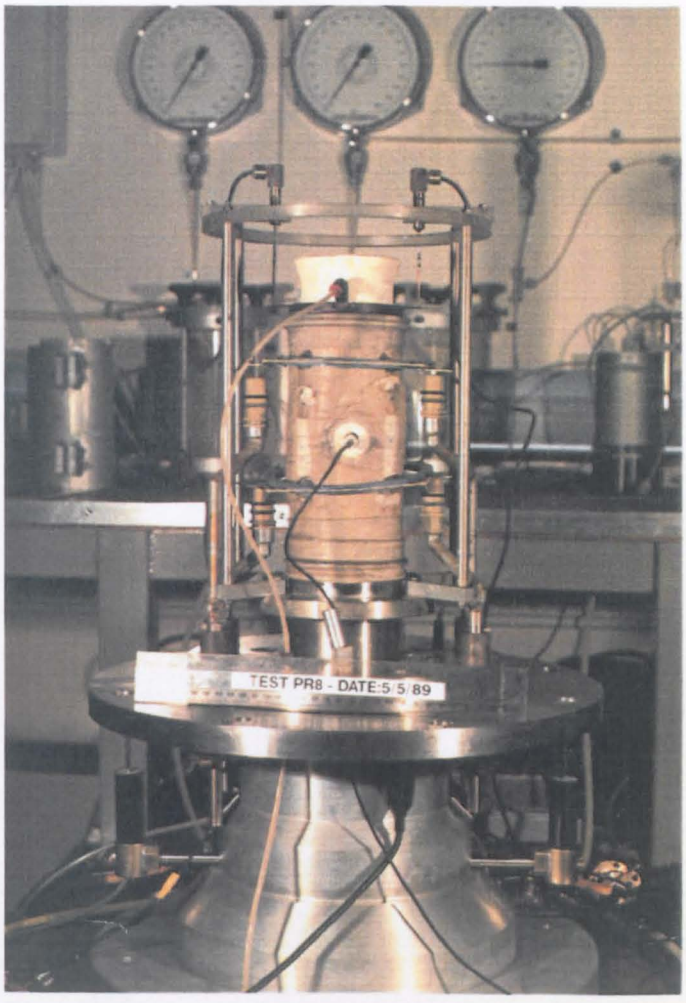

Plate 3.5 Proximity transducers mounting for axial strain measurement

parameter	value
LL %	72
PL %	40
PI %	36
G	2.65
%<200 mm	77.8

Table 3.1 Classification parameters assumed for kaolin

parameter	value
λ	0.19
k	0.05
N	3.26
M	0.96
Γ	3.16

Table 3.2 Critical state parameters of kaolin

pressure kPa	period days
20	8
38	5
75	6
150	> 10

Table 3.3 Sequence of pressure increments during slurry consolidation

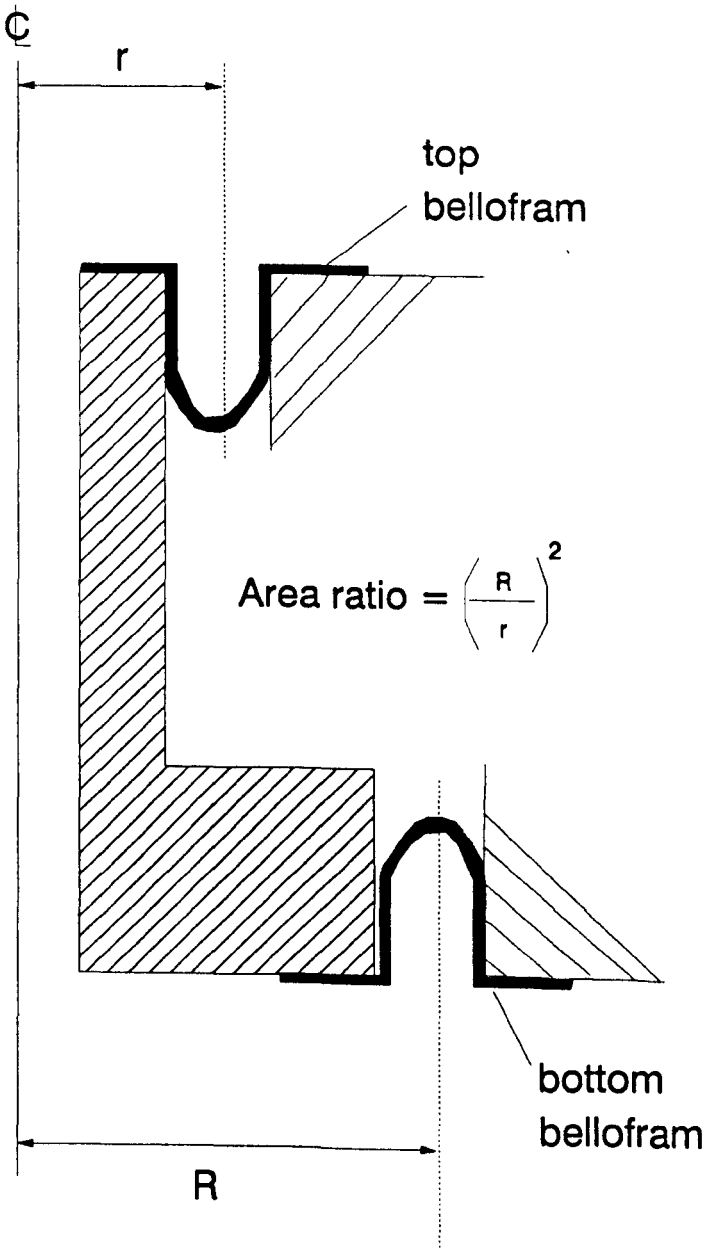

Fig 3.1 Bellofram area ratio

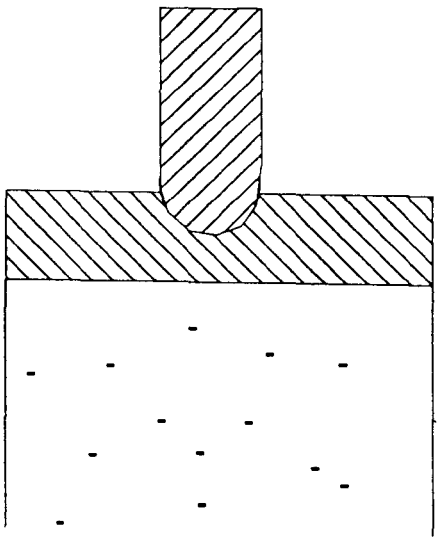

(a) curved recess

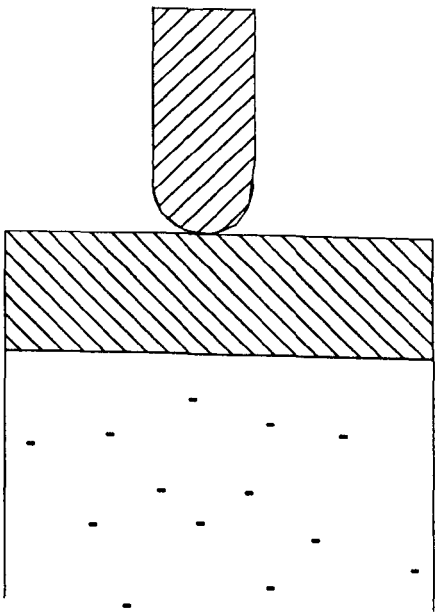

(b) flat surface

Fig 3.2 Top cap-load cell connections

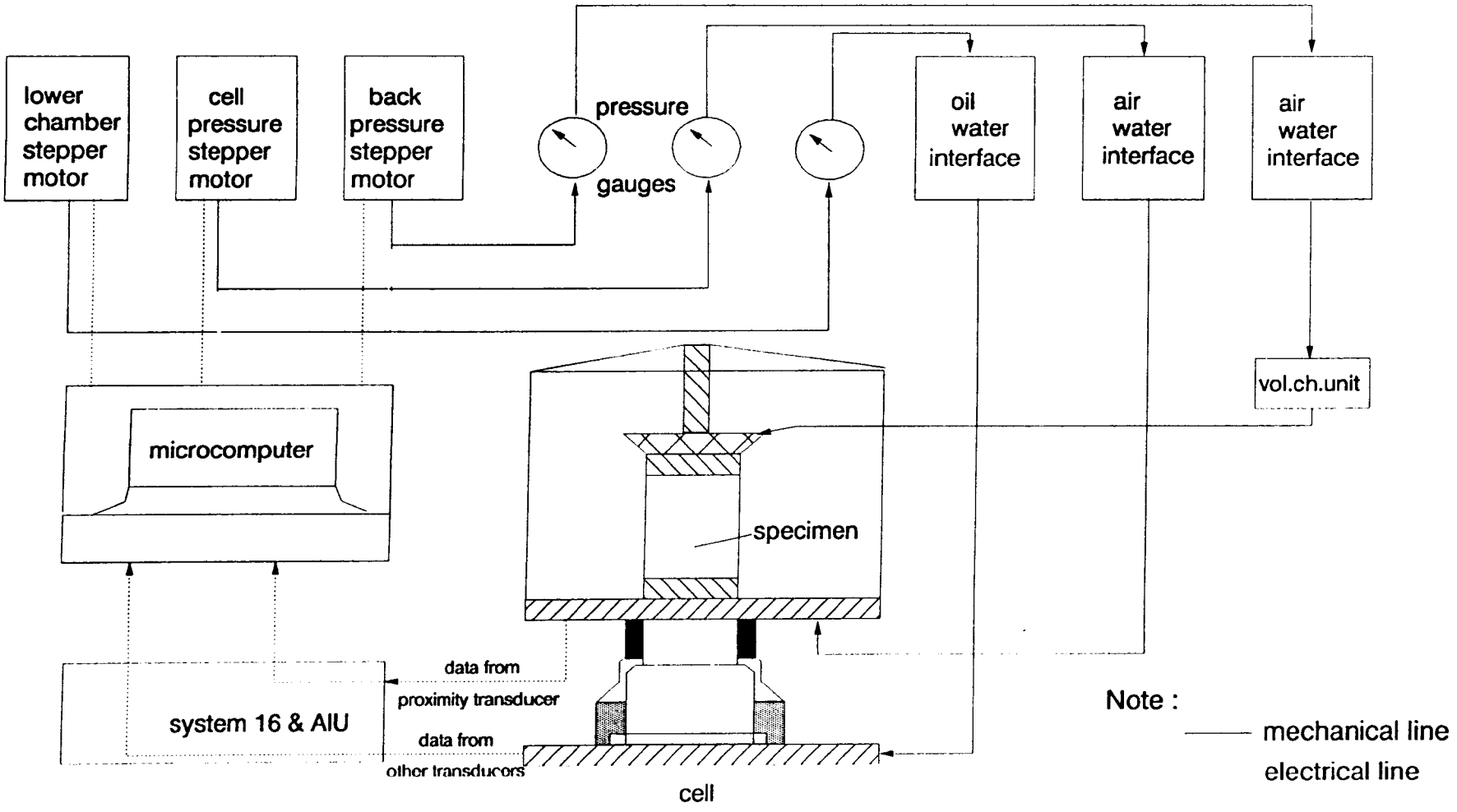

Fig 3.3 Schematic representation of the control system for the 100 mm cell

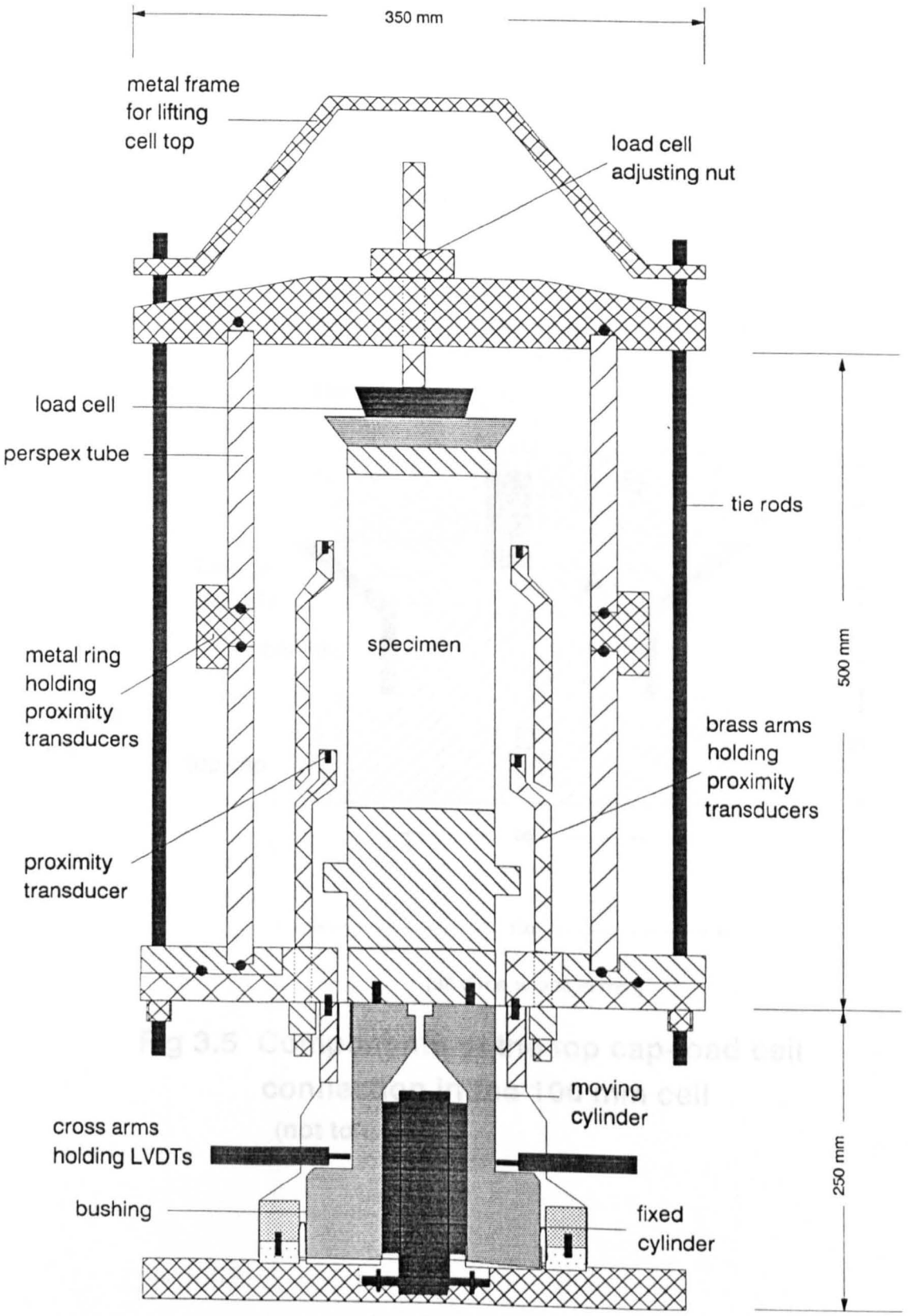

Fig 3.4 The 100 mm triaxial apparatus

(not to scale)

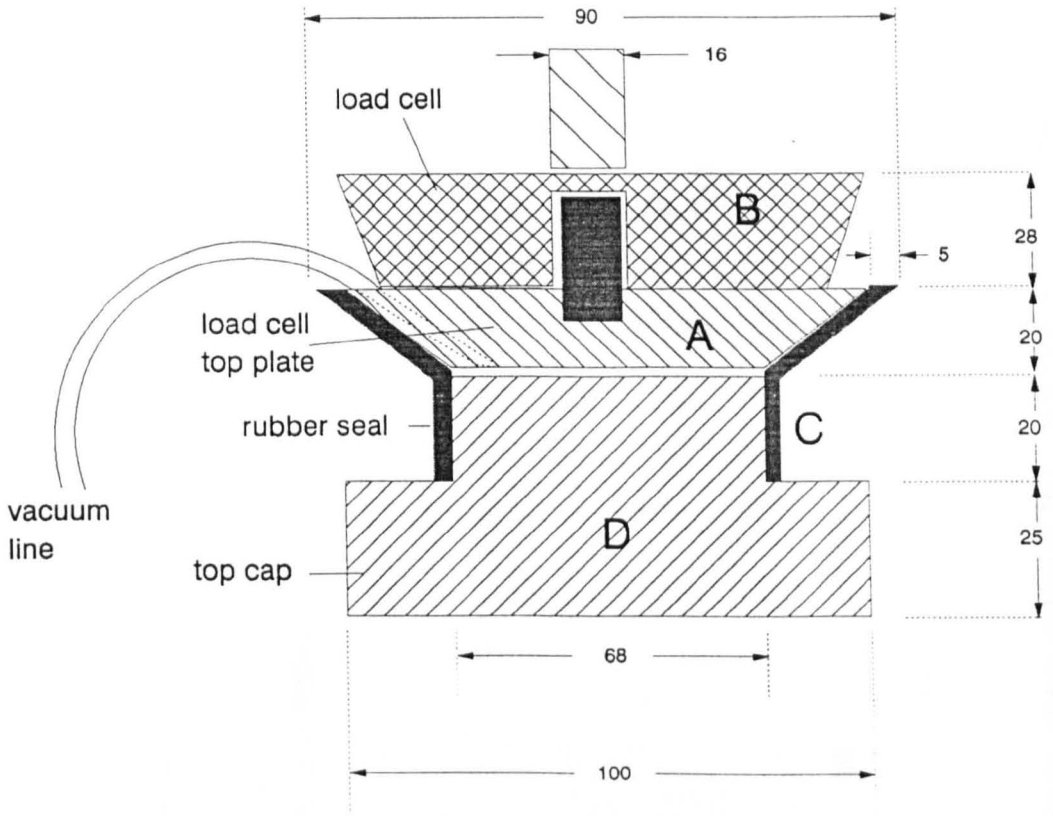

Fig 3.5 Components of the top cap-load cell connection in the 100 mm cell
(not to scale)

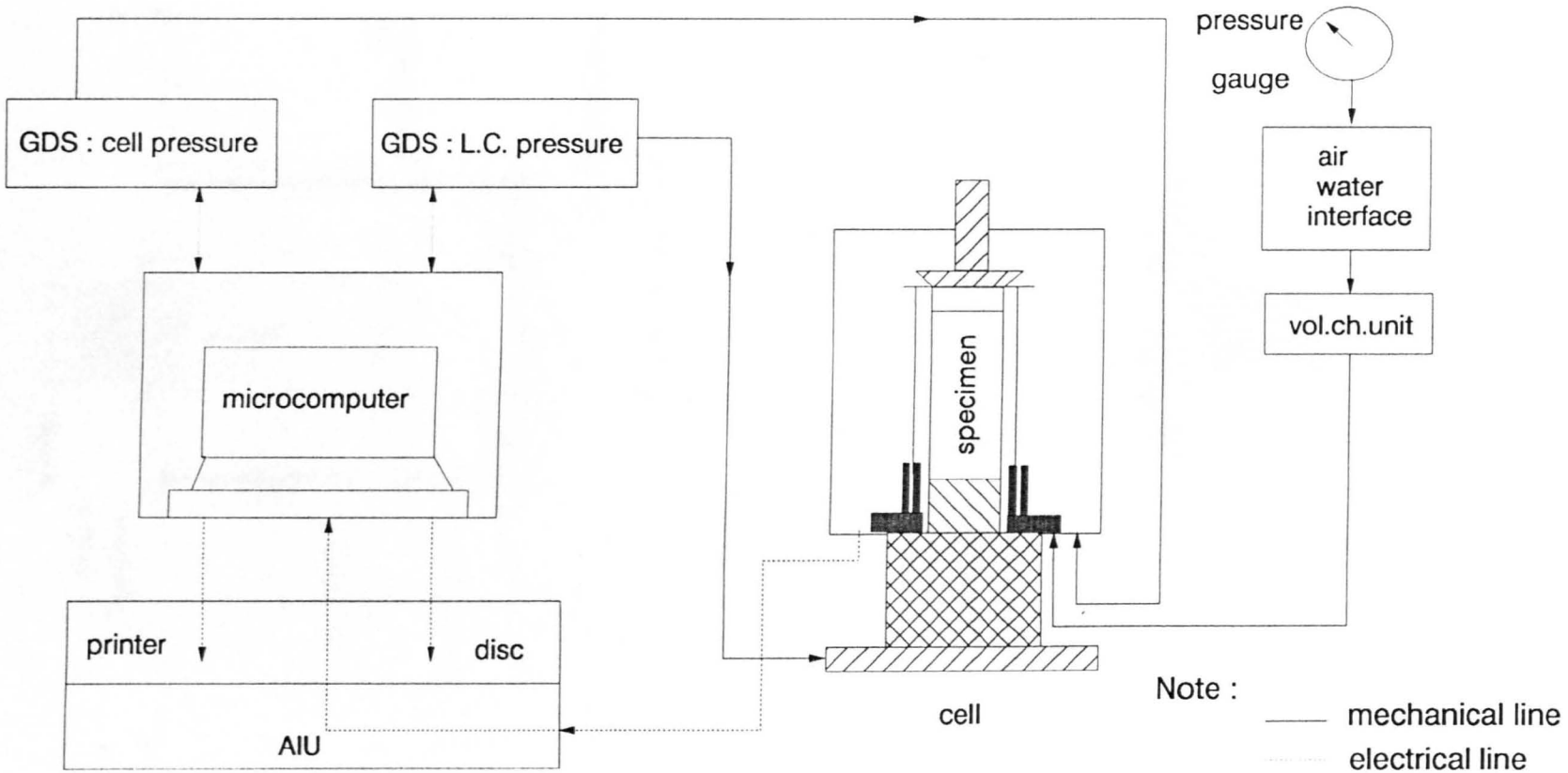

Fig 3.6 Schematic representation of the control system for the 38 mm cell

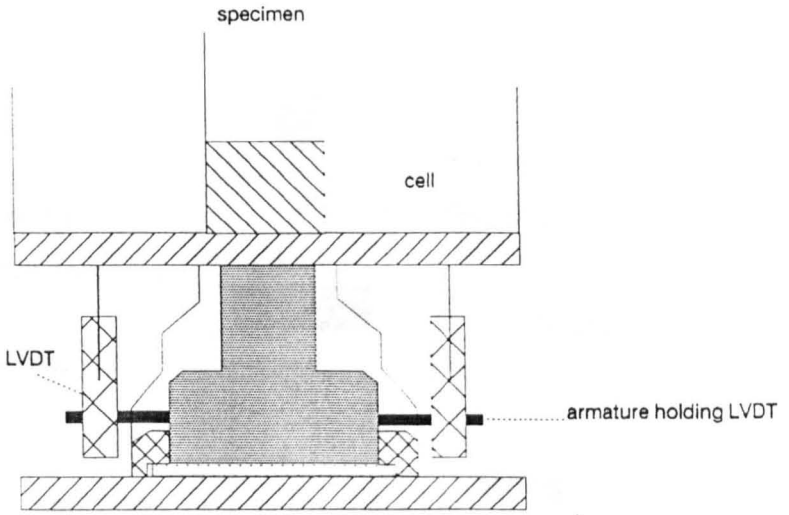

Fig 3.7 External strain measurement in the 100 mm cell

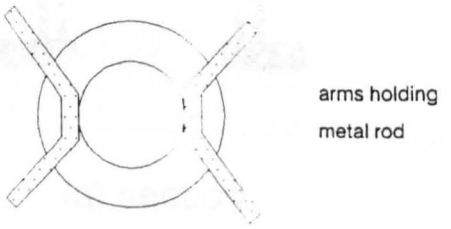

(a) plan view at bottom pedestal (A-A)

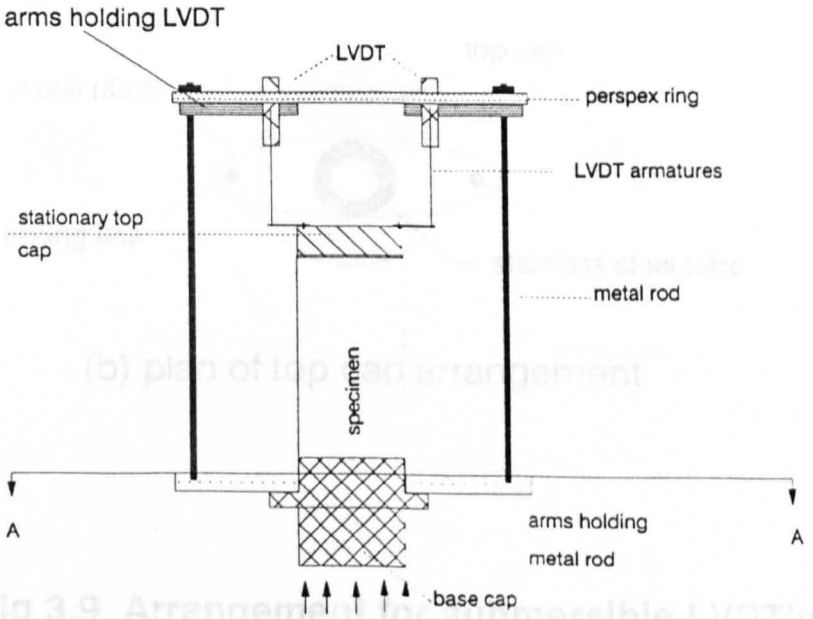

(b) sectional view

Fig 3.8 End cap strain measurement in the 100 mm cell

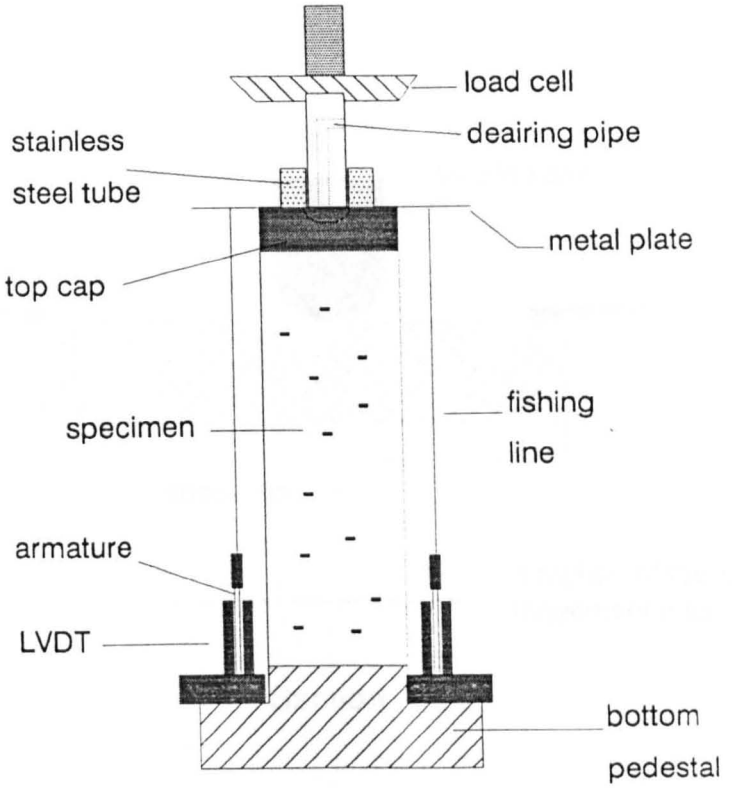

(a) section

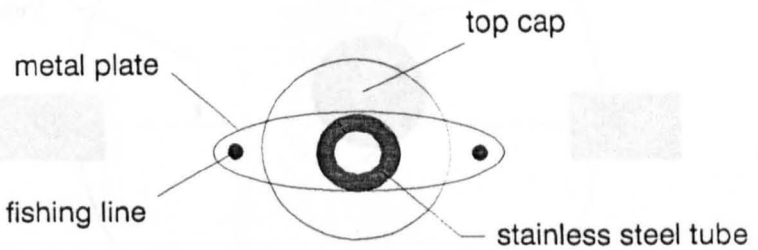

(b) plan of top cap arrangement

Fig 3.9 Arrangement for submersible LVDT's in the 38 mm cell

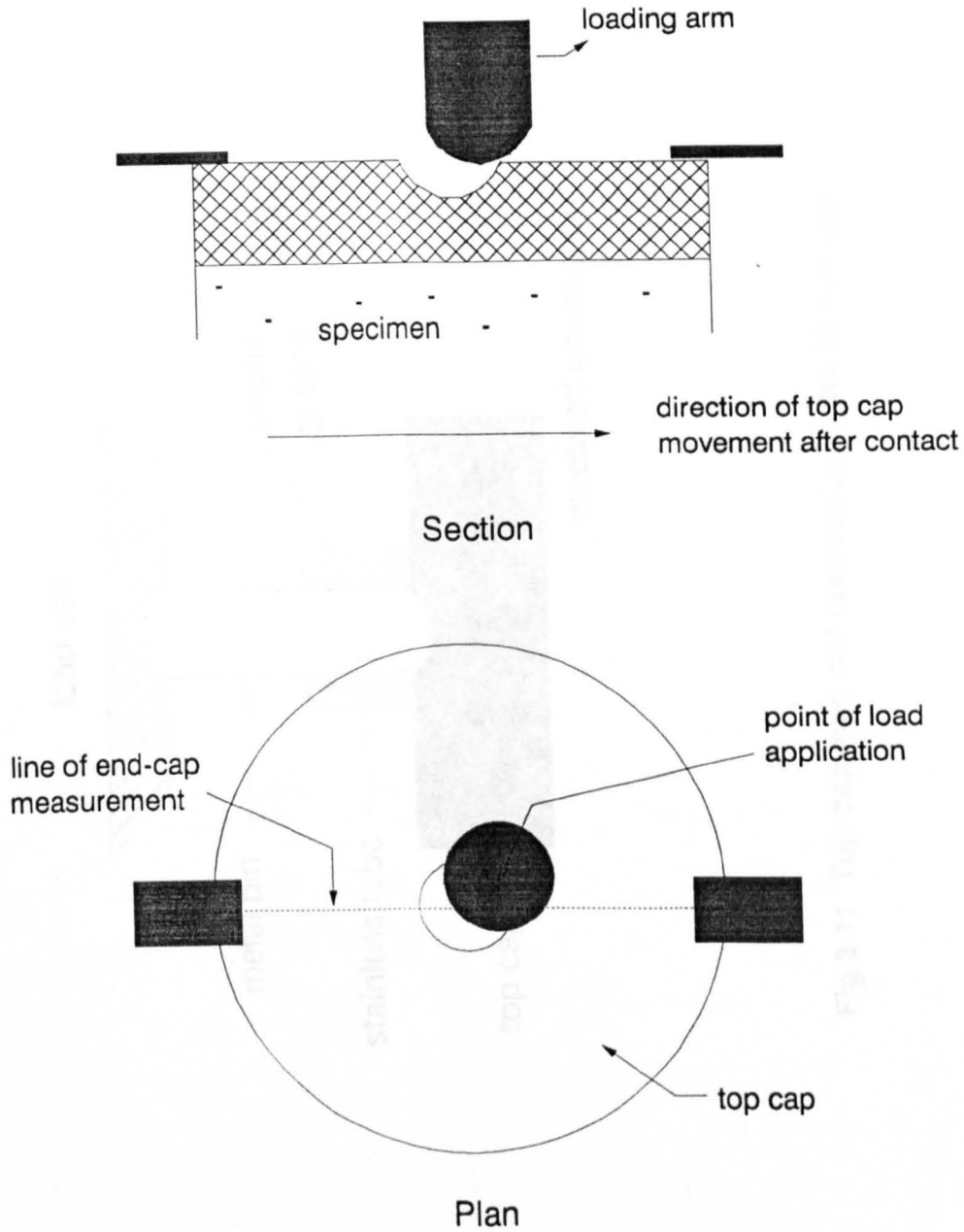

Fig 3.10 Possible point of contact between loading arm and top cap after isotropic consolidation

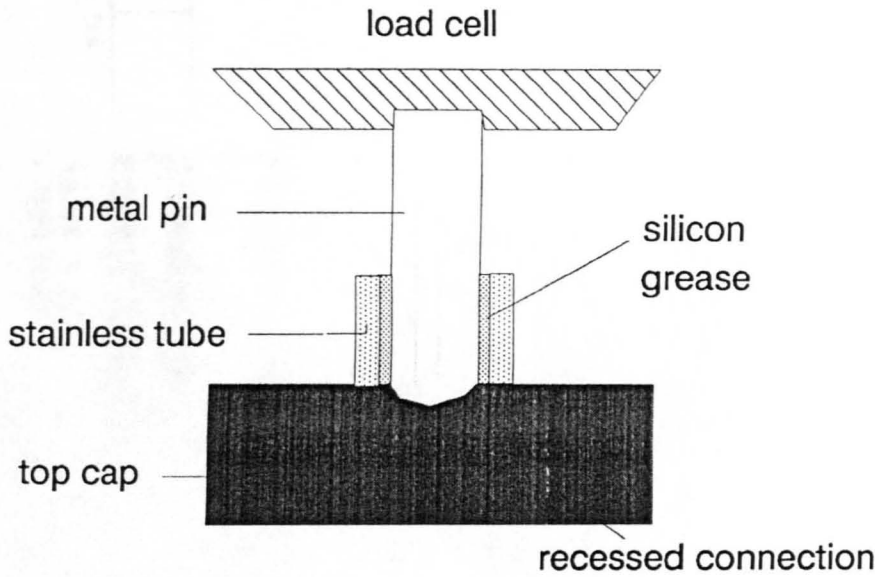

Fig 3.11 Top cap-load cell connection in the 38 mm cell

SLIDE MAT.L BRASS

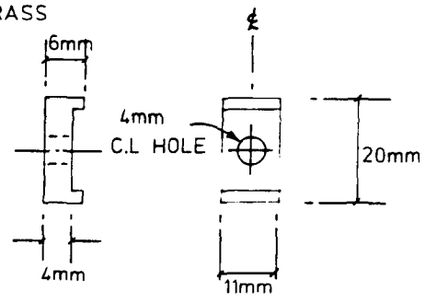

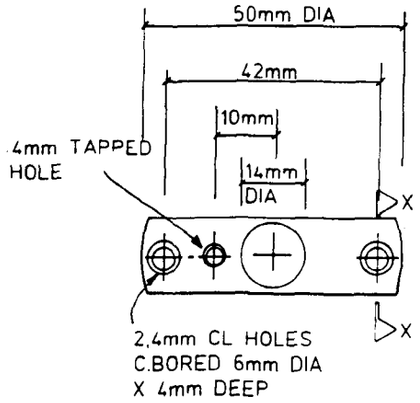

KEEPER MAT.L BRASS

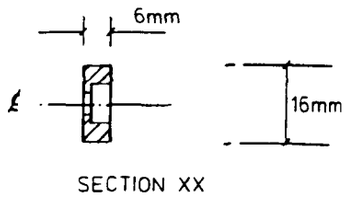

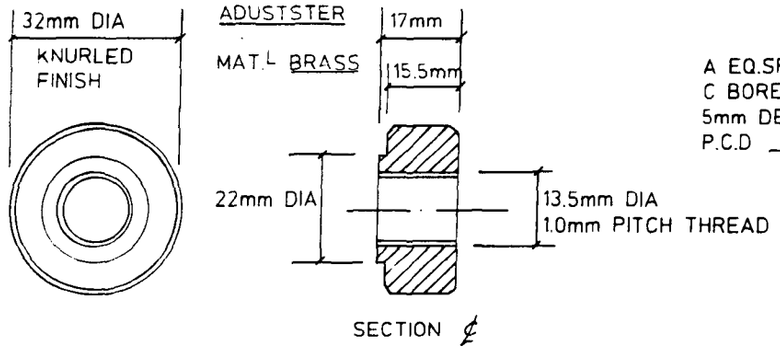

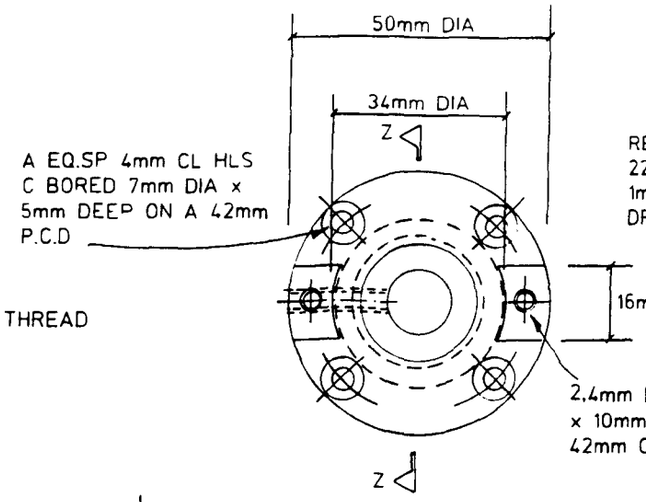

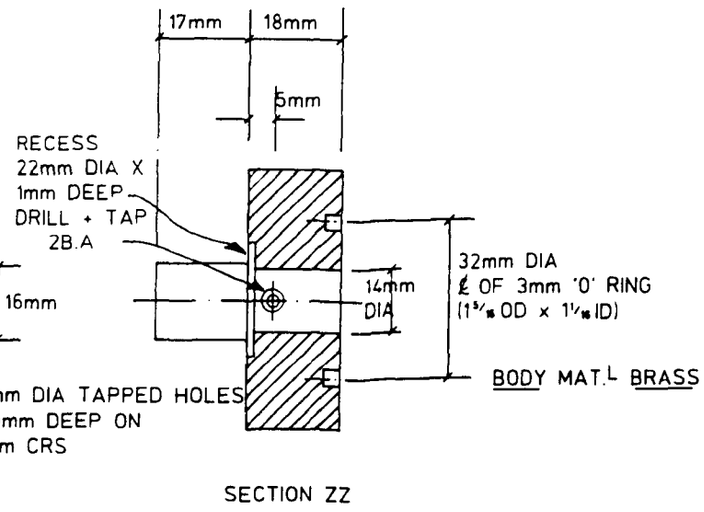

SECTION ZZ

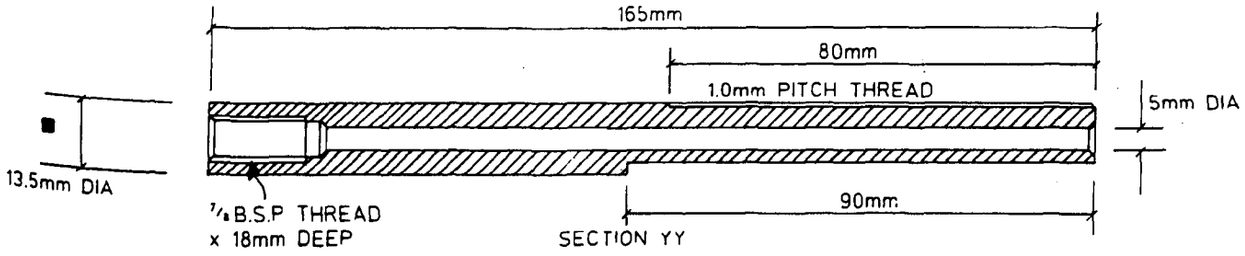

LEADSCREW MAT.L ST STEEL

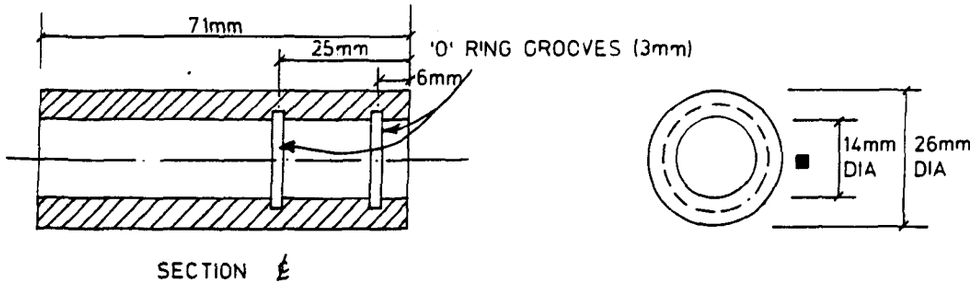

SLEEVE MAT.L Ph.B

N.B 26mm DIA. PUSH FIT IN CENTRAL RING (DRG.NoG219-9)
14mm DIA ■ REAMED FINISH

FIG 3.12
DETAILS OF THE PROXIMITY TRANDUCER MOUNTING UNIT

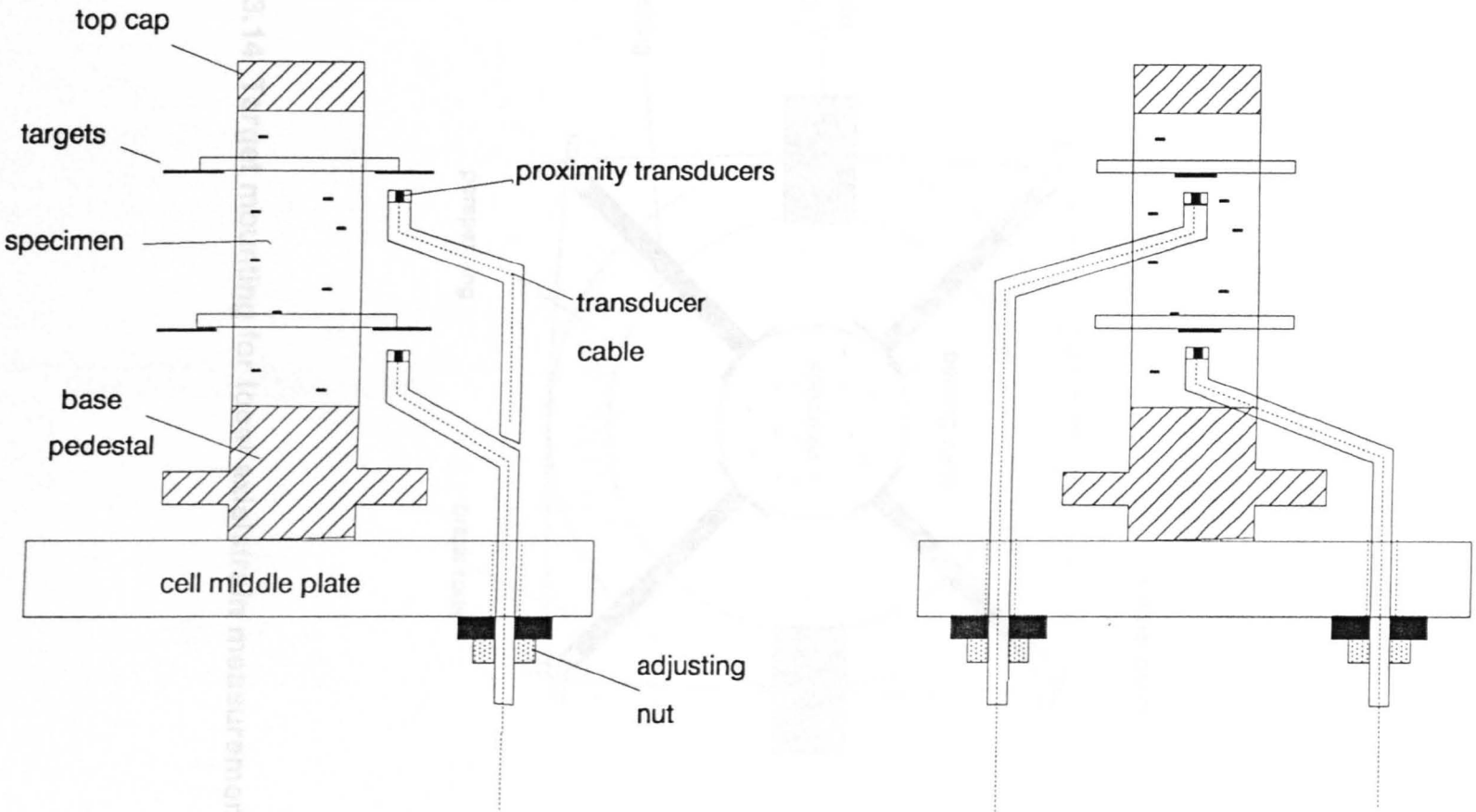

Fig 3.13 layout for local axial strain measurment (Elevation)

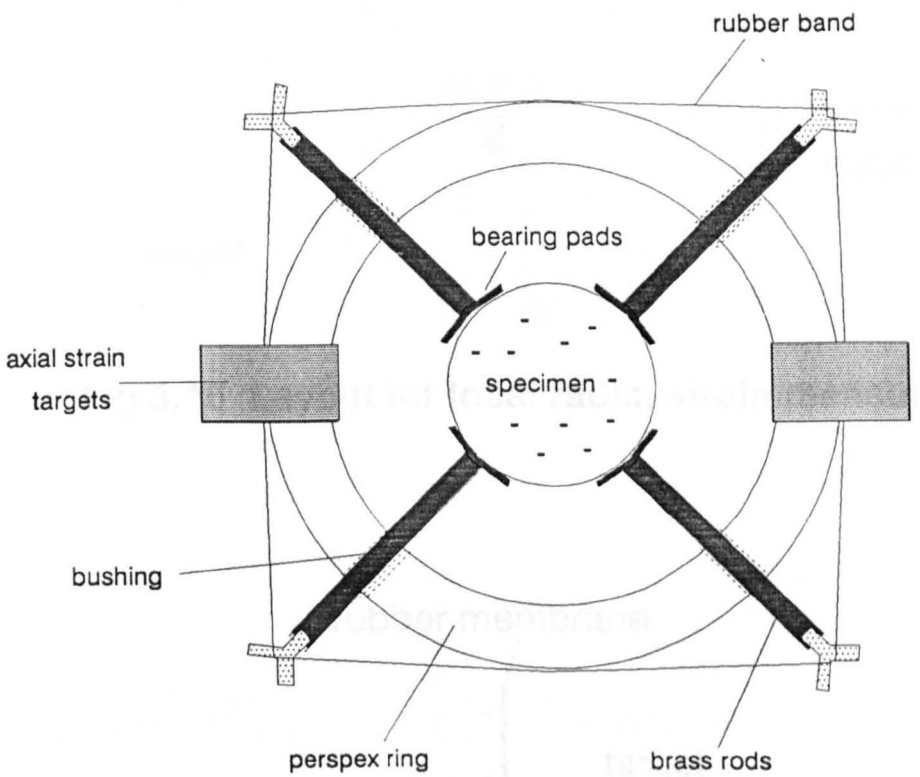

Fig 3.14 Target mounting for local axialstrain measurement

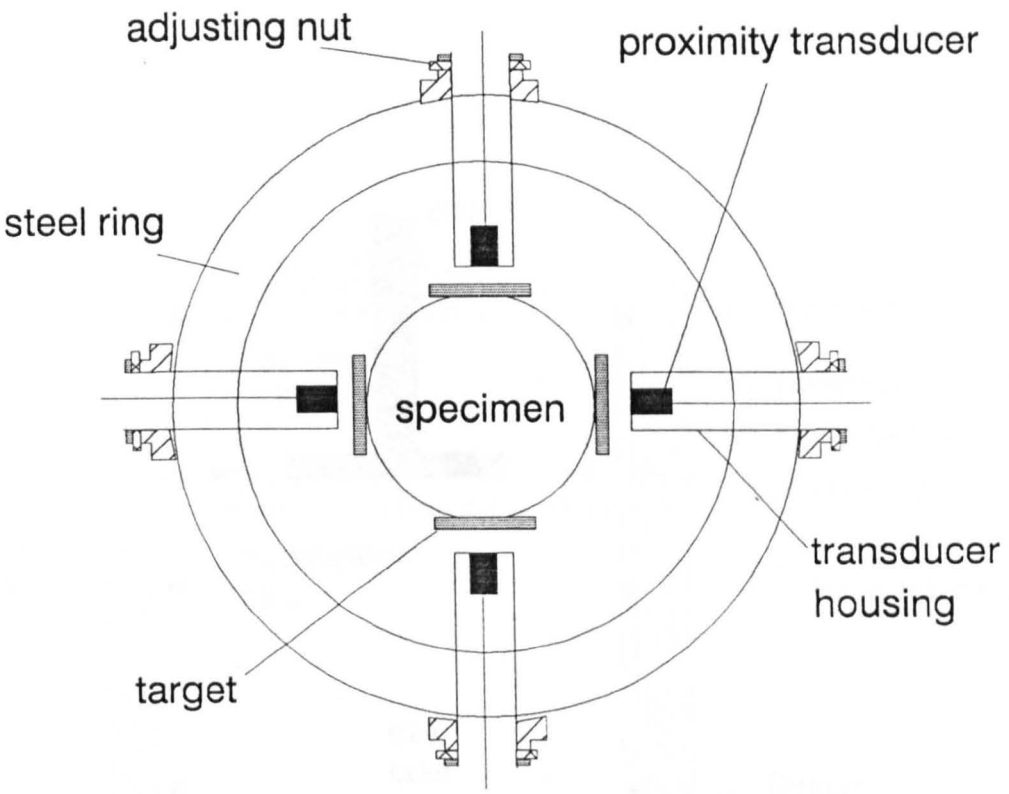

Fig 3.15 Layout for local radial strain measurement

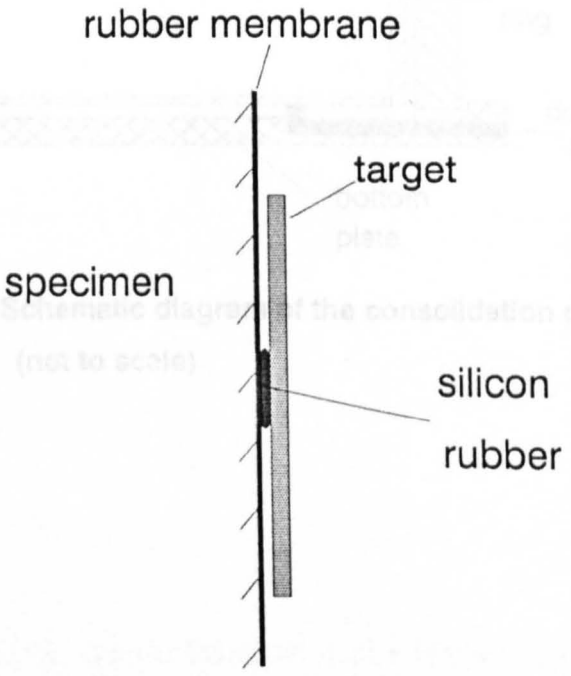

Fig 3.16 Method of attaching radial targets to specimen

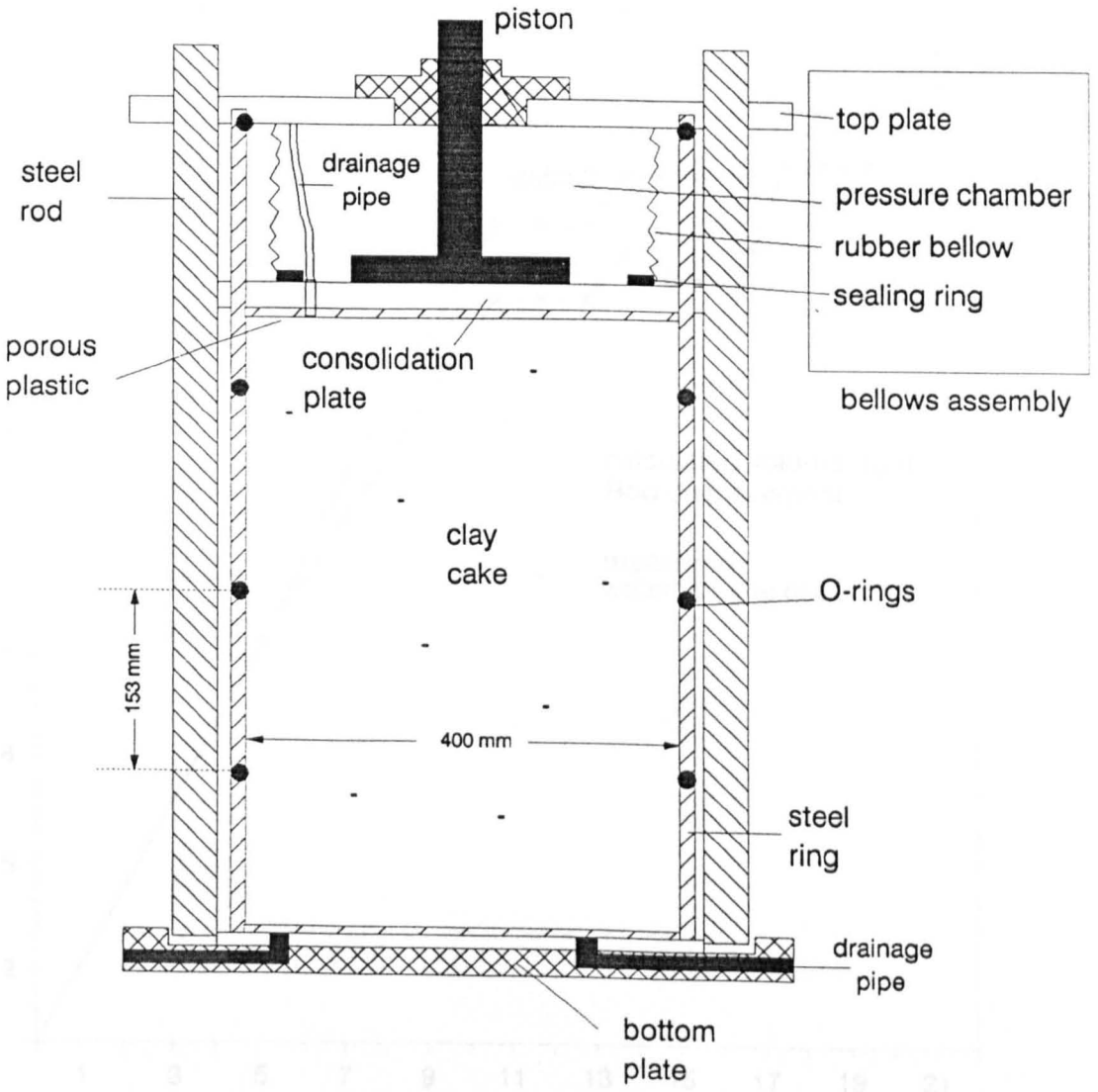

Fig 3.17 Schematic diagram of the consolidation pot (not to scale)

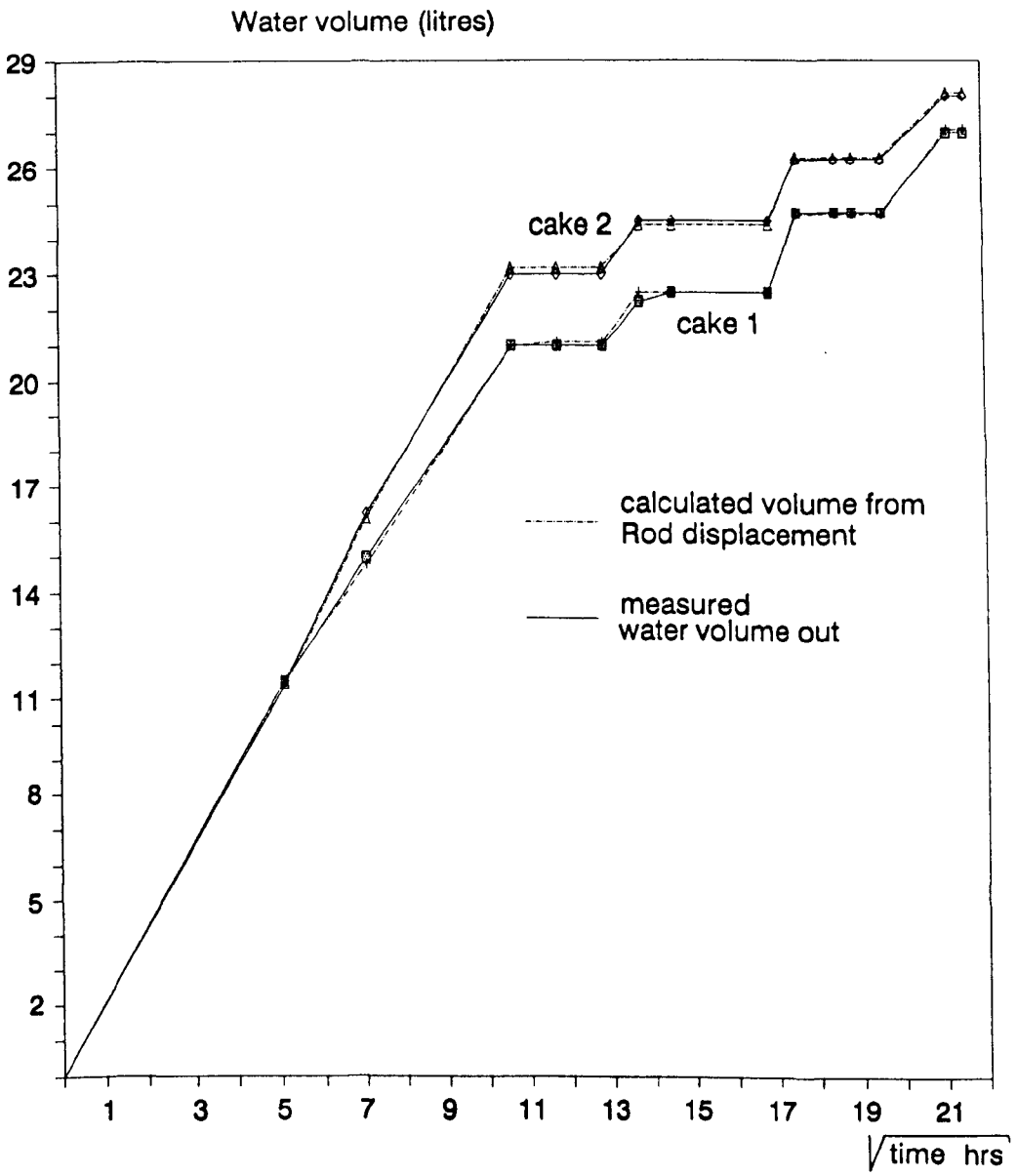

Fig 3.18 Consolidation histories of cakes 1 and 2

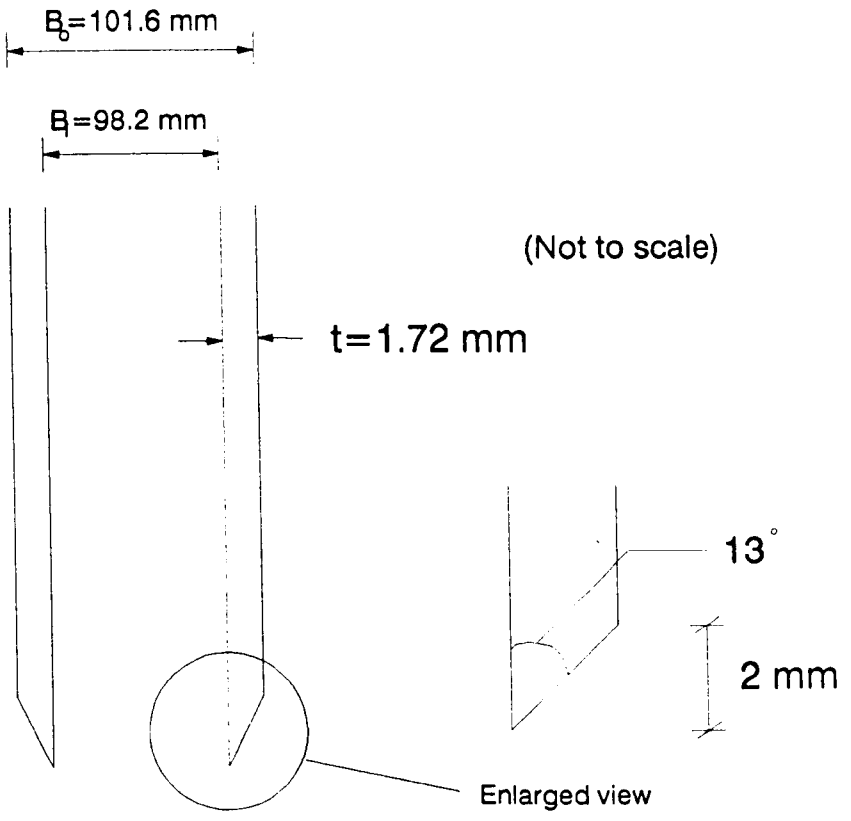

Fig 3.19 Geometry of the 100 mm sampler used for triaxial specimen preparation

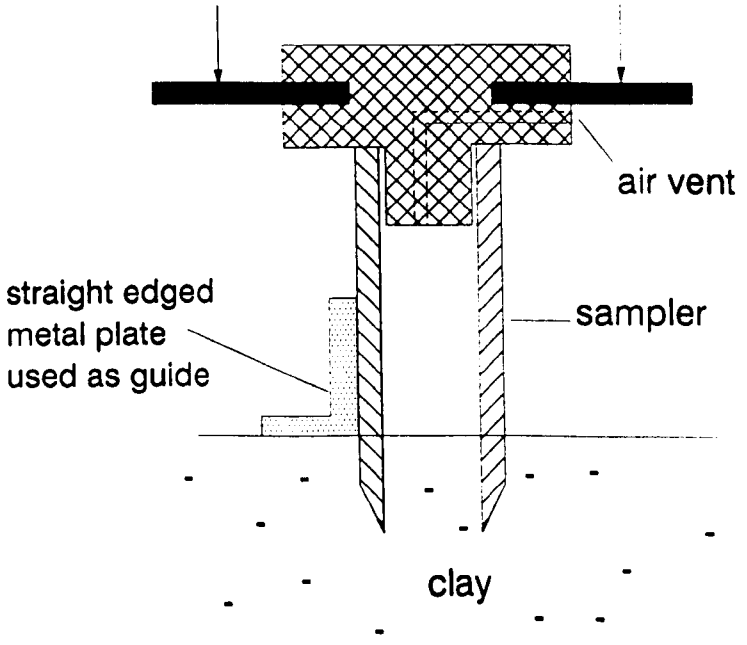

Fig 3.20 Method of sampler driving in the clay cake

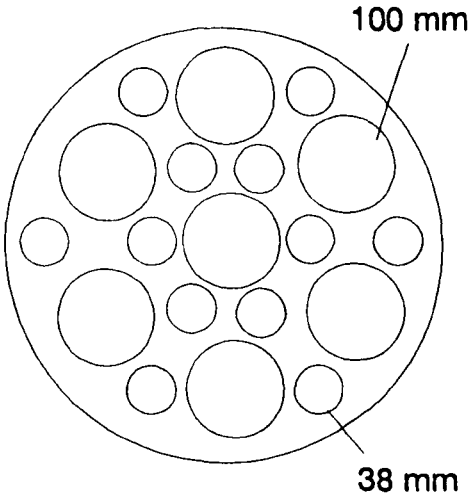

Fig 3.21 Positions of samplers pushed into the clay cake

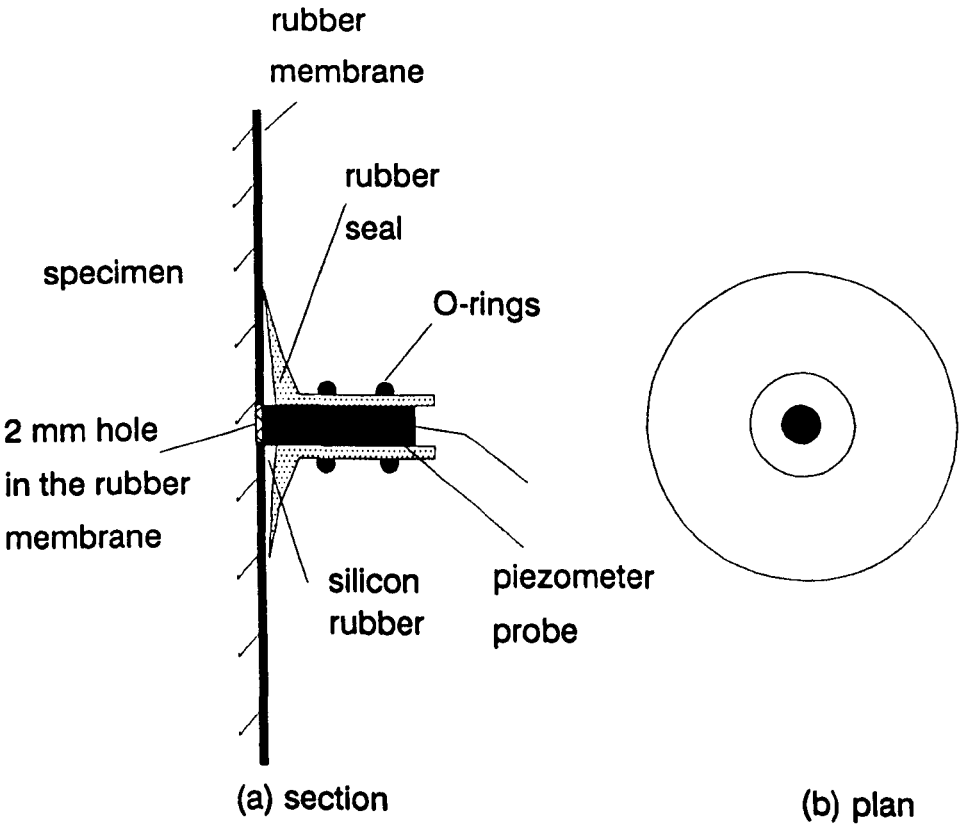

Fig 3.22 Rubber compartment for the mid-height pore pressure probe

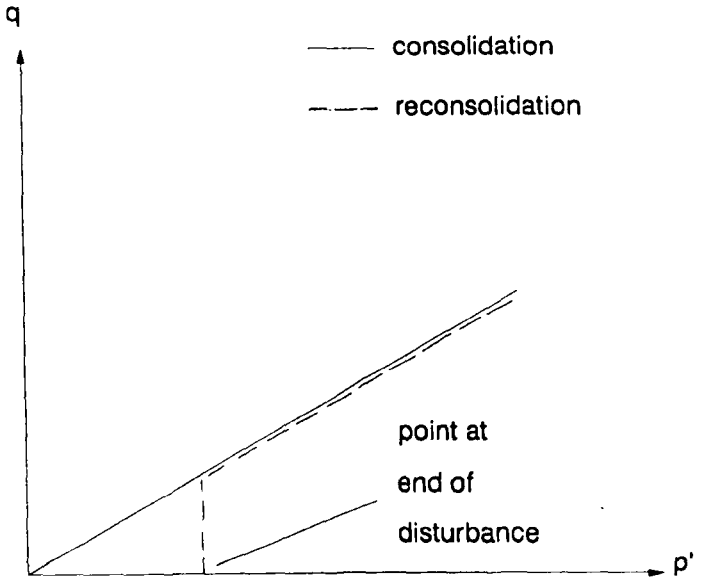

(a) normally consolidated

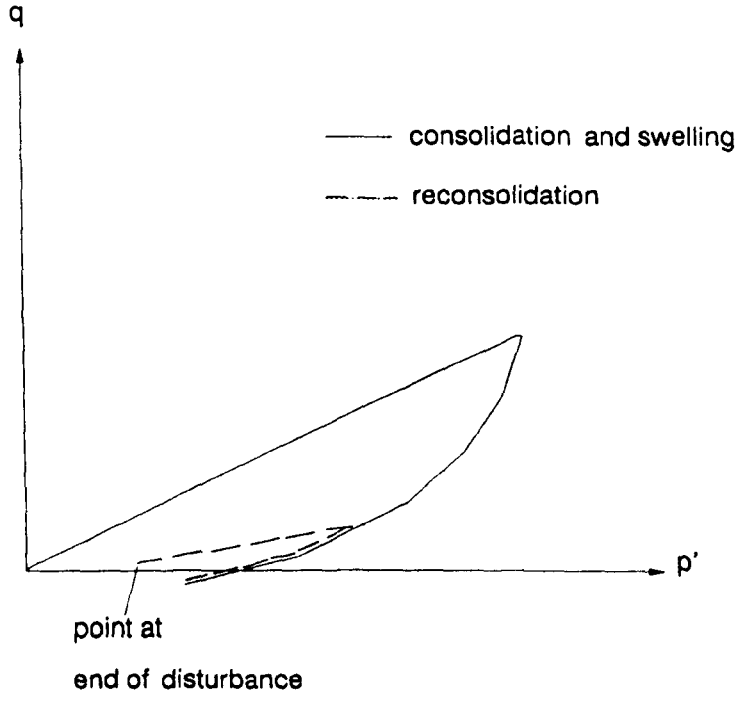

(b) overconsolidated

Fig 3.23 Diagrammatic representation of adopted reconsolidation paths

Chapter 4

COMPUTER PROGRAMS

4.1 Introduction

In order to implement the testing procedures described in the previous chapter (Section 3.6), a computerised control system was essential. In this chapter, the software used for both the 100 mm and 38 mm cells will be described, although the emphasis is placed on the former .

For the 100 mm cell, Yung (1987) had previously developed a computer program for stress path testing using the BASIC language on an Apple 2 Plus microcomputer (see Section 3.2.3). Although the software performed satisfactorily, it was difficult for anyone else to use, since information given to (and interaction with) the operator was kept to a minimum. It could have taken the Author longer to learn how to use this program and develop it further than to develop a completely new one. Some of the peripheral hardware used by the Author was different from that used by Yung and therefore the control statements would have been quite different. Fur-

thermore, the computer and the programming language used by Yung had become outdated. Running speed and storage capacities have increased tremendeously in recent years. For similar reasons, the 38 mm test system used by Ilyas (1983) needed further development in respect of both computer control and interfacing equipment.

For these reasons, it was decided to develop new computer software which would not only perform the desired tasks, but also would give the experimenter continuous information on the progress of the test and options to correct mistakes in input data or to change the course of a test. In addition to the computer software prepared for stress path testing, programs were developed for the analysis of data, as will also be briefly described in Section 4.3.5.

4.2 Requirements and General Approach

4.2.1 Test Control

The main requirements of the software were as follows :

- To initialise the hardware, select the channels to be scanned and set the corresponding gains.
- To take channel readings from the data logging interface and to convert these into engineering values using the appropriate calibration coefficients.
- To calculate stresses and strains along with other parameters (e.g. Poisson's ratio and B-value)

- To use these results to determine commands to be sent to the stepper motors so as to perform the desired test stage.

- To store data on the hard disc in both processed and unprocessed forms and provide back-up copies.

Depending on the microcomputer, hardware, and software language, a given task may take different times to complete. In programs which perform several functions, timing is important and the present generation of microcomputers cannot carry out a certain task unless the previous one has been completed succesfully. In this research, care had to be taken to prevent the computer from attempting to apply loads and retrieve data simultaneously.

4.2.2 Interaction with Operator

The main functions of the computer software in this respect were :

- To display channel readings and calculated parameters in an easily comprehended way on the screen and on a hard copy.

- To give information about the stepper motor command currently being carried out and the status of the computer (e.g. memory available).

- Wherever possible, to provide a graphical display of data on the screen and on a plotter during the test.

- To allow checks on input data and any necessary corrections to be made.

Interaction with the operator was carried out by making the computer present as many options as possible in the form of menus. This kept to a minimum the amount of typing required by the operator.

4.3 Description of the Computer Programs

Two different stress path programs were developed, one for the IBM compatible microcomputer, used to control the 100 mm cell, and one for the BBC microcomputer, for use with the 38 mm apparatus. Because both programs have similar basic features and adopt the same logic for controlling the stress path, only the software developed for the large cell will be described in detail.

4.3.1 Stress Path Program for the 100 mm Apparatus

The program is written in Microsoft QuickBasic 4 and made up of three modules called 'SM.BAS', 'SMLIB.BAS' and 'SMPATH.BAS', Figure 4.1. 'SM.BAS' is the main or controlling module, which performs tasks such as initialising the hardware, declaring and calling subroutines, and setting the updating interval (see Section 4.3.2). The other two modules are made up of subroutines only. 'SMLIB.BAS' contains those dealing with data logging and presentation, file management, and menu displays. 'SMPATH.BAS' contains some subroutines for controlling the stepper motors and others for data conversion into engineering values and error trapping.

As shown in Figure 4.2, the program involves a main menu of three options :

4.3.1.1 The 'Test' option

When this option is chosen, the program first carries out a survey of the existing files in the directory allocated for stress path testing (see Section 4.2.2). This ensures that no existing file gets overwritten or deleted. Readings from the nineteen channels are then displayed on the screen as shown in Figure 4.3. In addition, the average local axial strain ϵ_ℓ, the two radial strains ϵ_{r1} and ϵ_{r2}, the average end cap strain ϵ_{ec}, the average external strain ϵ_{ex}, and the average pore water pressure in the specimen u_{avg} are calculated and displayed. Figure 4.4 shows how the screen is divided into four windows. Window 1 is where the data are displayed, window 2 displays information about the current operation being carried out by the computer, window 3 displays the current stage of the test (i.e saturation, consolidation or shearing), and window 4 contains a submenu of options as follows.

- The 'Units' option : data in window 1 can be presented in either engineering units (see Figure 4.4) or unprocessed form (mV). The latter mode is useful when the operator wants to check that the transducers are working in their calibrated range. The display can be switched from one mode to another by pressing the Ctrl + U keys. When a transducer is out of range, the term 'O.o.R.' starts flashing to indicate so.

- The 'Values' option : this allows the operator to display the last values logged on the disc in either engineering units or unprocessed form and, by pressing the Ctrl+V keys, a comparison with the current values is possible. As will be described in Section 4.3.2, the computer updates the channel readings every 5 seconds, but the logging interval on the disc is usually much larger and depends on the test stage. This option is useful in deciding when to stop the test and in checking whether the logging interval is satisfactory.

- The 'Pause' option : it is sometimes desirable in stress path testing to allow the test to be stopped for a period and then continued from the stoppage point. This was certainly necessary in the present research. As explained in Chapter 3, the local axial and radial strain measurements were carried out using proximity transducers which could be manoeuvered from outside the triaxial cell. From time to time adjustments were required to bring the targets back within range. Pressing of the Ctrl+P keys stops all the operations being carried out by the computer, except the updating and display of the channel readings on the screen. Adjustment of the positions of the transducers can then be performed, at the end of which pressing of the Ctrl+C keys allows the test to be resumed. On average the transducer adjustment takes about 5 minutes and therefore does not affect the implementation of stress paths that have reasonably low stress or strain rates.

  Feed back is very important if the stress path is to be followed accurately. Special commands have been included in the program which check whether the channel readings are reasonable and if not, the test is paused automatically until the operator has made sure that it is sensible to continue.

- The 'Stage' option : when the stress path program is first started, the display shown on the screen after the 'Test' option has been selected from the main menu contains in window 3 the instruction "Select a stage to start". By pressing of the Ctrl+S keys a submenu of the test stages shown in Figure 4.2 appears in window 3. These stages will be discussed in detail in Section 4.4. Once the stage selection has been completed, the name of the stage and its corresponding data filename are displayed.

- The 'Graph' option : a graphical display of certain parameters, as indicated in Table 4.1, is available during any test stage. When the Ctrl+G keys are

pressed, the numerical display shown in Figures 4.3 and 4.4 disappears and is replaced by the graphical display. Hard copies of these graphs can be obtained at any time. To return to the numerical display, the same keys are again pressed. This option permits the behaviour of the specimen and progress of the test to be rapidly assessed.

- The 'Quit' option : although this option is not actually displayed in window 4, the program can be permanently stopped (rather than paused) by pressing the Ctrl+Q keys at any time. The main menu is again displayed and the test can only be continued by reselecting the test stage.

4.3.1.2 The 'File' option

Subroutines are provided to make sure that back-up copies of data are automatically taken as soon as a test stage finishes. The files for each stage are properly named and stored in the relevent directory. As shown in Figure 4.2, a submenu of the following options is provided .

- The 'View' option : this option permits the operator to look at the data from a completed or partially completed test stage before moving on to another one. The operator is provided with some extra information (e.g. file size and logging interval).

- The 'Print' option : a hard copy of data can be obtained. This is important since data on the storage discs of the computer can be lost or corrupted.

- The 'Delete' option : unwanted files in the stress path testing directory can be deleted.

- The 'Quit' option : when this option is chosen the operator is taken back to the main menu.

4.3.1.3 The 'Quit' option

This option allows the operator to quit the program and return to the Quick Basic 4 editor environment.

4.3.2 Algorithms of Test Stages in the 100 mm Apparatus

The stress path test is divided into five main stages, namely saturation, isotropic consolidation, one-dimensional consolidation, one-dimensional swelling and shearing. Each stage can be carried out independently of the others. For example, if saturation is not required, the operator can choose to go straight to a consolidation or shearing stage.

4.3.2.1 Saturation

The logic of this stage is shown in Figure 4.5. Although it is controlled by the computer, valves to open and close the drainage lines to the specimen have to be operated manually. Incremental cell and back pressures are applied and a check on the B-value is subsequently carried out. At the beginning of the stage, values of cell and back pressure increments must be fed to the computer as well as the desired value of B. Once the data file name and logging interval have also been specified, the saturation starts and a display similar to that shown in Figures 4.3 and 4.4 appears on screen. The current B-value is displayed in window 1. After

an increment of cell pressure has been applied, the computer waits until the pore pressure reading at the middle of the specimen is within 2.5 kPa of those at the top and bottom before displaying the average calculated value of B (If the operator wishes to continue the stage without waiting until the above specified condition is achieved, then it is possible to press the Enter key and proceed). If the average B-value is larger than the desired value, the computer applies the last back pressure increment and terminates the stage. If, on the other hand, this value is not achieved, a back pressure which is less than the cell pressure by about 7 kPa is applied and the computer waits until the pore pressure in the specimen is uniform (within ± 2.5 kPa) before applying the next cell pressure increment. (Again, the operator can also proceed without waiting by pressing the Enter key).

4.3.2.2 Isotropic consolidation

This stage is completely controlled by the computer. The required input data are the desired change in effective pressure and the number of steps to achieve it. The current cell presssure is calculated from the equation :

$$\sigma_3 = \sigma_{3i} + \Delta\sigma_3^{'}/(nn - (f - 1)) \tag{4.1}$$

where σ_{3i} and $\Delta\sigma_3^{'}$ are the total cell pressure at the beginning of the consolidation stage and the desired change in effective pressure respectively, and nn and f are the number of steps and the current step number respectively. The computer waits until 90% dissipation of the average excess pore water pressure has been achieved during the current step before moving on to the next one. (Pressing the Enter key would make the computer go to the next step without waiting for 90% pore pressure dissipation).

Isotropic swelling can be carried out using the same algorithm by specifying

a negative value for the desired change in effective cell pressure ($\Delta\sigma_3'$).

4.3.2.3 K_0-Consolidation

After completion of the saturation stage, the load cell is connected to the specimen top cap as described in Section 3.3.1. During K_0-consolidation the specimen is consolidated to a specified vertical effective pressure without allowing the lateral strain and the excess pore water pressure to exceed specified limits of $\pm 0.005\%$ and 10 kPa respectively (see Section 3.6.2).

The flow chart for this stage is presented in Figure 4.6. Once the maximum vertical effective pressure and the logging interval have been specified, the computer starts the stage by applying small increments of lower chamber pressure (equivalent to about 0.9 kPa of axial stress) and checks on the radial strain as well as the excess pore pressure at the middle of the specimen. If the values are within the specified limits, another increment of axial stress is applied. If, however, the radial strain exceeds either the upper or lower limit, the radial stress is altered in small increments (about 0.4 kPa) accordingly until the strain is back in range. The radial strain used in this stage is the average of two measurements, each calculated from the readings of a pair of proximity transducers (see Figure 3.15). It was realised that any of these transducers could accidentally go out of range (e.g. due to detachment of the metal target, as happened during one of the tests). If this happens, the computer ignores the faulty reading and takes the radial strain from the other pair of transducers providing these are still in range. Otherwise the test is paused. Proving tests (Section 5.5) showed that, even after the maximum effective pressure had been achieved, some volume change still took place which could be attributed to secondary compression. Therefore, the computer continues to log data indefinitely

until the operator decides to terminate the stage.

K_0-swelling is carried out in a similar manner to K_0-consolidation. However, a desired OCR value is specified instead of a target effective pressure.

At the end of these two stages, the drainage valves have to be closed manually if loading is to be performed under undrained conditions.

4.3.2.4 Shearing stage

This stage involves two main subroutines, one for stress path testing and the other for simulating sampling disturbance by applying a strain cycle (see Section 3.6.4).

As shown in Figure 4.7, once the shearing stage has been selected, the operator is given the option of applying a strain cycle or going straight into a stress path application. When the first option is selected, the operator is asked to specify the magnitude of the strain cycle to be applied, the logging interval and the data file name. The axial stress is then varied so as to achieve the strain cycle, while the cell pressure is kept constant. The increments of axial stress decrease in size as the strain approaches the specified limit to avoid overshooting it.

In the present work after the strain cycle had been completed, the axial stress was altered slowly until the deviator stress became very small, i.e. within a range of ± 1 kPa. In the case of normally consolidated clays, the pore pressure in the specimen after the strain cycle was much higher than the initial back pressure. The axial and radial stresses were therefore decreased in parallel until the pore pressure in the specimen became equal to the back pressure. Changes in pore pressure resulting from the strain cycle in the case of overconsolidated clays were very small. Therefore,

no such changes in total pressure were required. When the drainage valves were reopened, the reconsolidation to the initial stresses (see Section 3.6.4) could be started. Reconsolidation was carried out using the second option available in the shearing stage (i.e. stress path application). A stress path for reconsolidation was specified which lay as close as possible to the original consolidation stress path, with a similar rate of axial stress change.

In the Bishop and Wesley apparatus, the radial stress can be controlled directly, while the axial stress is controlled indirectly via the lower chamber. The relationship between the axial stress and the lower chamber pressure is given by the following eqaution :

$$\sigma_1 = \sigma_{lc}(a/A_c) + \sigma_3(1 - a/A_c) - W/A_c \tag{4.2}$$

where σ_{lc} is the lower chamber pressure, a is the bellofram seal area, A_c is the cross-sectional area of the specimen and W is the weight of the piston and other moving components including the specimen and top cap. It is possible to measure or calculate the quantities a, A_c and W and develop software based on Equation 4.2. However, experience in this and previous research has shown that friction losses usually occur in the bellofram seals and the bushing (or bearing) in which the piston slides, thus making Equation 4.2 inaccurate. By using an internal load cell to measure the deviator stress this problem can be avoided. Then axial stress is simply calculated as :

$$\sigma_1 = q + \sigma_3 \tag{4.3}$$

where q is the deviator stress measured by the load cell.

When taking the option of applying a stress path, the operator is asked whether it is to be specified in terms of the principal stresses (σ_1 and σ_3) or the parameters q and p . As shown in Figure 4.8, the stress path can be divided into a

number of sections with different directions. The number of sections for the complete stress path must be entered. For each section the coordinates of the starting and finishing points are specified, along with the axial stress rate R_1. The radial stress rate is calculated by the computer as

$$R_3 = \frac{\sigma_{3f} - \sigma_{3i}}{\sigma_{1f} - \sigma_{1i}} \times R_1 \tag{4.4}$$

where the subscripts f and i stand for the end and beginning of a section on the stress path respectively. With the aid of the computer timer, the desired changes of axial and radial stress are calculated from any given point reached on the stress path according to the following equations

$$\Delta\sigma_1 = R_1 \times \Delta t \tag{4.5}$$

$$\Delta\sigma_3 = R_3 \times \Delta t \tag{4.6}$$

where Δt is the change in time. As soon as either of these changes exceeds 0.9 kPa, the new values of σ_1 and σ_3 to be applied are calculated from the following equations

$$\sigma_1 = q_c + \sigma_{3c} + \Delta\sigma_1 \tag{4.7}$$

$$\sigma_3 = \sigma_{3c} + \Delta\sigma_3 \tag{4.8}$$

where the subscript c stands for the current values. The appropriate stepper motors are then activated by the computer until the axial and radial stresses are within $\pm$ 0.2 kPa of their desired values. This range has been specified after taking into consideration the sensitivity of pressure control via the lower chamber (i.e. area ratio a/A) and the accuracy of deviator stress measurement.

As the specimen approaches failure, two conditions are specified to avoid any damage to the specimen or the instrumentation. The test will stop, firstly, if the

axial strain rate exceeds 20 %/hr or, secondly, if the external axial compressive strain exceeds 10 %. At any time during the shearing stage, the 'Pause' option (see Section 4.3.1) can be used to temporarily disable the computer control and allow manual operations to be carried out.

4.3.3 Stress Path Program for the 38 mm Apparatus

Many of the options and facilities available within the software developed for the IBM computer and the 100 mm cell could not be provided in the corresponding software for the BBC computer and the 38 mm cell. This was mainly due to the limitations of the BBC computer concerning memory size, graphical display, and programming language. However, software with as much flexibility as possible was prepared based on the principles explained in the previous section. K_0-consolidation and K_0-swelling routines were not developed since the present work on the 38 mm cell only involved isotropic consolidation. The program consists of one module which incorporates all the statements and subroutines.

4.3.4 The Use of Lotus 123 and Other Programs for Data Analysis

Lotus 123 is a commercially available computer package that can be used on IBM compatible microcomputers for data processing and manipulation. Mathematical and statistical analyses can be carried out as well as graphical representations. Data from both cells were loaded into the Lotus 123 spreadsheet where they could be easily viewed and checked. However, all the original data files had first to be reformatted to be accepted by Lotus 123, by means of some QuickBasic 4 programs specially

developed for this purpose. These programs carry out checks on the conversion of the channel readings into engineering values, allocate titles and arrange miscellaneous information for each test. A variety of 'macro' programs were developed within Lotus 123 to carry out regression analysis and curve fitting by different methods. Calculations of tangent and secant stiffness could also be carried out, as described in more detail in Chapter 6.

Stage	Graphic Display
Saturation	B-value vs σ_3 ; σ_3 and σ_{bp} vs σ_3
Consolidation	Δ V vs $\sqrt{t}$; q vs p' ; u_{avg} vs σ_1'
Swelling	ditto
Shearing	q vs ε_1 ; u vs ε_{ex} ; ε_r vs ε_1 and q vs ε_1 ε_{ec} and ε_{ex}

Table 4.1 Graphic display of parameters during testing

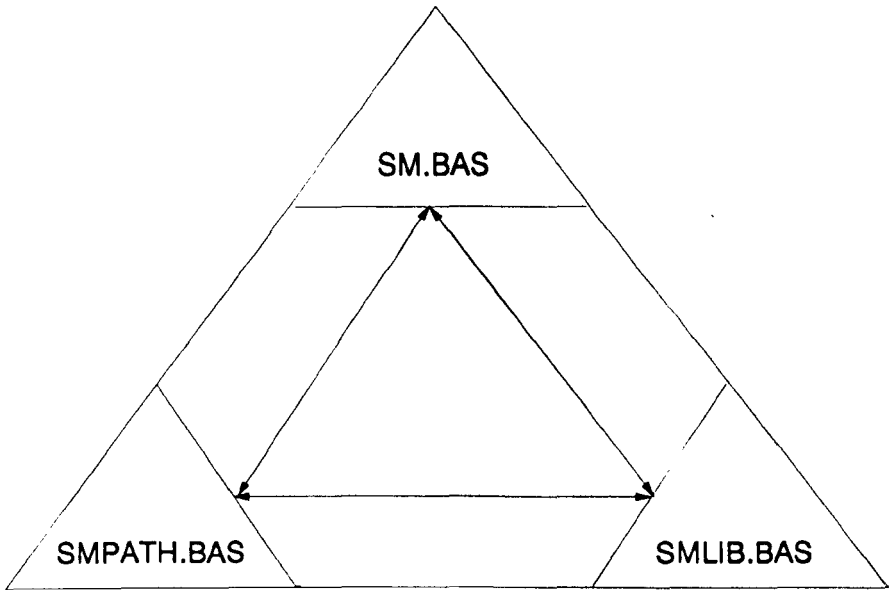

Fig 4.1 Structure and main modules of the computer program for the 100 mm cell

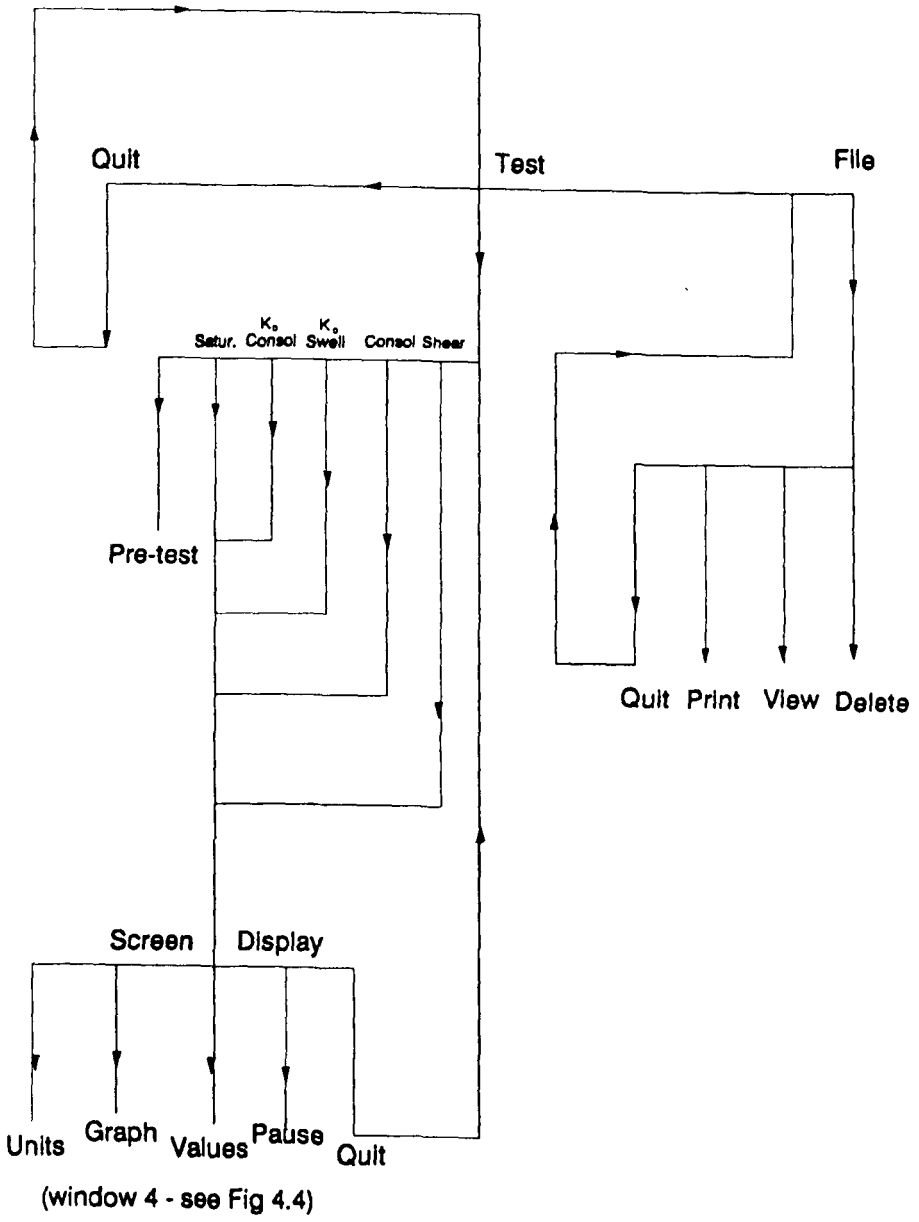

Fig 4.2 Available menus in the 100 mm cell stress path program

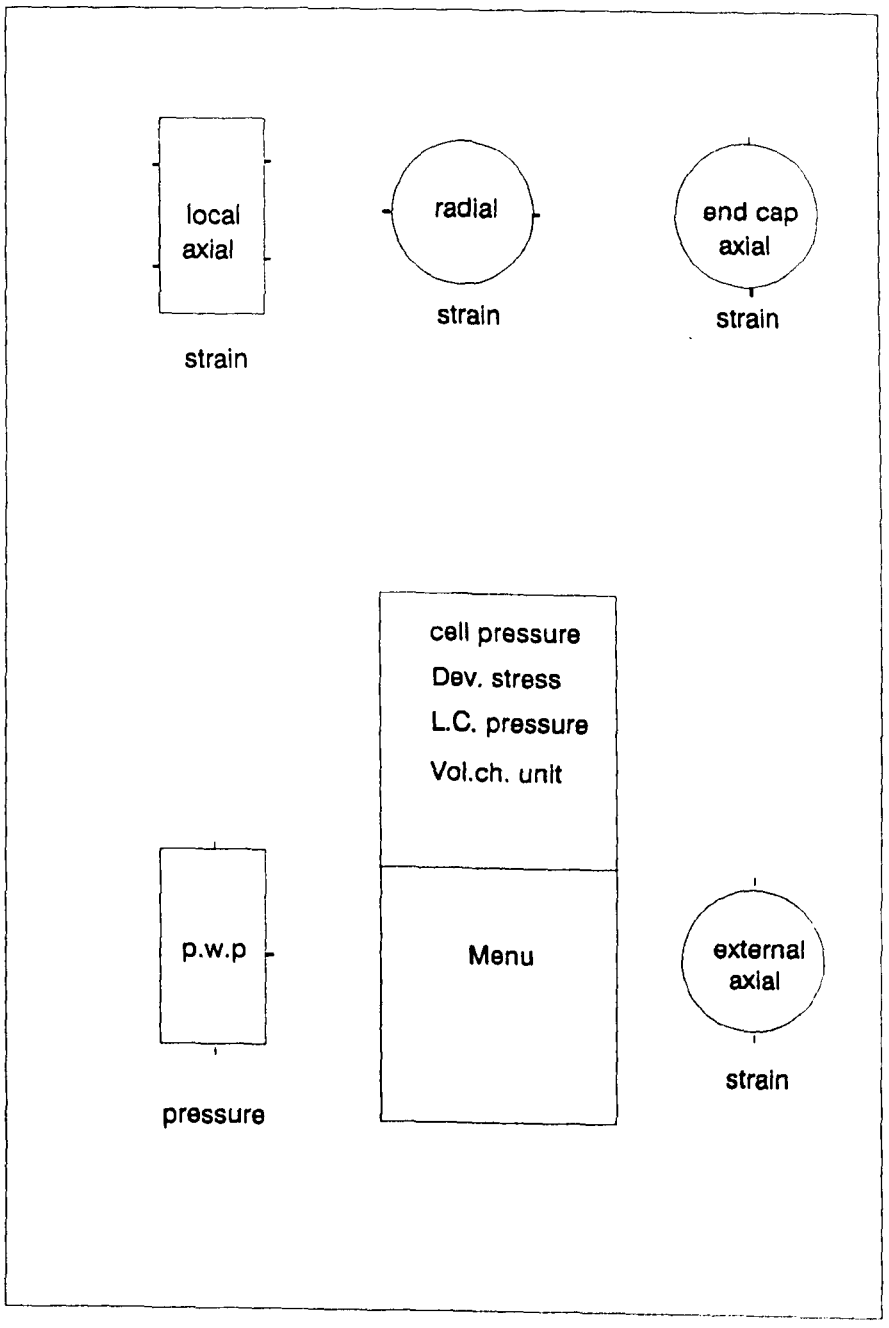

Fig 4.3 Layout of channel readings on the computer screen

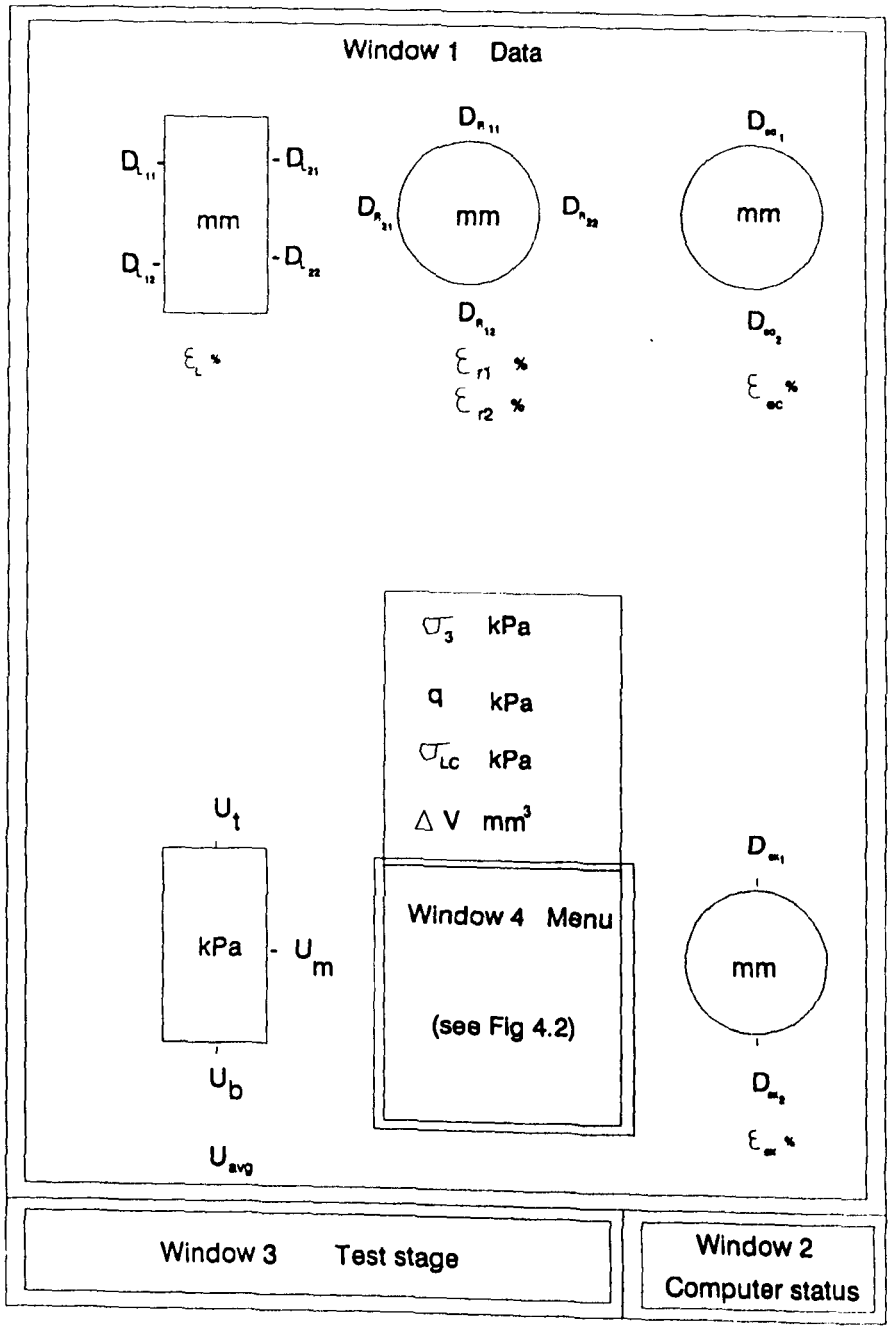

Note : D represents displacement in mm

Fig 4.4 Division of computer screen into windows

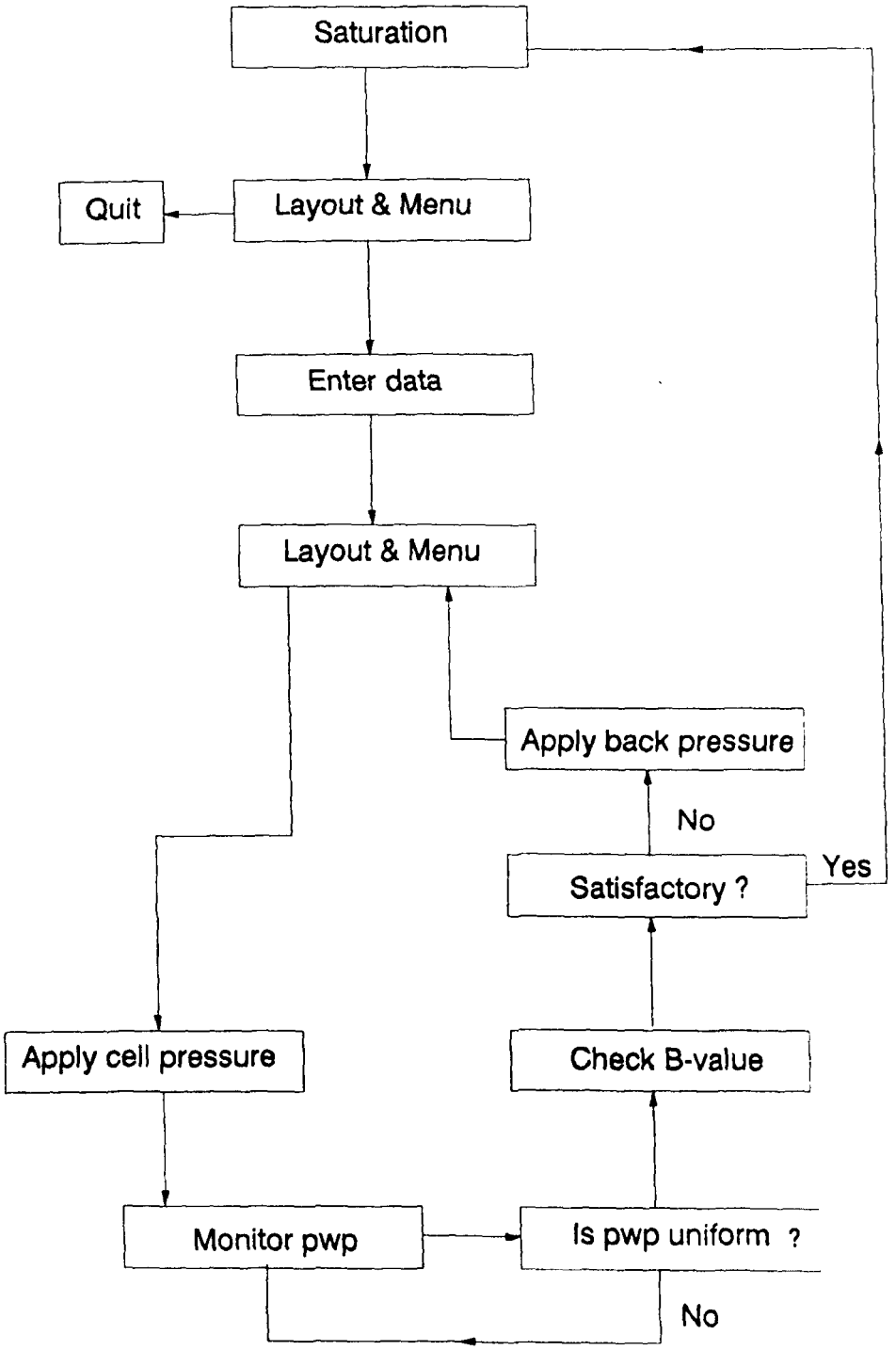

Fig 4.5 Flowchart for the saturation stage

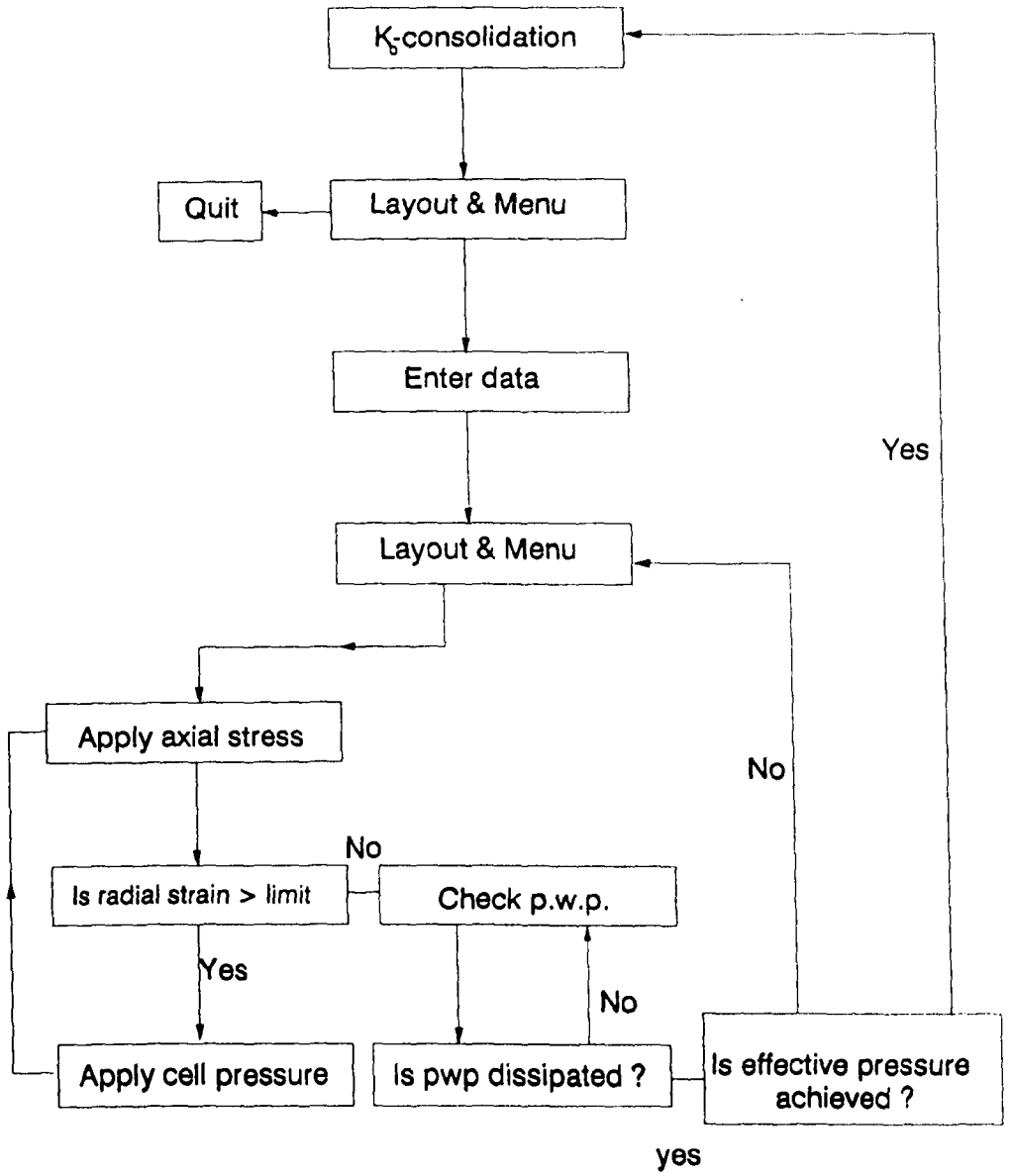

Fig 4.6 Flowchart for the K-consolidation stage

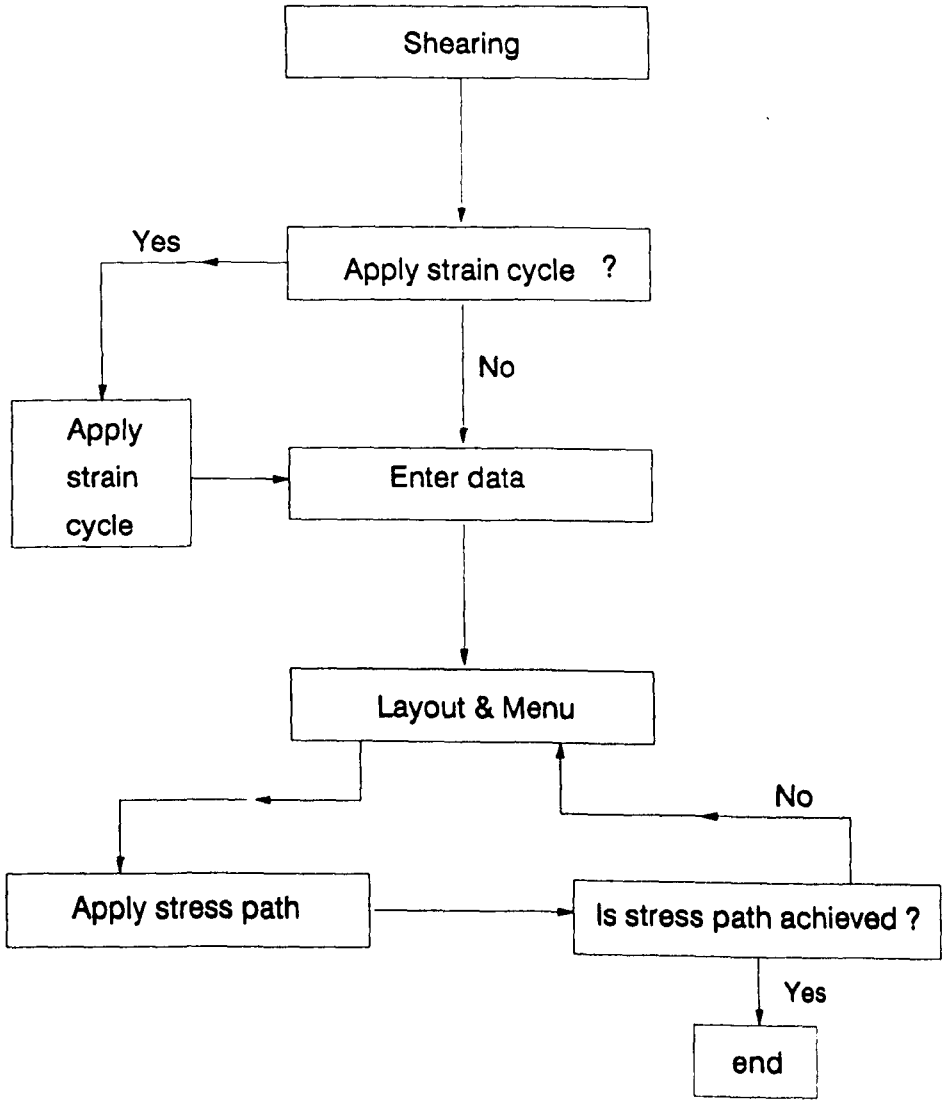

Fig 4.7 Flowchart for shearing stage

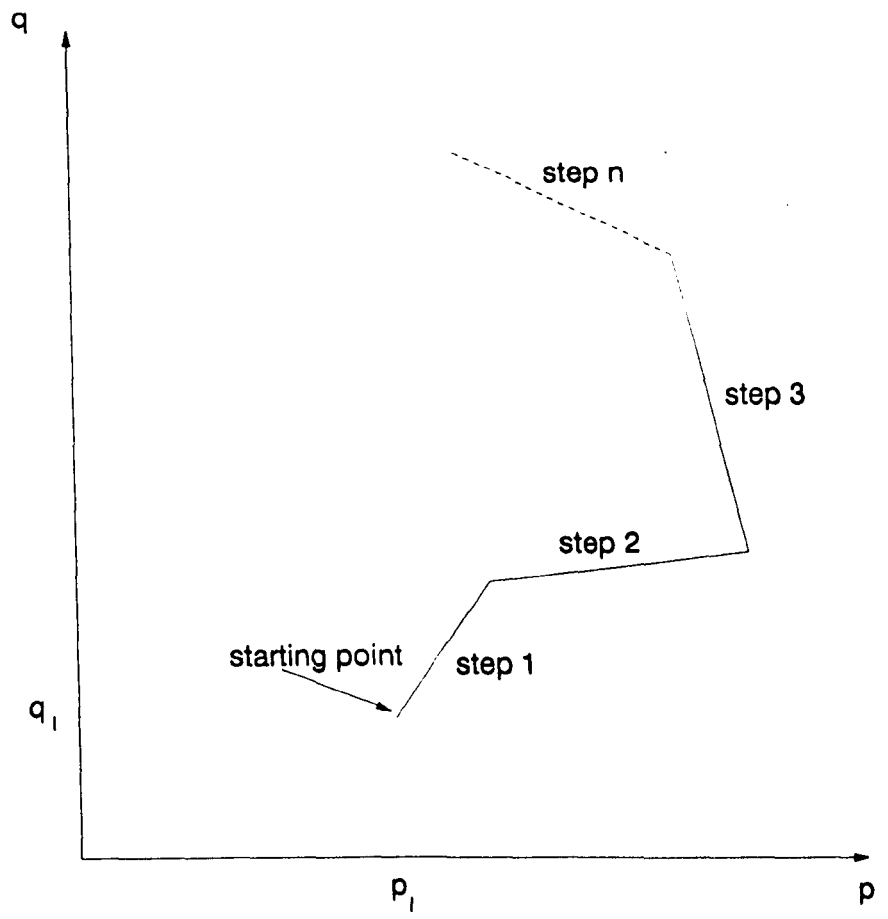

Fig 4.8 Schematic representation of a computer specified stress path

Chapter 5

CALIBRATION METHODS AND PROVING TESTS

5.1 Introduction

In the research being described, careful attention has been given to the determination of calibration factors for the transducers. The first section of this chapter describes the methods of calibration adopted and contains a discussion of the factors affecting the calibration results. Stresses and strains may be readily calculated from the readings of the transducers using the calibration factors. However, it is important to quantify the errors in the calculations, if a proper evaluation of the small strain stiffness of the soil is required. In the second section of the chapter the errors in the strains and the deviator stress are analysed; a similar analysis could be performed for other parameters. Proving test results are presented in the third section, along with a discussion of their implications for the main testing programme (outlined in Section 1.3 and described in Section 6.2)

5.2 Calibration of Transducers

In order to achieve reliable calibration data, it was important to minimise the difference between conditions during calibration and those during actual testing. All the calibration tests were performed in the temperature controlled room where the stress path testing was to be done. Additional tests were sometimes carrried out to check whether a change in the ambient conditions would have a significant impact on the calibration data.

Special computer programs were prepared for calibration purposes and changes in the output of the transducers during calibration were recorded automatically. Electronic arrangements (e.g. wiring and gain setting) during calibration were similar to those during testing. A minimum of three cycles of pressure, load or displacement was adopted for each transducer as appropriate. The methods of data analysis varied from one transducer type to another depending on the output (i.e. degree of non-linearity) and the level of precision required. Precision is defined as the scatter of measurements above and below a mean value and involves random errors only. All values of precision in this chapter are quoted with not less than 95% confidence unless otherwise stated. During calibration the errors include those in the calibration device. To take account of the systematic errors in the calibration device, it was necessary to rely on the quoted accuracy.

The determination of the calibration factors was carried out using two statistical computer packages. The first one, called MINITAB and available on the University's mainframe computer, was used to carry out regression analyses with different mathematical functions including various degrees of polynomial. Data points with exceptional deviations could be ignored and their effect on the overall precision

determined. The second one was the Lotus 123 spreadsheet package (see Section 4.4) This enabled checks on the calibration factors to be carried out and plots of fitted and actual calibration data to be produced.

Before the calibration of each type of transducers is described in detail, some general factors with potential effects on the calibration results or their use will be briefly discussed.

5.2.1 Non-linearity and Hysteresis

As mentioned above a minimum of three cycles of the measured quantity was used in the calibration of every transducer. Therefore the effects of non-linearity and hysteresis defined in Figure 5.1 could be taken into account, by fitting the calibration curve to all of the data collected. However, these effects were not serious since in all cases the precisions obtained were satisfactory. The load cells and pressure transducers did show some hysteresis so that the precision based on data from one half cycle was slightly better than that for all three cycles. Although separate calibrations could have been adopted for loading and unloading directions, this would have made the transformation to engineering units during testing more complicated, especially for applications where the readings from the transducer were liable to fluctuate.

5.2.2 Temperature Variations

Both the calibration and testing were carried out at a temperature of 20 $^{\circ}C \pm 1\ ^{\circ}C$. Thus, the temperature fluctuations were too small to cause any detectable

changes in transducer output. Although water used to fill the cells often had a temperature considerably lower than 20 $^{\circ}C$ and therefore could have affected the transducer output, by the time the specimen had been saturated the cell water had reached room temperature. The effect of any temporary temperature variation was disregarded.

5.2.3 Noise and Drift

Noise is fluctuation in transducer output caused by electrical effects. In the present work steps were taken, wherever possible, to reduce or eliminate noise (e.g. installation of filters). Each measurement from a proximity transducer was actually the average of ten readings, in order to minimise the effects of noise.

The drift of transducer output with time was also investigated. The results showed that the drift over a period of one month (a typical test period) was very small compared to the precision achieved during calibration. Calibration factors of transducers may also change with time. This was checked by carrying out calibration tests on selected transducers after all testing had been completed (all the transducers were initially calibrated before testing started). It was found that no significant changes in the calibration characteristics had taken place over the testing period. In addition, the last test carried out in the 100 mm cell was a repeat of the first test. Similar results from the two tests indicated that gross changes did not take place.

5.2.4 Proximity Transducers

As explained in Section 3.4, the proximity transducers were used in the 100 mm triaxial cell to measure local axial and radial displacements, from which the corresponding strains in the specimen can be calculated.

Figure 5.2 shows the calibration arrangement. It involved the use of a micrometer mounted above a V-shaped steel block (A) (Figure 5.2a) on a metal frame (B) so that the micrometer spindle head (C) is within the two inclined sides of the block. The micrometer was used only as a convenient seating arrangement, i.e. the spindle head was not adjusted during calibration. A proximity transducer within the housing described in Section 3.4 and Figure 3.12 was mounted on the metal frame so that its head was opposite the micrometer spindle head within the sides of the steel block. A 30 mm × 30 mm × 1 mm thick magnetic stainless steel plate (D), used as a target (see Section 3.4.6), was attached to a 20 mm × 20 mm × 10 mm steel block (E) as shown in Figure 5.2b. The assembly was placed in front of the transducer with block E in contact with the micrometer spindle. By wringing together a given number of slip gauges in accordance with the British Standard (1968) and placing them between block E and the micrometer spindle (Figure 5.2c), the target position was altered by a known amount and the resulting proximity transducer output was recorded. The stated accuracy of the slip gauges was 0.2 μm (British Standard (1968)), but in practice it was difficult to achieve such accuracy when wringing together a number of slip gauges. For each target position, an average of 10 readings was taken to reduce noise effects. Although the manufacturers claimed that the proximity transducers had a working range of about 2 mm, it was decided to use a range of only 1.16 mm starting from the minimum transducer-target distance, as indicated in Figure 5.3, and to calibrate the transducer in steps of 0.04 mm. This

helped to reduce the effects of non-linearity when computing the calibration factors. A smaller range was acceptable since, as explained in Section 3.4.5, the transducers could be moved at any time during a test.

Two different methods for the calculation of the calibration factors were investigated. In the first method the output range was first divided into six intervals within each of which a polynomial fit was carried out for the calibration curve. This method had the drawback of involving discontinuities in the overall calibration curve and was found to be cumbersome. Although the method would have presented no major problems in being incorporated in the computer programs of Chapter 4, it was felt that a second method which did not divide the curve into intervals might be better. Yung (1987) adopted a 'linearisation' technique which involves calculating the function :

$$f(\beta) = ln(\beta - \beta_t) \tag{5.1}$$

where β and β_t are the transducer's output at a given target position and when no target is placed in front of it respectively. This technique was found to be superior and was again used in the present research. The function $f(\beta)$ was then plotted against displacement, Figure 5.4, and a polynomial curve, with a degree varying between 4 and 8 according to the transducer characteristics and the level of precision achieved, was fitted to the data. Table 5.1 shows the precision achieved for each transducer. The overall average value was 2.7 μm. As will be shown later (Section 5.3) this overall precision was found to be satisfactory for the purpose of measuring strains.

5.2.5 Load Cell

Imperial College type load cells were calibrated for use with the two triaxial cells. The results for that used in the 100 mm cell are summarised in Table 5.2. The load cell was used to measure the deviator force on the specimen from which the deviator stress can be calculated. The testing programme involved compression and extension loading and therefore calibration of the load cell was carried out in both directions. Special attention was paid to calibration of the load cell at low loads, such as would occur in tests on an isotropically consolidated specimen or any specimen with an initially small deviator stress.

Two different methods of calibration were adopted over different ranges. A Budenburg dead weight pressure system was used to calibrate the load cells in compression over a range 0 to 3000 N in steps of 200 N. Unfortunately, this apparatus could not be used for calibration in extension and another method, using dead weights placed directly on a plate connected to the load cell, had to be adopted. This produced less accurate but still tolerable results over the range 0 to 1600 N. This second method was also used to calibrate the load cells in compression in the range 0 to 400 N with smaller load steps than was possible with the Budenburg apparatus. A polynomial of degree 4 was fitted to data (in the latter range) while another of degree 3 was fitted to data from the Budenburg apparatus (in the range 400 to 3000 N). Correspondingly, two sets of calibration factors were then used in the computer program. A small difference (equivalent to a load of 1.2 N) between the results of the two calibration equations at a load of 400 N was tolerated. The precisions achieved during calibration are shown in Table 5.2 in terms of both force and deviator stress.

5.2.6 LVDTs

As mentioned in Section 3.4, submersible LVDT's were used in both triaxial cells to measure the end cap displacements from which axial strains in the specimen can be calculated. LVDTs were also deployed to measure the displacement of the piston of the 100 mm cell.

Whilst it was accepted that a digital micrometer with an accuracy of 3 μm was a potentially less accurate calibration device, it was used in preference to the slip gauges to reduce the time involved. In a preliminary trial it was found that a similar precision was achieved using both methods, indicating that stated accuracy of the slip gauges could not be achieved, as mentioned in Section 5.2.1. During calibration, as well as during a test, the armature in each submersible LVDT was able to move slightly in the direction perpendicular to the axial displacement, as shown diagrammatically in Figure 5.5. However, it was found that the changes in the output of the transducer due to such movements were very small. Table 5.3 summarises the results of the LVDT calibrations. The precisions of the submersible LVDTs for use in the 100 mm cell, 3.7 μm on average, are not too different from those of the proximity transducers shown in Table 5.1. The precision of the LVDTs used in the 38 mm cell were found to be higher and in one case very much higher at 49 μm. Another calibration was carried out to check this result and a similar precision was achieved. Yung (1987) calibrated similar transducers and reported a typical precision of 70 μm which cannot be considered satisfactory for small strain measurement. Unfortunately, it was not possible to obtain any better transducers during the time available.

5.2.7 Pressure Transducers

In the 100 mm triaxial cell, pressure transducers of a similar type were used to measure the cell and lower chamber pressures as well as the top and bottom pore water pressures of the specimen. The mid-height pore water pressure in the 100 mm cell and bottom pore water pressure in the 38 mm cell were measured by another (miniature) type of transducer, referred to in Section 3.4.2. De-airing of all these transducers prior to calibration was carried out by placing them under water in a triaxial cell and applying a relatively high vacuum pressure to remove not only the air trapped in the transducers but also that dissolved in the water. A Budenburg deadweight tester was used for the calibration and the results are shown in Table 5.4. A typical precision of about 1 kPa was achieved.

5.2.8 Volume Change Units

Two Imperial College volume change units were calibrated using a method developed by Goodwin (1991). After the two GDS controllers mentioned in Section 3.3 and the volume change unit had been de-aired, one GDS controller was connected to the top of the volume change unit and the other to the bottom, as shown in Figure 5.6. The computer instructed one GDS controller to apply a certain volume change which was then recorded by the volume change unit and checked by the other GDS controller to make sure that no air existed in the system. Table 5.5 shows the results for both volume change units.

5.3 Analysis of Errors in Stresses and Strains

5.3.1 Axial Strains

The analysis developed and the results presented in this section relate to the 100 mm cell only. However, a similar, if not identical, approach could be adopted for the 38 mm cell. As described in Section 3.4, three methods of axial strain measurement (local, end cap and external) were adopted, Figure 5.7. The errors in the local measurement will first be discussed, following closely the analysis presented by Hird and Yung (1989).

As shown in Figure 5.7, the local strain on one side of the specimen, $\epsilon_{\ell 1}$, is given by :

$$\epsilon_{\ell 1} = \frac{x - y}{L_{gc}} \tag{5.2}$$

where x,y, and L_{gc} are the displacements of the upper and lower targets and the consolidated gauge length respectively. The maximum error in $\epsilon_{\ell 1}$ is given by :

$$\delta\epsilon_{\ell 1} = \frac{\delta x + \delta y}{L_{gc}} + \frac{|\epsilon_{\ell 1}|}{L_{gc}}\delta L_{gc} \tag{5.3}$$

where δx, δy, and δL_{gc} represent the uncertainties in x, y, and L_{gc} respectively and $|\epsilon_{\ell 1}|$ is the absolute value of $\epsilon_{\ell 1}$. From Table 5.2, it can be seen that a representative value of proximity transducer precision is 2.7 μm. This was achieved through calibration against the slip gauges referred to in Section 5.2. The total uncertainty in x or y equals 5.8 μm ($= 2.7 + 0.2 + 2.7 + 0.2$) since the displacement of the target is calculated as the difference between the current and datum readings of the proximity transducer. This uncertainty includes both random and systematic errors.

The initial gauge length L_g was measured six times by a digital vernier. The error in a single measurement of the gauge length consisted of two components. The

first, a systematic component due to inaccuracy of the vernier, was taken as 20 μm (BS 4311 (1968)) and the second, a random component evaluated by measuring a constant distance of 100 mm about 50 times, was found to be about 80 μm. Following Taylor (1982), the error in the average gauge length is equal to the error in a single measurement divided by the square root of the number of measurements. Therefore, the error in the gauge length prior to consolidation is 40.8 μm ($= (20 + 80)/\sqrt{6}$). Since all the specimens underwent anisotropic consolidation, the consolidated gauge length had to be calculated as

$$L_{gc} = L_g - \Delta L_g \tag{5.4}$$

where ΔL_g is the change of gauge length during consolidation. Therefore, the error in L_{gc} is given by :

$$\delta L_{gc} = \delta L_g + \delta(\Delta L_g) \tag{5.5}$$

where δL_g and $\delta(\Delta L_g)$ are the errors in the measurement of the initial gauge length ($= 40.8\mu m$) and the change during consolidation respectively . The volume change in the specimen during consolidation is measured by the volume change unit (see Section 3.4.3). For the tests conducted in the 100 mm cell no lateral strain was allowed to take place during consolidation. In this case, the change in specimen height, ΔL, is given by :

$$\Delta L = \frac{\Delta V}{A_c} \tag{5.6}$$

where ΔV and A_c are the volume change and the specimen cross-sectional area respectively. Therefore the error in the specimen height change after consolidation is :

$$\delta(\Delta L) = \frac{\delta(\Delta V)}{A_c} + \frac{|\Delta V|}{A_c}\delta A_c \tag{5.7}$$

where $\delta(\Delta V)$ is the error in the evaluation of the volume change of the specimen and δA_c is the error in calculating the cross-sectional area of the specimen. Under normal circumstaces, the second term of the above equation is much smaller than the first term. From Table 5.5, for the 100 mm specimens, the random error in a volume measurement from the volume change unit is about 189 mm^3. To this must be added a possible systematic error during calibration against the GDS controllers of 20 mm^3, giving a total error of 209 mm^3. The error in a volume change $\delta(\Delta V)$ can be evaluated as 418 mm^3 since it involves errors in both the datum and current readings of volume. This corresponds to an error in the specimen height change, $\delta(\Delta L)$, of 53 μ m. Assuming that the change in the gauge length is proportional to that in the specimen height :

$$\delta(\Delta L_g) = \frac{\delta(\Delta L) \times L_g}{L_0} \tag{5.8}$$

where L_0 is the initial height of the specimen. For $L_0 = 200\ mm$ and $L_g = 100\ mm$ the overall error $\delta(\Delta L_g)$ is equal to about 26.5 μ m. Therefore, the error in the gauge length after consolidation, δL_{gc}, is equal to 67.3 μ m (= 40.8 + 26.5). This value may be less than the actual error, since the above analysis does not take into account the existence of small amounts of air in the specimen and the drainage pipes which influence the volume change measurement.

In Equation 5.3 the second term (involving the error in the consolidated gauge length) is small compared to the first, especially at small strains. Additional errors in the gauge length due to misalignment of the targets could occur but are negligible for the same reason. If only random errors are considered, then the error in strain measurement can be written as :

$$\delta\epsilon_{\ell 1} = \frac{\sqrt{(\delta x)^2 + (\delta y)^2}}{L_{gc}} \tag{5.9}$$

where $\delta\epsilon_{\ell 1}$ is now the largest probable error in $\epsilon_{\ell 1}$ and δx and δy are each equal

to the precision of the proximity transducers, i.e. 2.7 μm since the errors in the gauge length and the datum reading become systematic. The results obtained from Equations 5.3 and 5.9, expressed as percentage errors, are plotted versus strain level in Figure 5.8 .

A similar analysis to that presented above can be carried out for the end cap axial strain measurement. Under ideal conditions, where bedding errors and compression of the top and bottom caps and porous discs are equal to zero and where the specimen behaves in a right cylindrical manner, the end cap axial strain on one side, ϵ_{ec1}, is given by :

$$\epsilon_{ec1} = \frac{z}{L_c} \tag{5.10}$$

where z and L_c are the displacement recorded by the submersible LVDT and the consolidated height of the soil specimen respectively. The maximum error in ϵ_{ec1} is therefore

$$\delta\epsilon_{ec1} = \frac{\delta z}{L_c} + \frac{|\epsilon_{ec1}|}{L_c}\delta L_c \tag{5.11}$$

where δz and δL_c are the magnitudes of the uncertainties in z and L_c. The largest probable error in ϵ_{ec1} is given by :

$$\delta\epsilon_{ec1} = \frac{\delta z}{L_c} \tag{5.12}$$

where δz is either the maximum error or random error in z, as appropriate. Results from equations 5.11 and 5.12 are presented in Figure 5.9.

The largest probable percentage errors from local and end cap strain measurements are compared in Figure 5.10. This figure shows that under ideal conditions, the end cap measurement is more accurate than the local one, despite the fact that the proximity transducers have a better precision. The closest situation to the ideal one arises when the specimen end surfaces are flat, the specimen is initially relatively

soft, a high axial stress is applied prior to making small strain measurements and a rigid load cell - top cap connection is used (see Section 3.3.1) to prevent tilting.

Since the local and end cap measurements are carried out on both sides of the specimen, it was argued by Yung (1987) that the errors quoted above could be reduced by a factor of $\sqrt{2}$ if an average result was taken. However, it was later stated by Hird and Yung (1989) that the measurements on each side were not completely independent, because of the target mounting arrangements, and therefore the reduction factor should not be applied.

5.3.2 Radial Strains

The analysis for errors in radial strain measurement can be carried out in a similar way to that for the local axial strains in the previous section. The radial strain, ϵ_{r1}, from one pair of proximity transducers (Figure 3.15) is given by

$$\epsilon_{r1} = \frac{k+l}{2R_s} \tag{5.13}$$

where k and l are the inward movements of the targets calculated from the current and datum readings of the proximity transducers (In a compression test the radial strain is negative). Therefore, the maximum error in radial strain is

$$\delta\epsilon_{r1} = \frac{\delta k + \delta l}{2R_s} + \frac{|\epsilon_{r1}|}{R_s}\delta R_s \tag{5.14}$$

where δk and δl are the errors in k and l (= 5.8μ m) and δR_s is the uncertainty involved in measuring the radius of the specimen. Employing the same digital vernier as used to measure specimen length, the diameter of the specimen, D_s, was measured six times and therefore the maximum error, δD_s, is again equal to 40.8 μm. The uncertainty in R_s is

$$\delta R_s = \delta D_s \tag{5.15}$$

so that $\delta R_s = 40.8\ \mu$m.

If only random errors are taken into consideration and assuming the second term in Equation 5.15 is negligible, the largest probable error in radial strain is given by

$$\delta\epsilon_{r1} = \frac{\sqrt{(\delta k)^2 + (\delta l)^2}}{2R_s} \tag{5.16}$$

where $\delta k = \delta l = 2.7\mu$m.

Since there are two pairs of proximity transducers making independent readings of radial strain, it can be argued that the error in the average reading, $\delta\epsilon_r$, is lower and given by

$$\delta\epsilon_r = \frac{\delta\epsilon_{r1}}{\sqrt{2}} \tag{5.17}$$

where $\delta\epsilon_r$ and $\delta\epsilon_{r1}$ refer to either maximum error or largest probable error. Figure 5.11 shows the resulting variations with strain of the maximum and the largest probable errors in the average radial strain measurement.

5.3.3 Poisson's Ratio

Poisson's ratio, ν, is calculated as

$$\nu = \frac{\epsilon_r}{\epsilon_\ell} \tag{5.18}$$

where ϵ_r and ϵ_ℓ are the average radial and local axial strains. The maximum and largest probable errors in ν are given by

$$\delta\nu = \frac{\delta\epsilon_r}{\epsilon_r} + \frac{|\nu|}{\epsilon_\ell}\delta\epsilon_\ell \tag{5.19}$$

and

$$\delta\nu = \sqrt{\left(\frac{\delta\epsilon_r}{\epsilon_r}\right)^2 + \left(\nu\frac{\delta\epsilon_\ell}{\epsilon_\ell}\right)^2} \tag{5.20}$$

respectivly, where $\delta\epsilon_r$ and $\delta\epsilon_\ell$ are the errors in radial and axial strains respectively. Results from equations 5.20 and 5.21 are shown in Figure 5.12 which reveals the difficulty in measuring Poisson's ratios at small strain levels.

5.3.4 Deviator Stress

An internal load cell was used to measure the deviator force on the specimen. The deviator stress is simply calculated as

$$q = \frac{F_d}{A_c} \tag{5.21}$$

where F_d is the deviator force. The maximum error in deviator stress is

$$\delta q = \frac{\delta F_d}{A_c} + \frac{|q|}{A_c}\delta A_c \tag{5.22}$$

and the largest probable error is

$$\delta q = \sqrt{\left(\frac{\delta F_d}{A_c}\right)^2 + \left(\frac{q\delta A_c}{A_c}\right)^2} \tag{5.23}$$

The current cross-sectional area of the specimen can be calculated knowing the change in the diameter, measured by the proximity transducers and assuming that the specimen deforms as a right cylinder. With one pair of proximity transducers readings the current diameter, D_{sc}, is thus :

$$D_{sc} = D_s + (k + l) \tag{5.24}$$

Therefore, the maximum error in measuring the current diameter is

$$\delta D_{sc} = \delta D_s + \delta k + \delta l \tag{5.25}$$

As in Section 5.3.2, $\delta D_s = 40.8$ μm and $\delta k = \delta l = 5.8$ μm . Therefore $\delta D_{sc} = 52.4$ μm. By assuming that the two radial strain measurements are independent, δD_{sc}

becomes 37.0 μm ($52.4/\sqrt{2}$) The error in the current area of the specimen is given by

$$\delta A_c = \frac{\pi}{2} D_{sc} \delta D_{sc} \tag{5.26}$$

which amounts to 5.8 mm^2. For deviator forces of up to 400 N, the precision of the load cell is approximately 3 N (Table 5.3). The accuracy of the calibration equipment is quoted by the manufacturers as 0.16 N. Therefore, δF_d is equal to 3.16 N. Figure 5.13 shows the variation, with deviator stress, of the maximum and largest probable percentage errors in the deviator stress for a 100 mm specimen.

5.3.5 Stiffness

For a conventional test $\Delta\sigma_3 = 0$, the tangent stiffness can be defined as

$$E = \frac{\Delta q}{\Delta \epsilon_\ell} \tag{5.27}$$

where $\Delta\epsilon_\ell$ is the change in local axial strain. Following the same reasoning as adopted in the previous sections, the maximum error in stiffness is

$$\delta E = \frac{\delta q}{\Delta \epsilon_\ell} + \frac{E}{\Delta \epsilon_\ell} (\delta(\Delta \epsilon_\ell)) \tag{5.28}$$

where δq and $\delta\epsilon_\ell$ are the maximum errors in deviator stress and axial strain respectively. On the other hand, the largest probable error in stiffness is given by

$$\delta E = \sqrt{\left(\frac{\delta q}{\Delta \epsilon_\ell}\right)^2 + \left(E \frac{\delta(\Delta \epsilon_\ell)}{\Delta \epsilon_\ell}\right)^2} \tag{5.29}$$

where δq and $\delta(\Delta\epsilon_\ell)$ are random errors. For secant stiffness $\Delta\epsilon_\ell$ is replaced by ϵ_ℓ in Equations 5.28 and 5.29. For typical data (from test AOCU1 which will be presented in Chapter 6) the results of the analysis are shown in Figure 5.14. This figure indicates that both the maximum and largest probable percentage errors in the

very small strain region are significant. It should be noted that the term involving δq in Equations 5.28 or 5.29 is relatively small and the error in stiffness is mostly a result of the errors in strain measurement.

5.4 Proving Tests

Upon completion of the transducer calibrations and the analysis of errors described in the previous sections, trial tests were performed for the following purposes :

- To gain experience in setting up the specimen, especially in the 100 mm cell where both care and skill are required.
- To check on the repeatability of the test results.
- To establish suitable values of certain parameters needed for testing, such as the rate of loading and the limits on radial strain during K_0-consolidation or K_0-swelling.
- To evaluate the loading system compliance.
- To evaluate the performance of the computer software, especially its ability to follow accurately a specified stress path and to store suitable readings for later analysis.

Stainless steel, rubber, and kaolin specimens with heights and diameters of 200 mm and 100 mm respectively were used for proving tests in the 100 mm cell.

Experience gained during the trial tests in the 100 mm cell was used in the 38 mm apparatus, especially in the automated control of testing. A small number

of trial tests was also carried out in the 38 mm cell but these will not be discussed. A summary of the proving tests along with the specimens used and their aims is presented in Table 5.6.

5.4.1 Tests on Stainless Steel Specimen

Two types of test were carried out on this specimen. These were designed, firstly, to check one aspect of the radial strain measurement method (test STE1) and, secondly, to evaluate the compression under stress of system components such as the top cap or the load cell (tests STE2 and STE3).

5.4.1.1 Radial strain measurement

As described in Section 3.4.6, radial strain measurement is carried out by mounting four proximity transducers on a stainless steel ring (Figure 3.15). The analysis presented in that section indicated that changes in cell pressure would have a negligible influence on the dimensions of the steel ring, and therefore on the proximity transducer readings.

In test STE1, the steel specimen was first surrounded by a rubber membrane on which the radial targets were attached at mid-height using a thin film of silicon rubber (Figure 3.16). Three cycles of cell pressure between 0 and 580 kPa were then applied and the resulting radial strain recorded. As shown in Figure 5.15, this strain did not exceed $\pm 0.005\%$ and did not depend on the cell pressure. The compression of the steel specimen itself is negligible. Thus neither changes in the mounting ring diameter nor compression of the silicon rubber had a significant effect on the radial strain measurement. In fact, all the sampling disturbance and shearing stages in

the test programme (see Section 6.2) were carried out with constant cell pressure, and therefore the radial strain measurement during these stages could not possibly have been influenced by cell pressure variations.

5.4.1.2 Loading system compliance

The compressiblity of certain parts of the triaxial apparatus was measured by carrying out two tests (STE2 and STE3) with external and end cap axial strain measurements only. A top cap and porous stones were installed at the ends of the specimen. A deviator stress of up to 440 kPa was applied slowly while strains were recorded. The results are shown in Figure 5.16. It should be mentioned that in both tests the end cap strain was very small (less than 0.0005%) while the external strain varied with deviator stress. Compression of the top cap and the porous stones, must therefore be negligible compared to that of the load cell-top cap connection (described in Section 3.3.1), the load cell itself and other components. When the deviator stress-external strain curves from the two tests are compared (Figure 5.16), it may be seen that test STE3 involved a significantly higher strain at low deviator stresses, which can be attributed to the lack of rigidity between the load cell and the top cap. This bedding error may not happen in every test and depends on the setting up procedure. A linear regression analysis was performed on the subsequent portions of the curves, the results of which are presented in Table 5.7. The slopes represented by the regression coefficients are similar, indicating that the compression is systematic or repeatable. Although it is possible to evaluate the elastic component of compression and allow for it in the calculation of the external axial strain, the initial bedding referred to above is much more difficult to evaluate.

The results of these tests were also used to check on the ratio between the

lower chamber pressure and the axial stress. Theoretically this ratio should equal the bellofram area ratio (a/A) of 2.25. The regression analysis of the two test results, presented in Table 5.7, shows that the deduced ratio ranges between 2.08 and 2.50 with an average of 2.26. The relationship between σ_{lc} and σ_1 is not perfectly linear due to the friction between the piston and its bushing. Tilt of the piston can be checked by plotting the movements of the cross arms, measured externally on both sides of the apparatus. A significant tilt occured initially in test STE2 while in test STE3 the tilt was negligible. When the cylinder is at its very lowest position, a certain amount of tilt may take place but the tilting becomes relatively small once the cylinder is above that position. Thus all tests should be conducted after ensuring that the cylinder is not at its lowest position to avoid non-uniform strains in the specimen.

5.4.2 Tests on Rubber Specimen

Tests were conducted on the rubber specimen for several purposes, namely to check the application of stress paths (RUB2), the application of strain cycles (RUB3 and RUB4), the measurement of local strains by evaluating Poisson's ratio (RUB5 and RUB6 among others), and the effect of other factors such as stiffening of the specimen due to the mounting of the small strain instrumentation (RUB7) and membrane slippage (RUB8). The specimen deployed had a hardness of about 55 (British Standards Institution (1957)). In the course of these tests, different techniques were tried to find the most satisfactory ways of setting up the local strain targets and of connecting the load cell to the top cap without applying any significant deviator stress to the specimen.

5.4.2.1 Application of stress paths

Trial tests were carried out to find the most accurate method of implementing a desired stress path. Suitable limits on the axial and radial stress increments which were specified in the computer software were determined (see Section 4.3.3). Results shown in Figure 5.17, taken from proving test RUB2, show a satisfactory agreement between the applied and intended stress paths. A regression analysis showed that the precision achieved in the deviator stress was $\pm$ 1.22 kPa.

5.4.2.2 Application of strain cycles

The simulation of sampling disturbance involved the application of a strain cycle in the manner described in Section 2.3. Proving tests RUB3 and RUB4 were performed to check the ability of the software to apply strain cycles of 0.05% and 0.1% respectively. In order to maintain a positive deviator stress throughout the cycle, the specimen was initially subjected to a deviator stress of about 7 kPa. The results are shown in Figure 5.18 which shows that the maximum and minimum values of axial strain during the cycle were within $\pm$0.005% of the specified limits. Figure 5.18 indicates that the strain cycle could be applied sufficiently accurately over a relatively short period of time (about 10 minutes). The figure also shows a fairly good agreement between the average local and end cap strains. The external strain shows poor agreement and a much larger scatter.

5.4.2.3 Poisson's ratio

Although the determination of Poisson's ratio, ν, in the small strain range is not very accurate (Section 5.3.3), results from proving tests RUB5 and RUB6, among

others, gave a value of ν very close to 0.5, as indicated in Table 5.8. These values have been calculated by performing linear regression between the radial and axial strains over the whole range of local strain in each test (i.e. beyond the small strain range). The overall range of 0.47 to 0.50 agrees well with that quoted for rubber by Kaye and Laby (1973) of 0.46 to 0.49.

5.4.2.4 Membrane slippage and stiffening effects of target mountings

Membrane slippage was checked by carrying out four proving tests. Two of these, RUB8 and RUB9, involved the use of a rubber membrane around the specimen with the targets for the proximity transducers mounted in the usual way, while in the other two, RUB10 and RUB11, no rubber membrane was used. Because the surfaces of the soil specimens used for the main tests were contaminated with a thin layer of silicon grease after extrusion from the sampling tubes, a similar layer of grease was applied to the rubber specimen in tests RUB8 and RUB9. The results are shown in Figure 5.19 where the deviator stress was varied between 2 kPa and 15 kPa. No significant effect of membrane slippage is apparent. The scatter in each set of results is within the known uncertainties of the stress and strain measurements, as described in Section 5.3.

A check on the effects of mounting the local strain targets on the stiffness of the specimen was carried out by comparing the end cap stiffness from test RUB7, which did not involve the mounting of local targets, with those from other tests. As shown in Table 5.9, there was no significant difference between the results.

5.4.2.5 Repeatability checks

The data retrieved from the proving tests on the rubber specimen permitted the repeatability of the techniques for stress and strain measurement to be assessed. Good repeatabilty was obtained for both Poisson's ratio, Table 5.8, and stiffness, Table 5.9. The stiffness was determined by carrying out a linear regression analysis of the data of deviator stress versus strain. Variations in the 'end cap' and 'local' stiffnesses were much lower than those in the 'external' stiffnesses reflecting both the low precision of the external LVDT's and the additional errors involved as discussed in Section 5.2.3. The 'local' stiffnesses were larger in every case than the 'end cap' ones which may be explained by bedding and seating errors. This illustrates a situation where a local strain measurement is more reliable than an end cap one.

5.4.3 Tests on Soil Specimens

Despite the satisfactory test results obtained for the stainless steel and rubber specimens, it was considered important to carry out some trial tests on soil specimens to investigate how the apparatus and the controlling software would operate under conditions similar to those in the main tests. Certain parameters also had to be determined before the start of the testing programme, some of which could only be evaluated by running trial tests. Two tests TR1 and TR2 were performed using kaolin specimens prepared in the manner described in Section 3.5 but taken from a slurry consolidated under a higher vertical effective pressure of 280 kPa. Discussion will focus first on test TR1.

The setting up of the soil specimens proved more difficult than that of the steel or rubber specimens, since they were much softer. The pressure lines also had

to be de-aired. Saturation of the specimens was carried out as described in Section 4.3.2. A satisfactory B-value was achieved with a back pressure of about 200 kPa.

After saturation, K_0-consolidation was performed. The results showed a considerable scatter in the stress path data, although the direction of the stress path was similar to that expected. This scatter was blamed on the large limit on radial strain initially adopted in the software (0.01%) as well as the large increments (about 5 kPa) of axial and radial stress initially allowed. The maximum radial strain actually measured was found to be 0.018% which was clearly unsatisfactory. The excess pore water pressure recorded by the midheight pressure transducer did not exceed the allowable limit of 10 kPa. The average rate of loading achieved was about 2 kPa/hr of axial stress.

K_0-swelling was next carried out. Although the desired OCR was achieved accurately, an even larger scatter in the stress path data occured than during consolidation. This scatter was equivalent to a variation in deviator stress of $\pm$ 5 kPa and was again attributed to both the large limit on radial strain and the high increments of stress. The rate of axial stress unloading of 2 kPa/hr ensured that the mid-height pore water pressure deficit did not exceed 10 kPa.

Sampling disturbance was then simulated by applying a strain cycle of amplitude 0.3%. The results indicated that the cycle was not followed accurately. As the compressive strain approched 0.3%, the apparatus did not respond quickly enough in reversing the strain direction due to friction losses in the loading system. Consequently, the specimen was sheared in compression to a strain of about 0.5% before the strain started to decrease. This problem was not encountered when applying strain cycles to the rubber specimen since material creep was virtually non-existent.

Finally, the specimen was sheared conventionally (σ_3 = constant) in undrained compression at an axial stress rate of 2 kPa/hr without being recompressed to its initial stress state. No significant non-uniformity of pore water pressure in the specimen was noticed at this rate of loading. However, the stress strain data showed significant scatter, which was attributed to the large increments of axial stress (about 5 Kpa) initially adopted in the controlling software.

Experience from test TR1 was used to plan another test on a similar soil specimen to make sure that all the problems encountered with TR1 could be avoided.

In test TR2 K_0-consolidation was carried out by adopting the smallest possible increments of axial and radial stress (0.85 kPa and 0.38 kPa respectively) and attempting to limit the radial strain to $\pm 0.005\%$. The variation of radial strain with axial stress is shown in Figure 5.20, which indicates that only occasionally did the radial strain exceed $\pm 0.005\%$ and never did it exceed $\pm$ 0.007%. Figure 5.21 shows the stress path for this stage which can be considered satisfactory. The regression analysis showed that $K_0 = 0.67 \pm 0.006$. The rate of loading was found to be similar to that achieved in test TR1.

The K_0-swelling stage was carried out under the same control limit for lateral strain ($\pm 0.005\%$). Figure 5.22 shows that during swelling the measured radial strain rarely exceeded $\pm 0.006\%$. A larger scatter in the stress path data for this stage than for the consolidation stage was obtained but the scatter was smaller than in test TR1. Since the desired OCR was achieved accurately with no significant lateral strain, the irregularities in the stress path were considered tolerable.

Sampling disturbance was then simulated by following a strain cycle with an amplitude of 1.0%. Quicker procedures were adopted in the software than in test

TR1. The resulting strain cycle is shown in Figure 5.23 which indicates that the performance of the software was now satisfactory.

As in test TR1, shearing in compression at a rate of 2 kPa/hr of axial stress was applied straight after the sampling disturbance stage, without any reconsolidation of the specimen. The stress-strain data for the shearing stage over the small strain range had a maximum scatter found from a regression analysis equivalent to about $\pm$ 1.22 kPa of deviator stress. This is satisfactory considering the errors involved in the determination of the deviator stress and the local axial strain.

Following the above tests on the soil specimens all the control parameters required for the main test series could be finalised.

Transducer code	95 % Conf. interval (μm)
PR1	2.470
PR2	2.537
PR3	3.110
PR4	2.878
PR5	2.447
PR6	2.699
PR7	2.723
PR8	2.705

Table 5.1 Results of proximity transducer calibrations

Loading	Method of Calibration	Range (N)	Increment (N)	95 % Conf. Interval (N)
Compression	Budenburg Apparatus	0-3000 (382)	200 (25)	5.07 (0.65)
Compression	Dead Weights	0-400 (51)	20 (2.5)	3.00 (0.38)
Extension	ditto	0- -1600 (-204)	-100 (12.5)	10.89 (1.39)
Extension	ditto	0- -360 (-46)	-20 (2.5)	2.25 (0.29)

Note : Numbers in brackets represent values of deviator stress on a 100 mm specimen (kPa)

Table 5.2 Results of load cell calibration

Transducer code	Range (mm)	Increment (mm)	95% Conf. interval (mm)
LVDT92	0-10	0.5	3.82×10^{-3}
LVDT546	0-10	0.5	3.60×10^{-3}
LVDT56	0-10	0.5	9.35×10^{-3}
LVDT91	0-10	0.5	4.90×10^{-4}
LVDT21	0-50	1.0	0.164
LVDT98	0-50	1.0	0.118

Table 5.3 Results of LVDT calibrations

Transducer code	Range (kPa)	Increment (kPa)	95% Conf. interval (kPa)	used for	triaxial cell
L112793	0-700	50	0.684	cell pressure	100 mm
L117292	0-700	50	0.429	l.c. pressure	100 mm
L102671	0-700	50	1.110	top p.w.p.	100 mm
L33090	0-700	50	1.280	bottom p.w.p.	100 mm
253	0-700	50	0.592	mid-height p.w.p.	100 mm
-	0-500	VARIABLE	0.782	bottom p.w.p.	38 mm

Table 5.4 Results of pressure transducer calibrations

Range mm^3	Increment mm^3	95 % Conf Interval mm^3	Triaxial cell
0-95000	5000	188.9	100 mm
0-95000	5000	271.5	38 mm

Table 5.5 Results of volume change unit calibrations

Test	Specimen material	Cell pressure kPa	Loading rate kPa/hr	Purpose
STE1	steel	variable	10	to check radial strain measurement method and cell components compressibility
STE2	steel	----	10	
RUB2	rubber	----	40	to check stress path application
RUB3	ditto	variable	60	
RUB4	ditto	53	60	
RUB5	ditto	53	20	to check Poisson's ratio
RUB6	ditto	15	7	
RUB7	ditto	200	18	to check stiffening of the specimen
RUB8	ditto	200	2	
RUB9	ditto	200	2	to check membrane slippage
RUB10	ditto	200	2	
RUB11	ditto	200	2	
TR1	kaolin	200	2	to evaluate behaviour of the cell with actual soil specimens and determine certain parameters
TR2	kaolin	variable	2	

Table 5.6 Summary of proving tests

Test	System compressibility		
	Constant kPa	Coefficient kPa/%	
STE2	0.0187	0.0007	
STE3	0.136	0.0007	
	pressure ratio σ_{lc}/σ_1		
	initial	intermediate	overall
STE2	2.08	2.33	2.44
STE3	2.10	2.31	2.50

Table 5.7 Regression results from data in tests STE2 and STE3

Test	U
RUB2	0.48
RUB3	0.47
RUB4	0.48
RUB5	0.50
RUB6	0.49
RUB7	-----
RUB8	0.48
RUB9	0.48
RUB10	0.48
RUB11	0.48

Table 5.8 Summary of U values for tests on the rubber specimen

Test	local	end cap	external
RUB2	4240	3503	3808
RUB3	3947	3555	3852
RUB4	3920	3492	3918
RUB5	4384	3599	3931
RUB6	4274	-------	3339
RUB7	------	3692	3745
RUB8	4208	3350	2120
RUB9	3980	3640	3898
RUB10	4061	3605	3182
RUB11	4156	3502	3503
Average	4130	3549	3536

Note : Stiffness in kPa calculated by regression to 0.1 % strain

Table 5.9 Summary of stiffness values from tests on the rubber specimen

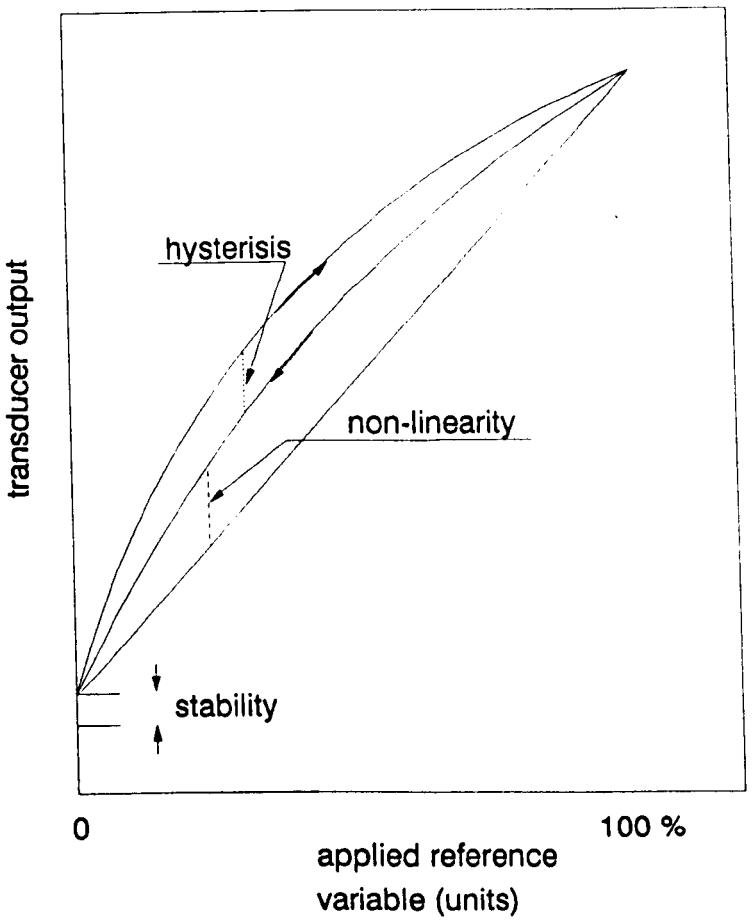

Fig 5.1 Definitions of terms relating to transducer output

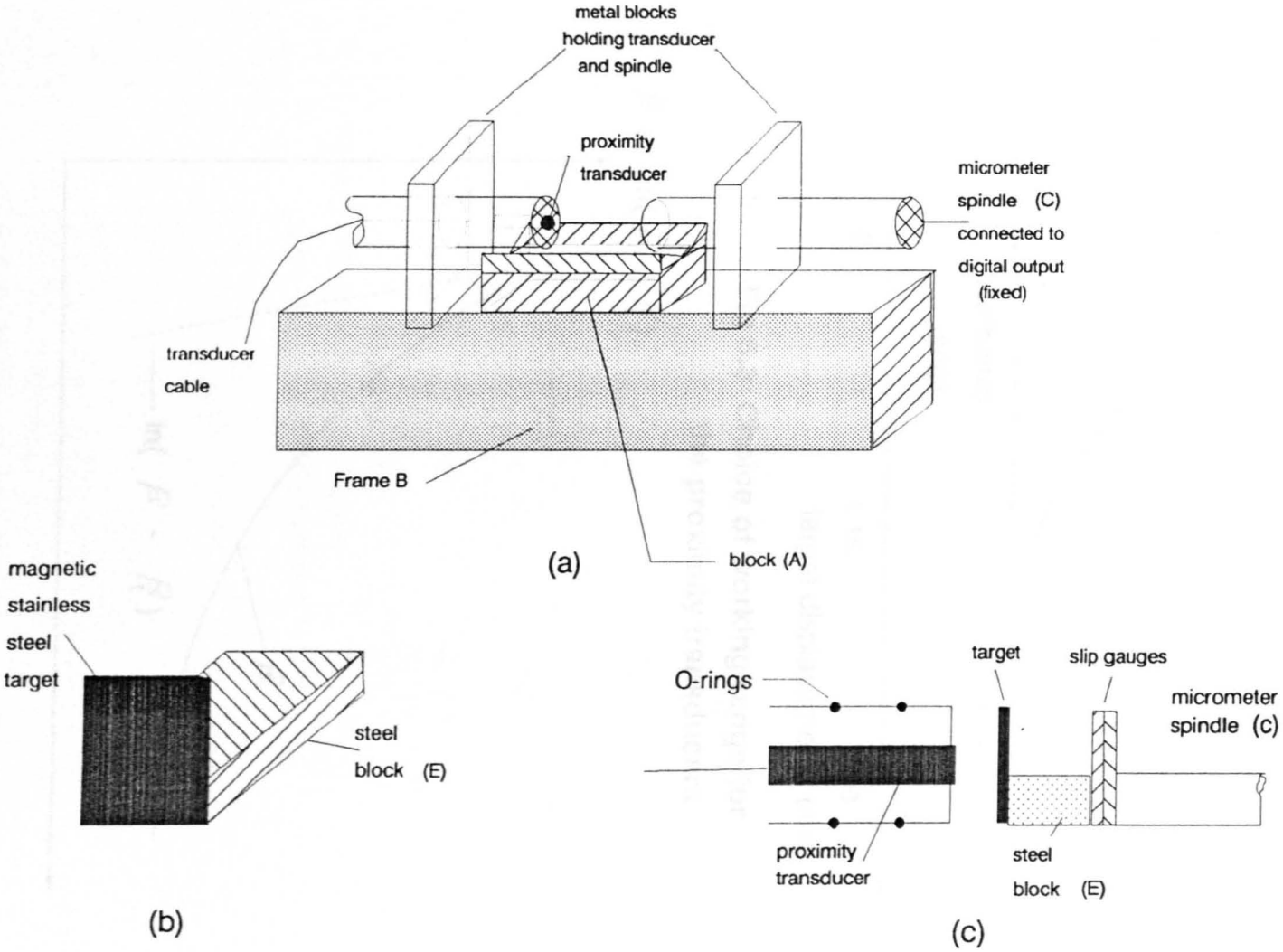

Fig 5.2 Calibration arrangement for the proximity transducers

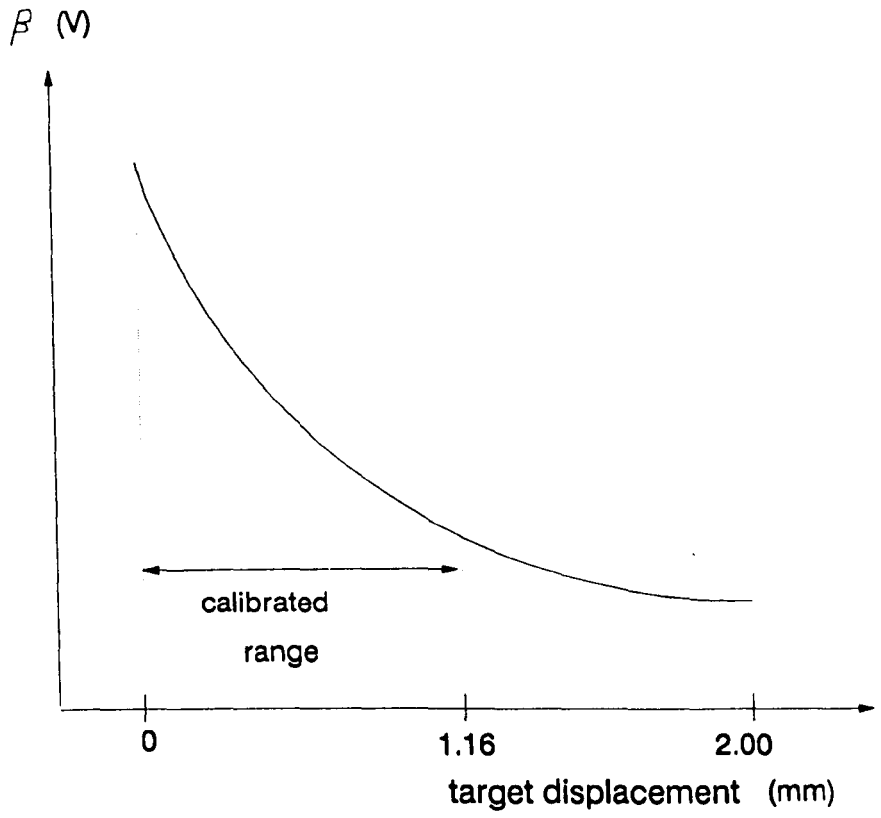

Fig 5.3 Choice of working range for the proximity transducers

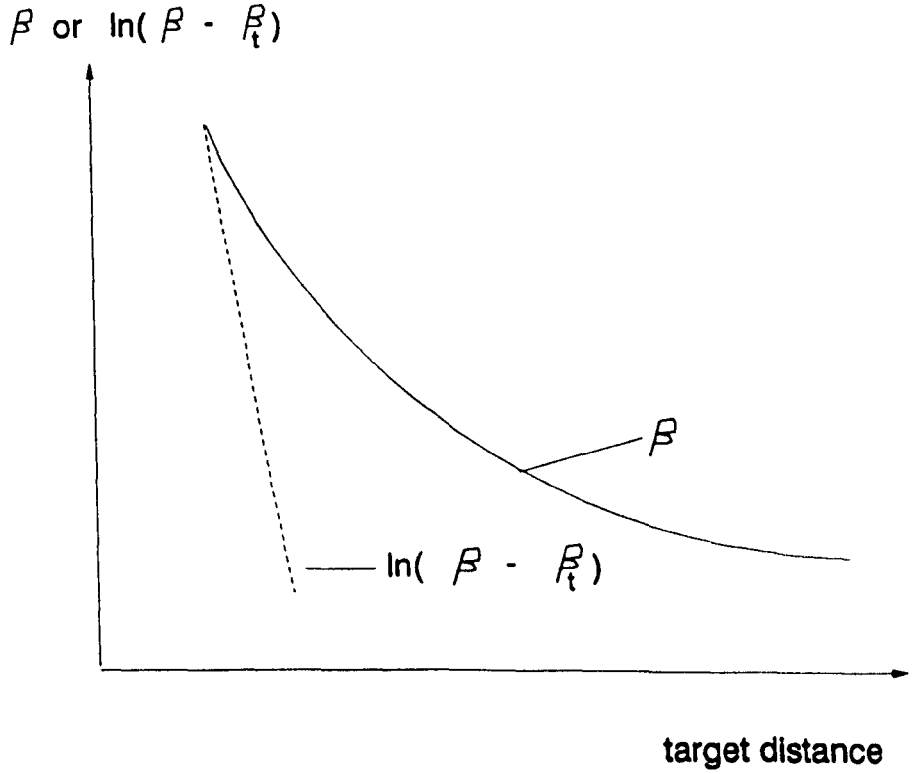

Fig 5.4 'Linearisation' of proximity transducer output

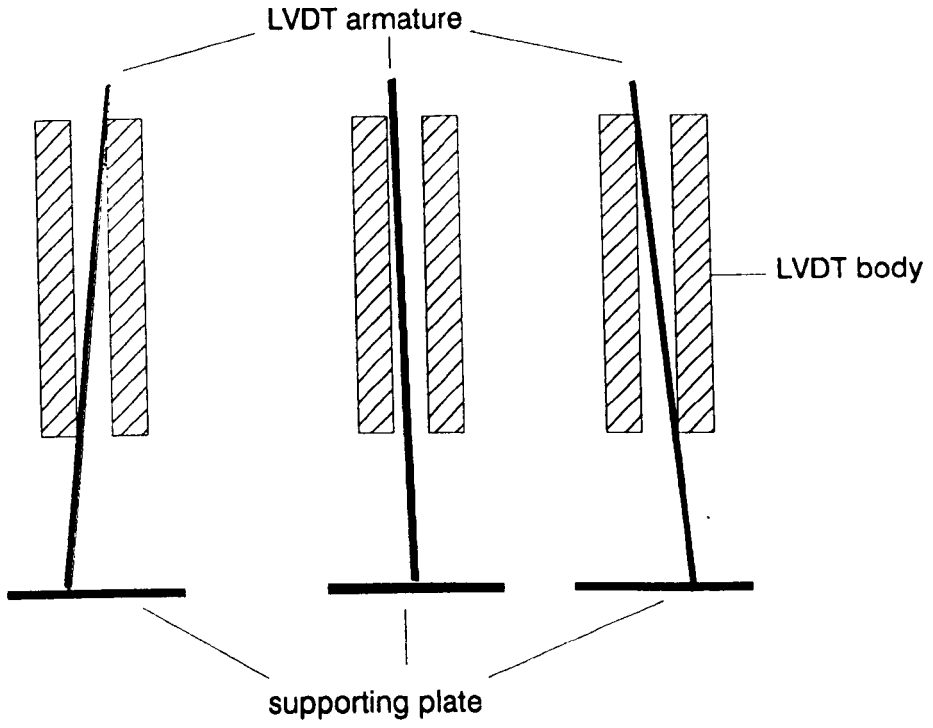

Fig 5.5 Possible positions of submersible LVDT armature during testing or calibration

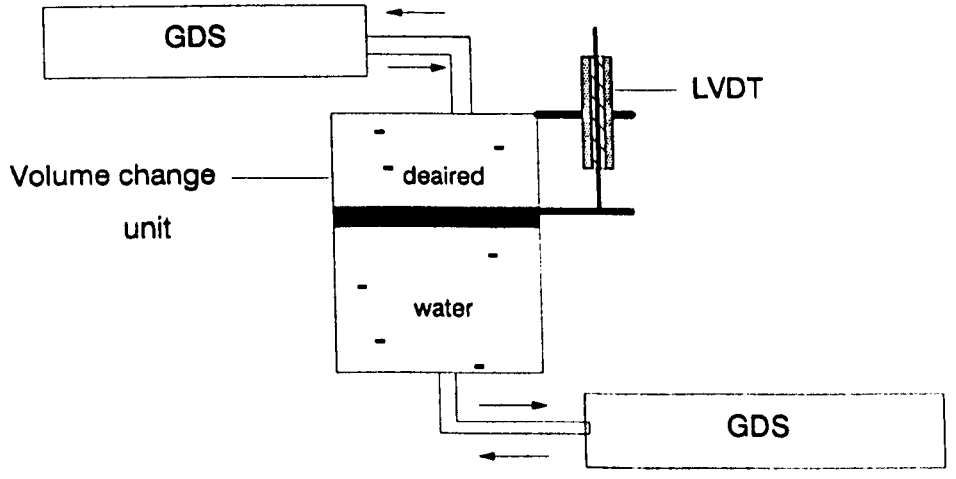

Fig 5.6 Method of calibrating the volume change units

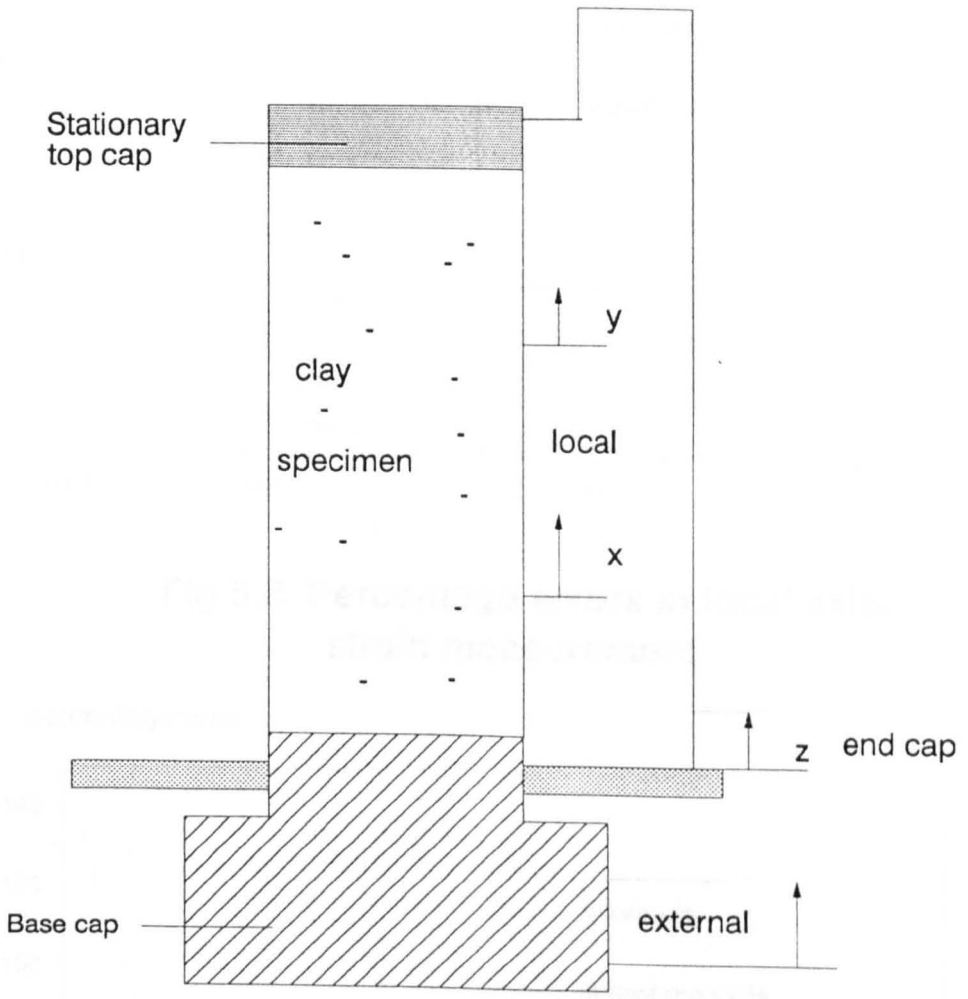

Fig 5.7 Diagrammatic representation of the three methods of axial strain measurement

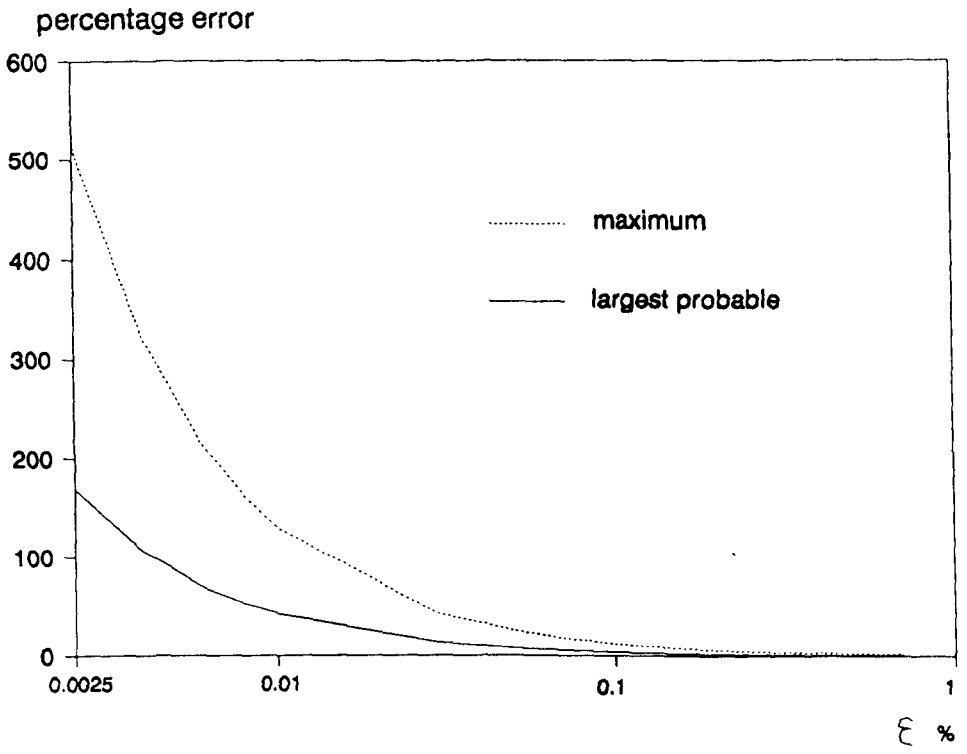

Fig 5.8 Percentage errors in local axial strain measurement

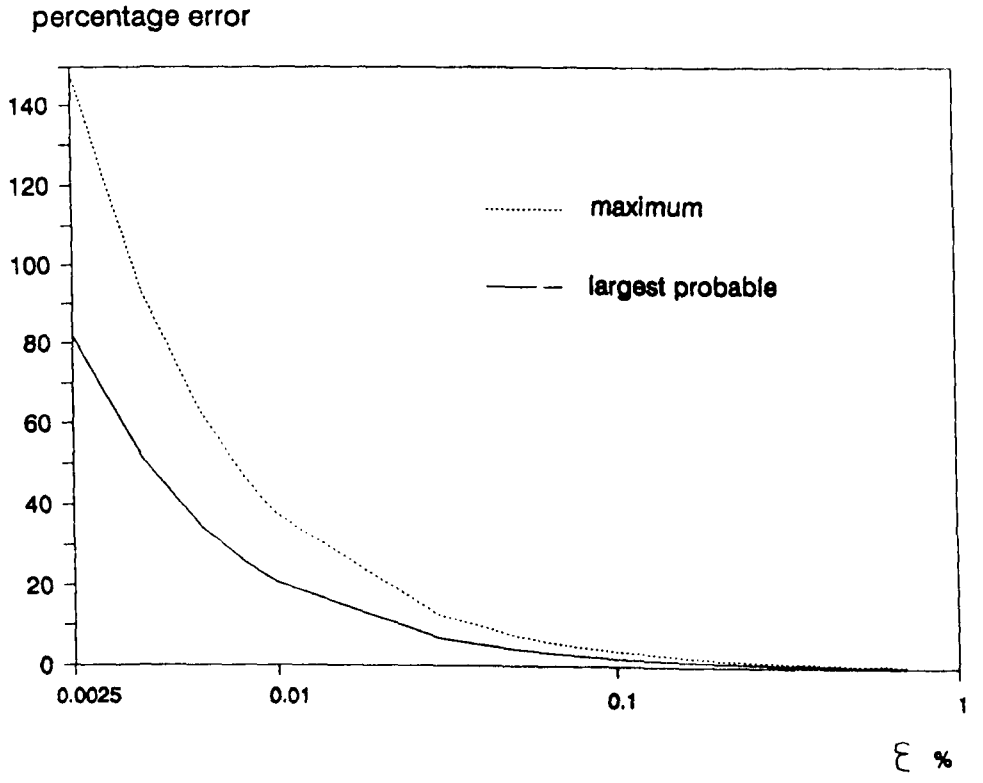

Fig 5.9 Percentage errors in end cap axial strain measurement

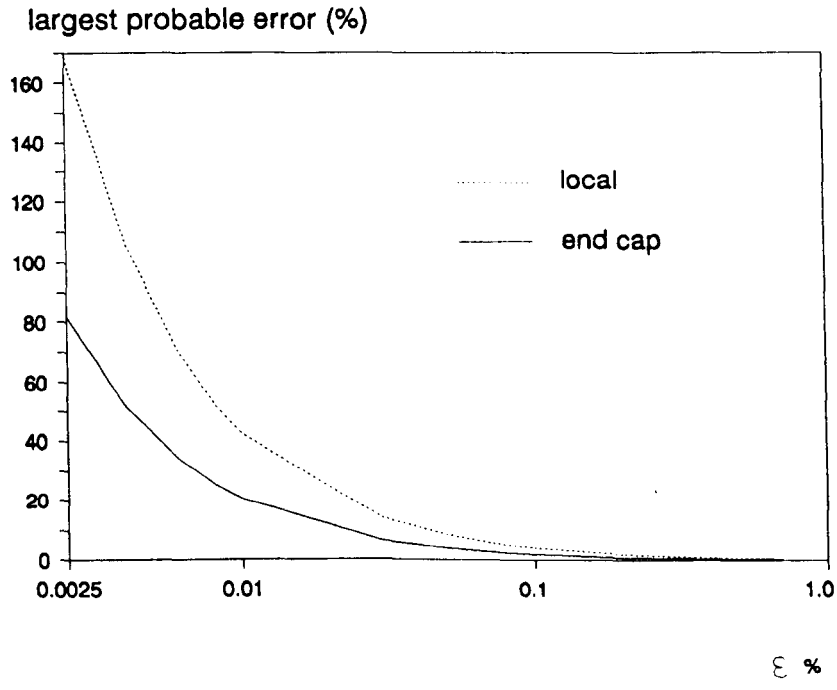

Fig 5.10 Comparison of errors in local and end cap strains

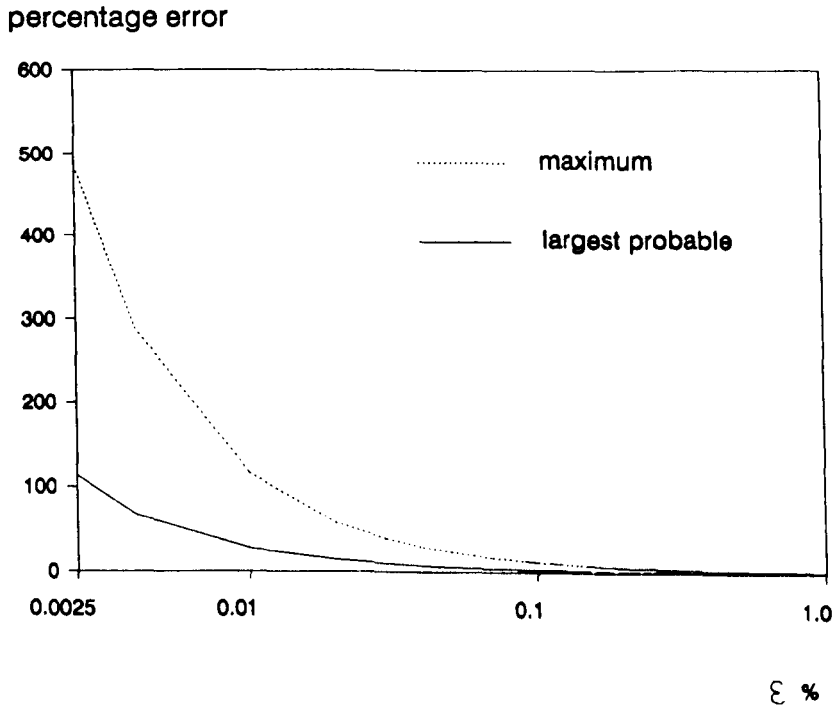

Fig 5.11 Percentage errors in local radial strain measurement

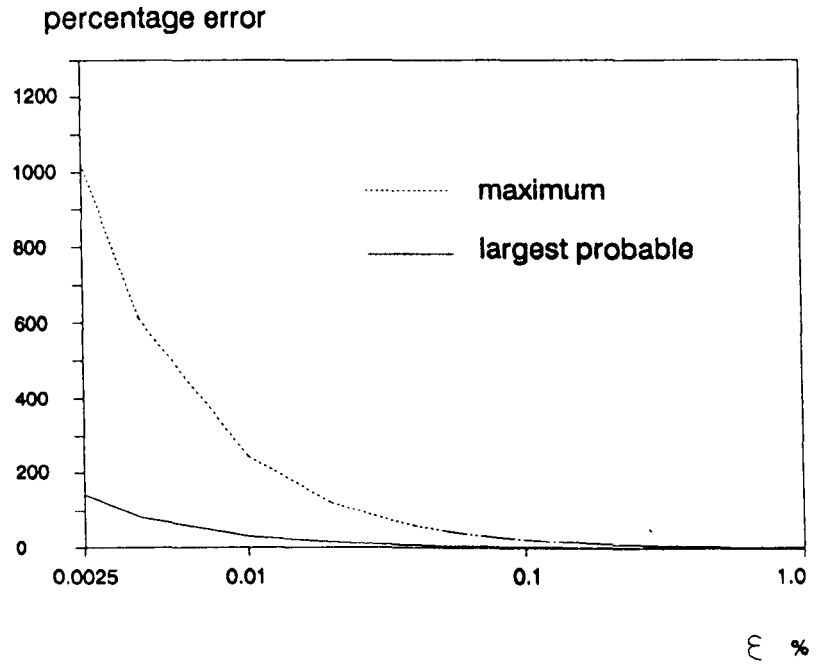

Fig 5.12 Percentage errors in Poisson's ratio

ν = 0.5

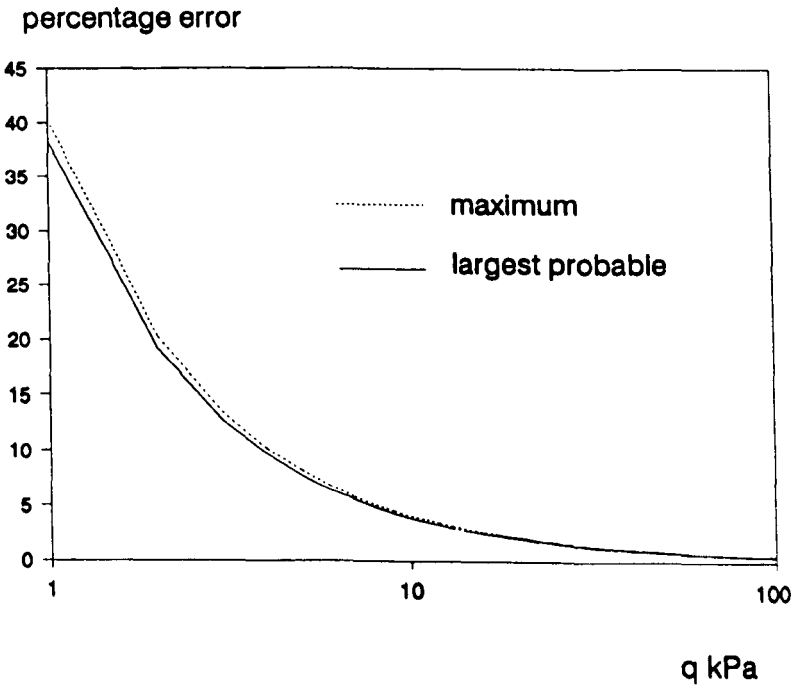

Fig 5.13 Percentage errors in deviator stress

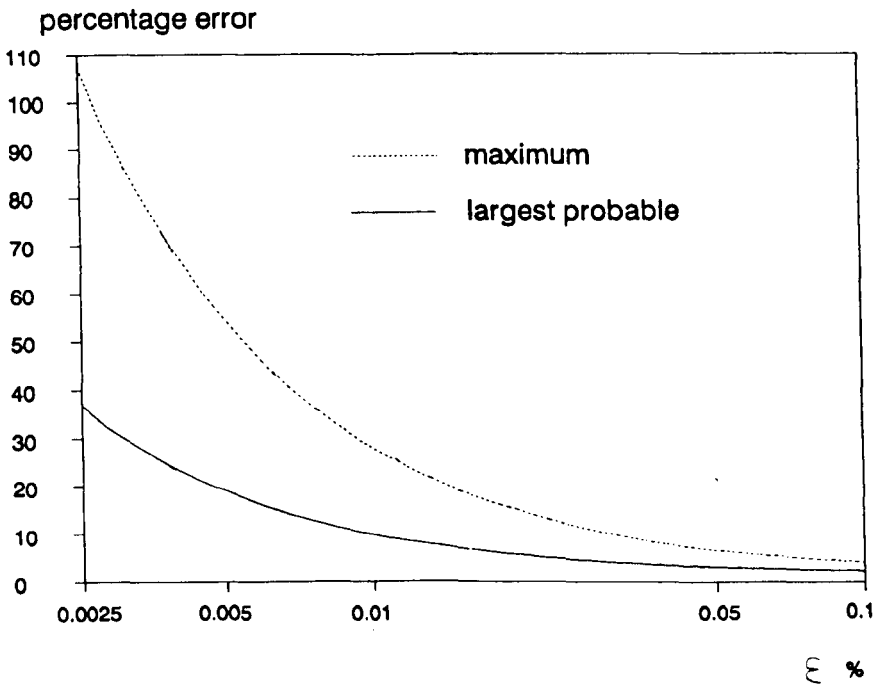

Fig 5.14 Percentage errors in tangent stiffness

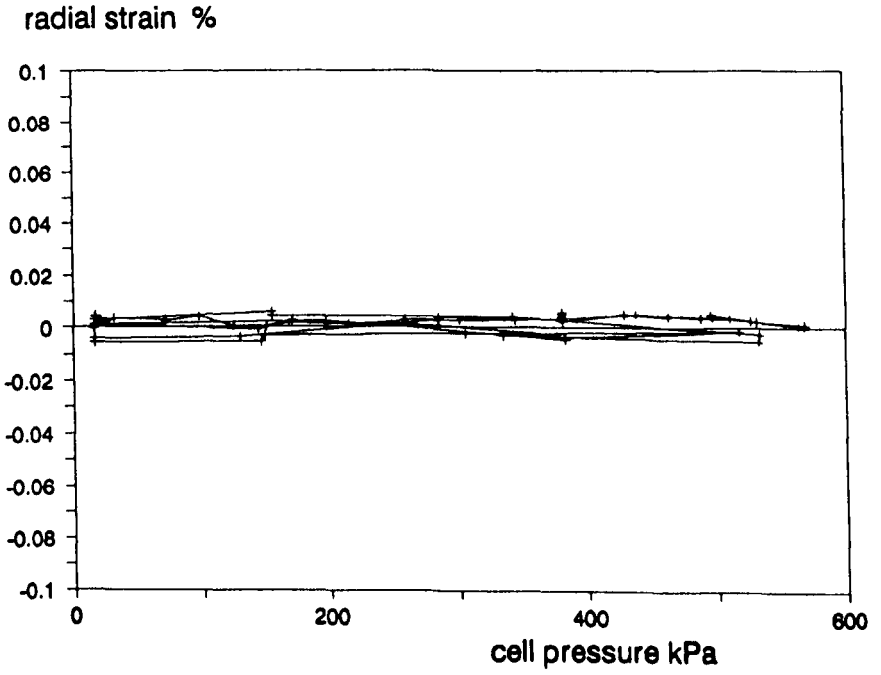

Fig 5.15 Effect of changing cell pressure on radial strain

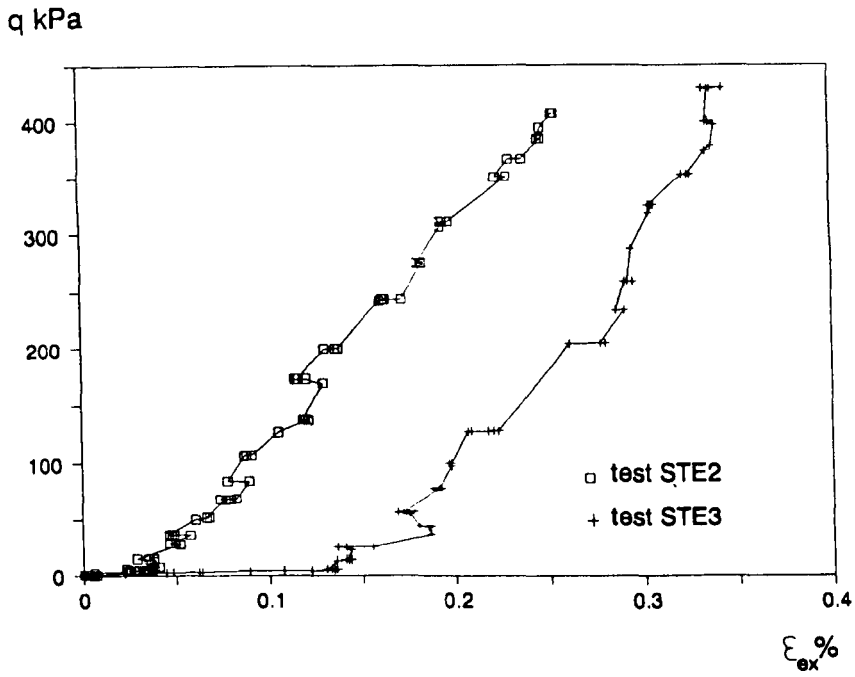

Fig 5.16 Stress strain curves during loading of the steel specimen

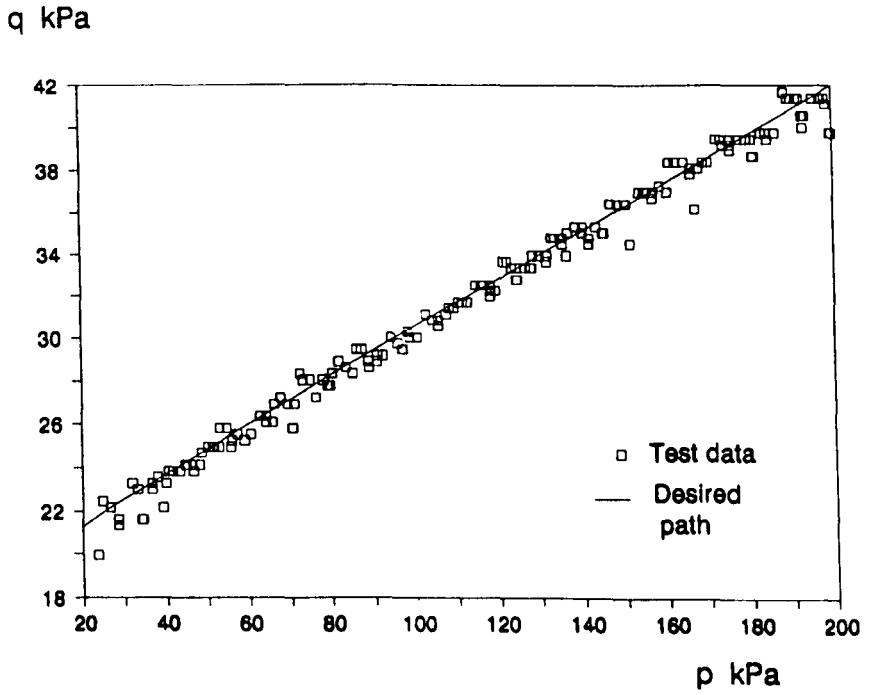

Fig 5.17 Comparison between desired and actual stress paths (test RUB2)

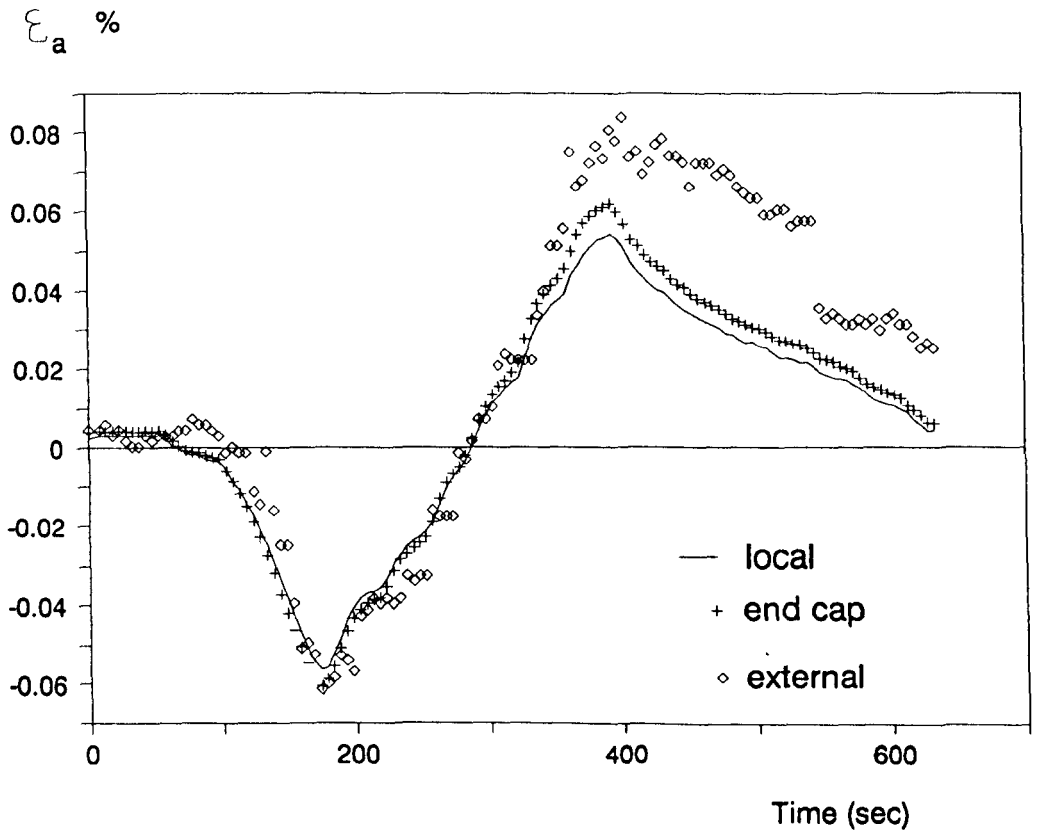

(a)

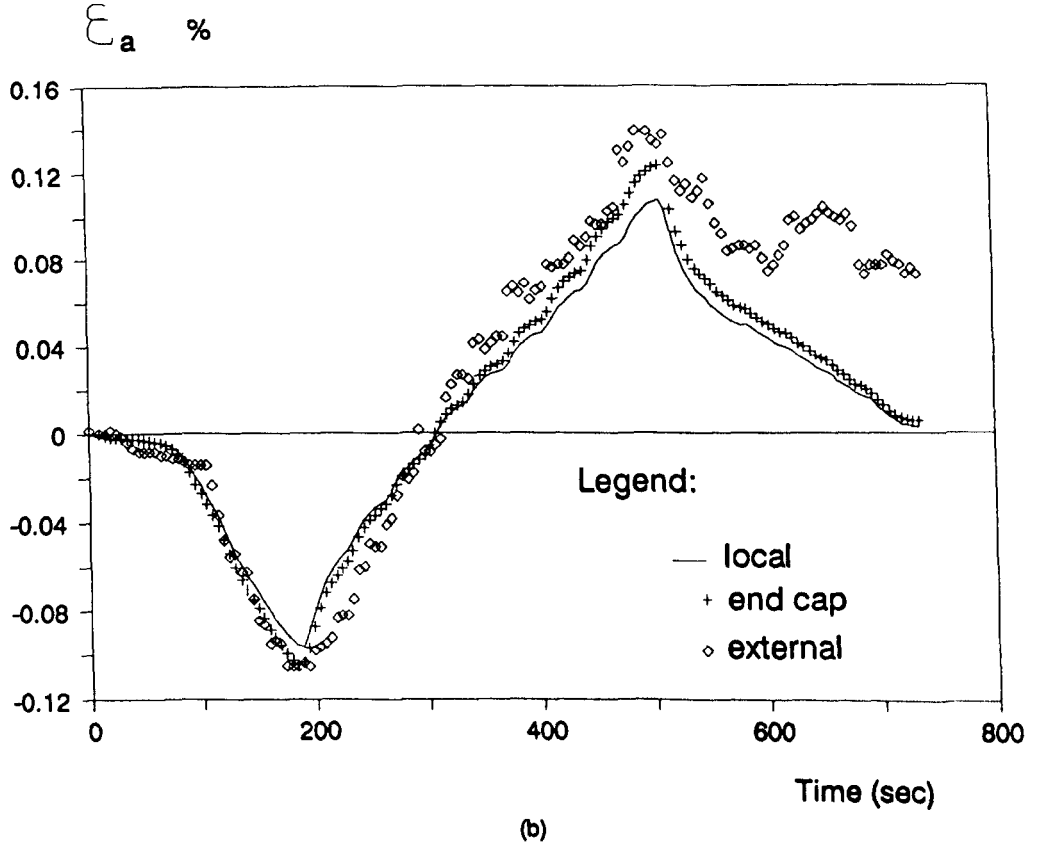

(b)

Fig 5.18 Strain cycles on the rubber specimen
(a) 0.05% ; (b) 0.1%

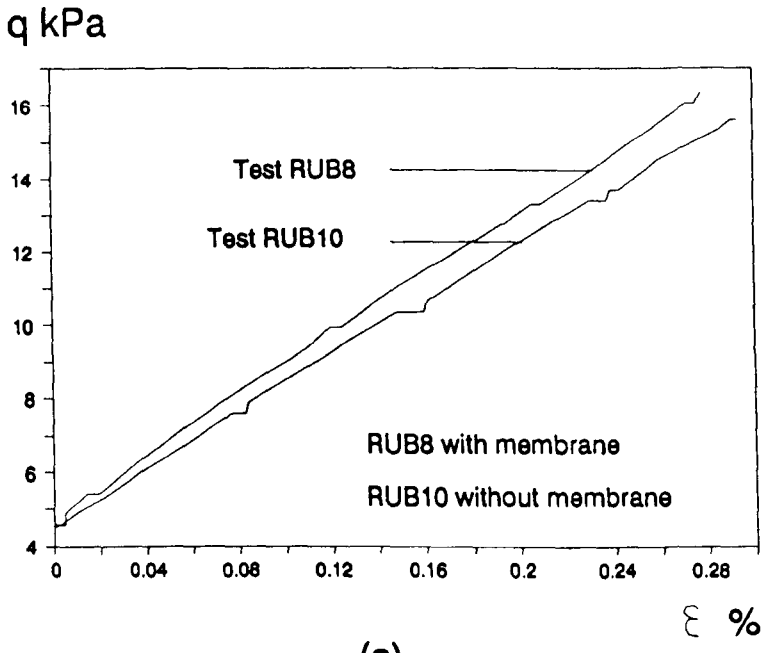

(a)

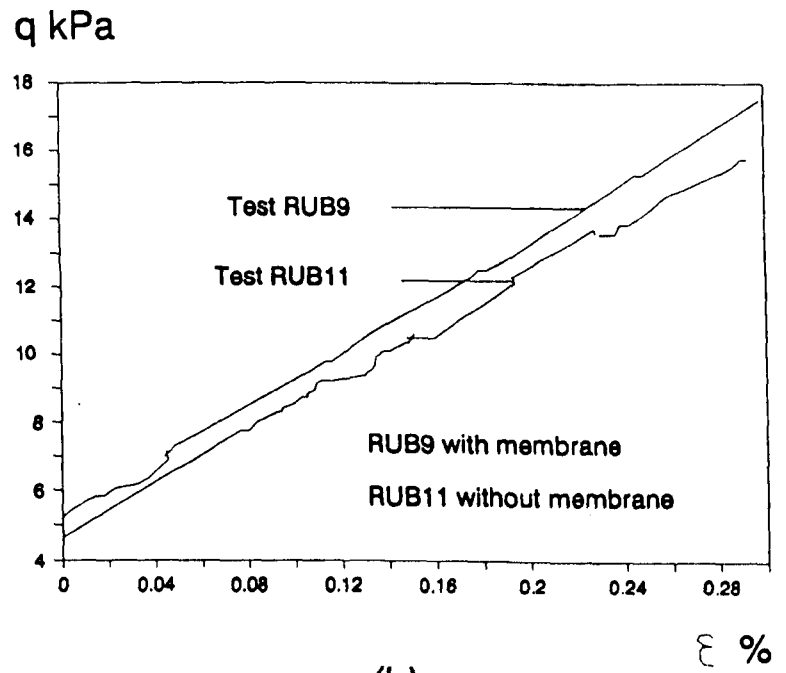

(b)

Fig 5.19 Tests to investigate membrane slippage

(a) series 1; (b) series 2

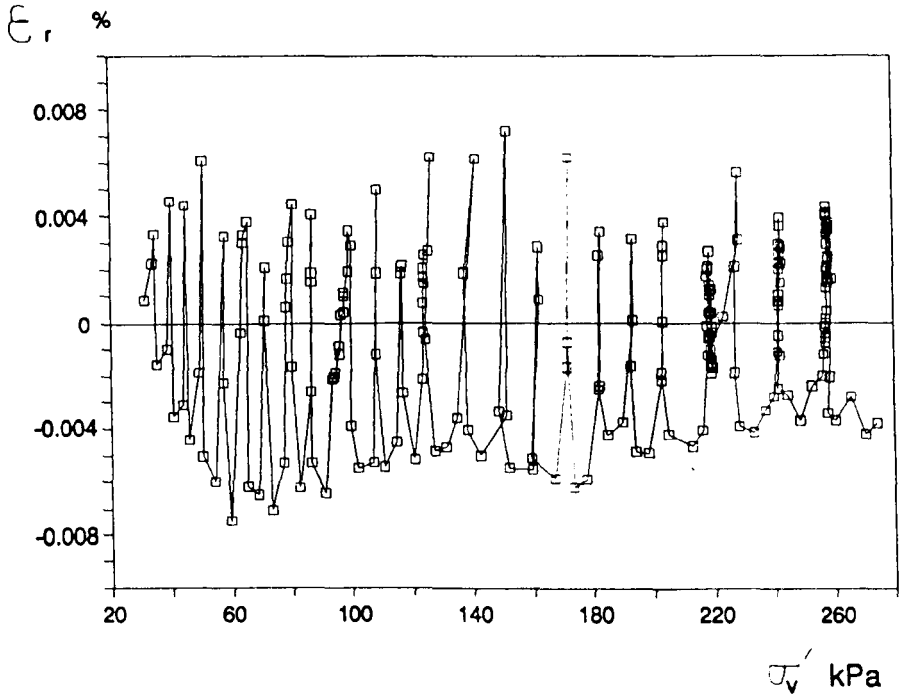

Fig 5.20 Variation of radial strain with vertical effective pressure during Ko-consolidation (Test TR2)

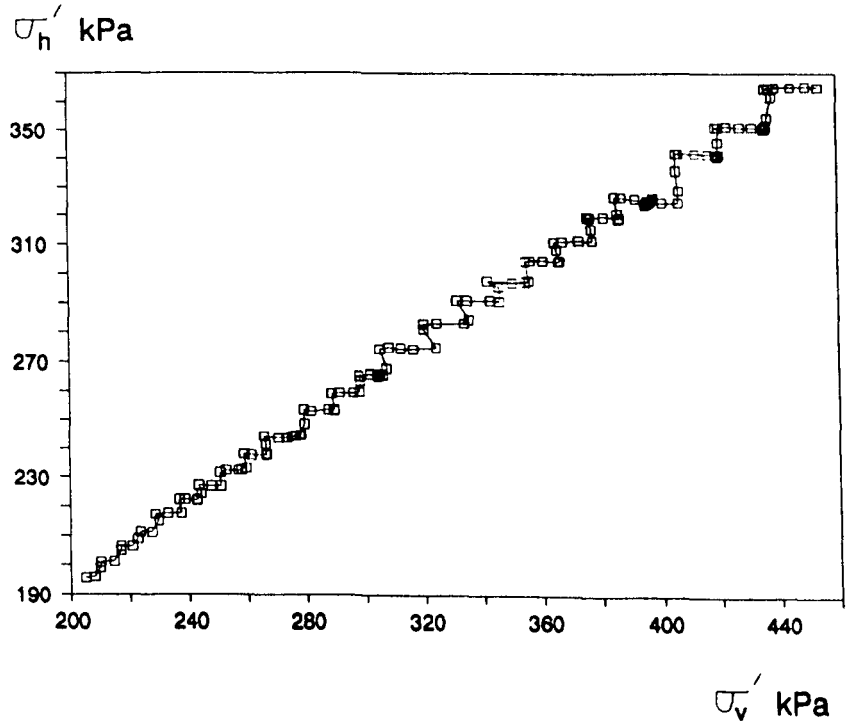

Fig 5.21 Stress path during Ko consolidation (Test TR2)

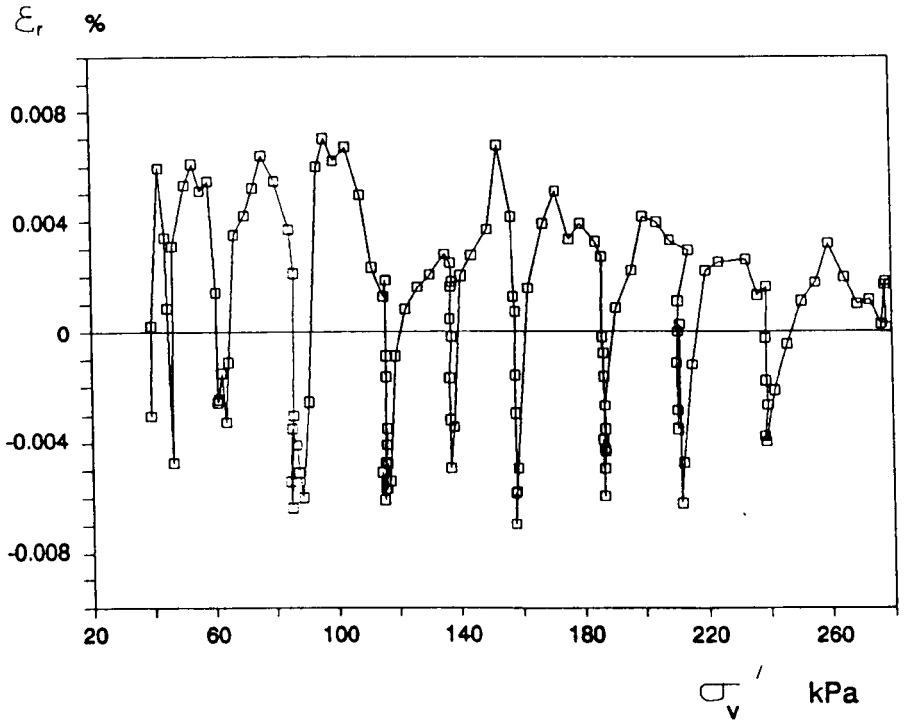

Fig 5.22 Variation of radial strain with vertical effective pressure during Ko-swelling (Test TR2)

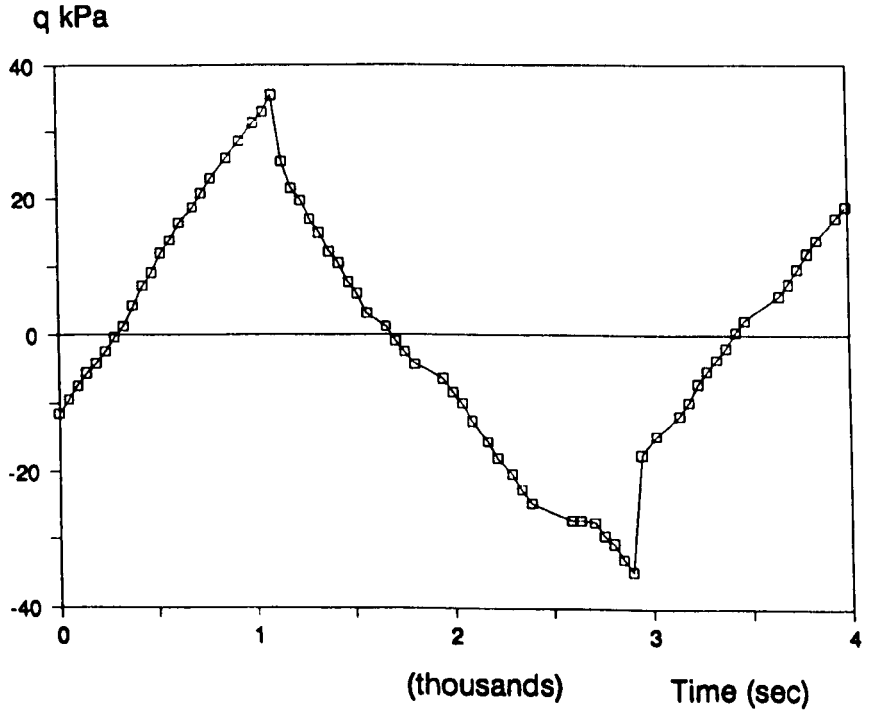

Fig 5.23 Change of deviator stress during strain cycle of amplitude 1% (Test TR2)

Chapter 6

EXPERIMENTAL RESULTS

6.1 Introduction

In this chapter the main test programme is described and the results are presented in a mainly factual manner. The results are discussed and interpreted in Chapter 7.

The test programme and the methods of processing the data and evaluating the stiffness parameters are described in the first two sections. Results from the consolidation and swelling stages of the tests in the 100 mm cell are then presented and compared with other published data. An evaluation of the axial strain measurement methods is presented in the fourth section. The final sections of the chapter deal with the shearing stage results from both normally consolidated and overconsolidated specimens. Stress paths obtained during the shearing stages (including the application of strain cycles) are compared with those published by other researchers.

6.2 Description of the Test Programme

The overall aim of the test programme was to provide an insight into tube sampling effects on the small strain behaviour of soils over a wide range of initial conditions (see Sections 1.3 and 2.5). Most natural soils are encountered in an overconsolidated condition and small strains are often associated with engineering works in heavily overconsolidated soils (e.g. Burland et al (1979)). Nevertheless, several of the present tests were carried out on normally consolidated specimens.

6.2.1 Tests in the 100 mm Apparatus

Ten tests were carried out in the 100 mm apparatus. These are listed in Table 6.1 where it can be seen that six tests (including two repeatability tests) involved normally consolidated specimens, while four tests were carried out on overconsolidated specimens. Figure 6.1 shows the stages involved in the tests. All the specimens were consolidated under zero lateral strain conditions using the technique described in Section 4.3. Half the specimens were then sheared in undrained compression, the other half in undrained extension. For each type of loading disturbed and undisturbed specimens were tested. The notation for the test names used in Table 6.1 is explained in Table 6.2. For example, test ANCU1 involved one-dimensional consolidation (A) of a normally consolidated specimen (N), was loaded in compression (C) without disturbance (U), and was the first of its type (1).

Ideally, every test would have been repeated but due to time constraints (each test took about one month to complete) this was not possible. It was decided instead to carry out two repeatability tests, one at the beginning of the testing period (ANCU2) and the other at the end (ANCD2). The latter permitted the

stability of the measuring devices and the applicability of the previously determined calibration factors to be checked. In addition, although the number of complete repeatabilty tests was limited, processes of consolidation, swelling and simulated sampling disturbance were repeated more than once.

6.2.2 Tests in the 38 mm Apparatus

In support of the tests in the 100 mm cell, isotropically consolidated and swollen specimens were tested in the 38 mm cell with special axial strain instrumentation (Section 3.4.5). Only one overconsolidation ratio (OCR = 4) was adopted in the 100 mm apparatus. Therefore, the tests in the 38 mm cell were designed, firstly, to provide more data about the effects of OCR on the small strain deformation behaviour. Secondly, tests were conducted at different shearing rates to provide information about undrained creep effects on the small strain deformation behaviour. These were carried out on normally consolidated specimens, where rate effects would be expected to be most pronounced.

Seventeen tests were carried out in the 38 mm apparatus, as listed in Table 6.3. A test name comprises the letter S followed by three numbers representing the overconsolidation ratio, the rate of shearing and the order of testing for repeatability. These numbers are separated by the symbol '/'. For example, test S2/2/1 is a test carried out in the 'small' 38 mm cell (S), at an OCR of 2 and an axial stress rate during shearing of 2 kPa/hr, and is the first of its type.

It was found in the proving tests, as in other research (e.g. Atkinson (1985)), that as long as the rate of undrained shearing was small enough, no significant gradients of pore water pressure developed in the specimen. In the investigation

of shearing rate effects three different 'slow' rates of axial stress increase of 0.5 kPa/hr, 2kPa/hr and 4 kPa/hr were adopted. In addition, much higher loading rates (about 100 kPa/hr) were adopted to provide data for comparison with the tests in the 100 mm cell involving high rates of shearing during the simulation of sampling disturbance.

As can be seen in Table 6.3, each test was repeated once. This was possible since tests in the 38 mm cell involved relatively short periods of time compared to those in the 100 mm cell.

A higher mean effective consolidation pressure was adopted in the 38 mm cell than in the 100 mm cell because it was thought that the 38 mm specimens suffered greater disturbance when they were initially set up (Section 3.5.3). For overconsolidated specimens with high OCRs (over 40) it was difficult to achieve the desired overconsolidation ratio accurately because of fluctuations in the cell pressure (see Section 3.2.2).

6.3 Data Processing

As mentioned in Section 4.3.4, test data were loaded into Lotus 123 spreadsheets before processing and the production of graphs were carried out. Extensive use was made of the least squares regression option available in Lotus 123. With this option, a curve is fitted to the experimental points, Figure 6.2. The curve is a polynomial of the form :

$$y = a_0 + a_1 x + a_2 x^2 + a_3 x^3 + ... + a_n x^n \qquad (6.1)$$

where $a_0, a_1, ...a_n$ are the coefficients calculated by Lotus 123 (along with their standard deviations), x is an experimentally determined value (independent variable)

and y is the calculated value (dependent variable). The slope of the curve at any point, $x = x_0$, is therefore :

$$y'_{x_0} = \left(\frac{dy}{dx}\right)_{x_0} = a_1 + 2a_2x_0 + 3a_3x_0^2 + ... + na_nx_0^{n-1} \tag{6.2}$$

Alternatively, by taking very small increments of x and y :

$$y'_{x_0} = \left(\frac{\delta y}{\delta x}\right) = \frac{y_2 - y_1}{x_2 - x_1} \tag{6.3}$$

with x_0 being the mean of x_1 and x_2. The above method of slope determination was found to be satisfactory in most cases (e.g evaluation of ν and K_0). However, when it was used to evaluate the tangent stiffness (i.e. $x = \epsilon$ and $y = \Delta q$) it was noticed that the fitted curve depended significantly on the polynomial degree and the amount of scatter of the data points. Thus spurious fluctuations of slope occurred, as indicated in Figure 6.3 at strains of more than 0.05 %.

Atkinson et al (1986) developed a different computerised method to evaluate the tangent stiffness. This makes use of least squares fitting to produce overlapping sections of the stress-strain curve, Figure 6.4. For each group of data points a quadratic function is fitted which is then differentiated at each point. The tangent stiffness is determined as the average of the differentials so calculated. Experience of using this method with the present data showed that, to be successful, it required evenly distributed data (i.e. data points located at constant intervals of stress or strain). Also, as illustrated in Figure 6.5, some trials were required to determine the optimum number of points in each group, n_g, and the number of points within each increment between groups, n_i, to give a smooth variation of tangent stiffness with strain.

It was desirable to develop a method for calculating both tangent and secant stiffnesses which could be used with any distribution of stress-strain data without involving the above mentioned disadvantages. When the stress-strain data are plotted

on a semi-logarithmic scale, the data plot is in the form shown in Figure 6.6. When polynomial fitting is carried out, a much better fit is obtained and the irregularities shown in Figure 6.3 disappear. The tangent stiffness can be determined as

$$E_{ut} = \frac{q_b - q_a}{\epsilon_{\ell b} - \epsilon_{\ell a}} \tag{6.4}$$

where $\epsilon_{\ell b}$ and $\epsilon_{\ell a}$ are suitably close axial strains and q_b and q_a are corresponding deviator stress values determined from the regression analysis. The secant stiffness can be calculated as :

$$E_{us} = \frac{\Delta q}{\epsilon_\ell} \tag{6.5}$$

A computer program was written in Lotus 123 'macro' language to calculate the tangent and secant stiffnesses and provide appropriate graphical output.

The sensitivity of this method to the polynomial degree (n) was examined. Figure 6.7 compares the stiffnesses based on polynomials with n of 3, 4 and 6. It can be seen that for strains of more than 0.004 %, the differences are less than 7 %. The larger difference at strains lower than 0.004 % may be the result of increased scatter in the stress-strain data due to the proportionately larger measurement errors involved (Section 5.4). An investigation was also carried out to evaluate the sensitivity of this method to the upper limit of the strain range over which the curve fitting was carried out. The results indicated that the method was relatively insensitive to this limit.

Figure 6.8 shows the superiority of the above method over Atkinson's method. It should be mentioned that, in applying Atkinson's method, the number of points on each overlapping section of the stress-strain curve (see Figure 6.4) was 40. This is much larger than the number used by Atkinson et al (1986) because the total number of data was much larger.

6.4 Consolidation and Swelling Results

As mentioned in Section 6.2.1, the tests in the 100 mm cell involved one-dimensional consolidation and swelling while tests in the 38 mm cell involved isotropic consolidation and swelling. The consolidation and swelling stages in the 38 mm cell were carried out under one increment of loading and limited data were retrieved. Therefore, only the more worthwhile data from the 100 mm cell will be presented.

In the following sections the results from consolidation and swelling stages will be presented separately. Typical data are presented in graphical form, but individual data points are too numerous to show on the graphs. Instead, in most cases curves passing through the data points are shown. In addition, appropriate critical state parameters are evaluated and compared with other published data.

6.4.1 Consolidation

In Section 3.6.2 it was explained that one-dimensional consolidation was carried out by increasing the axial and radial stresses in small increments while monitoring the radial strain. The value of K_0 was determined from a graph of the type shown in Figure 6.9, using the curve fitting procedure described in Section 6.3. As expected the plot of σ_3' versus σ_1' is linear indicating that the value of K_0 is constant during normal consolidation. Table 6.4 shows the value of K_0 from each test. The average value of 0.70 compares well with other published values, as shown in Table 6.5. However, using the empirical Equation 3.1 developed by Jaky (1944) and taking $\phi' = 23°$ (Roscoe and Burland (1968) and Al Tabbaa (1987)), a lower value of K_0 is

predicted, $K_0 = 0.61$. Brooker and Ireland (1965) suggested a revised relationship :

$$K_0 = 0.95 - \sin\left(\phi'\right) \tag{6.6}$$

which gives an even smaller value of K_0. Therefore, in the present case, the empirical formulae developed to predict K_0 do not seem to be satisfactory.

A typical variation with σ_1' of the ratio of axial to volumetric strain (ϵ_a/ϵ_v), determined from the external LVDTs and the volume change unit respectively (Sections 3.4.3 and 3.4.4) is shown in Figure 6.10. Theoretically, the ratio should be constant and equal to 1. However, Figure 6.10 indicates that during the initial stages of consolidation ϵ_a is much smaller than ϵ_v. The ratio ϵ_a/ϵ_v then increases rapidly until a constant average ratio of 0.9 is achieved. Gens (1983) reported a value of 0.88 from tests on natural soils. This result can perhaps be explained by a limited amount of membrane penetration into cavities in the vicinity of the porous stones or in the surface of the specimen. The latter is less likely in the present case.

6.4.2 Swelling

The value of K_0 during one-dimensional swelling, K_{0u}, is not constant but depends on OCR. Al-Tabbaa (1987) reported that a plot of K_{0u} versus OCR on a semi-logarithmic scale produces a straight line. However, in the present research, it was found that the relationship is visibly non-linear, Figure 6.11. As OCR approached the desired value of 4, the unloading stress path lay very close to the p' axis and hence the value of K_{0u} approached 1.

Attempts to evaluate K_{0u} theoretically (e.g. Pender (1978)) using constitutive laws have not proved successful. However, many empirical (or semi-empirical)

relationships have been proposed. For example, Schmidt (1966) suggested that :

$$K_{0u} = K_0(OCR)^{\alpha} \tag{6.7}$$

where α is a parameter which depends on the soil type. Values of α for kaolin determined by different researchers are shown in Table 6.6. Mayne and Kulhawy (1982) carried out a statistical analysis to determine K_{0u} for a wide range of soils. Using Equation 6.7 and assuming $\alpha = \sin\phi'$, K_{0u} can be evaluated as :

$$K_{0u} = (1 - \sin\phi')(OCR)^{\sin\phi'} \tag{6.8}$$

with $\phi' = 23°$ for kaolin. Wroth (1975) noticed that for small OCRs the swelling stress path in q, p' space could be represented by a straight line. Using the principles of elasticity, he suggested the following equation :

$$K_{0u} = K_0(OCR) - \frac{\nu'}{1-\nu'}(OCR - 1) \tag{6.9}$$

where ν' is the 'drained' Poisson's ratio determined from a correlation with the plasticity index. Al-Tabbaa (1987) reported an average value of ν' of 0.3 for kaolin. Equation 6.9 is only applicable for small overconsolidation ratios. At larger OCRs the assumption of elasticity becomes unrealistic but, by assuming a linear relationship between q/p' and $\ln p'$, Wroth (1971) arrived at the following equation :

$$m\left[\frac{3(1-K_0)}{1+2K_0} - \frac{3(1-K_{0u})}{1+2K_{0u}}\right] = \ln\left[\frac{(OCR)(1+2K_0)}{1+2K_{0u}}\right] \tag{6.10}$$

where m is a parameter related to the plasticity index. For kaolin, m values of 1.8 and 1.5 have been reported by Wroth (1971) and Al-Tabbaa (1987) respectively.

Mitachi and Kitago (1978) proposed the following equation for K_{0u} :

$$1 + 2K_{0u} = (1 + 2K_0)(OCR)^{\beta_1} \tag{6.11}$$

where β_1 is given by :

$$\beta_1 = -\log(1 + 2K_0/3)\log m_0 \tag{6.12}$$

and the value of m_0 can only be determined if K_{0u} is already known for a certain OCR larger than 1.

The spread of experimental data from all four of the present tests involving swelling is shown in Figure 6.12 along with the relationships reviewed above. For $OCR < 2$ reasonable agreement between the experimental results and most of the predicted values is seen. However, for $OCR > 2$ some of the equations predict far higher values for K_{0u} than those found experimentally. This discrepancy could possibly be due to differences between the methods of unloading adopted by different researchers. The rate of unloading could have a significant effect on the shape of the stress path and hence on K_{0u}.

During swelling the ratio ϵ_a/ϵ_v was found to be very close to 1 throughout the test stage, as expected.

6.4.3 Critical State Parameters

Critical state parameters from tests in the 100 mm apparatus are summarised in Table 6.7.

Figure 6.13 shows a typical plot of v versus $\ln p'$ during one-dimensional consolidation and swelling. The non-linearity of the $v - lnp'$ relationship during consolidation illustrated in this figure is mainly due to disturbance of the specimen during preparation. In the present work, λ has been calculated as the tangent to the final portion of the consolidation line. The average value of λ from 10 tests was 0.184 (see Table 6.7). A comparison of the approximately linear portion of the one-dimensional normal consolidation line with other published work is shown in Figure 6.14. Although the positions of the lines differ significantly, their slopes are

similar. A comparison of the values of λ is given in Table 6.8. Al-Tabbaa (1987) reported that a plot of $\ln v$ versus $\ln p'$ produced a straight line with a slope λ^* and found that that $\lambda/\lambda^* = 2.2$. A typical graph of $\ln v$ versus $\ln p'$ from the present research is shown in Figure 6.15. There does not appear to be any improvement on the previous plot (i.e. $v - lnp'$). A regression analysis carried out on the present data to determine the average λ^* gave a value of 0.083 and hence a ratio of $\lambda/\lambda^* = 2.22$. Both values are similar to those reported by Al-Tabbaa.

The swelling line shown in Figure 6.13 has a slope, denoted by κ, which depends on OCR, in contrast to the common assumption that κ is constant. Again, Al-Tabbaa suggested plotting $\ln v$ versus $\ln p'$ and defined κ^* as the slope of the swelling line on this plot. For values of OCR_p between 1 and 1.4, where OCR_p is defined as the ratio of p'_{max}/p' where p'_{max} is the maximum mean effective pressure the specimen has been subjected to, the average value of κ^* based on the present data was 0.0074 (see Table 6.7) which compares well with the value of 0.0078 reported by Al-Tabbaa. Over the same OCR_p range the ratio of κ/κ^* was found to be 2.19. Richardson (1988) proposed the use of two parameters, κ_1 and κ_0, representing the slopes of two straight lines fitted to the swelling data on the $v - lnp'$ plot. He reported values of 0.0057 and 0.047 for κ_1 and κ_0 respectively. The average of these two values (0.026) compares well with that reported by Al-Tabbaa (0.028) and that found during the present work (0.026).

Table 6.7 shows also the values of N_0, the reference specific volume under one-dimensional conditions (Figure 6.16), found by extrapolating the straight line portion of the consolidation line. Comparisons with other published values are shown in Table 6.8.

Because most of the specimens tested in the 100 mm cell were not brought

to a critical state condition during shearing, it was not possible to determine Γ experimentally. However, use could be made of the following equations proposed by Al-Tabbaa

$$\ln(N/N_0) = (\lambda^* - \kappa^*) \ln \frac{p'_j}{p'_{1d}} \tag{6.13}$$

$$\ln(N/\Gamma) = (\lambda^* - \kappa^*) \ln \frac{p'_j}{p'_{cs}} = (\lambda^* - \kappa^*) \ln 2 \tag{6.14}$$

where p'_j, p'_{1d}, p'_{cs} and N are as defined in Figure 6.16. Using the average experimental values for λ^* and κ^* shown in Table 6.8 and taking Al-Tabbaa's value of 1.09 for p'_j/p'_{1d}, the ratio of N/N_0 can be evaluated from Equation 6.14 as 1.006. Taking $N_0 = 3.11$ (Table 6.7), Equation 6.15 then gives a value of Γ of 3.06 which falls within the range of 2.87 to 3.44 reported by various researchers. Since the critical state line is theoretically parallel to the normal consolidation line, the experimentally determined value of λ and the predicted value of Γ can be used to draw the critical state line, Figure 6.17. On the same graph the final data points obtained during shearing stages in the 100 mm cell are also shown and are consistent with the predicted line. Since the tests were not conducted on heavily overconsolidated soil, they could be expected to produce points either on the line or to the right of it, depending on when shearing was terminated. Only a couple of the experimental points lie to the left of the line and then only by a small amount.

6.5 Evaluation of Strain Measurement Methods

Discussion in this section will mainly concentrate on the strain measurement methods used in the 100 mm cell. As described in Section 3.4, during the shearing stages measurement of axial strain was carried out locally, between the end caps and externally. Radial strain was measured locally at approximately the mid-height of the

specimen.

Stress-strain curves from a typical compression test (test ANCU1) for the small strain range are shown in Figure 6.18. The good agreement between the local and the end cap strains indicates that bedding errors between the specimen and end caps are negligible. In this test, the external strain is only slightly larger than the local or end cap strain, but the measurements suffer from a larger scatter. After correcting for the errors due to the compression of the load cell and other components using the relationship developed in Section 5.4.1, the external strain agrees more closely with the local and end cap strains, Figure 6.19. On the other hand, the stress strain data from a typical extension test (test ANEU1) plotted in Figure 6.20 show a considerably larger discrepancy between the external and the local or end cap strain.

The above results show that axial strain measurement can be adequateley carried out either locally or between the end caps under the favourable conditions applying in this research, i.e. where the specimens were homogeneous, had flat end surfaces and were one-dimensionally consolidated to a high vertical effective pressure before shearing commenced. Two features were noticed as far as external strain measurement was concerned. The first was the significantly larger scatter in the stress-strain data, resulting from the inadequate precision of the LVDTs at small strains. The second was that in situations where a change in the direction of movement of the loading piston was involved, the external axial strain appeared to be larger than both the end cap and locally measured strains. Slackness at the load cell-top cap connection and the load cell bushing connected to the cell top plate may be behind this phenomenon. However, under the favourable conditions described above, it is possible that if more precise external instrumentation is adopted, no reversal in loading direction is involved, and a correction for the load cell compression is

applied the external strain measurement could be satisfactory, even at small strains.

Although the method of connecting the load cell to the specimen top cap (Section 3.3.1) should prevent any tilting of the top cap, the measured axial deformation of the specimen was not uniform, as illustrated by the typical results of Figure 6.21. In addition, the radial strains were found to display non-uniformities which varied randomly from one test to another, Figure 6.22. It is clear, therefore, that the evaluation of Poisson's ratio from a single pair of transducer readings cannot be satisfactory. This could be one of the reasons why Yung (1987) encountered unrealistic values of Poisson's ratio in his tests on Cowden Till. Results of radial strain measurement will be presented and discussed in Section 7.2.

Typical results from the 38 mm cell (test S/2/2/1) are shown in Figure 6.23 where axial strains derived from the lower chamber volume change are compared with the end cap measurements. There are the expected dicrepancies at small strains (Figure 6.23a) but there is good agreement at larger strains (Figure 6.23b). These results suggest that confidence can be placed in the end cap strains, which ought to be superior at small strain levels.

6.6 Results from Shearing Stages

The results presented in this section relate to the shearing stages both during the simulation of sampling disturbance and 'slow' undrained loading. Sections 6.6.1 to 6.6.4 relate to the results from tests in the 100 mm cell, while in Section 6.6.5 the results from tests in the 38 mm cell are presented.

6.6.1 Results from Normally Consolidated Undisturbed Specimens

Stress paths and stress strain curves from all three normally consolidated undisturbed specimens (ANCU1, ANCU2, ANEU1) are shown in Figures 6.24 and 6.25 respectively. Unfortunately, the tests had to be terminated before large strains were achieved because of the danger of damaging the submersible LVDTs which were moving towards the cell top plate as axial strain increased. Test ANCU2 was intended to be a repeat of test ANCU1. However, large differences were noticed in both the stress paths and the stress-strain curves. The main difference between the two tests is that due to an operational error, the specimen in test ANCU2 was given a shorter rest period at the end of the one dimensional consolidation stage (approximately a third of that allowed in test ANCU1). Effects of the rest period on the stress-strain behaviour of clay soils have been experimentally investigated at relatively large strains by Richardson (1988). He concluded that the increase in stiffness is approximately linear with the logarithm of the rest period so that :

$$\Delta E = C_1 \log \Delta t \tag{6.15}$$

where Δt is the elapsed time during the rest period and C_1 is an experimentally determined constant. By considering the relative durations of the rest periods in tests ANCU1 and ANCU2 it may be predicted that

$$E_{ANCU2} = 0.7 E_{ANCU1} \tag{6.16}$$

The present experimental result, based on average stiffnesses from tests ANCU1 and ANCU2 over the strain range of 0.005 to 0.01 %, is

$$E_{ANCU2} = 0.62 E_{ANCU1} \tag{6.17}$$

which is comparable to the prediction. It should be noted that the effect of rest period on tangent stiffness decreases as axial strain increases.

The stress paths shown in Figure 6.24 did not involve large stress increments and in the compression tests no stress reversals occurred. In extension tests some temporary stress reversals took place, but these did not exceed 2.5 kPa in magnitude and usually happened after the specimen had undergone a change of deviator stress large enough to take it beyond the small strain region.

The stress paths of Figure 6.24 compare well with those in other tests on kaolin carried out by Atkinson et al (1987) and Parry and Nadarajah (1974). This is seen most clearly by normalising the results with respect to p'_{max}, Figure 6.26.

6.6.2 Results from Normally Consolidated Disturbed Specimens

As mentioned in Section 3.6, disturbance to the specimen was simulated by applying a strain cycle of amplitude 1 %, followed by a release of deviator stress and reconsolidation to the initial conditions. The complete effective stress paths for tests ANCD1, ANCD2 and ANED1 are shown in Figures 6.27 to 6.29. Due to an operational error at the beginning of the testing programme, the reconsolidation path in test ANCD1 was achieved by initially dissipating the excess pore water pressure in the specimen after the strain cycle and then moving the stress state vertically towards the original K_0- line before following this line to the initial condition. Research carried out by Hight et al (1985) and Atkinson et al (1989) illustrated the importance of following the original K_0- line during reconsolidation if the effects of the recent stress history are to be minimised.

Variations of the mean effective pressure with time during the application of the strain cycle are shown in Figure 6.30 where the overall decrease in p' varies between 40 and 60 %. During loading phases (positive increments of axial stress) a large increase in the pore water pressure is noticed, while during unloading (negative increments of axial stress) the pore water pressure is relatively constant. Step changes in pore water pressure can also be seen which correspond to quick reversals of loading direction.

Changes in water content as a result of sampling disturbance and reconsolidation are shown in Table 6.9. The average drop in water content is about 1.5 % which is significant enough to cause changes in the strength and stiffness of the specimens as will be shown in Section 7.3.

For comparison purposes, in Figure 6.31 the strain cycle stress path from test ANCD1 is shown alongside that reported by Baligh et al (1987) for Boston Blue clay and that estimated by Hight et al (1985). The general shapes are fairly similar and the drop in p' found presently is comparable with that reported by Baligh et al. The shapes during the initial loading phase are closely similar, but both Baligh et al and Hight et al show a large decrease in p' during the unloading phase while the present data indicates a somewhat more moderate drop in p' during this phase. While Baligh's experimental curve shows a slight recovery in p' during the second (last) loading phase, Hight's estimation indicates no significant change in p' and the present data displays a fairly significant drop in p'. Such differences may be the result of differences in the method of application of the cycle. For example, Baligh's data does not show such a large change in deviator stress between the cycle phases as that seen in the current work, where the abrupt change in the loading direction was carried out quickly (with a sizeable change of deviator stress) to prevent the axial strain from overshooting. Indeed, the fact that in Baligh's work the stress

path during the initial compression phase was similar to that for a slowly tested undisturbed specimen suggests that the strain cycle was applied more slowly than in the present case, where axial stress rates over 100 kPa/hr were used (the effects of rate of loading on the position of the stress path and the deformation behaviour will be discussed in detail in Chapter 7).

The stress-strain curves from the three strain cycles are shown in Figure 6.32. Repeatability is evidenced by the closeness of these curves, especially during the initial compression phase. These stress strain curves compare well with those reported by Baligh et al, Figure 6.33. Scatter in the test data both within and between tests, starts to increase during the unloading and reloading phases, as can also be seen in the data of Baligh et al. In the present case, this could be partly due to the difficulty of applying a maximum positive axial strain of 1.0 % under stress control at high rates of loading, as discussed in Section 5.4.3. At a strain of about 0.4 %, the deviator stress becomes constant as strain increases, indicating that the specimens had failed. The failure of normally consolidated specimens during tube sampling was noted by Baligh et al. The deviator stress at the end of the strain cycle is slightly lower than that at the beginning, a feature also noticed in Baligh's data.

Stress-strain curves in the small strain region during shearing after reconsolidation are shown in Figure 6.34. Although test ANCD2 is a repeat of test ANCD1 it had a different reconsolidation path as explained above. However, both tests show similar deformation behaviour at small strains. Based on this limited experimental evidence, it can be concluded that, as long as the final stage of the reconsolidation stress path approaches the initial condition in the same way (i.e. along the original K_0-line), the same deformation behaviour at small strains will be obtained. However, there is likely to be a minimum distance which the specimen has to travel along

the K_0-line before the recent history effects can be effectively erradicated (Atkinson et al (1989)).

6.6.3 Results from Overconsolidated Undisturbed Specimens

Two tests, AOCU1 and AOEU1, on undisturbed overconsolidated specimens (OCR=4) were carried out, one in compression and the other in extension. The stress paths and stress-strain curves for these tests are shown in Figures 6.35 and 6.36 respectively.

The normalised stress paths from both tests are shown in Figure 6.26 where, although the starting points are different, the pattern of the current data is similar to that reported by other researchers.

6.6.4 Results from Overconsolidated Disturbed Specimens

Two tests were conducted on specimens with simulated sampling disturbance. The stress paths from these tests, AOCD1 and AOED1, are shown in Figures 6.37 and 6.38. In both tests the effective stress state after disturbance is very close to the initial state. Since the direction of approach of the stress path to the initial conditions during reconsolidation may influence the stiffness response, the reconsolidation was conducted in the manner illustrated in Figure 6.39 which relates to test AOCD1.

Changes in p' during the strain cycle in both tests are shown in Figure 6.40. At the end of the cycle a reduction of not more than 10 % is observed. Hight et al (1985) reported that during tube sampling heavily overconsolidated specimens

would exhibit an increase rather than a decrease in p', as would occur with normally consolidated soil. Hence, moderately overconsolidated specimens might be expected to exhibit a neutral response. This is confirmed by the results from the current tests. It is also reflected in the relatively small changes in water content during sampling and reconsolidation, Table 6.10. These changes might be expected to have a smaller effect on the stress-strain behaviour than in the case of normally consolidated specimens.

Stress-strain curves over the whole strain cycle for these specimens are shown in Figure 6.41 where good repeatability can be noticed. In contrast to the normally consolidated specimens, the overconsolidated specimens do not appear to have undergone failure.

Stress-strain curves for the disturbed specimens during shearing after reconsolidation are shown in Figure 6.42.

6.6.5 Results from the Isotropically Consolidated Specimens

Stress paths and stress strain curves from the eleven tests on isotropically consolidated and swollen specimens with a rate of axial stress increase of 2 kPa/hr are shown in Figures 6.43 and 6.44 respectively. The stress paths and stress-strain curves for tests with other rates of loading are shown in Figure 6.45 and 6.46 respectively. The more erratic stress path data from these tests, which were conducted in the 38 mm cell, can be blamed on the lower accuracy of the pressure control devices (see Section 3.2.2). The strain data are also of lower quality than those obtained from the 100 mm cell. Although the end cap strain data should perhaps have been of comparable

accuracy in the two cells, this was not the case since one of the submersible LVDTs used in the 38 mm cell had a significantly lower precision (see Section 5.2.6). As a result, the repeatability of data from this cell is less good than that of data from the 100 mm cell.

Comparison of the normalised stress paths with data published by other researchers is shown in Figure 6.47. General agreement between the current and published data sets is seen for both normally consolidated and overconsolidated specimens.

Test	OCR	$\lvert \varepsilon_{max} \rvert$ %	Loading	σ'_{v0} (kPa)	p'_0 (kPa)	w_i^* %	w_f^c %	Cake
ANCD1	1	1.0	Compression	351.5	285.5	52.0	42.08	1
ANCU1	1	0.0	ditto	350.0	285.3	52.0	44.2	1
ANCU2	1	0.0	ditto	342.8	277.1	51.5	43.8	1
ANEU1	1	0.0	Extension	347.0	281.0	53.4	43.13	1
ANED1	1	1.0	ditto	345.0	276.0	53.0	41.9	1
AOCU1	4	0.0	Compression	86.4	82.7	51.5	45.5	2
AOCD1	4	1.0	ditto	87.0	89.2	52.7	44.15	2
AOEU1	4	0.0	Extension	86.4	84.3	53.4	44.5	2
AOED1	4	1.0	ditto	81.8	82.1	53.0	44.53	2
ANCD2	1	1.0	Compression	347.9	279.9	53.5	42.60	2

Notes :

* Average of top and bottom trimmings (before test)

c Average of six portions (after test)

Table 6.1 Summary of the main tests in the 100 mm cell

Letter	Meaning
A	one-dimensionally consolidated
I	isotropically consolidated
N	normally consolidated
O	overconsolidated
C	compression loading
E	extension loading
U	undisturbed (no strain cycle)
D	disturbed (with strain cycle)

Table 6.2 Notation for test names in the 100 mm cell

Test	OCR	Rate kPa/hr	p'_0 kPa	w_i^* %	w_f^* %
S1/130/1	1	130	327	51.6	41.5
S1/2/1	1	2	329	51.3	42.0
S1/4/1	1	4	325	53.2	42.5
S1/0.5/1	1	0.5	321	51.7	42.7
S1/4/2	1	4	315	52.5	42.9
S1/0.5/2	1	0.5	313	53.0	41.6
S1/2/2	1	2	316	53.0	41.8
S1/100/1	1	100	329	51.8	42.4
S4/2/1	4	2	84	53.4	43.0
S4/2/2	4	2	84.6	53.0	42.8
S10/2/1	10	2	35	53.1	43.0
S8/2/1	8	2	46	52.5	45.8
S35/2/1	35	2	9	53.1	45.8
S45/2/1	45	2	7	53.8	46.0
S8/2/1	8	2	4	53.3	45.0
S2/2/1	2	2	163	53.6	42.0
S2/2/2	2	2	160	53.5	42.0

Notes:

* Average of top and bottom

i before test

f after test

Table 6.3 Summary of the main tests in the 38 mm cell

Test	K_o
ANCD1	0.71
ANCU1	0.72
ANCU2	0.68
ANEU1	0.72
ANED1	0.70
AOCU1	0.71
AOCD1	0.69
AOEU1	0.70
AOED1	0.70
ANCD2	0.70
Average	0.70

Table 6.4 Summary of K_o values during normal consolidation

Reference	K_o
Author	0.70
Calladine (1971)	0.71
Al-Tabbaa (1987)	0.69
Roscoe and Burland (1968)	0.70
Burland (1967)	0.69
Parry & Wroth (1976)	0.64
Sketchly and Bransby (1973)	0.66
Richardson (1987)	0.63

Table 6.5 Comparison of average experimental and other reported K_o values

LL %	PI %	Clay Content	ϕ'	OCR_{max}	α	Reference
72	32	-	22.6	2.6	0.66	Parry and Nadarajah (1973)
-	-	-	23.2	5.2	0.38	Parry and Wroth (1976)
76	37	68	20.7	4.0	0.29	Sketchley and Bransby (1973)
-	-	-	23.0	7.8	0.28	Burland (1967)
55	23	40	23.3	40	0.30	Singh (1966)
-	31	-	23.0	10	0.46	Al-Tabbaa (1987)
-	-	-	-	-	0.47	Schmidt (1966)
-	-	-	-	-	0.41	Schmertman (1975)
-	-	-	-	-	0.50	Meyerhof (1976)

Table 6.6 Reported values of α for kaolin
(partly after Mayne and Khulhawy (1982))

Test	$v^{\wedge}$	λ	λ^{*}	k^{+}	k^{*}	N_0	η'_0
ANCD1	2.111	0.186	0.084	-	-	3.189	0.345
ANCU1	2.105	0.188	0.086	-	-	3.130	0.341
ANCU2	2.110	0.185	0.083	-	-	3.110	0.354
ANEU1	2.100	0.188	0.085	-	-	3.140	0.355
ANED1	2.110	0.185	0.084	-	-	3.100	0.375
AOCU1	2.135	0.186	0.084	0.0172	0.0078	3.150	0.0661
AOCD1	2.136	0.180	0.082	0.0150	0.0068	3.120	0.0520
AOEU1	2.154	0.181	0.082	0.0150	0.0069	3.130	0.0200
AOED1	2.179	0.175	0.080	0.0174	0.0079	3.120	0.0050
ANCD2	2.128	0.185	0.084	-	-	3.110	0.361

Notes : ^ just before shearing

\+ over the initial part of swelling

Table 6.7 Summary of the critical state parameters from the present work

Ref.	λ	λ^*	k	k^*	N_0	M	η'_0
Author	0.184	0.083	0.162	0.0079	3.12	0.9	0.34
Al-Tabbaa	0.187	0.085	0.171	0.0078	3.13	0.9	-
Pender	0.180	-	0.06	-	-	1.0	0.4
Atkinson	0.180	-	-	-	-	0.92	0.32
Richardson	0.190	-	0.05	-	3.26	0.95	-

Table 6.8 Comparison between experimental and other reported critical state parameters

Test	w % (before)	w % (after)	Change %
ANCD1	43.70	42.08	1.62
ANCD2	43.90	42.60	1.30
ANED1	43.40	41.89	1.51

Table 6.9 Changes in water content due to disturbance of normally consolidated specimens

Test	w % (before)	w % (after)	Change %
AOCD1	44.21	44.15	0.06
AOED1	44.38	44.53	-0.15

Table 6.10 Changes in water content due to disturbance of overconsolidated specimens

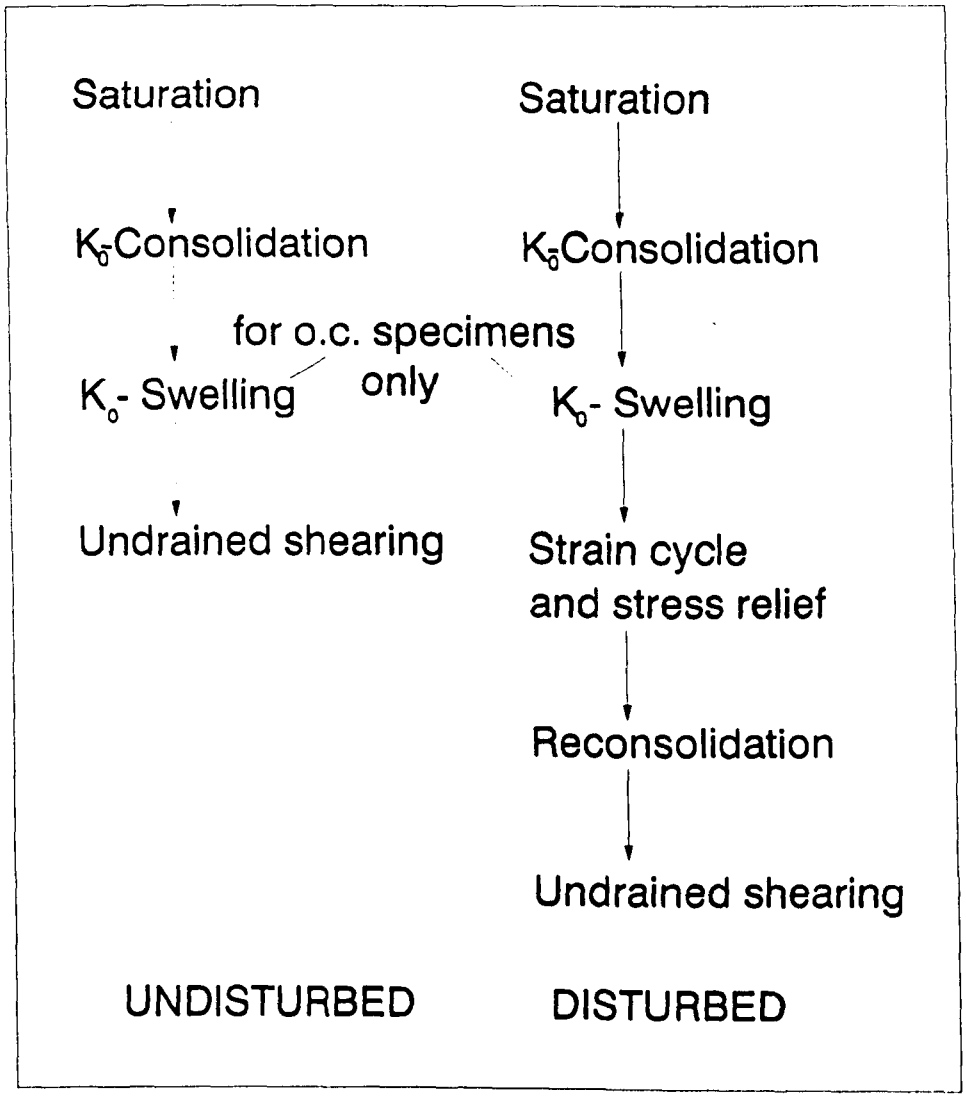

Fig 6.1 Test stages in the 100 mm cell

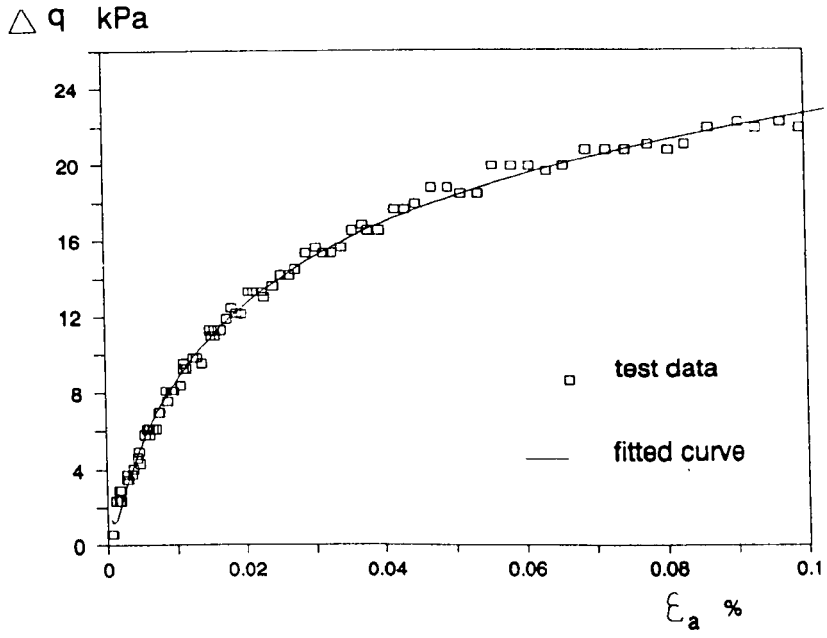

Fig 6.2 Curve fitting to experimental stress-strain data (test ANCU1)

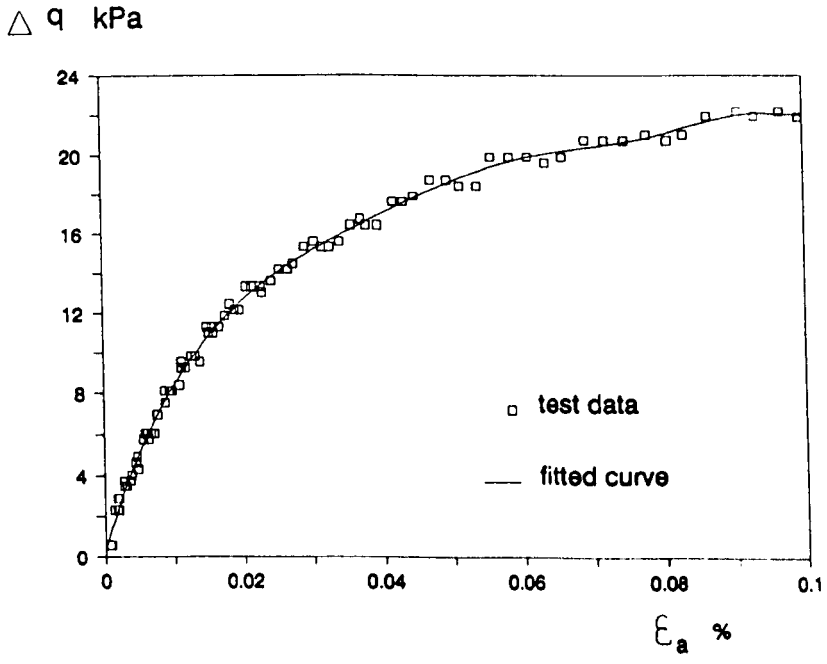

Fig 6.3 Fluctuations in the fitted curve due to fitting technique (test ANCU1)

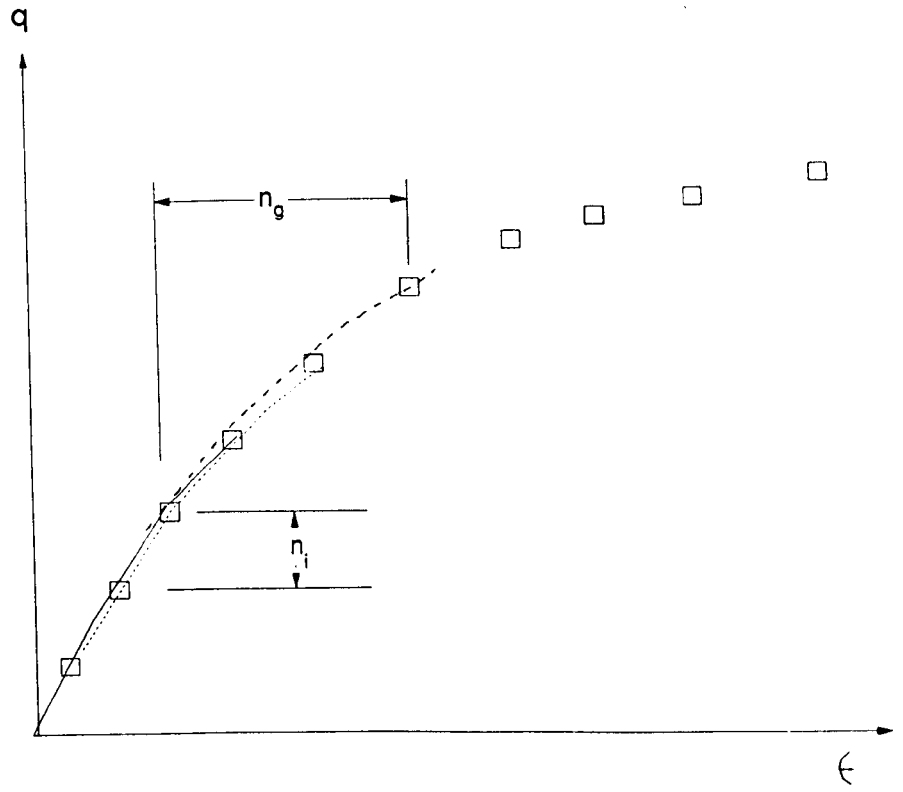

Fig 6.4 Polynomial fitting for overlapping portions of the stress-strain curve

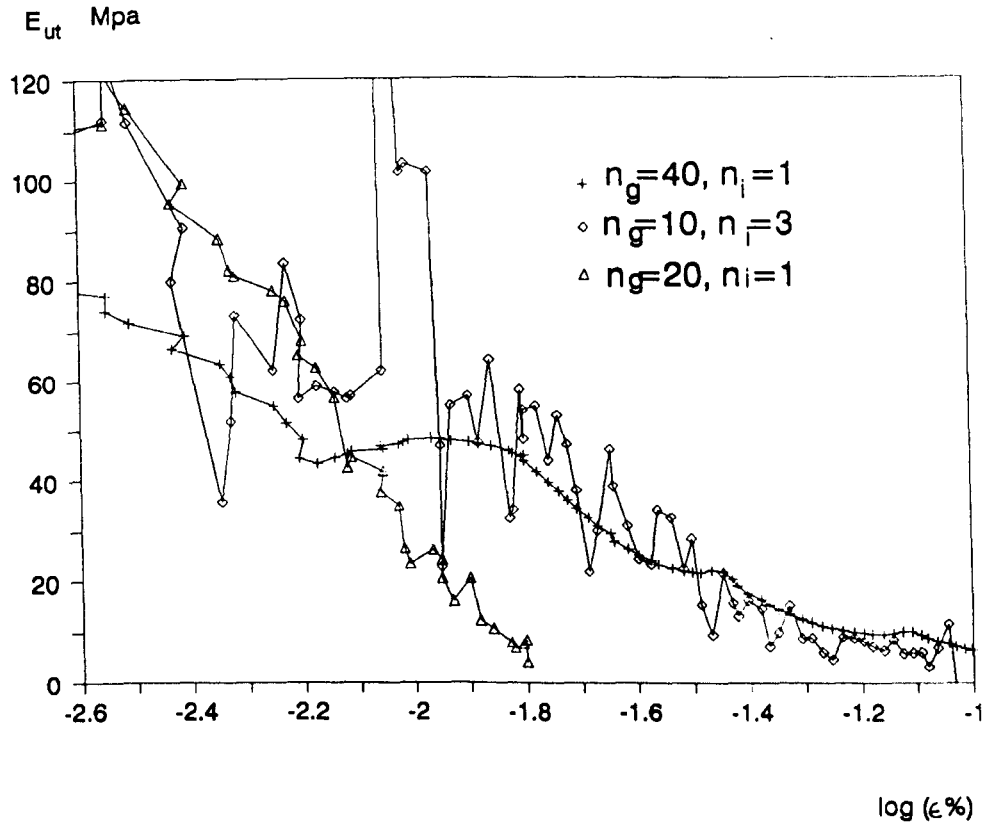

Fig 6.5 Sensitivity of Atkinson et al's method to n_g and n_i (test ANCU1)

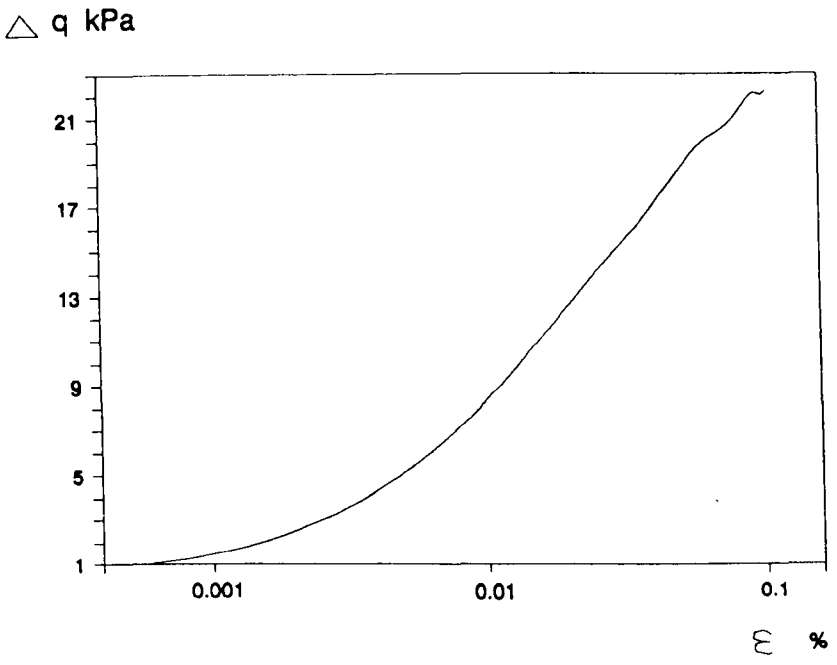

Fig 6.6 Typical stress-strain plot on a semi-logarithmic scale (test ANCU1)

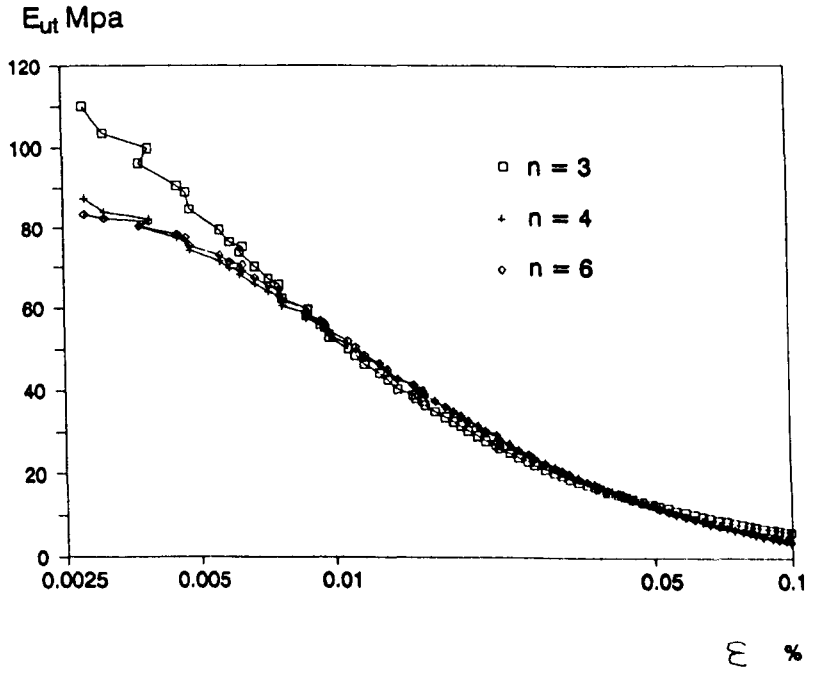

Fig 6.7 Sensitivity of the proposed fitting method to the polynomial degree (test ANCU1)

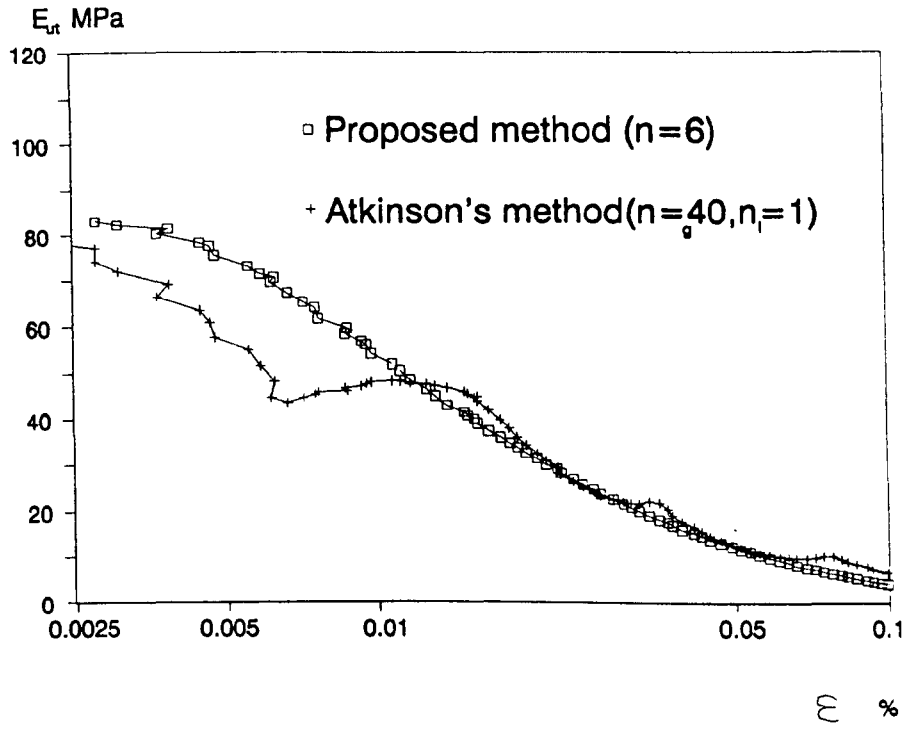

Fig 6.8 Comparison between proposed and Atkinson et al's fitting methods (test ANCU1)

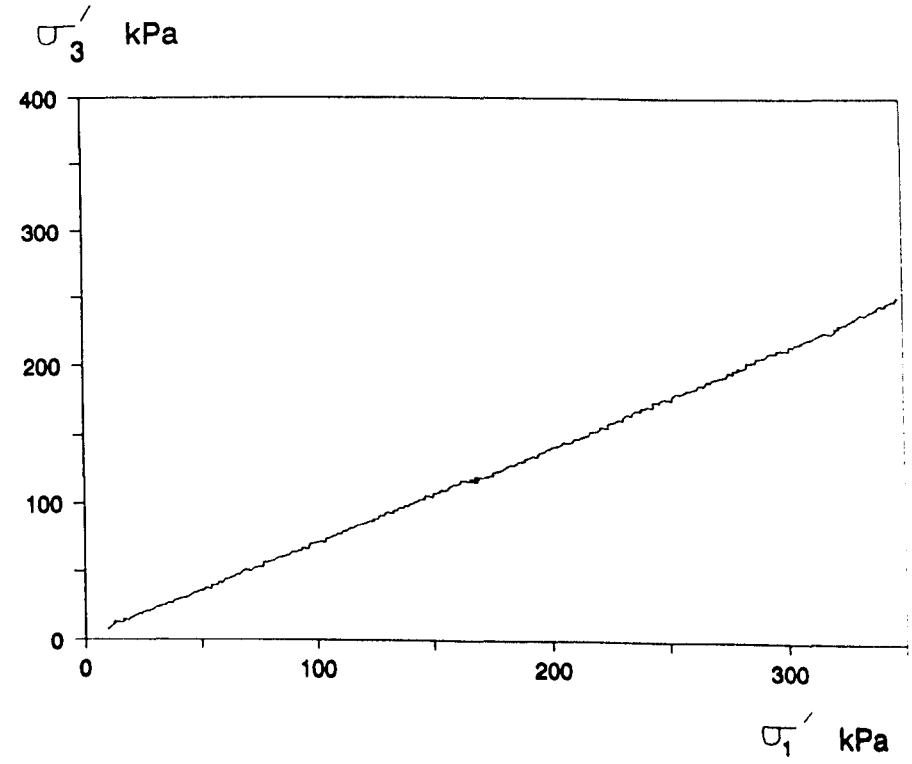

Fig 6.9 Typical stress path during K_o-consolidation (test AOCU1)

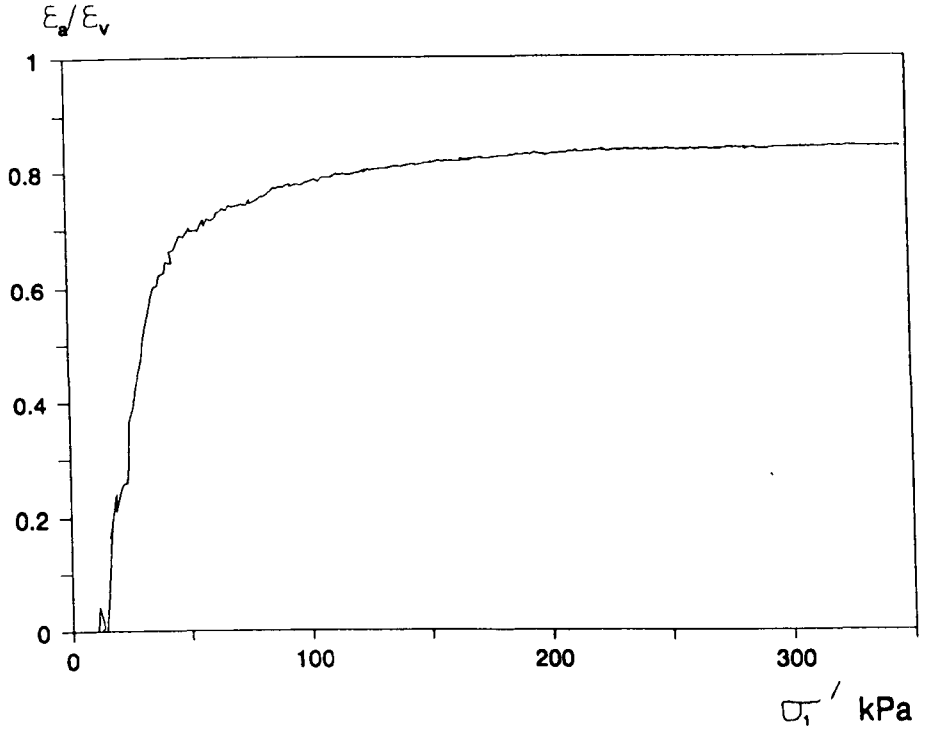

(a) strain ratio versus vertical stress

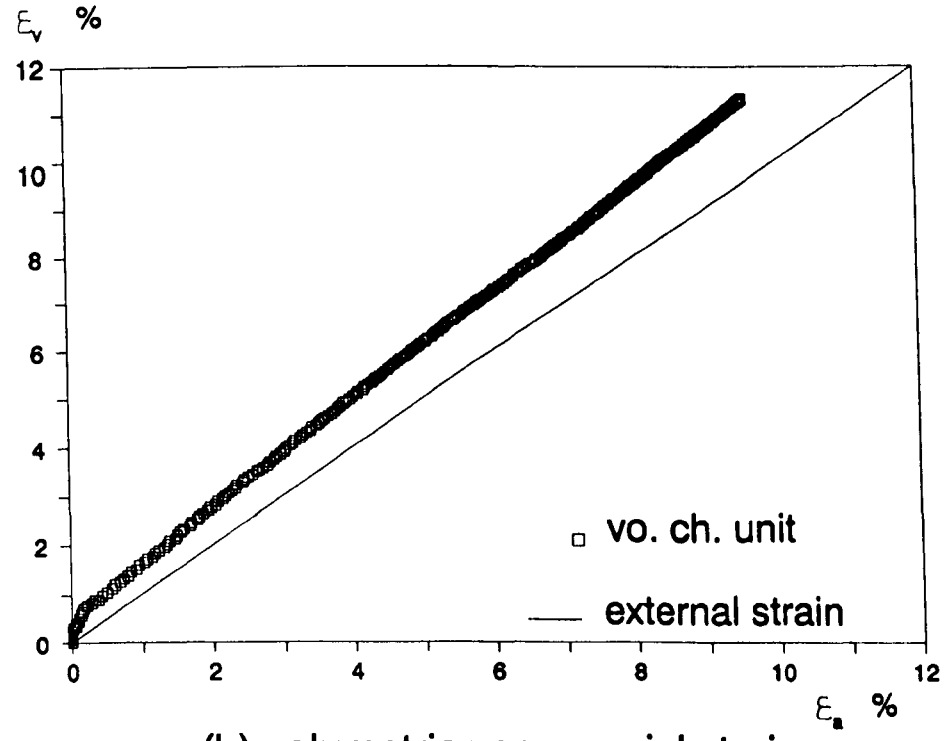

(b) volumetric versus axial strain

Fig 6.10 Relationship between axial and volumetric strains during $K_o$consolidation

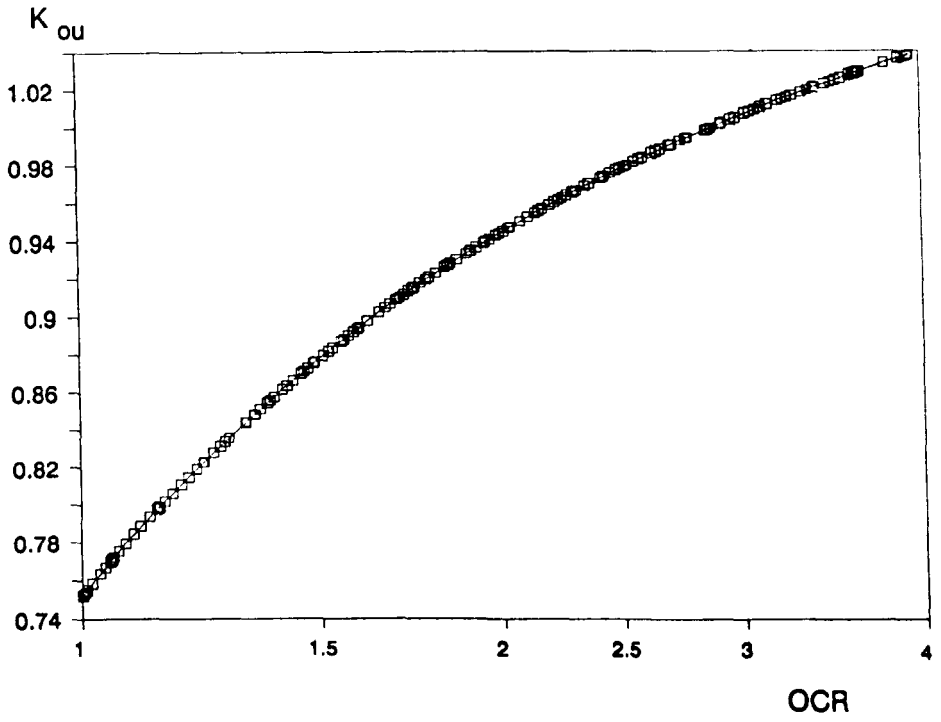

Fig 6.11 Typical variation of K_{ou} with ln(OCR) (test AOCU1)

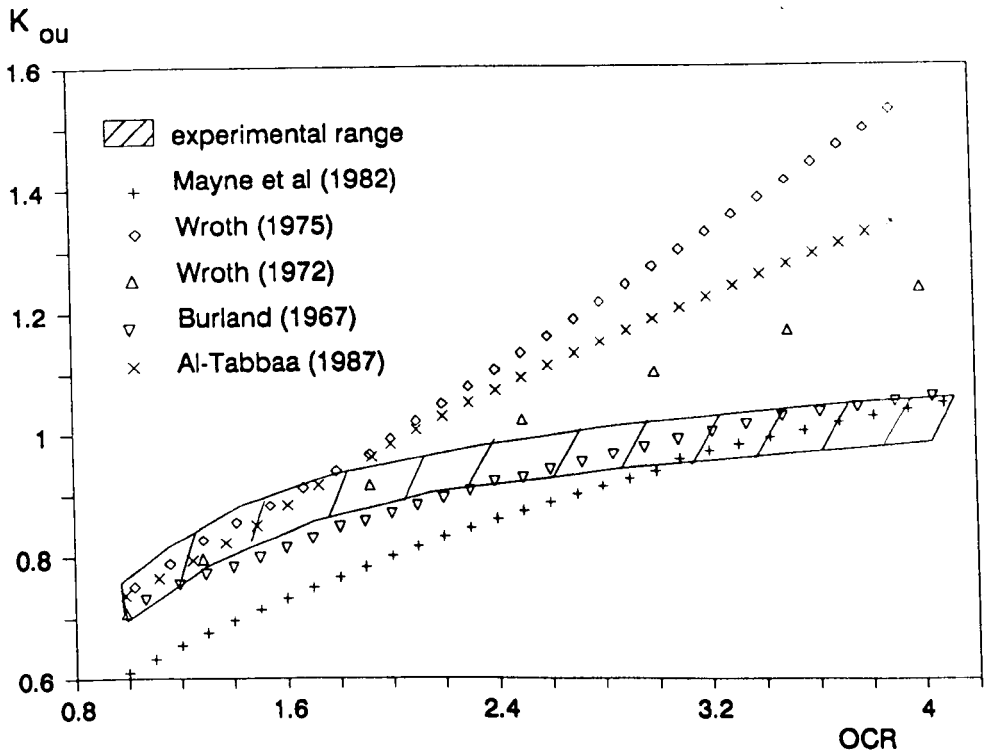

Fig 6.12 Comparison between experimental and reported K_{ou}-OCR relationships

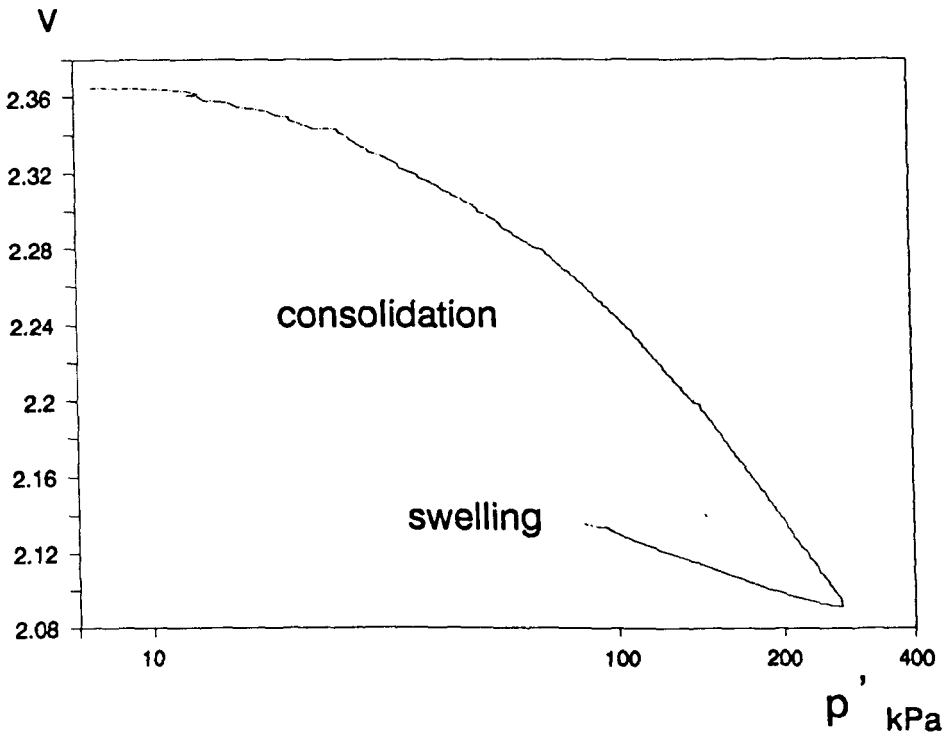

Fig 6.13 Typical v-ln p' plot during K_o consolidation and swelling (test AOCU1)

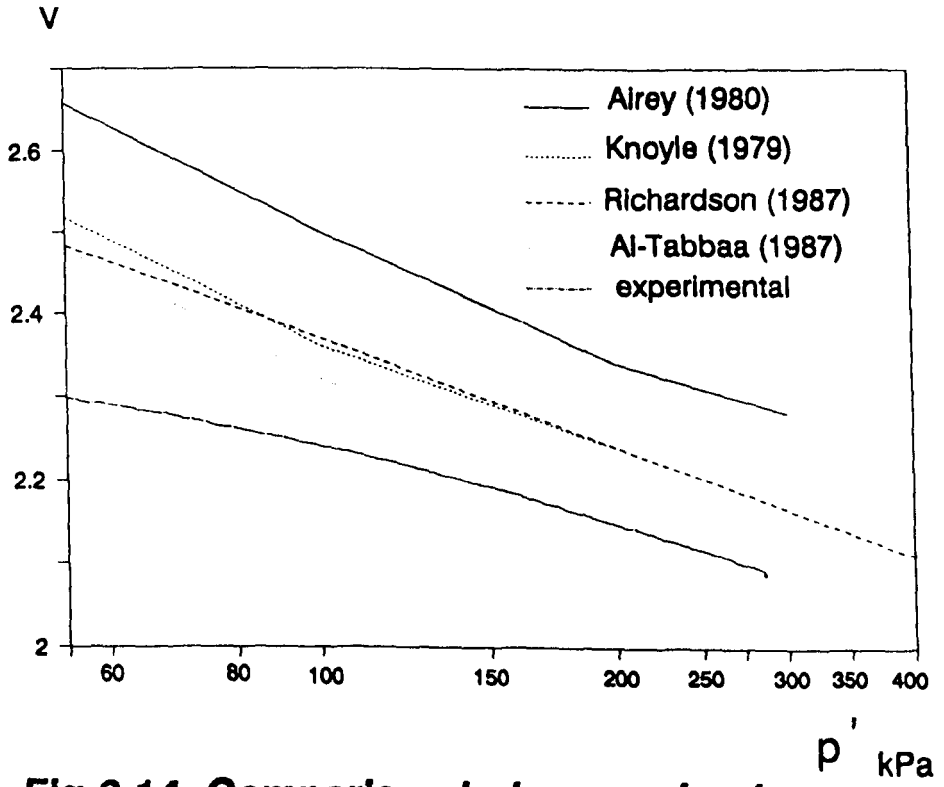

Fig 6.14 Comparison between v-ln p'curve during K_o consolidation with curves from other researchers

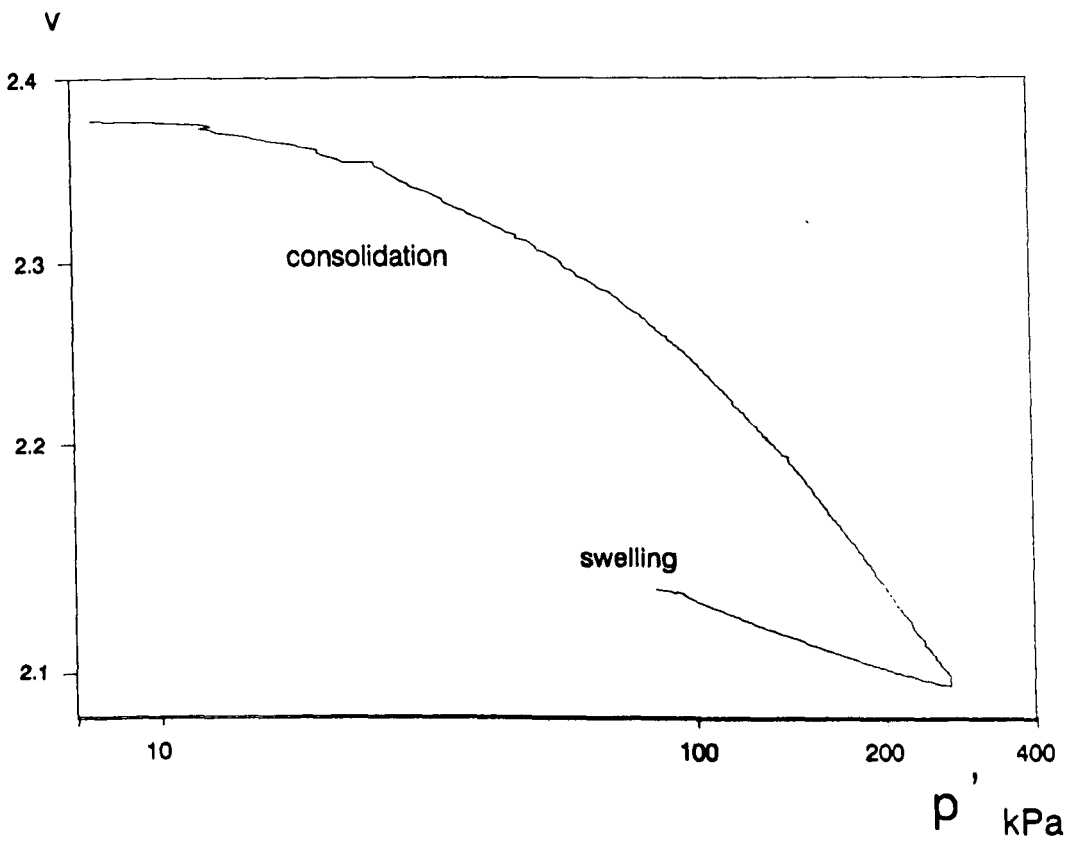

Fig 6.15 Variation of ln v with ln p' during K_o consolidation and swelling (test AOCU1)

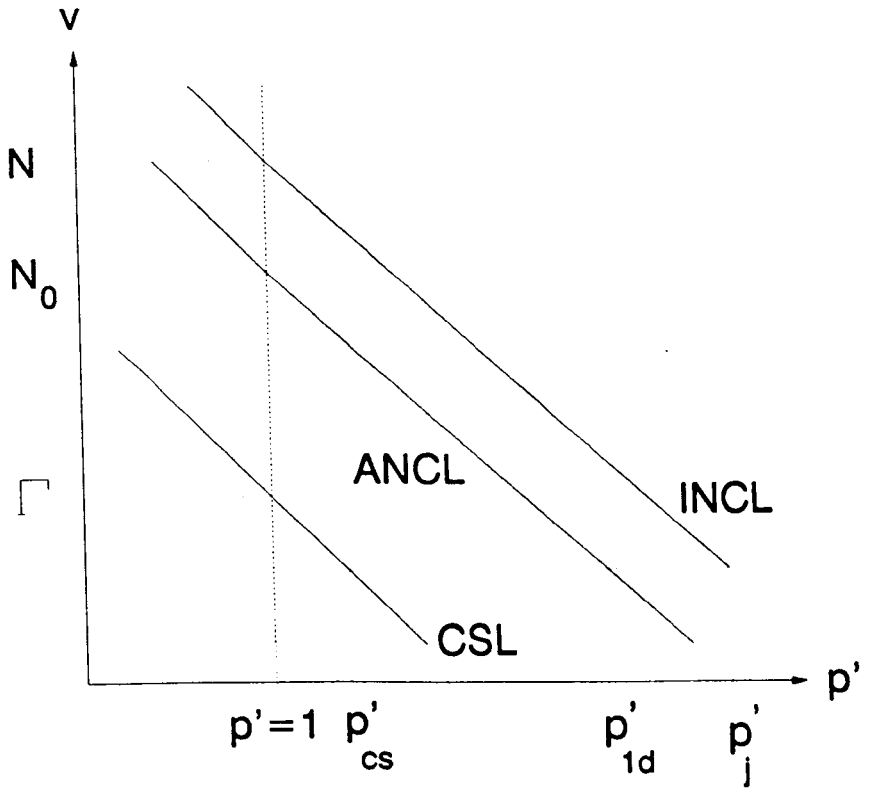

INCL : Isotropic normal consolidation line
ANCL : Anisotropic normal consolidation line
CSL : Critical state line

Fig 6.16 Definition of parameters used in equations 6.13 and 6.14

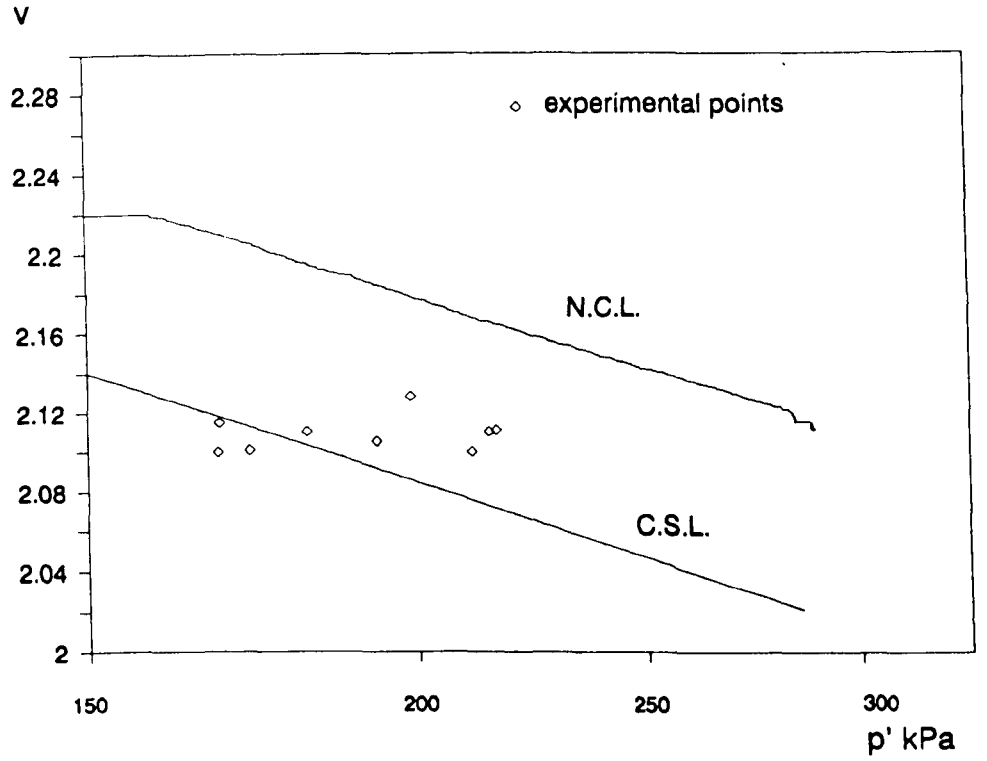

Fig 6.17 Position of experimental data points at the end of shearing with respect to the estimated critical state line

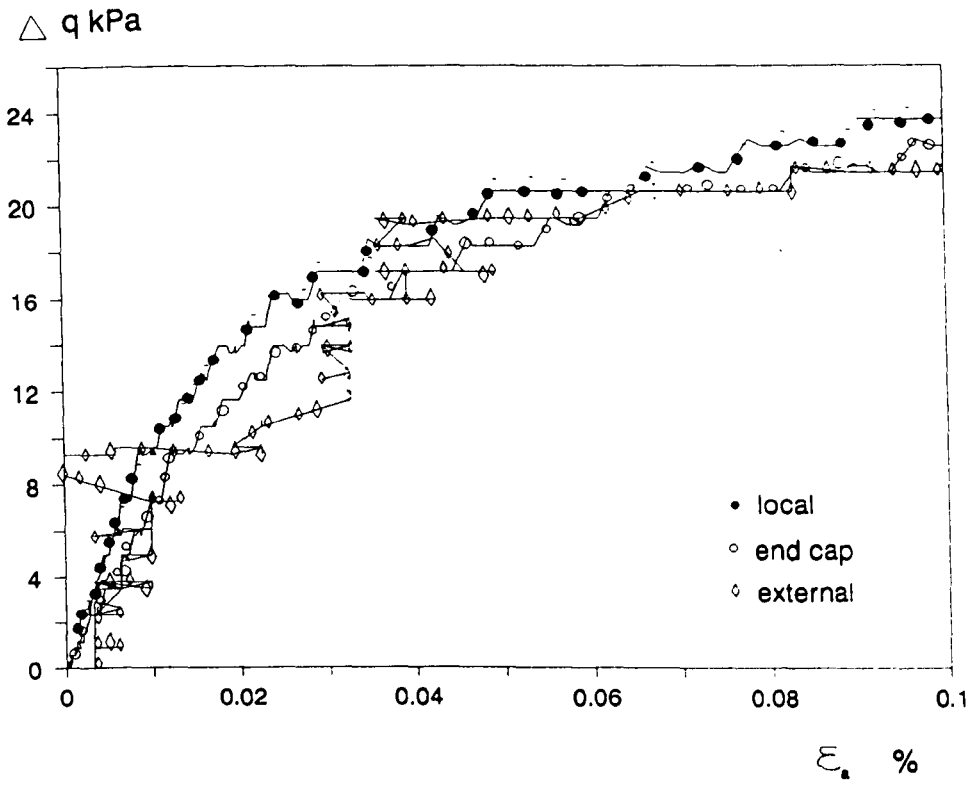

Note : only selected data points are shown

Fig 6.18 Stress-strain curves from local, end cap and external measurements. compression loading - test ANCU1

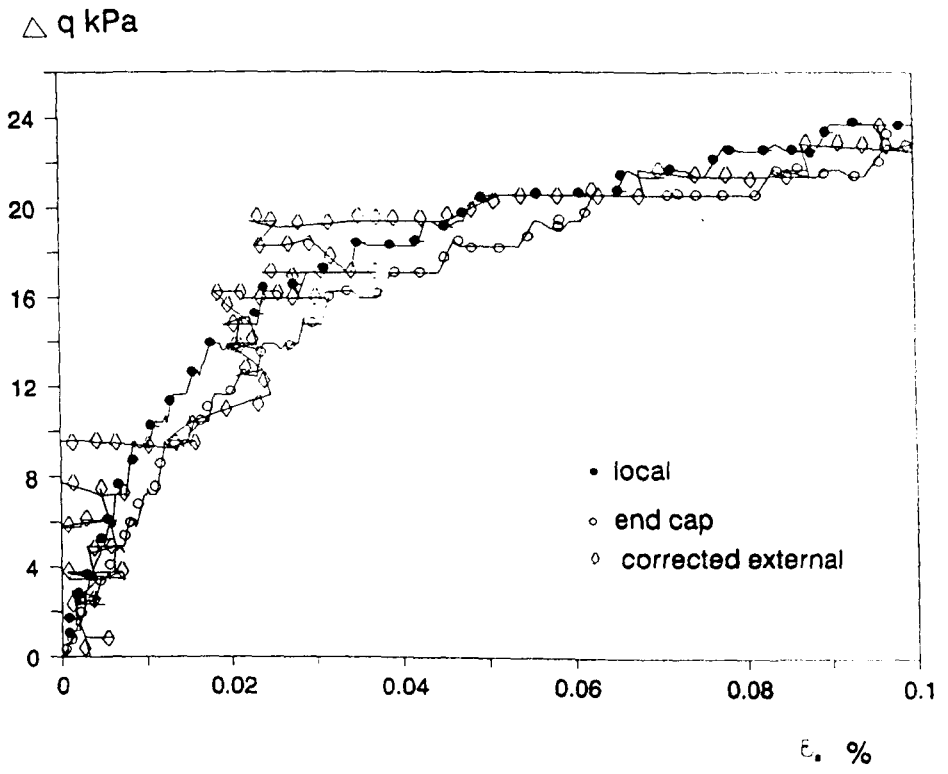

Note : only selected data points are shown

Fig 6.19 Stress-strain curves from local, end cap and corrected external measurements . compression loading-test ANCU1

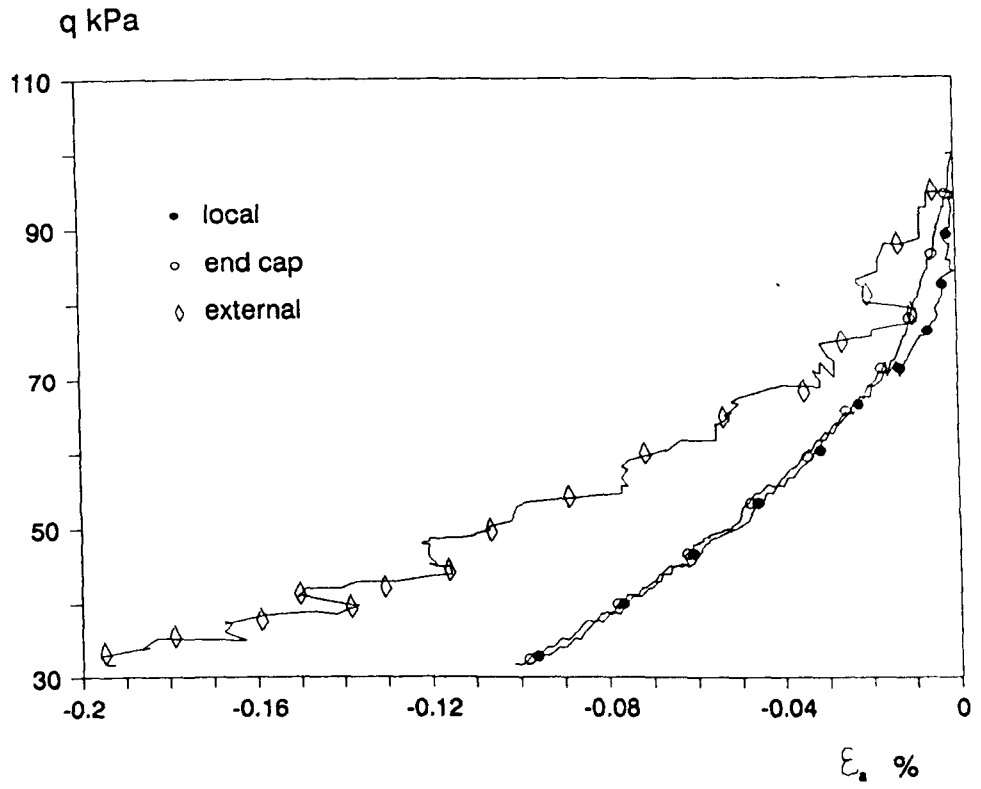

Note : only selected data points are shown

Fig 6.20 Stress-strain curves from local, end cap and external strain measurements. extension loading-test ANCE1

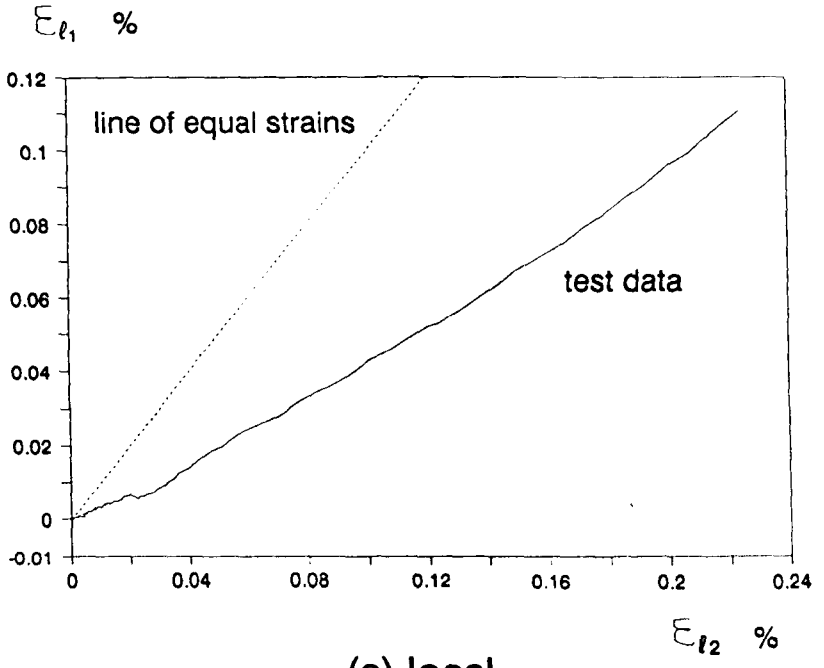

(a) local

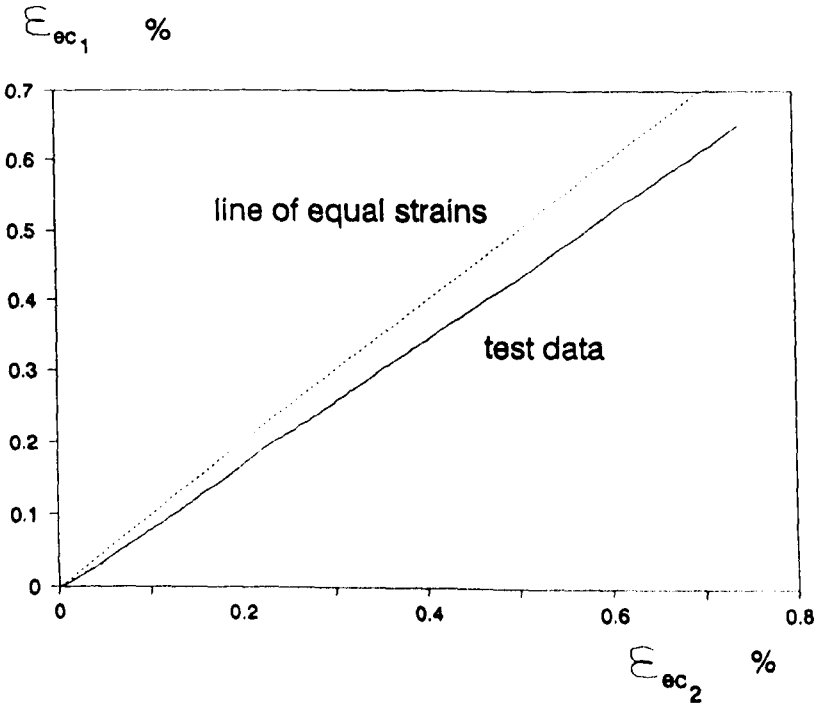

(b) end cap

Fig 6.21 Non-uniformity in axial strains (test ANCD1)

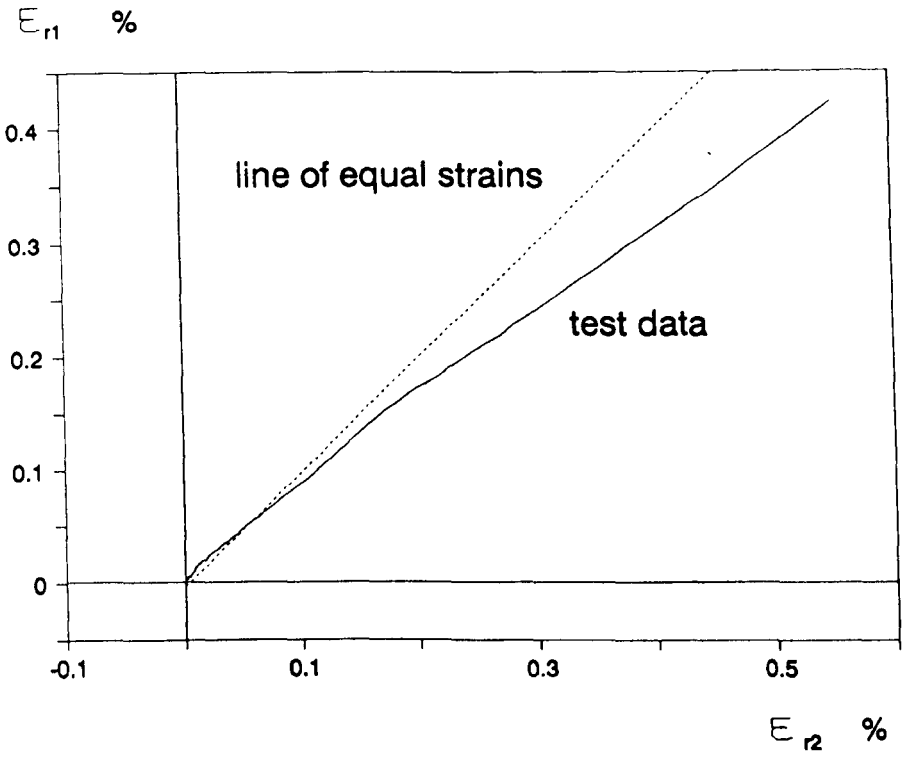

Fig 6.22 Non-uniformity in radial strains (test ANCU1)

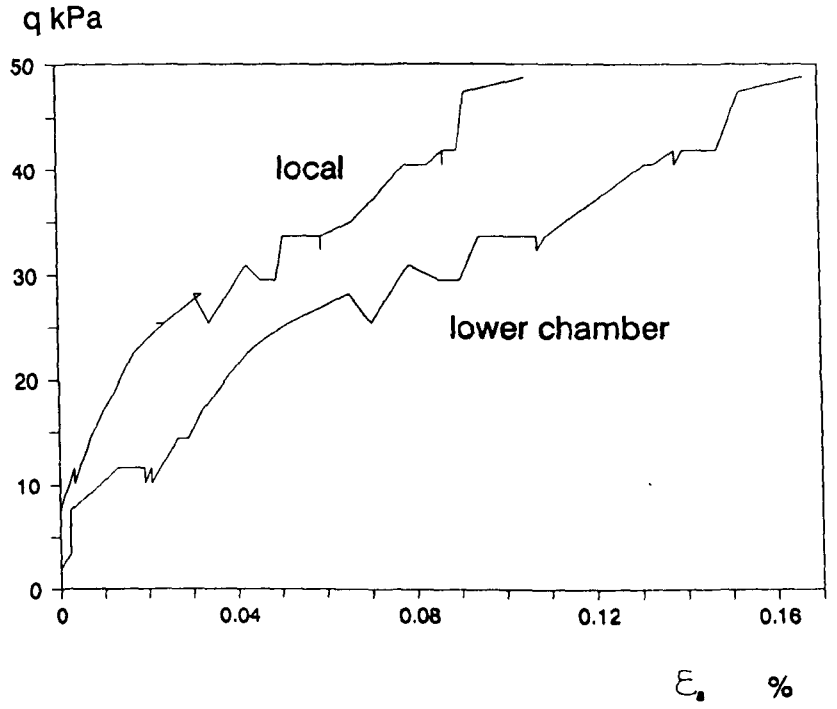

(a) small strain range

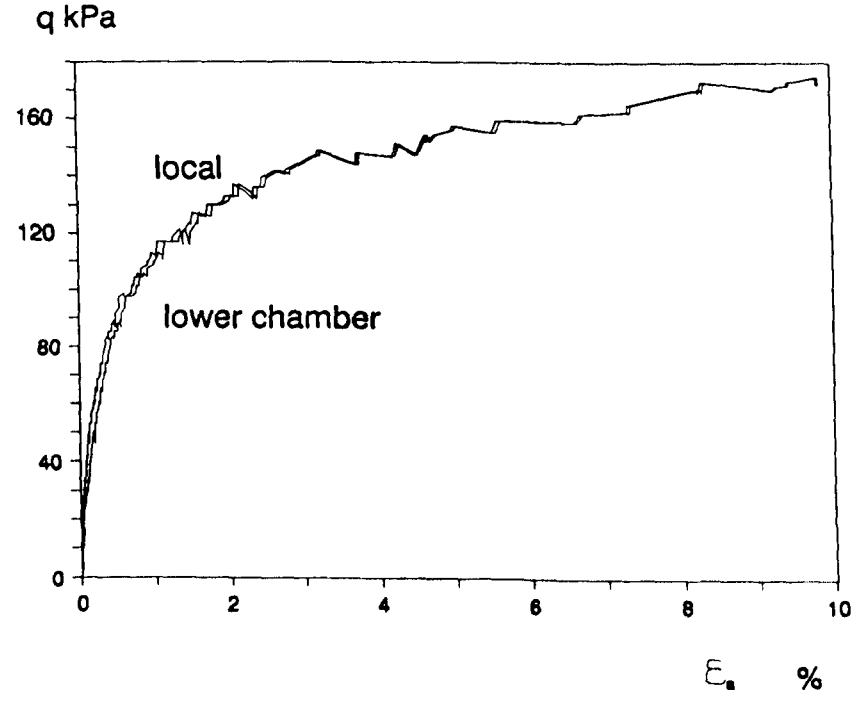

(b) large strain range

Fig 6.23 Stress-strain curves from a typical test in the 38 mm cell (test S/2/2/1)

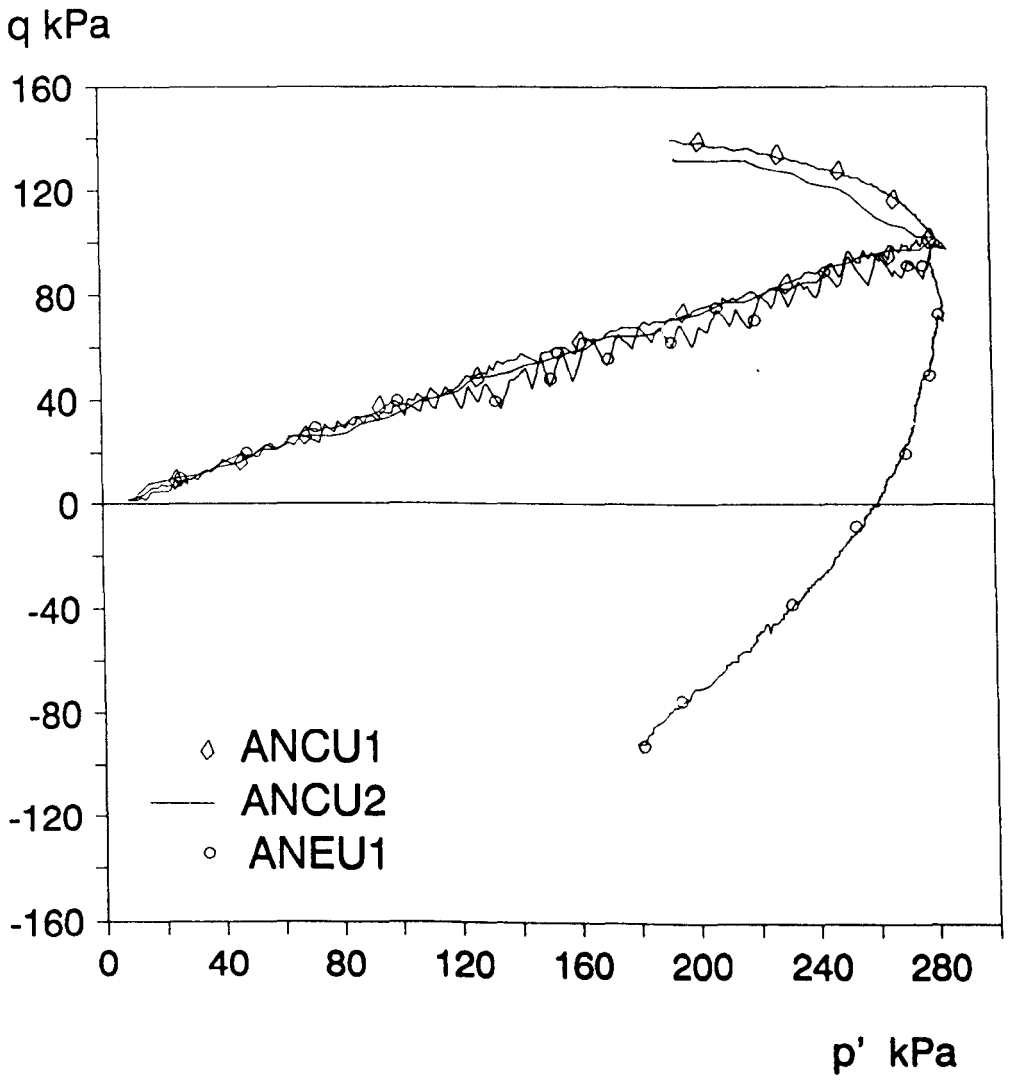

Note : only selected data points are shown

Fig 6.24 Stress paths for normally consolidated undisturbed specimens

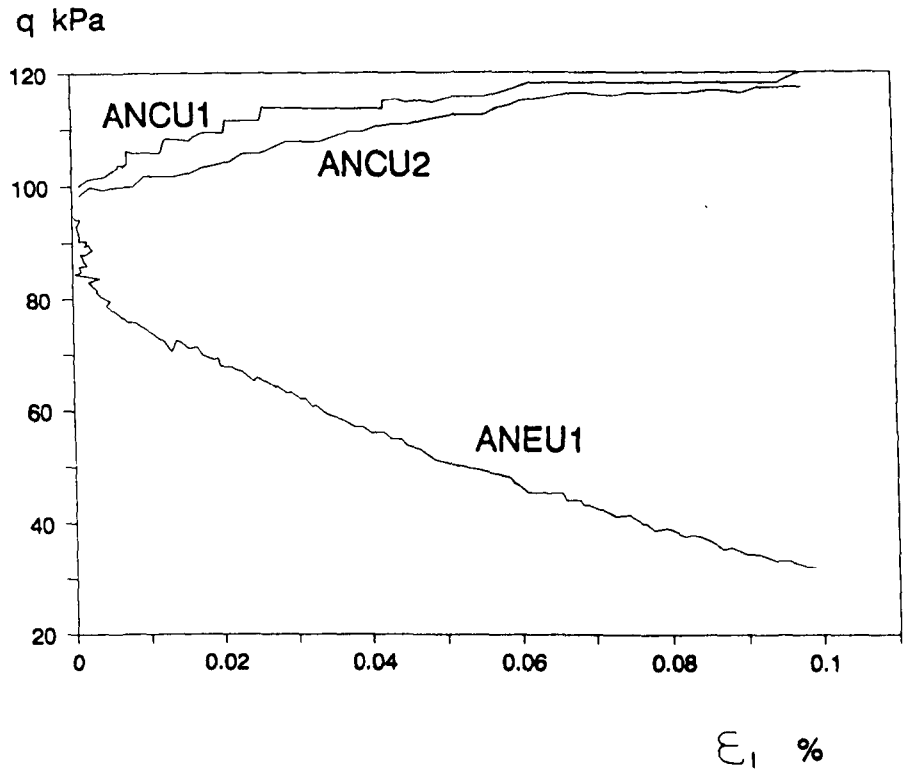

Fig 6.25 Stress-strain curves for normally consolidated undisturbed specimens

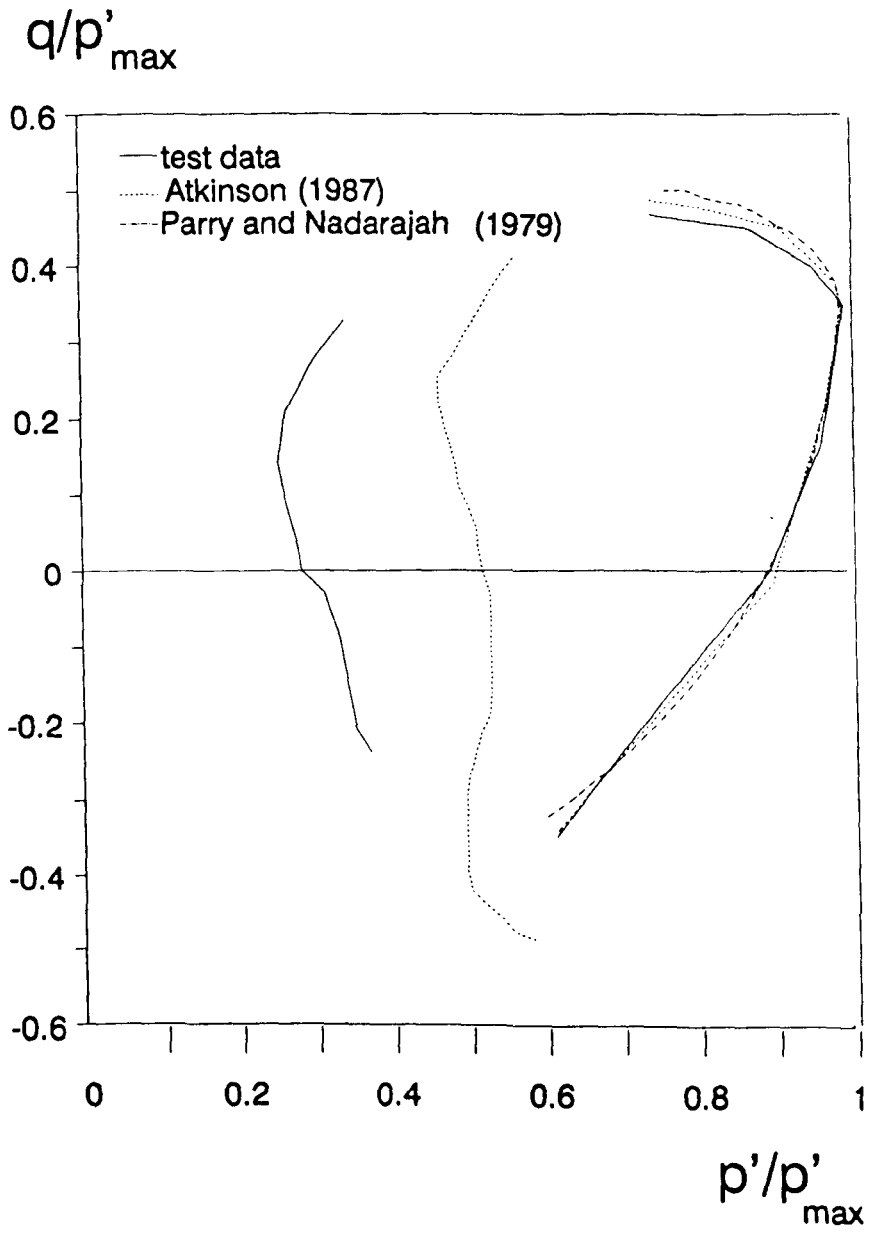

Fig 6.26 Comparison of experimental normalised stress paths with other published data

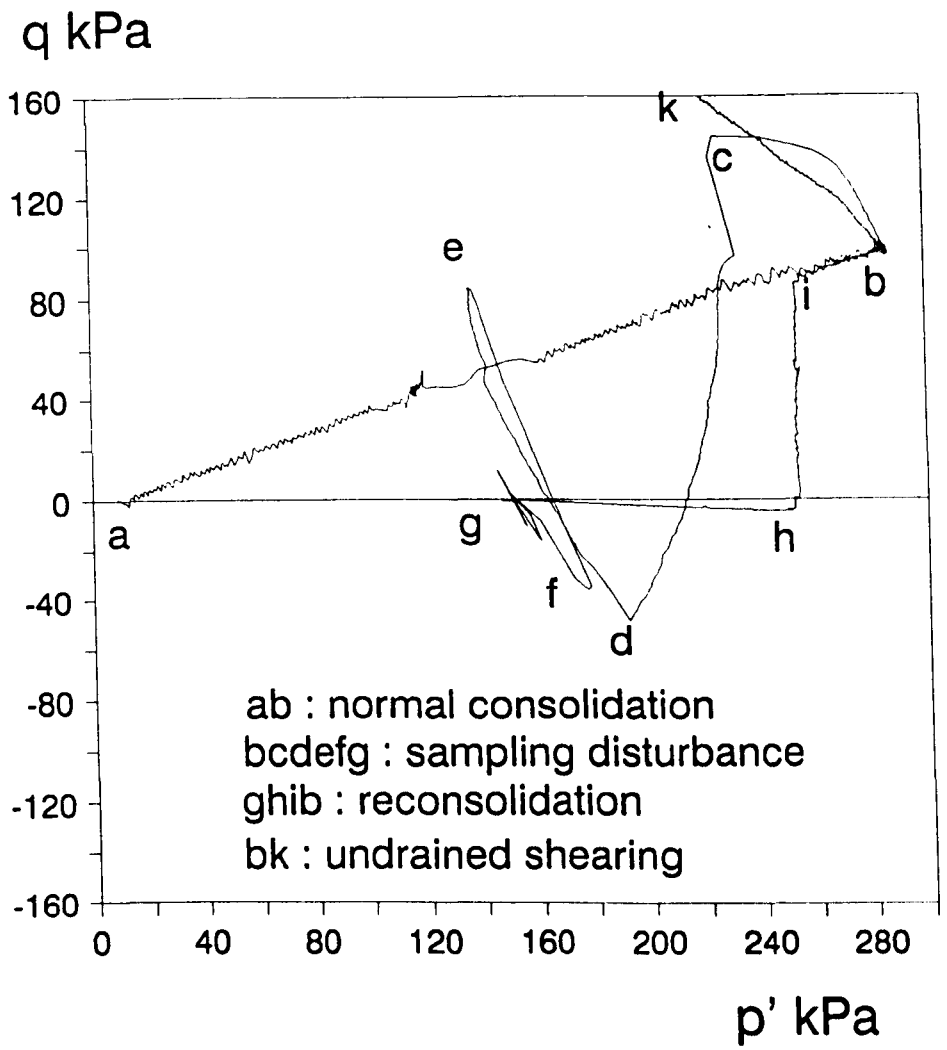

Fig 6.27 Stress path for test ANCD1

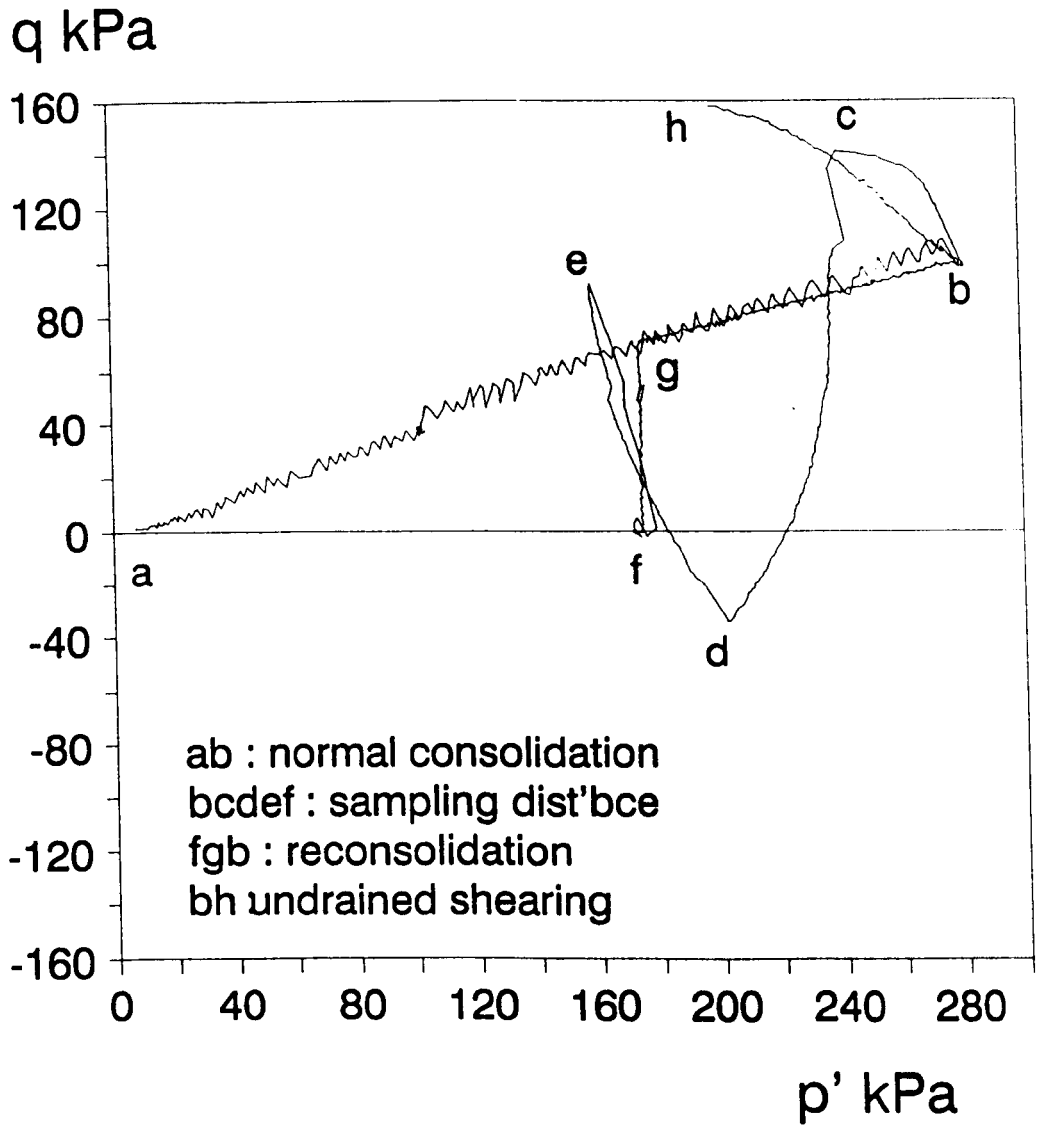

Fig 6.28 Stress path for test ANCD2

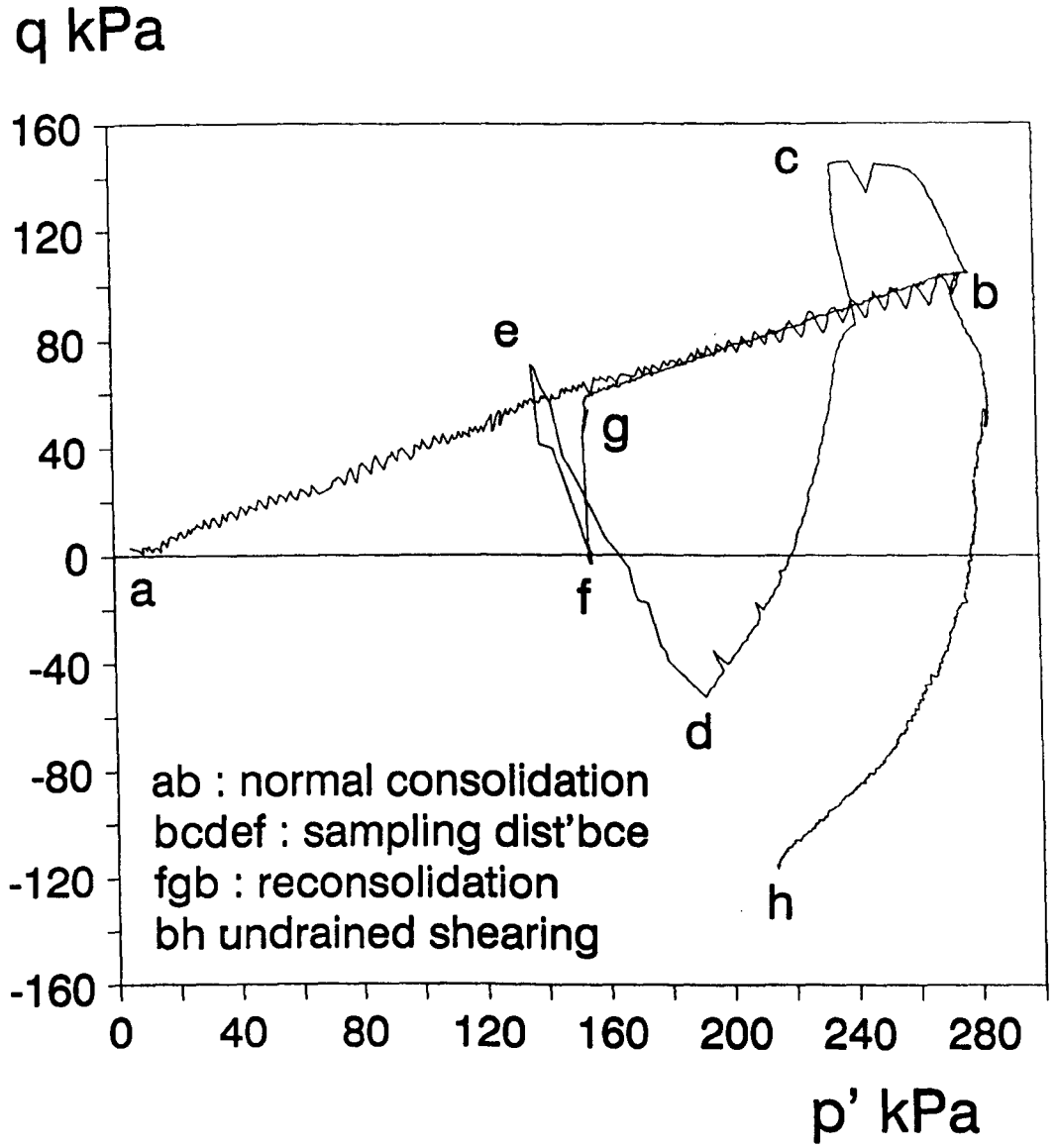

Fig 6.29 Stress path for test ANED1

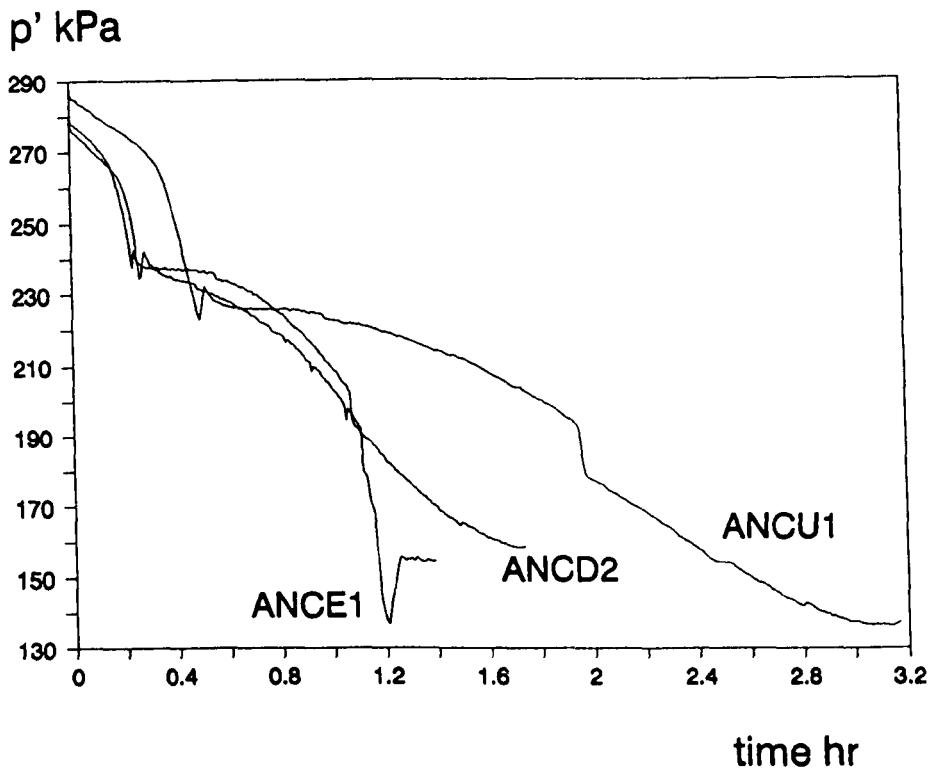

Fig 6.30 Variation of p' with time during strain cycles for normally consolidated specimens

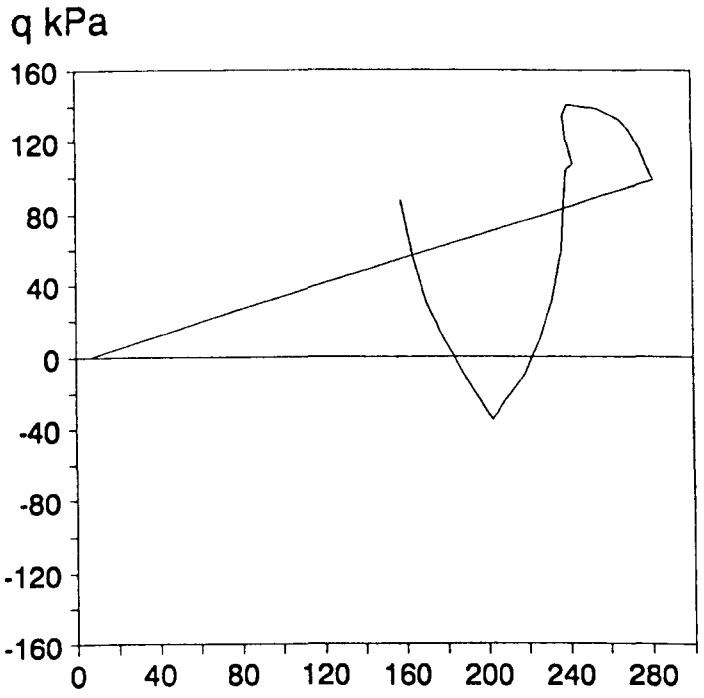

(a) experimental data (test ANCD2)

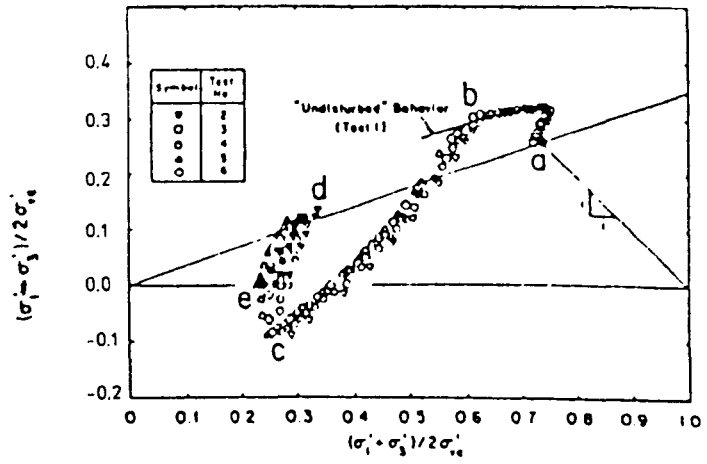

(b) Baligh et al (1987)

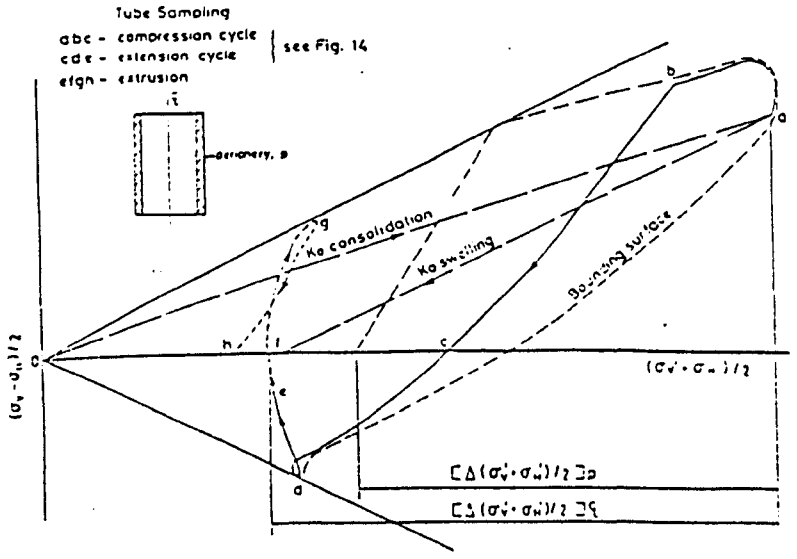

(c) Hight et al (1985)

Fig 6.31 Comparison of strain cycle stress paths for normally consolidated soils

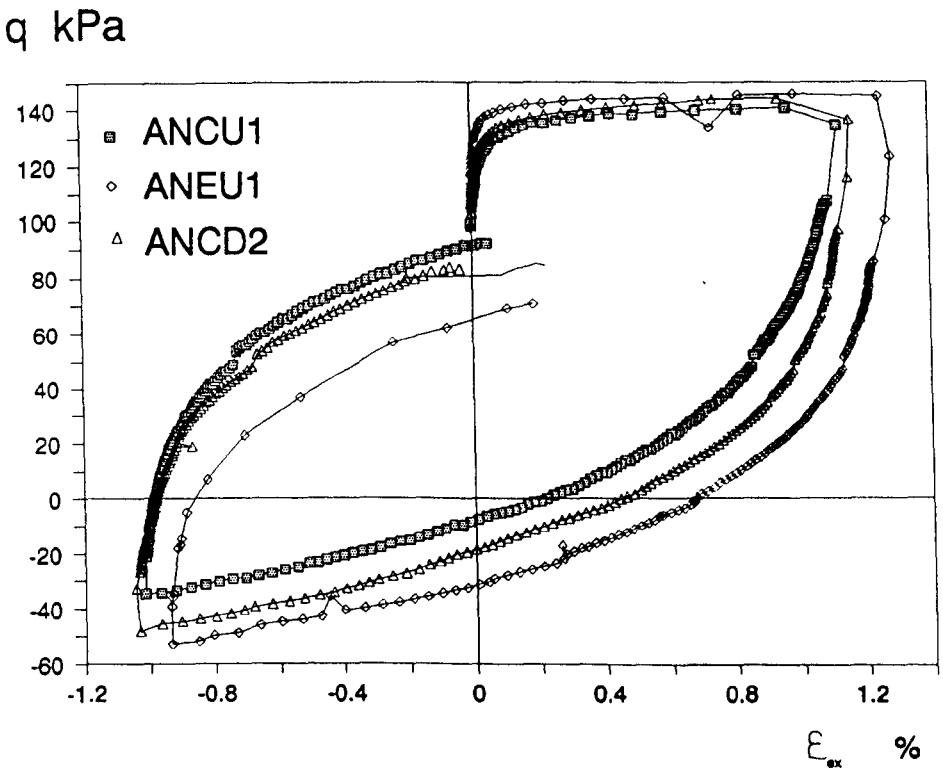

Fig 6.32 Stress-strain curves during strain cycles for normally consolidated specimens

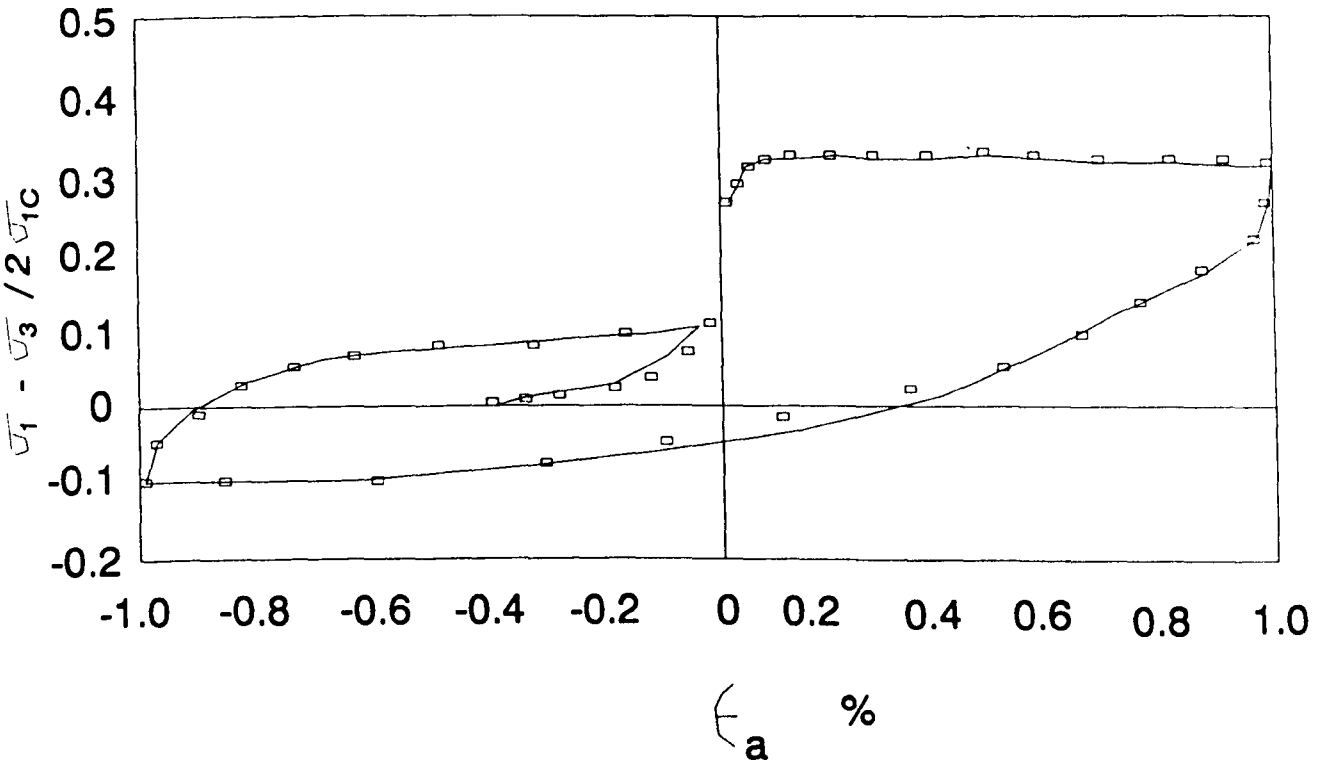

Fig 6.33 Stress-strain during cycle application on normally consolidated Boston blue clay

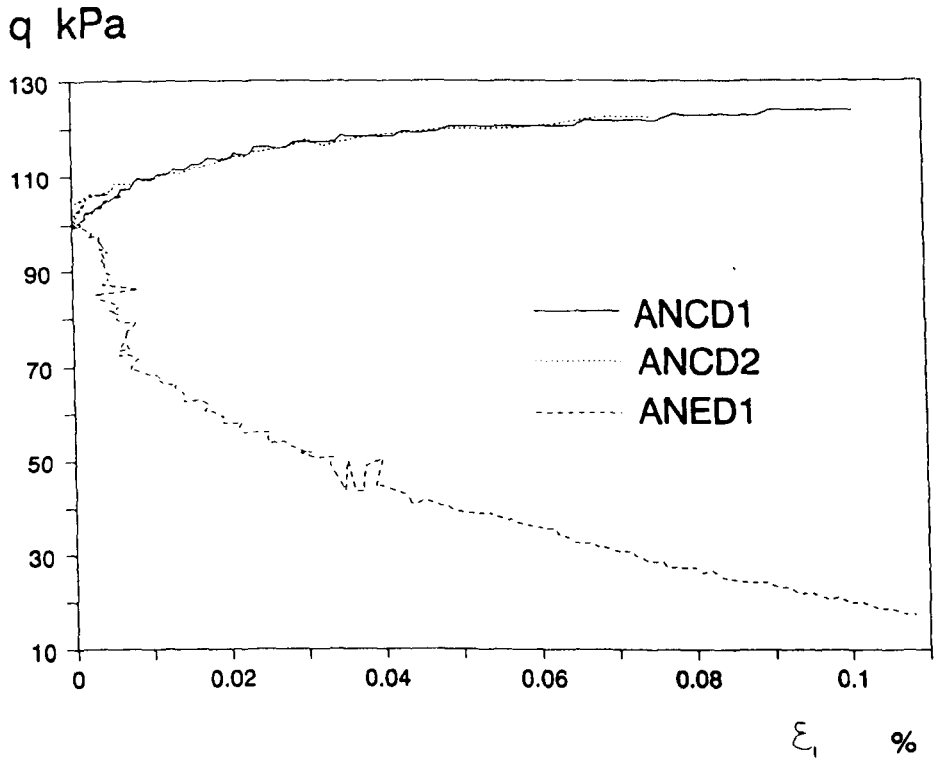

Fig 6.34 Stress-strain curves for normally consolidated disturbed specimens

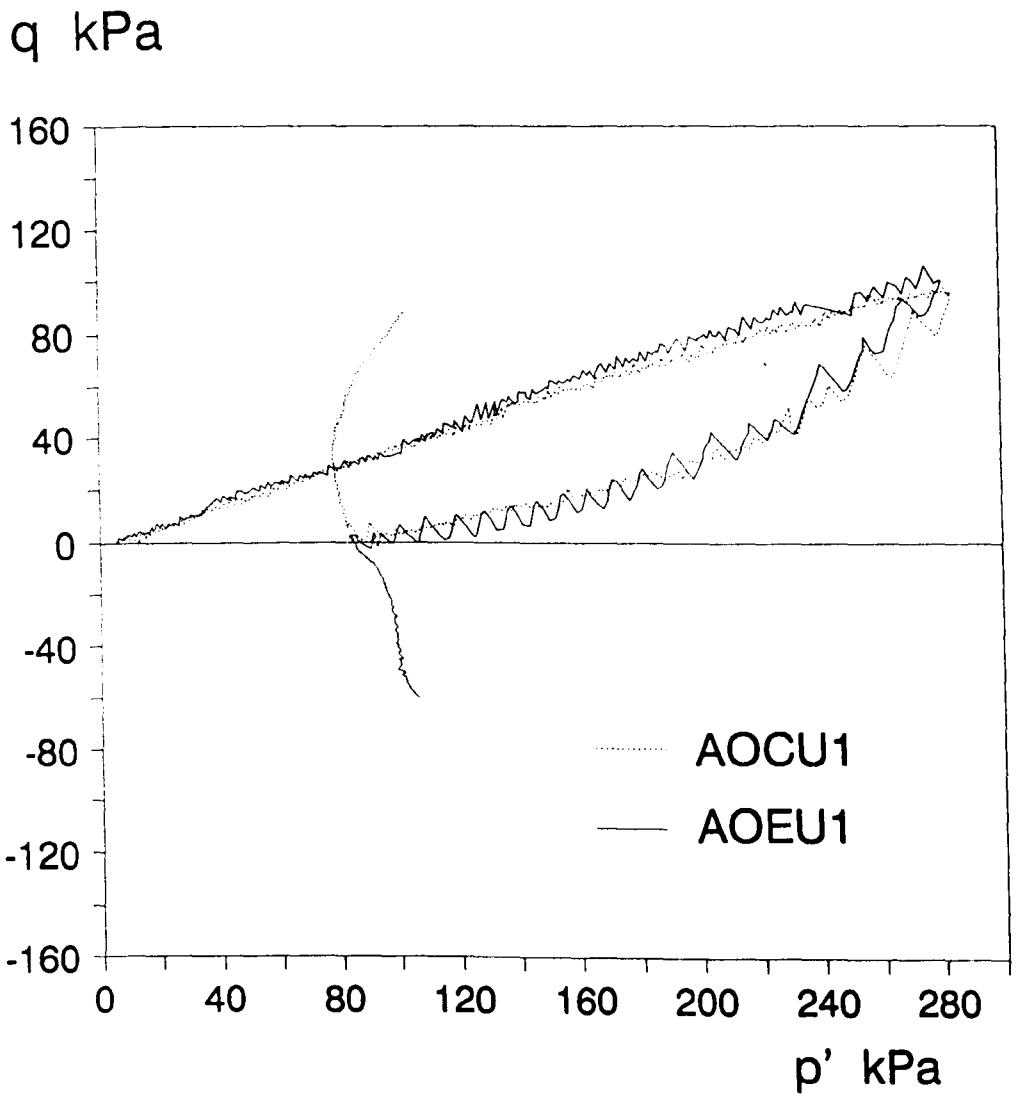

Fig 6.35 Stress paths for overconsolidated undisturbed specimens

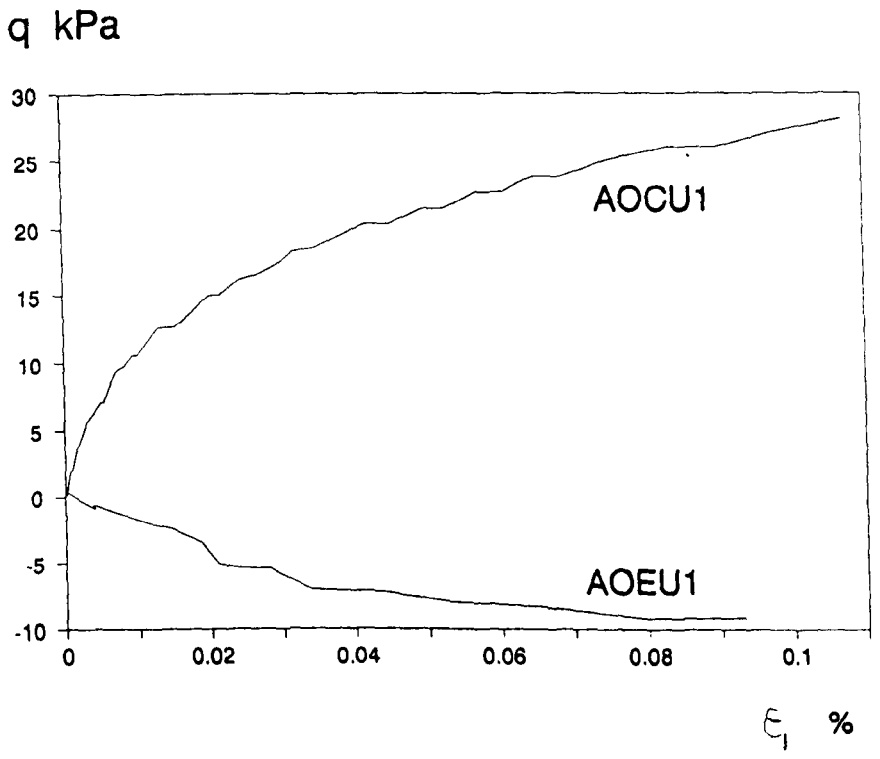

Fig 6.36 Stress-strain curves for overconsolidated undisturbed specimens

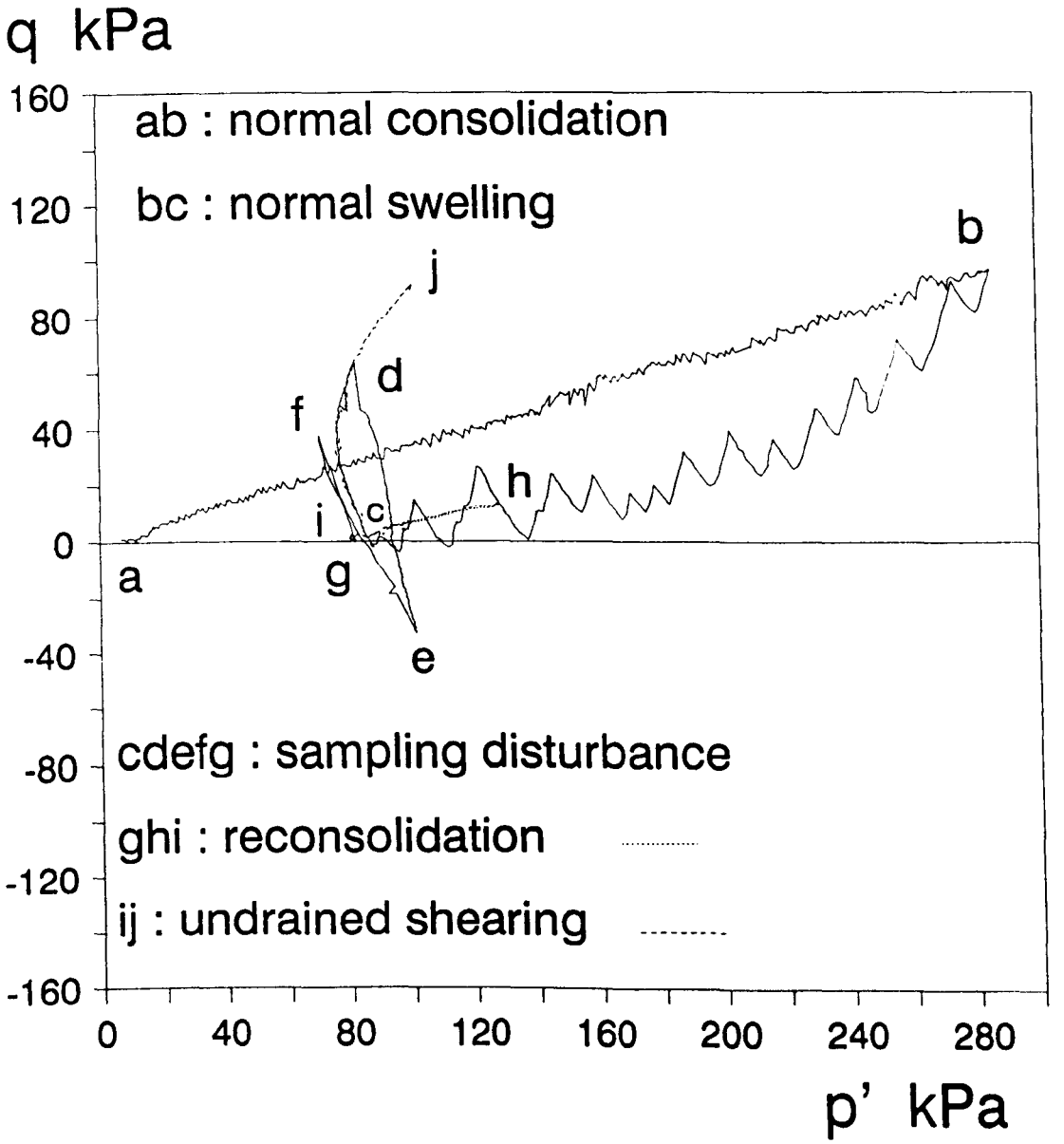

Fig 6.37 Stress path for test AOCD1

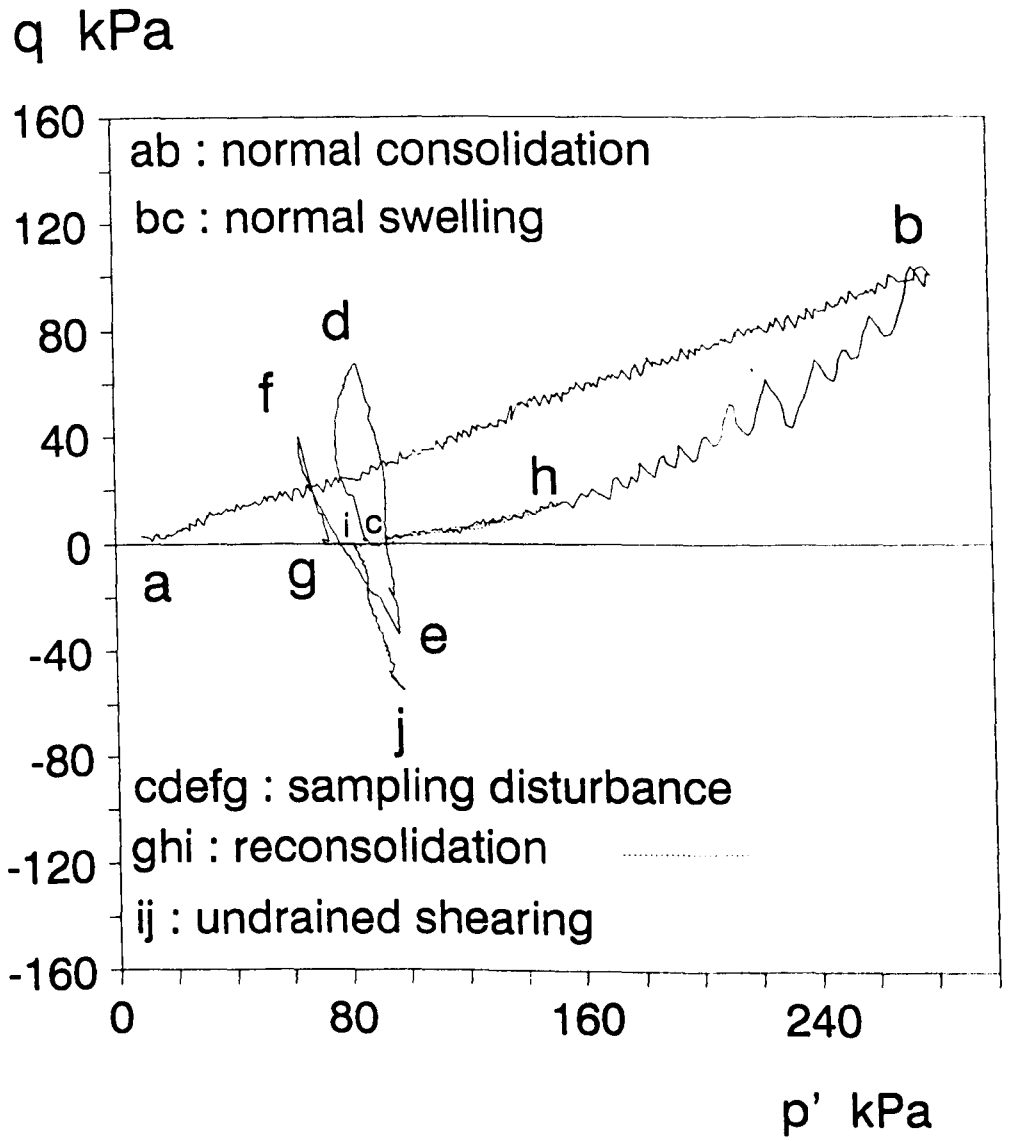

Fig 6.38 Stress path for test AOED1

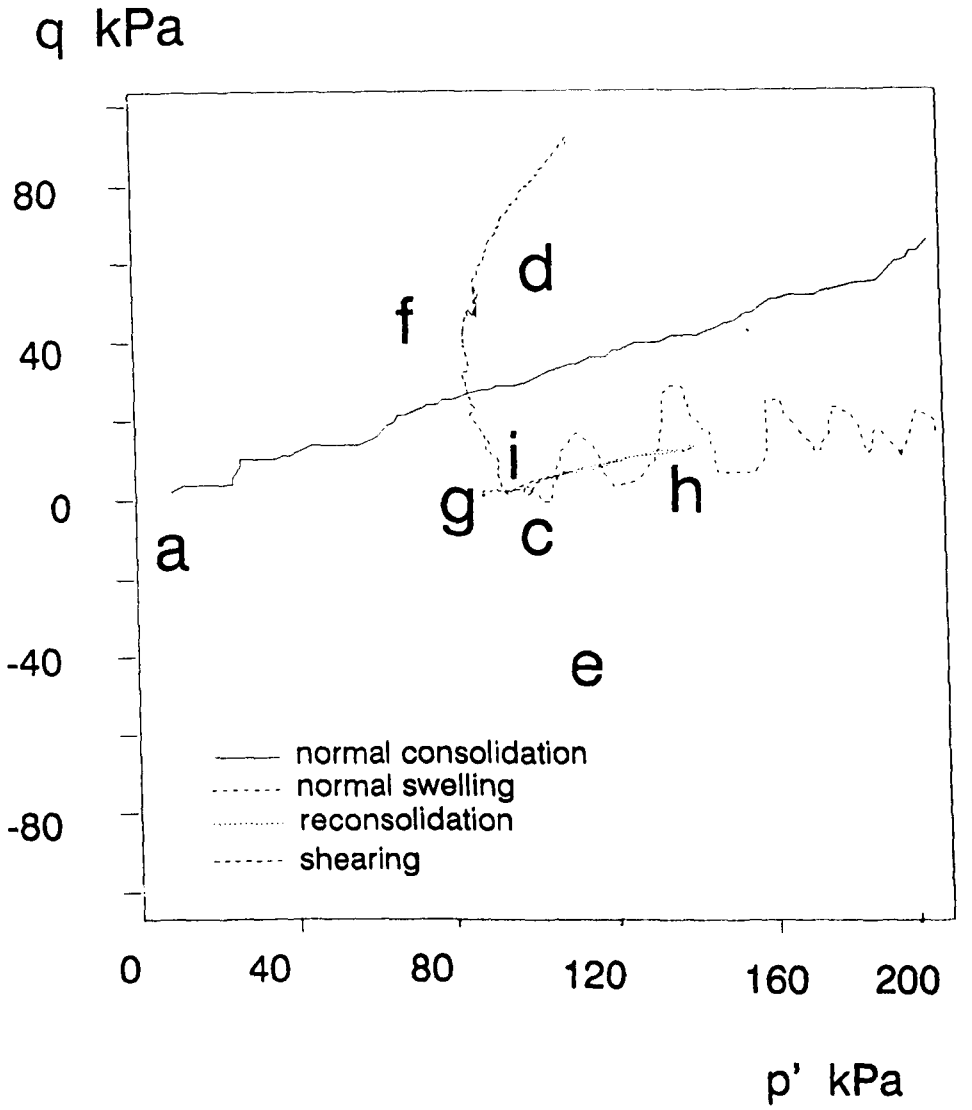

Fig 6.39 Typical reconsolidation stress path for an overconsolidated specimen (refer to Fig 6.37)

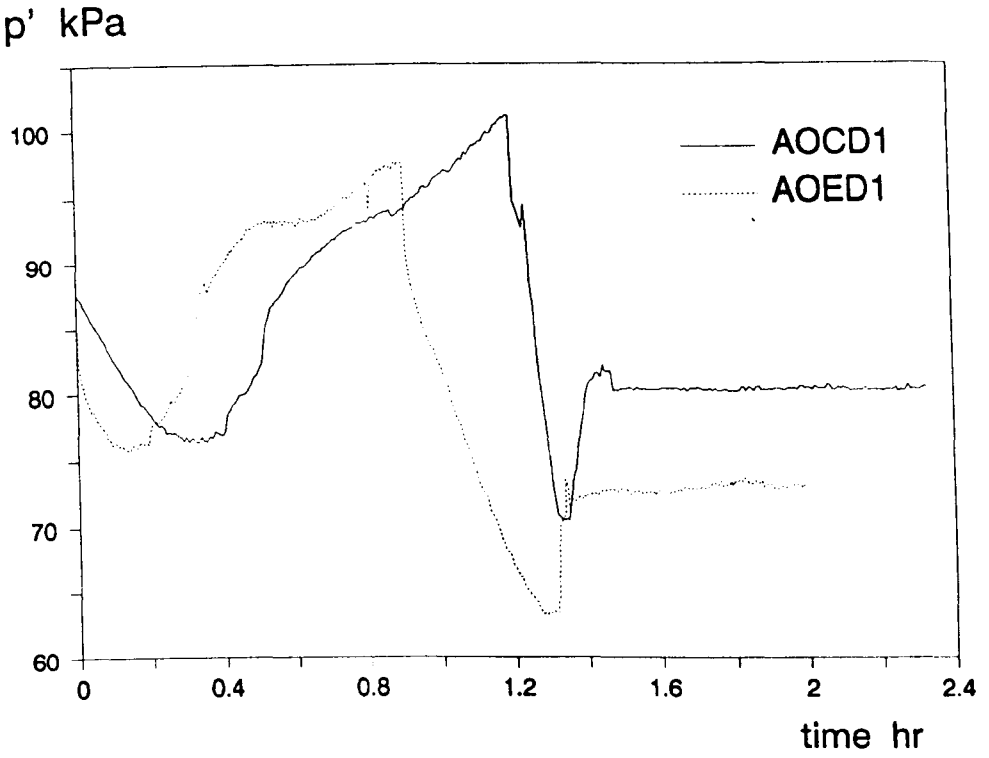

Fig 6.40 Variation of p' with time during strain cycles for overconsolidated specimens

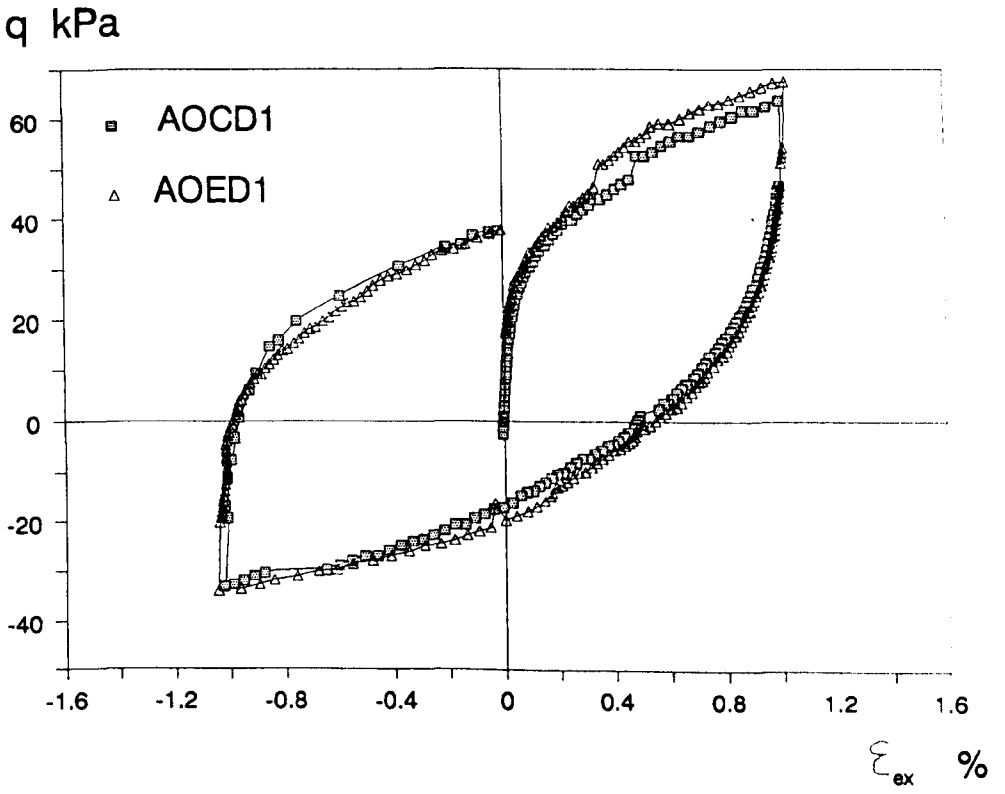

Fig 6.41 Stress-strain curves during strain cycles for overconsolidated specimens

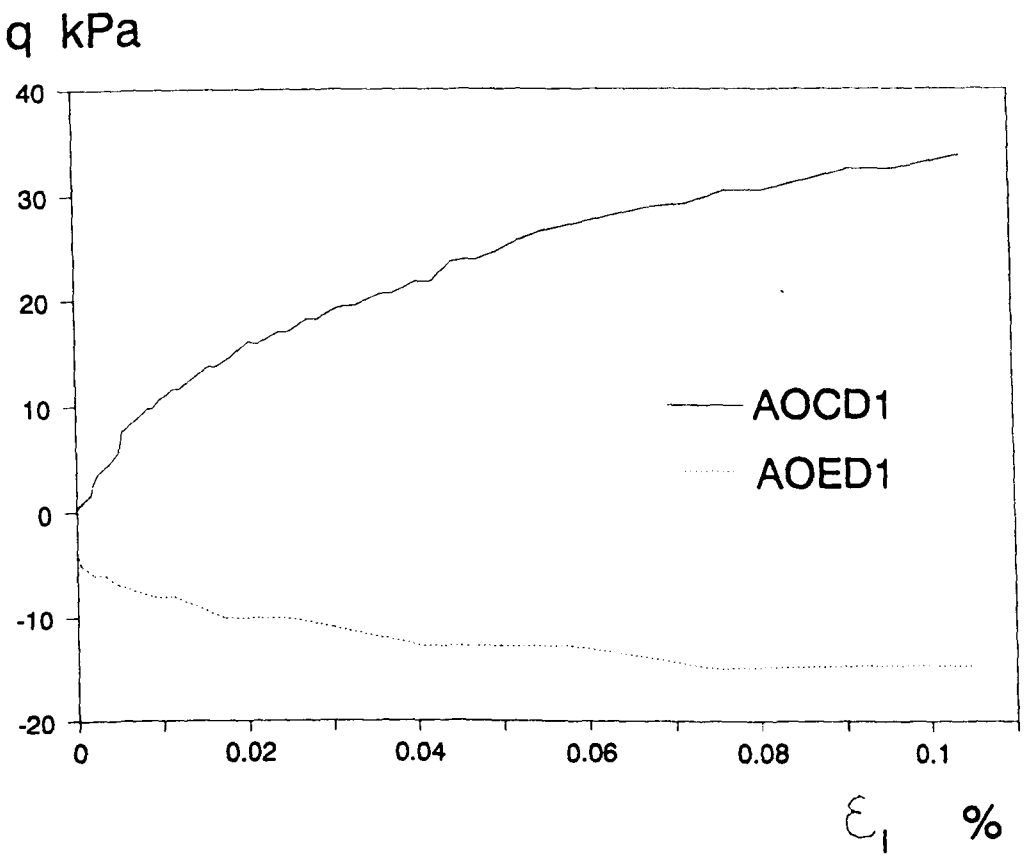

Fig 6.42 Stress-strain curves for overconsolidated disturbed specimens

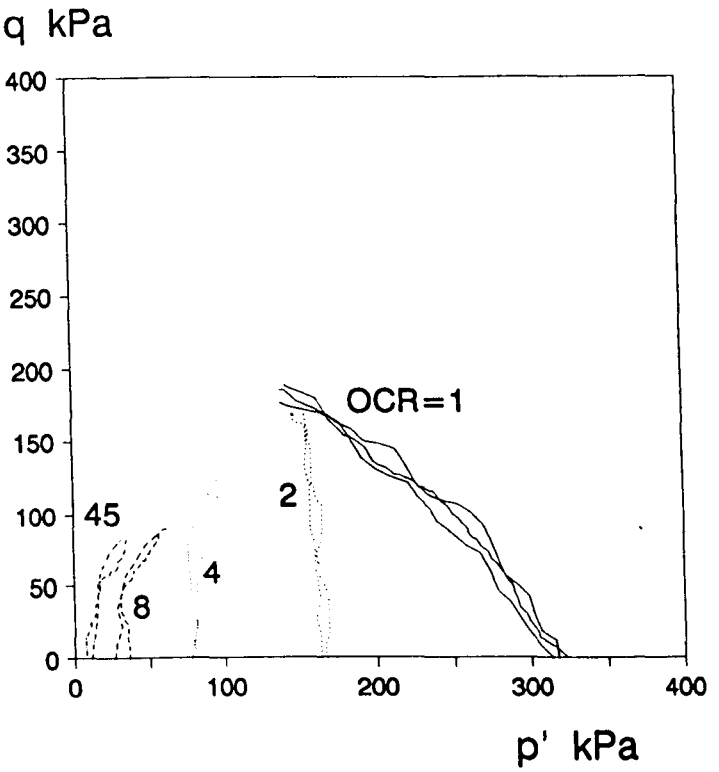

Fig 6.43 Stress paths for tests in the 38 mm cell (loading rate=2kPa/hr)

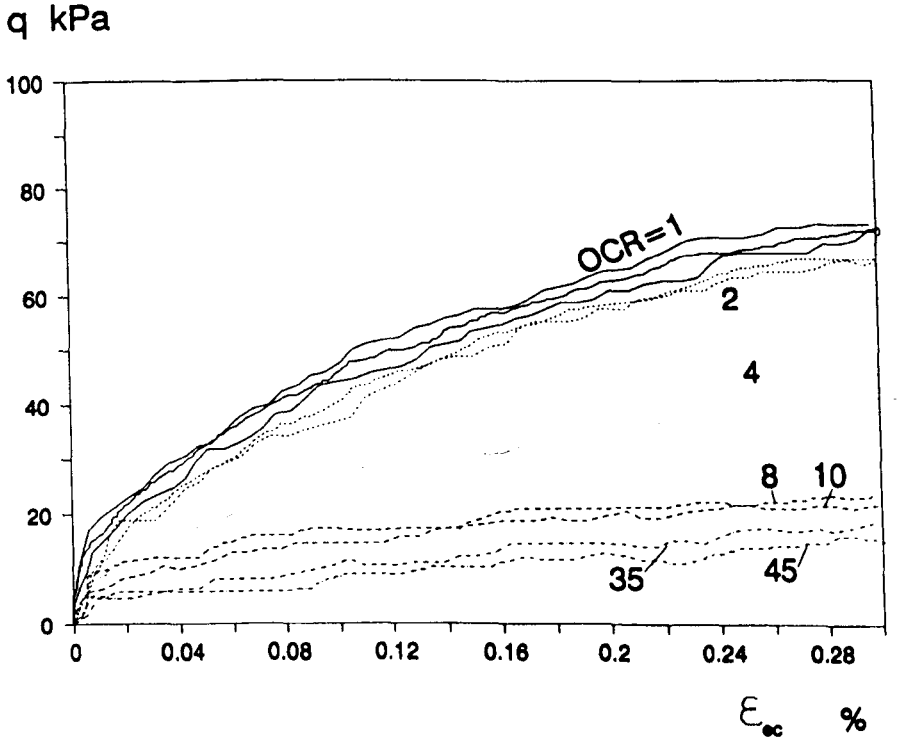

Fig 6.44 Stress-strain curves for tests in the 38 mm cell (loading rate=2kPa/hr)

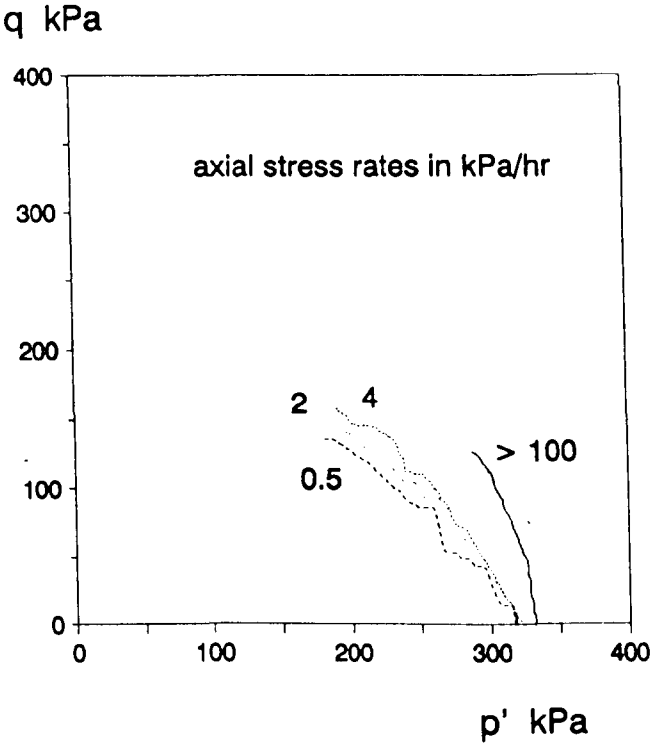

Fig 6.45 Stress paths for normally consolidated specimens in the 38 mm cell with different loading rates
(Note : each curve represents average of two tests)

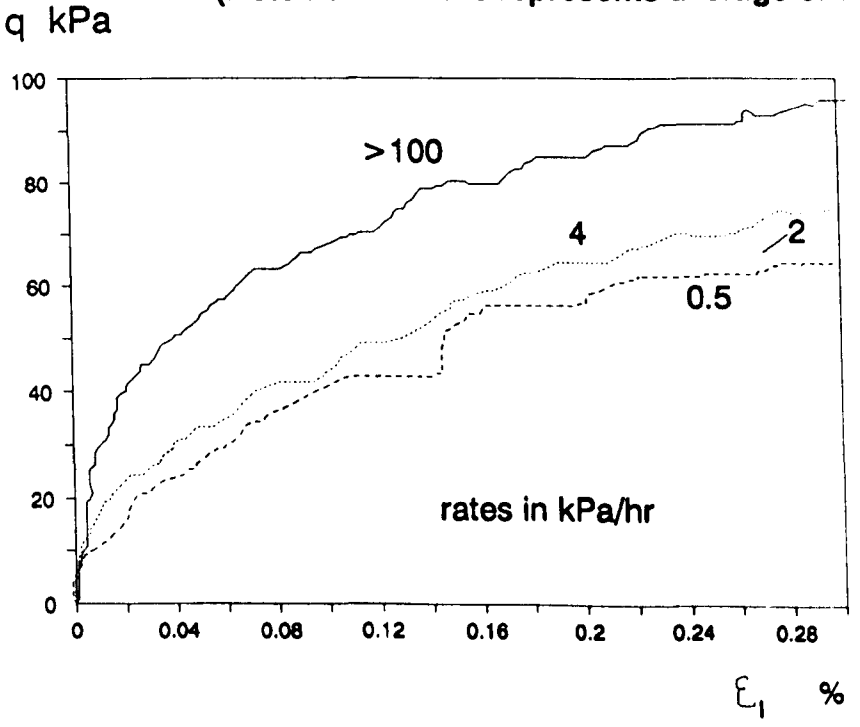

Fig 6.46 Stress-strain curves for normally consolidated specimens in the 38 mm cell with different loading rates
(Note : each curve represents average of two tests)

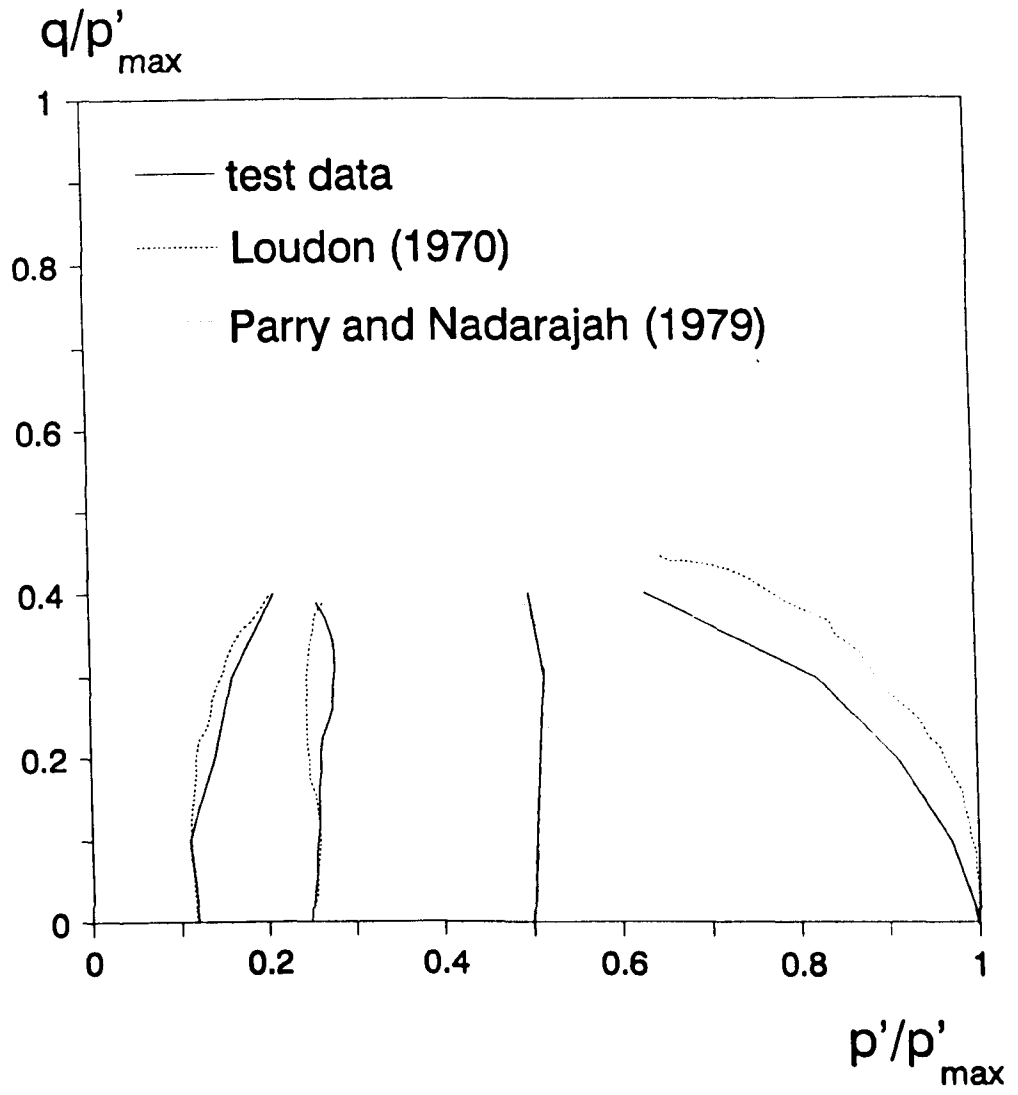

Fig 6.47 Comparison of experimental normalised stress paths in the 38 mm cell with other published data

Chapter 7

DISCUSSION OF EXPERIMENTAL RESULTS

7.1 Introduction

This chapter contains a discussion of the small strain deformation behaviour of kaolin under undrained conditions. The first section is concerned with the relevant parameters, such as the tangent stiffness, that can be derived from the tests described in Chapter 6. In the following sections, the effects of sampling disturbance, rate of shearing, and overconsolidation ratio on the small strain deformation behaviour are examined. A comparison is then made between the behaviour of one-dimensionally and isotropically consolidated specimens. In the final section, comparisons are made between the experimental results and the predictions of some of the models discussed in Chapter 1. The discussion will centre on the small strain region where these models have not been adequately checked.

7.2 Stiffness Parameters

The stiffness parameters calculated from the results from the 100 mm triaxial cell will be presented in this section. In Section 1.1.1, it was indicated that stiffness can be evaluated either as a tangent or a secant value. A typical plot of stiffness versus axial strain on a semi-logarithmic scale is shown in Figure 7.1. Theoretically the secant stiffness, E_{us}, should be always larger than the tangent stiffness, E_{ut}. In the present case, this is true except at very small strains where scatter in the stress strain data may result in a fitted polynomial curve with a reversal of curvature, as illustrated in Figure 7.2. For discussion purposes, unless otherwise stated, only tangent stiffnesses will be used, which have been evaluated according to the method described in Section 6.3.

Non-linearity of the stress-strain behaviour is clearly shown by the large differences between the stiffness values at different strain levels in Figure 7.1 and Table 7.1. A linearity index L (Jardine et al (1984)) may be defined as

$$L = \frac{E_{ut0.1}}{E_{ut0.01}} \tag{7.1}$$

where $E_{ut0.01}$ and $E_{ut0.1}$ are the stiffness values at axial strains of 0.01 % and 0.1 % respectively. This index is tabulated in Table 7.2. For compression tests, a general increase in L with OCR can be noticed. A similar trend was reported by Hight et al (1985). It also shows that tests with high rate of shearing exhibit generally a more non-linear response.

The evaluation of Poisson's ratio, ν, for tests in the 100 mm cell was carried out using the average local radial strain and the average local axial strain (for details of measurement techniques see Section 3.4.6). The test results are shown in Figure 7.3. Calculation of ν was carried out according to the method described in Section

6.3. Due to end restraint (see Section 2.5.1) the radial strain can be expected to be larger over the middle part of the specimen than near the end caps. End restraint effects on the evaluation of Poisson's ratio have been analytically examined by Moore (1976) using the theory of elasticity. Moore concluded that if ν is to be evaluated correctly, a correction factor should be applied which depends on ν and the height to diameter ratio of the specimen. However, this was found to be unnecessary in the present research. As argued in Section 2.5.1, at small strains (where both axial and radial strain measurements are made) the middle part of the specimen remains closer to a right cylinder than the whole specimen does, as shown diagrammatically in Figure 7.4.

The results of linear regression analyses carried out on the data of the type shown in Figure 7.3 are presented in Table 7.3. Over the axial strain range of 0 to 0.7 %, the values of ν are acceptably close to the theoretical value for undrained loading of saturated soil, $\nu = 0.5$. On the other hand, values calculated over larger axial strain ranges were found to be higher than 0.5 suggesting that barrelling effects become more significant as shearing progresses.

7.3 Effects of Sampling Disturbance

In this section, results from the tests carried out in the 100 mm apparatus will be analysed to provide a comparison between the responses of 'undisturbed' and 'disturbed' specimens. It was shown in Section 2.3 that the tube sampling process is complicated and difficult to simulate accurately. Therefore, it should be re-emphasised that the application of a strain cycle to a specimen in the triaxial cell can be considered as significant but still, according to Baligh et al (1987), ideal

disturbance by comparison with that which might actually occur.

For comparison purposes, the changes in deviator stress and stiffness have been normalised with respect to p_0', the initial mean effective pressure prior to shearing. The reasons for using p_0' as the normalising parameter rather than the undrained shear strength, c_u, have been discussed by Jardine et al (1984). These include the fact that the value of c_u depends on several factors such as the rate of loading, total stress path, sampling disturbance and the soil microfabric. In particular, for anisotropically consolidated soil, the value of c_u in compression is different from that in extension. In any case, the value of c_u was not generally known for the present specimens, since the majority of the specimens were not brought to failure. A further point is that the ratio of E_u/p_0' is less dependent on the stress history than E_u/c_u.

7.3.1 Normally Consolidated Specimens

Stress-strain curves for normally consolidated disturbed and undisturbed specimens sheared in compression are compared in Figure 7.5a. The result for Test ANCU2 is omitted since, as explained in Section 6.6.1, this did not have the standard rest period before shearing. Although test ANCD1 involved a different reconsolidation path from test ANCD2 (see Section 6.6.1), the directions of the reconsolidation paths immediately prior to shearing were still similar. Therefore, it is likely that the effects of the recent stress history, as described by Atkinson et al (1989), have been minimised.

Corresponding stiffnesses, normalised with respect to p_0', are shown in Figure 7.5b. For strains below 0.01 %, the differences between the values of E_{ut}/p_0' may

be blamed on the inaccuracies in the data. As explained in Section 5.3.2, scatter in the stress-strain data at small strains can be mainly attributed to the larger random errors involved in measuring the strains. The maximum difference in the stiffnesses for strains between 0.01 % and 0.1 % does not exceed 7 % and therefore there is very good agreement between the disturbed and undisturbed behaviour.

Results from tests on disturbed and undisturbed specimens sheared in extension are compared in Figure 7.6. Agreement between disturbed and undisturbed behaviour in this case is not as good as that found with specimens loaded in compression. The stress-strain curve for the disturbed specimen (ANED1) lies above that for the undisturbed specimen (ANEU1) except at very small strains (Figure 7.6a).

7.3.2 Overconsolidated Specimens

Results from the overconsolidated specimens loaded in compression are presented in Figure 7.7. Very good agreement can be seen between stress-strain behaviour of disturbed and undisturbed specimens. This is in contrast to the data from tests on overconsolidated specimens loaded in extension, Figure 7.8 where the disturbed specimen displays a markedly stiffer response.

7.3.3 Overview

The results from the present work have shown that disturbed specimens, when reconsolidated to the initial stress conditions, exhibit similar small strain stiffnesses to those of undisturbed specimens, although somewhat higher stiffnesses have been

obtained from the disturbed specimens in the case of extension tests on both normally consolidated and overconsolidated soil. It is difficult to assess whether these latter differences are within the repeatability limits or not since none of the extension tests were repeated. Fluctuations in the deviator stress just before the start of the shearing stage may have contributed to these differences. This is particularly likely in the case of overconsolidated specimens loaded in extension from a nearly zero deviator stress since small absolute fluctuations may represent a large percentage error in the small strain region. Table 7.2 shows that except in the case of test ANEU1, the disturbed specimens exhibit similar non-linear behaviour as the undisturbed specimen.

Effective stress paths during shearing for all the specimens tested in the 100 mm cell are compared in Figure 7.9. Since strains are related to changes in effective stress, it is not surprising that the general agreement between the stress-strain curves of disturbed and undisturbed specimens at small strains is reflected in the agreement between the corresponding sections of the stress paths. For normally consolidated specimens, deviations of the stress paths of disturbed and undisturbed specimens at larger strains correspond to significant differences in large strain stiffness and strength, as indicated in Figure 7.10. However, in the case of overconsolidated specimens, the smaller difference between the stress paths reflects better agreement, Figure 7.11.

Most previous research on sampling disturbance effects (reviewed in Sections 2.3 and 2.4) has been concerned with undrained strength and stiffness at large strains under compression loading. Atkinson and Kubba (1981) reported from tests on normally consolidated kaolin that, despite the fact that the stress path of a reconsolidated perfect sample (i.e. one subjected to stress relief only) was similar to that of an undisturbed sample, the stiffnesses at large strains were not equal.

For tube samples they reported that, after reconsolidation to the initial stresses, the soil exhibited a different stress path from that of undisturbed soil and that the tube samples had higher stiffnesses. Similarly, Baligh et al (1987) found that, for normally consolidated Boston Blue clay, reconsolidation to the initial stresses after tube sampling and stress relief resulted in a higher stiffness at large strains and a larger shear strength. Therefore, the results from the present work are in agreement with previous research but indicate that, although reconsolidation does not result in similar stiffnesses at large strains, the small strain stiffness is fairly well recovered by reconsolidation (or swelling) along the original stress path, especially under compression loading.

Lacasse and Berre (1987) carried out similar tests to those described here and those performed by Baligh et al (1987), but did not make local strain measurements. Their results showed that, for both normally consolidated and overconsolidated soil, disturbed and undisturbed specimens loaded in compression attained similar strengths. Furthermore, the disturbed specimens showed lower stiffnesses. These results contradict the findings of Baligh et al (1987) and the present results. It is difficult to give an explanation for the difference in the results, since it is not known how Lacasse and Berre reconsolidated their specimens after the application of the strain cycle. As explained in Section 6.6.2, the stress path followed during reconsolidation could have a significant effect on the initial deformation behaviour. However, they report volumetric strains of 1 % and 0.13 % for normally consolidated and overconsolidated specimens respectively which are similar to the corresponding values of 1.8 % and 0.12 % found in the present work. Therefore diferences in the change in water contents upon disturbance between the two sets of tests could not be the reason for the disagreement between Lacasse and Berre's results and those from the present research. In contrast, the results from the extension tests carried out by

Lacasse and Berre, again on both normally consolidated and overconsolidated specimens, agree with the present results in that the stiffness for the disturbed specimen was higher than that of an undisturbed specimen.

The present normally consolidated disturbed specimens underwent a significant increase in mean effective stress during reconsolidation, which resulted in a reduction of water content as compared with the undisturbed specimens (Table 6.9). This explains the higher strengths and large strain stiffnesses of the disturbed specimens (Hight et al (1979) and Balasubramanian (1969)). The overconsolidated specimens exhibited a smaller change of water content upon disturbance and reconsolidation (Table 6.10). This agrees with the much better agreement between the large strain stiffnesses of the disturbed and undisturbed specimens (see Figure 7.11).

Differences between the water contents of corresponding disturbed and undisturbed specimens just before shearing were comparable for specimens tested in compression and those tested in extension. Therefore, water content variations cannot be responsible for the discrepancies in small strain stiffness seen in the extension tests, discussed above.

The results show that, in general, recovery of the small strain deformation behaviour in both normally consolidated and overconsolidated disturbed specimens is similar although, as noted above, the former had undergone a larger change in water content as a result of the disturbance.

7.4 Effects of Rate of Shearing

In Section 2.4 it was mentioned that isotropically consolidated specimens exhibit an increase in stiffness upon increasing the loading rate. During the application of the strain cycle in the 100 mm apparatus, the specimens were subjected to a much higher rate of shearing (axial stress rate of over 100 kPa/hr) than that adopted during normal shearing (axial stress rate of about 2 kPa/hr). The effect of this for normally consolidated specimens can be seen in Figures 7.12 and 7.13 showing the stress paths and stress-strain curves respectively. There is agreement here with the results reported by Graham et al (1988) in that a higher rate of loading produces not only a larger stiffness but also an expansion of the yield locus (see Section 2.4).

Corresponding data for overconsolidated specimens, Figures 7.14 and 7.15, show that the rate of shearing effects are not as significant especially in the case of stress paths. This is due to the fact that creep effects and associated changes in undrained pore water pressure response are not as significant in the case of overconsolidated clays. As illustrated in the diagram of Figure 7.16, under drained conditions it would take an overconsolidated specimen longer than a normally consolidated one to produce a given change of volume due to creep. Hence, under undrained conditions it would take longer for positive pore pressures to develop as a result of creep (Bjerrum (1973)).

As described in Section 6.2, an investigation of strain rate effects was conducted on isotropically consolidated specimens in the 38 mm apparatus. A plot of normalised stiffness against the rate of shearing for different strain levels is shown in Figure 7.17 where some data from the 100 mm cell are also included. The normalised stiffness is seen to increase with increasing rate of loading in a similar way

to that reported by Hight (1983). Furthermore, the results are in agreement with the finding of Graham et al (1983) in that the effect of loading rate on stiffness becomes less significant as the strain increases. On the same graph, the relationship between E_{ut}/p_0' and rate of shearing at 1% strain is shown. In terms of slope, this agrees well with the approximate relationship between strength and rate of loading, i.e. 10 to 20 % increase per log cycle (Graham et al (1983)).

In Figure 7.17, there is reasonable agreement between the data from the 38 mm and 100 mm cells. However, it should be noted that only two data points are available from the 100 mm cell for each strain level and therefore a definitive conclusion concerning this set of data cannot be drawn.

7.5 Effects of Overconsolidation

The discussion presented in Section 2.4 indicated that for isotropically consolidated specimens, the normalised stiffness varies linearily with OCR on a semi-logarithmic scale (Wroth et al (1979)). On the other hand, anisotropically consolidated specimens may be expected to exhibit a non-linear relationship (Gens (1983) and Jardine et al (1986)).

Tests in the 100 mm cell involved specimens with OCRs of 1 and 4 only. As expected, the latter had a higher stiffness when normalised with respect to the mean effective pressure just before shearing, Table 7.1.

Tests in the 38 mm cell involved a wider range of OCRs, as explained in Section 6.2.2. In these tests similarly, it was found that the higher the OCR, the larger the normalised stiffness. The data are included in Figure 7.18. This figure

shows an approximately linear relationship between the normalised stiffness, $E_{ut}/p_0^{'}$ and ln OCR at a given strain level. As in the case of the rate of shearing effects, the effects of overconsolidation are seen to become smaller as strain increases. Linear regression analysis carried out on the data in Figure 7.18 revealed that in the associated relationship

$$E_{ut}/p_0^{'} = \left(E_{ut}/p_0^{'}\right)_{n.c.}(1 + C \ln OCR) \tag{7.2}$$

$\left(E_{ut}/p_0^{'}\right)_{n.c.}$ and C take the values summarised in Table 7.4. Figure 7.18 shows similar patterns to those reported by Atkinson and Little (1988) testing natural clays and Georgiannou et al (1990) in tests on clayay sands who also reported that in the case of extension loading, the normalised stiffness decreases with the logarithm of OCR in a linear fashion.

7.6 One-dimensional versus Isotropic Behaviour

The influence of the method of consolidation on the deformation behaviour, touched on in the preceding section, has been appreciated by many researchers. The present research involved compression tests on both one-dimensionally and isotropically consolidated specimens and therefore a direct comparison between the corresponding small strain deformation behaviours can be made.

Figures 7.19 and 7.20 show the comparisons for normally consolidated and overconsolidated specimens respectively. There is reasonably good agreement between the stress strain curves from the normally consolidated specimens (Figure 7.19a). The anisotropically consolidated specimen exhibited a somewhat higher degree of non-linearity as shown in the plot of tangent stiffnesses against the loga-

rithm of axial strain (Figure 7.19b). Agreement in the case of the overconsolidated specimens (Figure 7.20a) appears less satisfactory. Once again, the anisotropically consolidated specimen shows a higher degree of non-linearity (Figure 7.20b). The larger discrepancy may be due to the definition of OCR which is in terms of vertical stress. If, instead, the overconsolidation ratio is defined in terms of the mean effective pressure, it becomes equal to about 3.5 rather than 4 for the specimens in the 100 mm cell. By examining Figure 7.18, a difference of 0.5 in OCR accounts for a small difference in the normalised stiffness and therefore could not be the main reason for the apparent discrepancy.

In general, the trends found in this work are similar to those reported by Gens (1983) and Richardson (1988).

7.7 Comparison between Model Predictions and Experimental Results

In this section comparisons are made between the experimental results and constitutive model predictions for behaviour during ordinary undrained shearing (slow monotonic loading) and behaviour during simulated tube sampling (fast cyclic loading). Most of the soil parameters used for the model predictions were determined in the laboratory, as shown in Section 6.4.3. Those which were not available experimentally were assumed equal to those given by the authors of the respective models. The model predictions are compared with experimental curves from all the available tests.

The models used in this section are those presented by Atkinson et al (1987),

Pender (1978 and 1979) and Al-Tabbaa (1988) which will be referred to as Atkinson's model, Pender's model and Al-Tabbaa's model respectively. These models are described in Section 1.2. Atkinson's model will be applied for normally one-dimensionally consolidated soils for the predictions of stress paths only during monotonic loading. The latter two models are applicable to isotropically or anisotropically normally consolidated and overconsolidated soils. They will be used to predict both stress paths and stress strain curves for both monotonic and cyclic loading.

7.7.1 Predictions of Undrained Behaviour During Monotonic Loading

7.7.1.1 Stress paths

The test results from the 100 mm cell are shown alongside Atkinson's model predictions on the diagram of Figure 7.21. In general terms the agreement is acceptable. However, the prediction for extension loading appears to be less accurate than for compression loading. Atkinson et al (1987) reported similar findings. Thevanayagam and Prapaharan (1988) thought that the poorer prediction of the extension stress path was due to a difference between the stress path and the state boundary surface, which Atkinson et al assumed to be coincident. They also reported, contrary to what was suggested by Atkinson et al, that the state boundary surface is symmetrical about the p' axis rather than the K_0 line. They suggested an alternative model but their predictions did not represent a major improvement.

Pender's model predictions for both normally consolidated and overconsolidated specimens are shown in Figure 7.22. As with Atkinson's model, acceptable agreement with the experimental data can be seen. As before, but to a lesser ex-

tent, for normally consolidated soils the agreement appears to be less adequate for extension loading than for compression loading. The prediction of the stress paths for the overconsolidated specimens is not as good as for the normally consolidated specimens. Pender's model was also used to predict the stress paths of isotropically consolidated specimens in the 38 mm cell. The results are shown in Figure 7.23 where fairly good agreement may be seen.

Al-Tabbaa's model predictions of stress paths for anisotropically consolidated specimens are presented in Figure 7.24. Once again, this model predicts the stress paths of normally consolidated specimens loaded in compression better than the rest . Corresponding predictions for the stress paths of isotropically consolidated specimens are shown in Figure 7.25. The performance of the model is similar to that of Pender's model.

7.7.1.2 Stress-strain curves and stiffnesses

Predicted and experimental stress strain curves and tangent stiffnesses for normally one-dimensionally consolidated specimens loaded in compression are shown in Figure 7.26. The tangent stiffness appears to be well predicted for strains larger than 0.01 %. Predictions of the deformation behaviour for the normally one-dimensionally consolidated specimens loaded in extension are shown in Figure 7.27 along with corresponding experimental data. Here, the agreement does not seem to be satisfactory.

In the case of one-dimensionally overconsolidated specimens, predictions and experimental data are compared in Figure 7.28 for compression loading and Figure 7.29 for extension loading. In the former case, both models used give comparable predictions but underestimate the tangent stiffness, while in the latter case the

model predictions are not as satisfactory. Nevertheless, for strains higher than 0.04 % the stiffness is adequately predicted.

Predictions for isotropically normally consolidated specimens are shown in Figure 7.30. Corresponding predictions for the overconsolidated specimens are presented in Figures 7.31 to 7.34 for OCRs ranging between 2 and 45. For the normally consolidated specimens, the predictions are markedly less satisfactory than those for the corresponding one-dimensionally normally consolidated specimens. For overconsolidated specimens, the predictions improve on average with increasing OCR.

7.7.2 Predictions of Undrained Behaviour during Cyclic Loading

As mentioned in Section 4.3.3, the strain cycle was applied to anisotropically consolidated specimens in the 100 mm cell by keeping the cell pressure constant, varying the axial stress in small increments and monitoring the axial strain. In making predictions it was assumed that the identical increments of deviator stress had been applied to the soil. For a given increment the resulting axial strain and change in mean effective pressure were calculated from the appropriate equations listed in Section 1.2. Parameters defining the state of the sample were updated before the calculations for the next stress increment were performed.

Predicted and experimental results for the normally consolidated specimens are shown in Figures 7.35 and 7.36. The general shape of the stress path (Figure 7.35) is fairly well predicted by both models. However, the final drop in p' is underpredicted because of the divergence of the actual and predicted stress paths during the final leg of the cycle (reloading stage). Both predictions of the stress path for

the initial compression phase lie below the experimental stress path. The general shape of the stress-strain cycle (Figure 7.36) is well predicted by both models.

Corresponding predictions of the models for the overconsolidated specimens are shown in Figures 7.37 and 7.38. The stress-strain cycle (Figure 7.38) appears to be better predicted than the stress path (Figure 7.37) and the predictions are especially good during the initial compression phase. As before, the greatest divergence of the predicted and experimental stress paths occurs during the reloading stage.

7.7.3 Overview of Model Performance

7.7.3.1 Monotonic loading

The models of Pender and Al-Tabbaa capture the general pattern of behaviour adequately. Stress paths are seen to converge on the critical state. For one-dimensionally overconsolidated specimens, the stress paths are initially symmetrical about the swelling line thus reflecting anisotropy of behaviour. This feature is not captured by either model. Atkinson's model is almost as good as those of Pender and Al-Tabbaa for normally consolidated specimens but would give unrealistic predictions for overconsolidated soils since the behaviour would be assumed elastic initially.

In the case of the stress-strain curve and stiffness, the model predictions are variable in accuracy, depending on the stress history and the type of test (i.e. compression or extension). At the 0.01 % strain level discrepancies in E_{ut} are up to 100 %. At the 0.1 % strain level agreement is more satisfactory; discrepancies are generally less than 20 %. More test data is required in some cases to assess the

accuracy properly in relation to repeatability limits.

The previous section indicated that the best predictions were obtained for compression tests on normally consolidated soil. Distinctly poorer predictions were noticed for extension tests. One reason for this may be that models have been developed largely on the basis of data from compression tests, where the model parameters may not take the same values as those under extension loading. For example, the value of M in extension has been found to be smaller than in compression (Atkinson et al (1987)) whereas the models employed above use the same value of M for both compression and extension cases.

7.7.3.2 Cyclic loading

For cyclic loading both Pender's and Al-Tabbaa's models capture the general pattern of behaviour remarkably well. However, major discrepancies in the stress paths arise in the final reloading stage of shearing. This is true for both normally consolidated and overconsolidated specimens. One reason may be the fact that both types of specimen approach a failure state towards the end of the first leg of the cycle and therefore major changes to the soil microfabric or the development of shear planes may take place, thus rendering the parameters adopted for the predictions unrealistic.

The stress strain loops are predicted to have larger areas (i.e. larger deviator stresses). This is thought to be due to loading rate effects, discussed in Section 7.4. The models have been developed on the basis of data obtained from tests conducted at relatively low loading rates.

Test	E_{sr}/p'_0		
	0.01%	0.05%	0.1%
ANCD1	199	45	22
ANCD2	214	54	24
ANCU1	180	44	23
ANED1	528	163	98
ANEU1	334	160	107
AOCD1	628	202	123
AOCU1	605	190	109
AOED1	244	73	20
AOEU1	161	43	15
ANCD1 *	375	42	7.7
ANCD2 *	340	54	17
ANED1 *	298	36	5.4
AOCD1 *	1009	224	30
AOED1 *	610	183	97

Note:

* data from the first phase of the strain cycle

Table 7.1 Summary of stiffness values from tests in the 100 mm cell

Test	L
ANCD1	0.11
ANCD2	0.15
ANCU1	0.13
ANED1	0.18
ANEU1	0.32
AOCD1	0.19
AOCU1	0.18
AOED1	0.10
AOEU1	0.09
ANCD1 *	0.02
ANCD2 *	0.05
ANED1 *	0.02
AOCD1 *	0.09
AOED1 *	0.16

Note:
* data from the first phase of the strain cycle

Table 7.2 Summary of linearity index values from tests in the 100 mm cell

Test	ν
ANCD1	0.501
ANCD2	0.481
ANCU1	0.490
ANED1	0.510
ANEU1	0.500
AOCD1	0.497
AOCU1	0.512
AOED1	0.499
AOEU1	0.511

Table 7.3 Summary of Poisson's ratio values

Strain Level %	$\langle E_{ur}/p'_0 \rangle_{n.c.}$	C
0.01	91	103
0.05	81	50
0.10	75	31

Table 7.4 Summary of $\langle E_{ur}/p'_0 \rangle_{n.c.}$ and C values

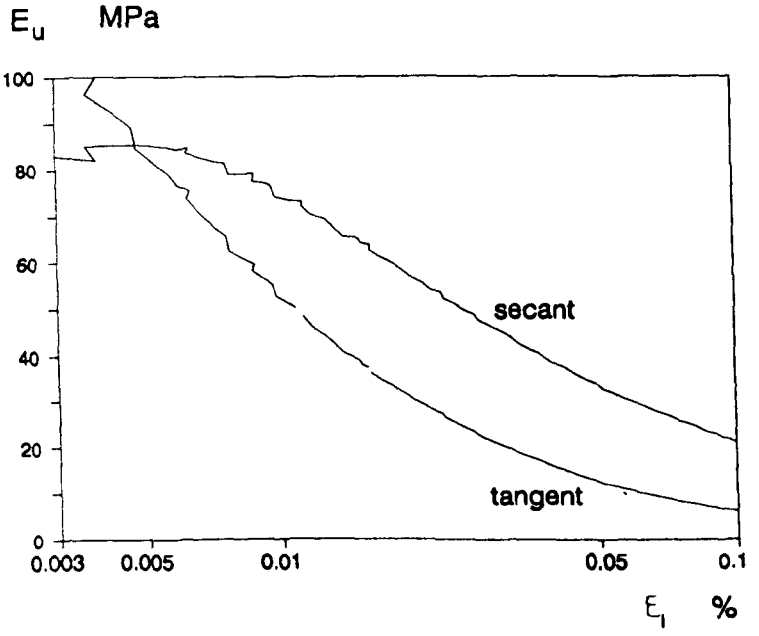

Fig 7.1 Typical stiffness-strain plot on semi-logarithmic scale

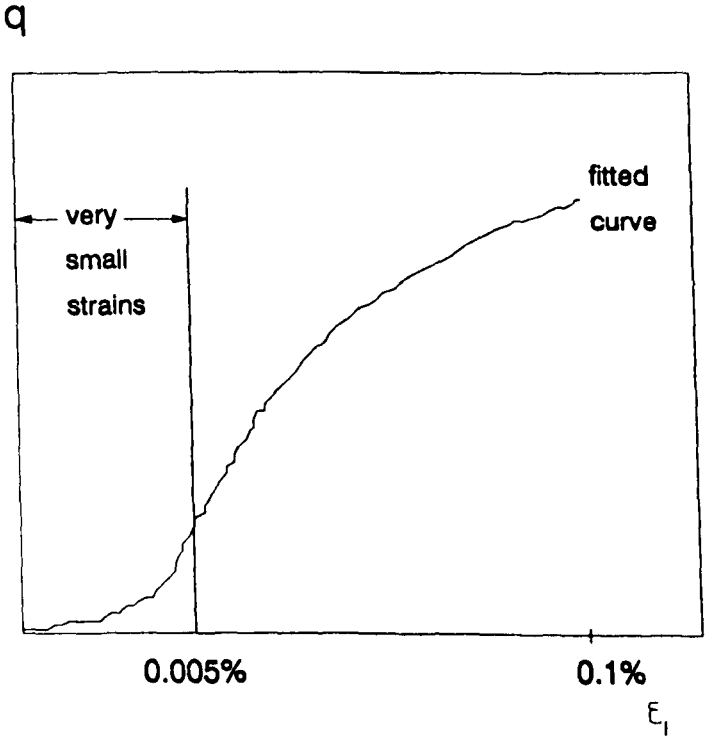

Fig 7.2 Exagerated representation of fitted curve at very small strains (not actual data)

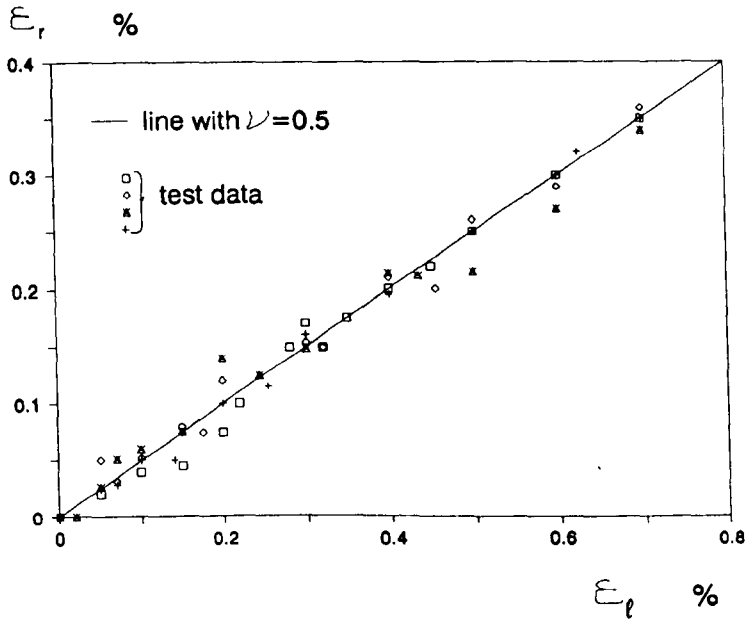

(a) OCR=1

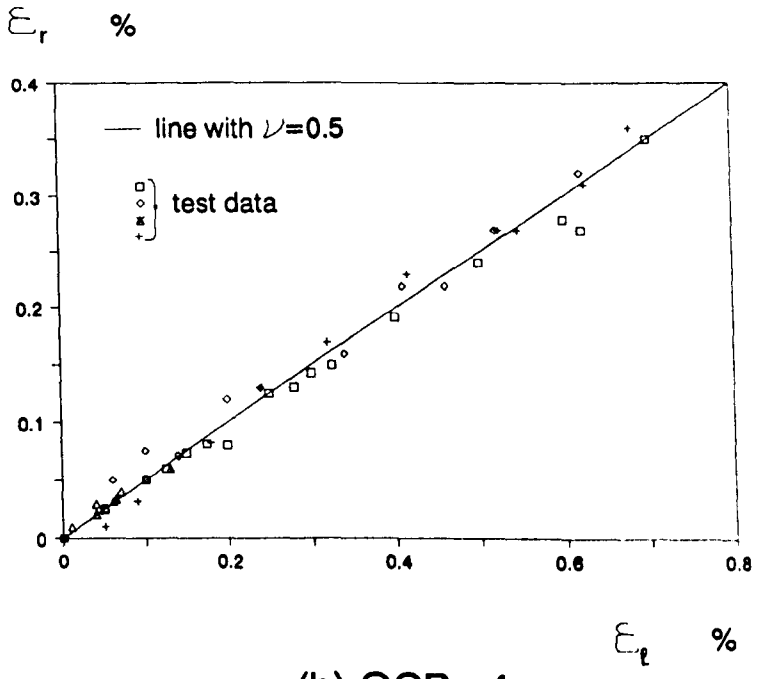

(b) OCR=4

Fig 7.3 Variation of radial strain with axial strain during undrained shearing

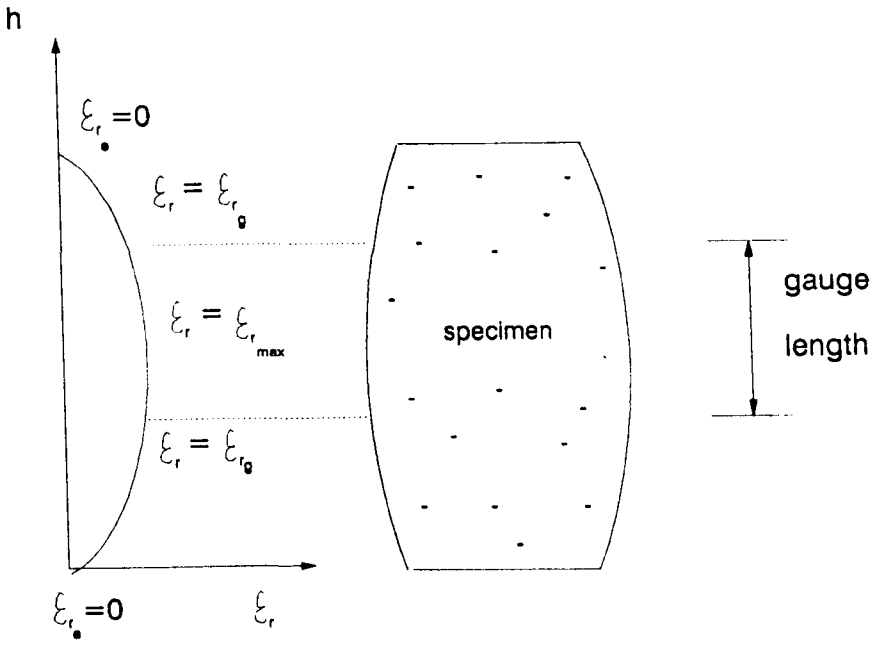

$$\varepsilon_{r_{max}} - \varepsilon_{r_g} < \varepsilon_{r_{max}} - \varepsilon_{r_e}$$

Fig 7.4 Schematic representation of the distribution of radial strain along the specimen height

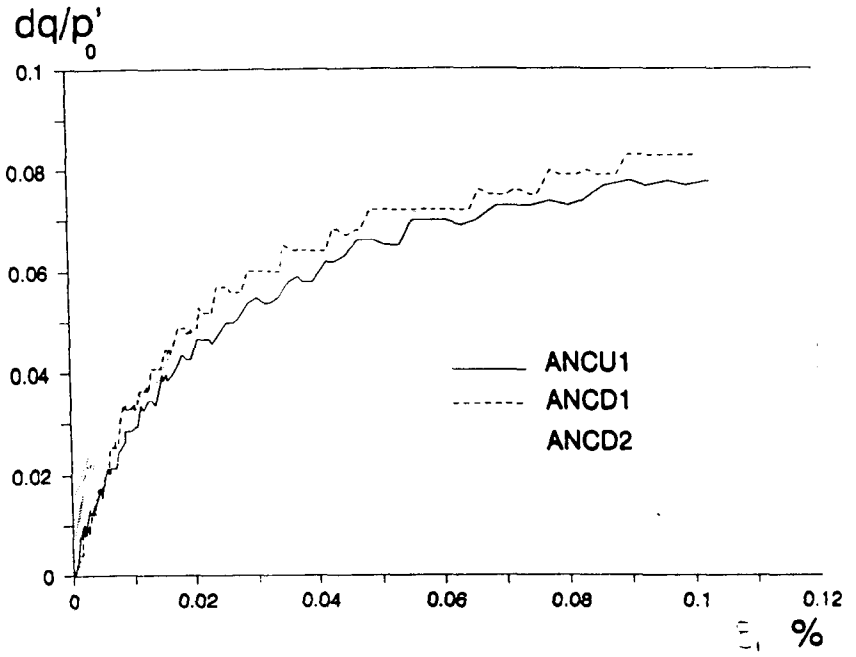

(a) stress-strain

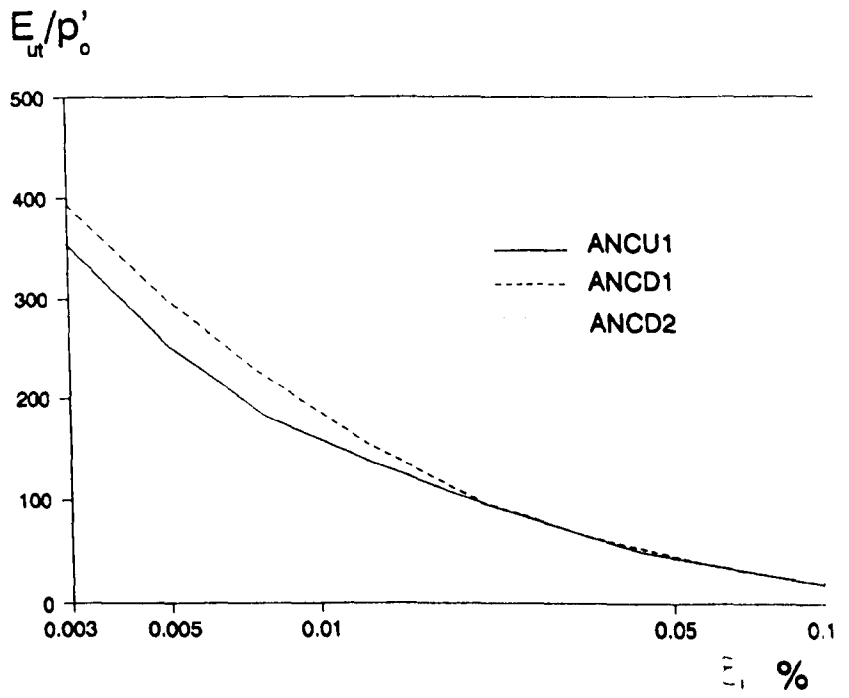

(b) stiffness-strain

Fig 7.5 Effect of sampling disturbance on the deformation behaviour of normally consolidated specimens-compression.

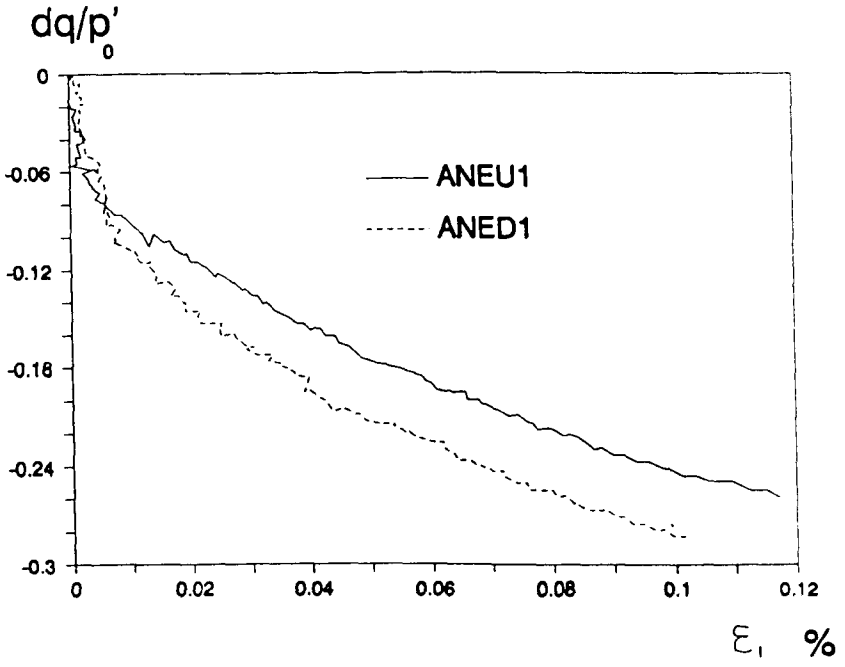

(a) stress-strain

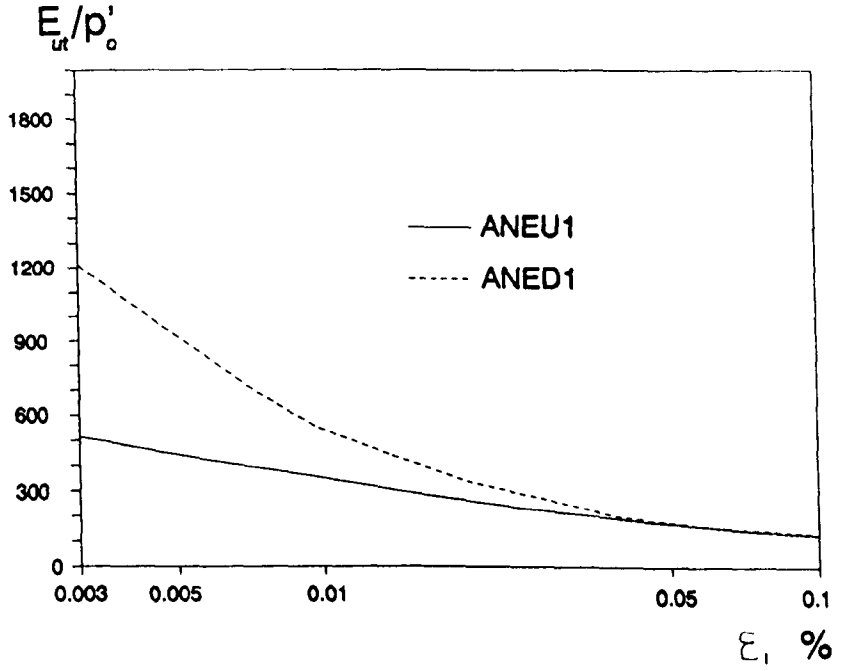

(b) stiffness-strain

Fig 7.6 Effect of sampling disturbance on the **deformation behaviour of normally consolidated specimens-extension**

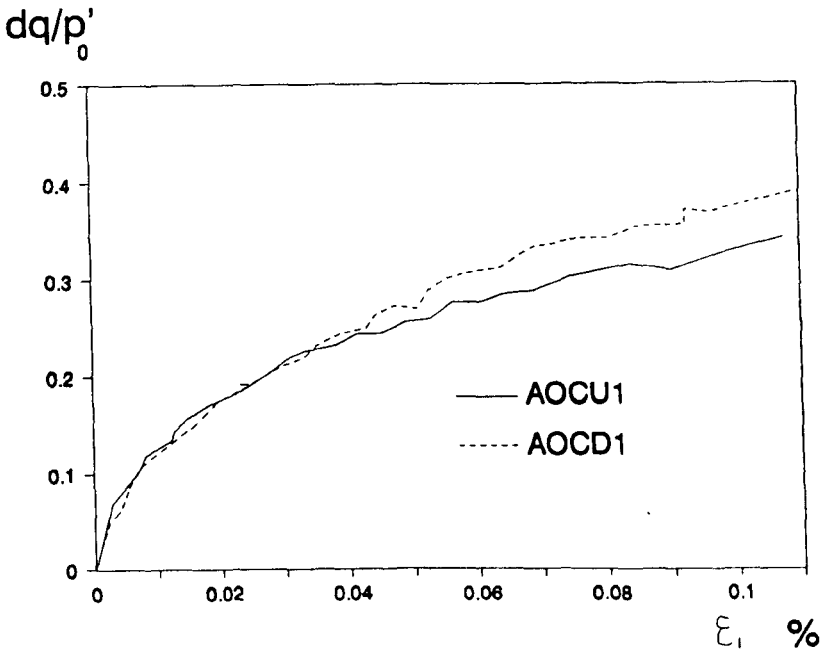

(a) stress-strain

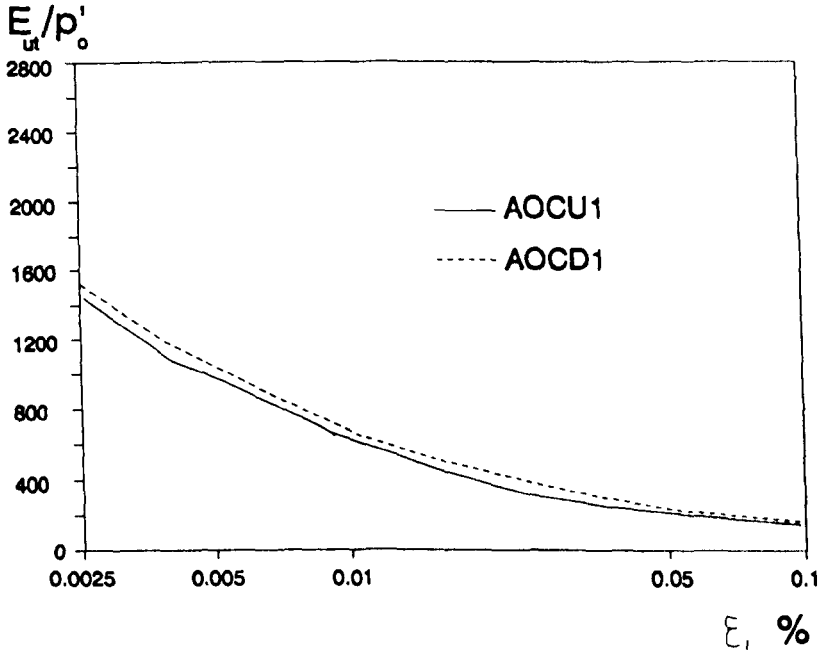

(b) stiffness-strain

Fig 7.7 Effect of sampling disturbance on the deformation behaviour of over-consolidated specimens-compression

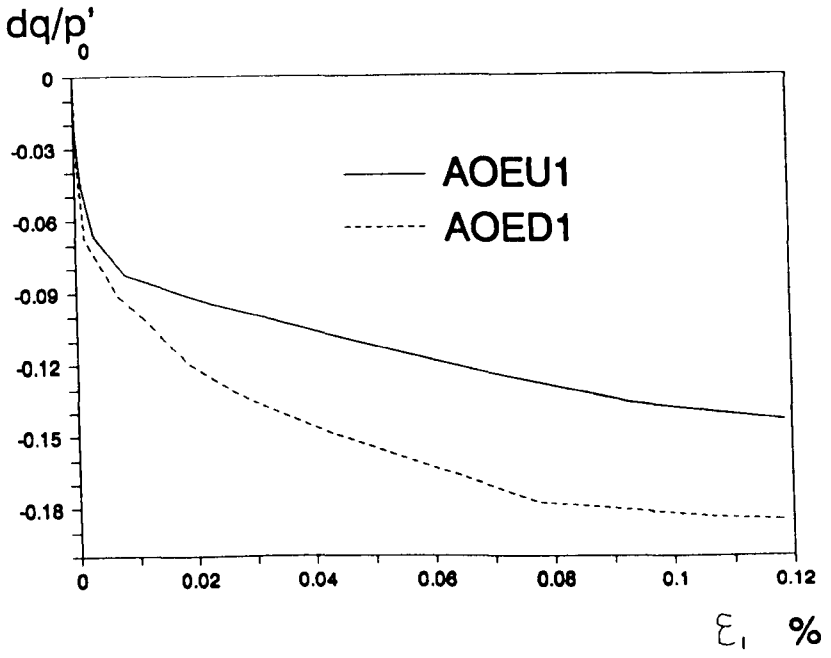

(a) stress-strain

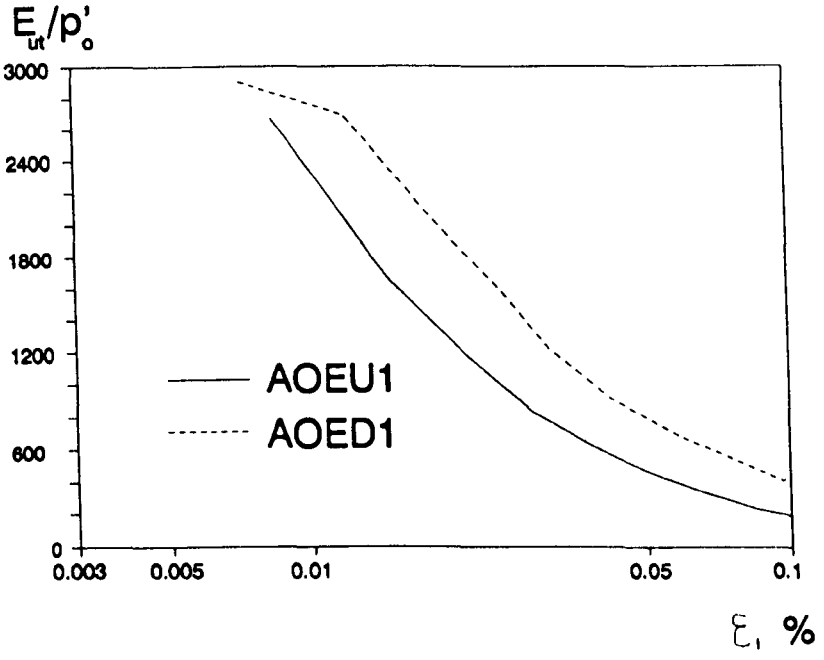

(b) stiffness-strain

Fig 7.8 Effect of sampling disturbance on the deformation behaviour of over-consolidated specimens-extension

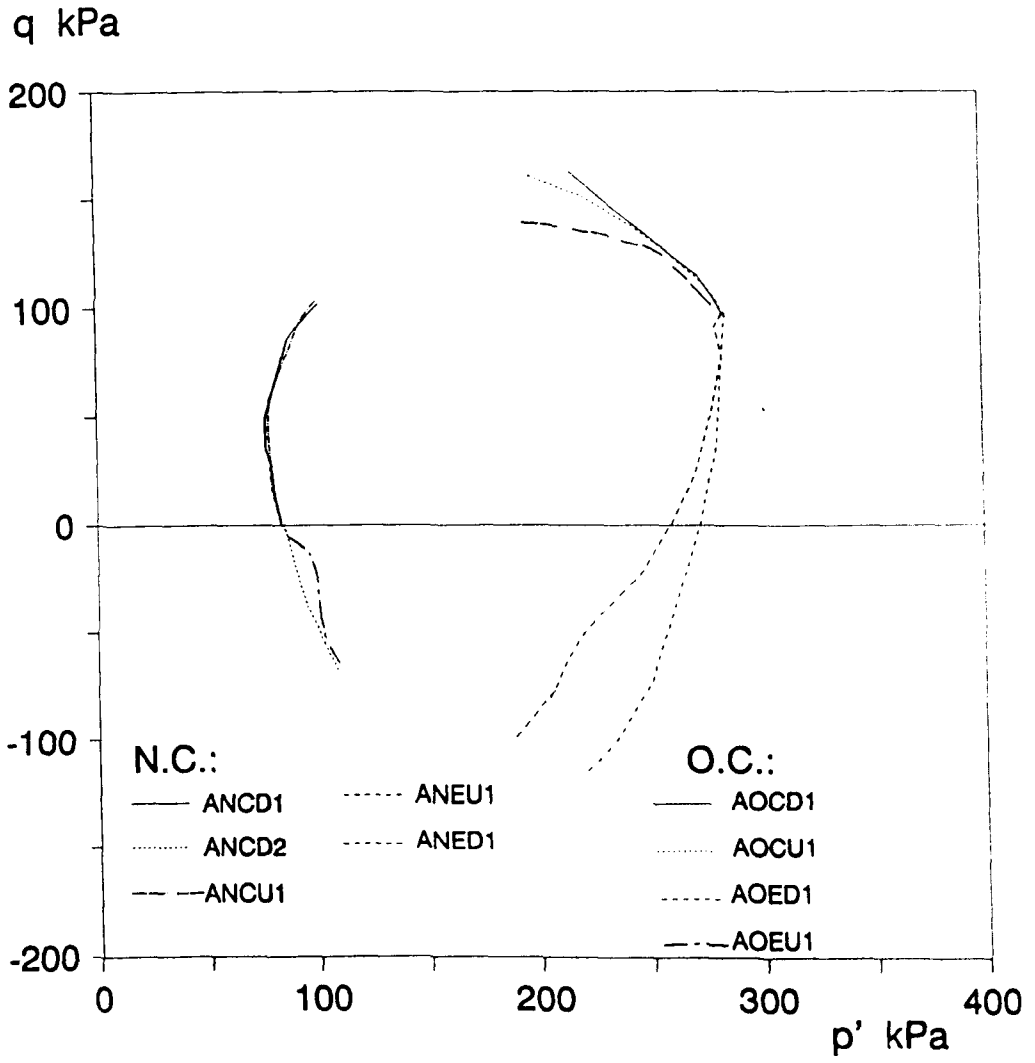

Fig 7.9 Stress paths during normal shearing for all the tests in the 100 mm cell

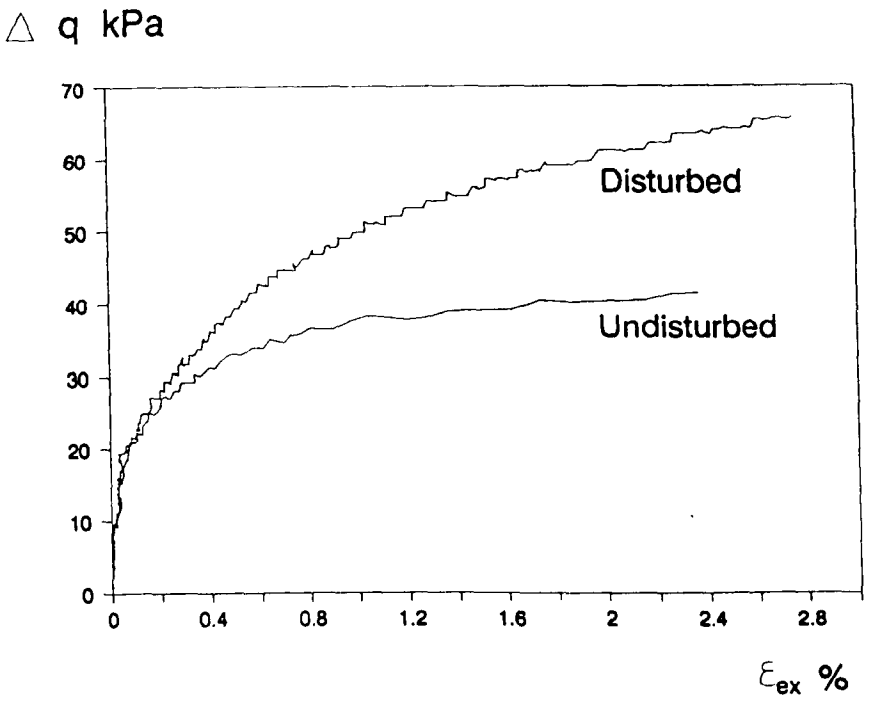

(a) compression loading

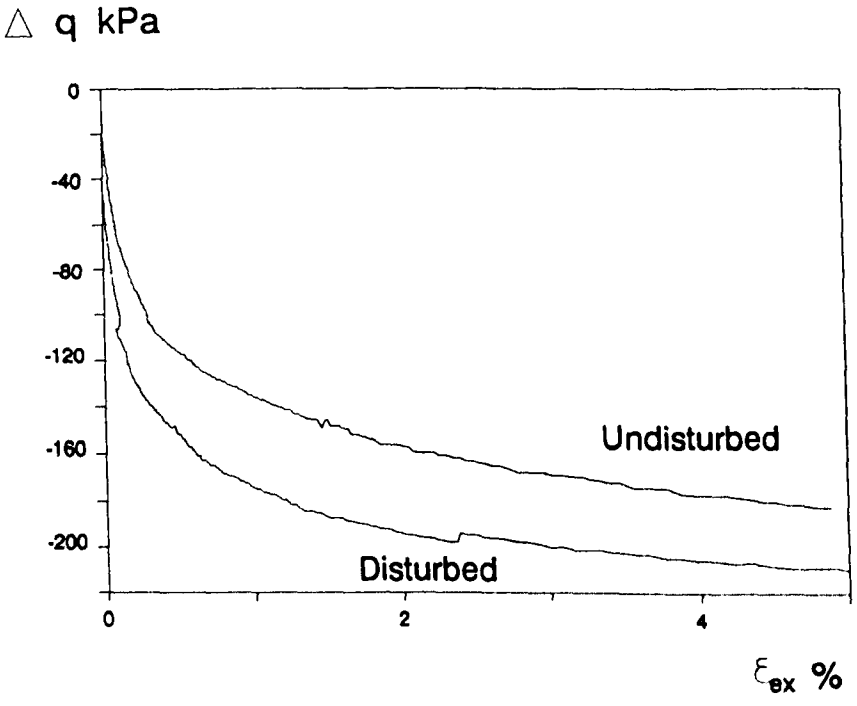

(b) extension loading

Fig 7.10 Effect of sampling disturbance on the large strain behaviour of normally consolidated specimens

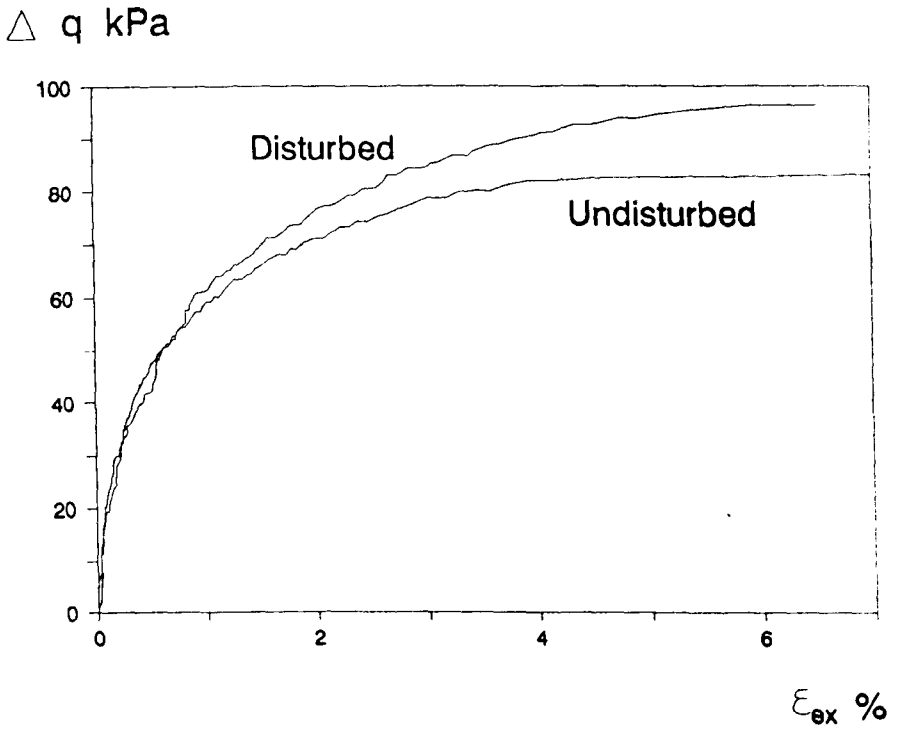

(a) compression loading

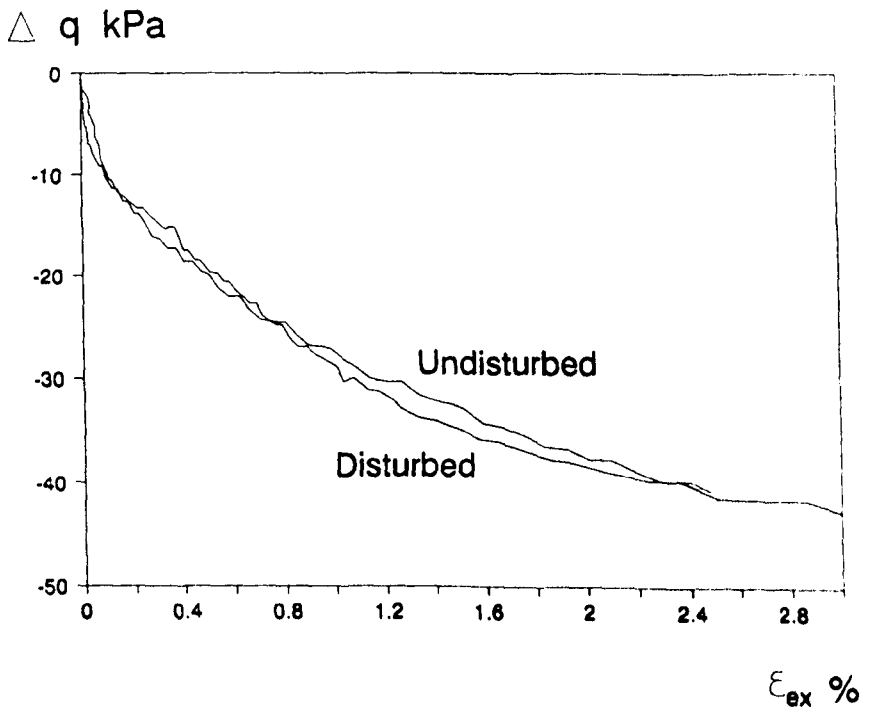

(b) extension loading

Fig 7.11 Effect of sampling disturbance on the large strain behaviour of overconsolidated specimens

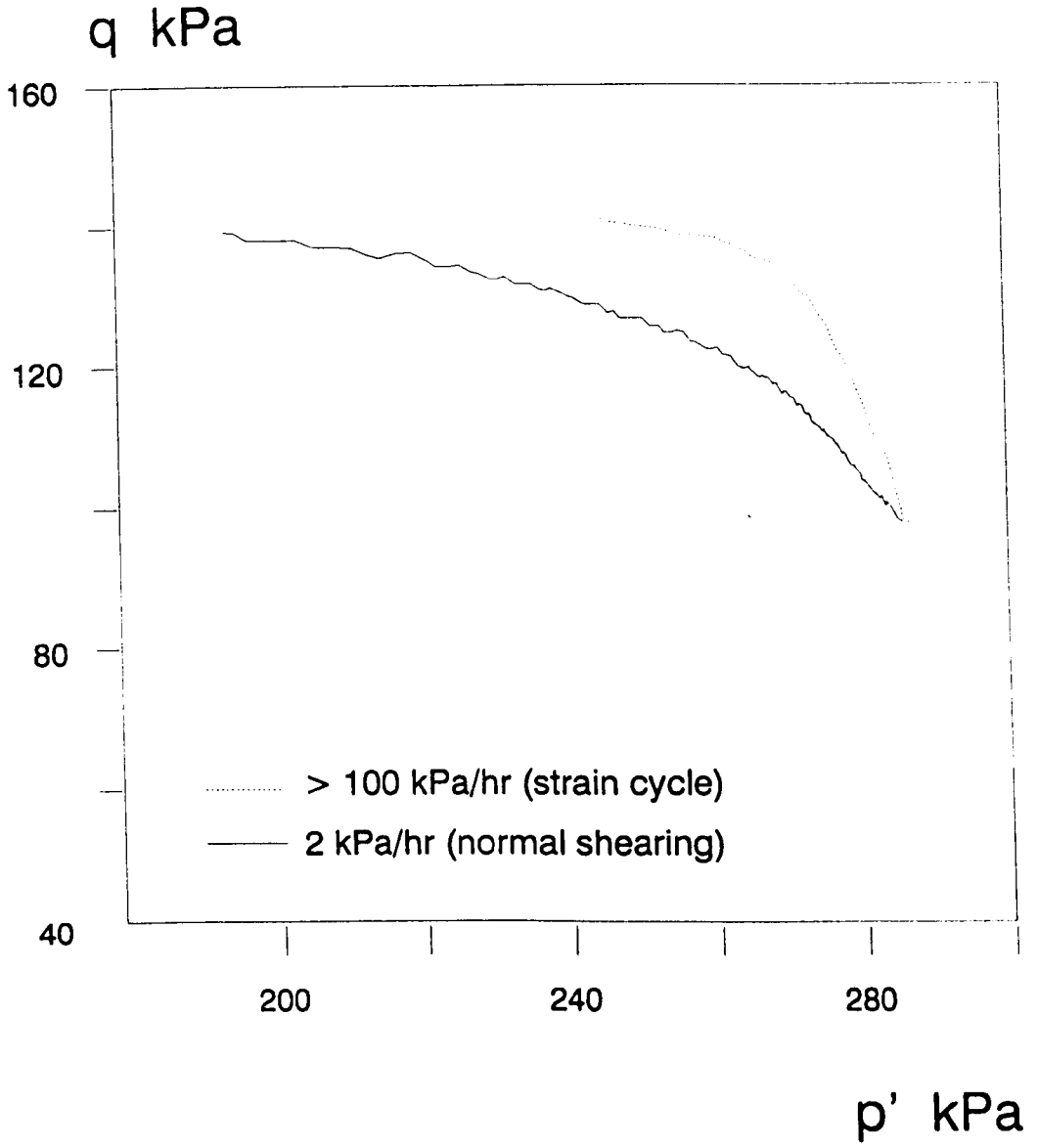

Fig 7.12 Effect of rate of shearing on the stress path of one-dimensionally normally consolidated specimens

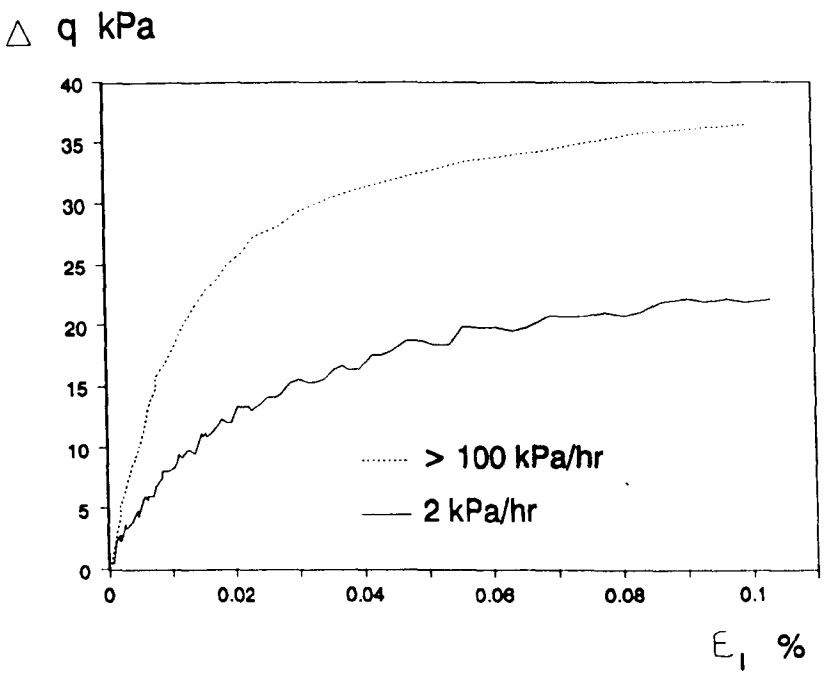

(a) stress-strain

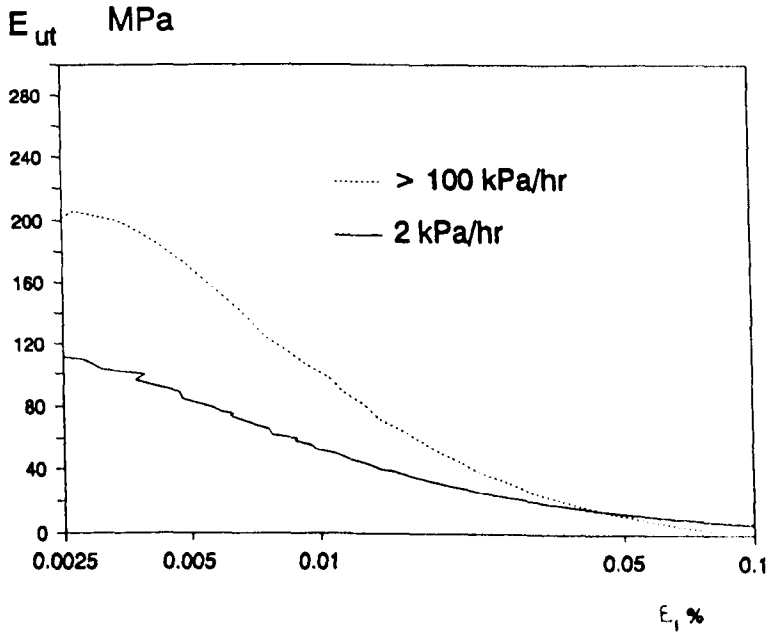

(b) stiffness-strain

Fig 7.13 Effect of rate of shearing on the deformation behaviour of one-dimensionally normally consolidated specimens

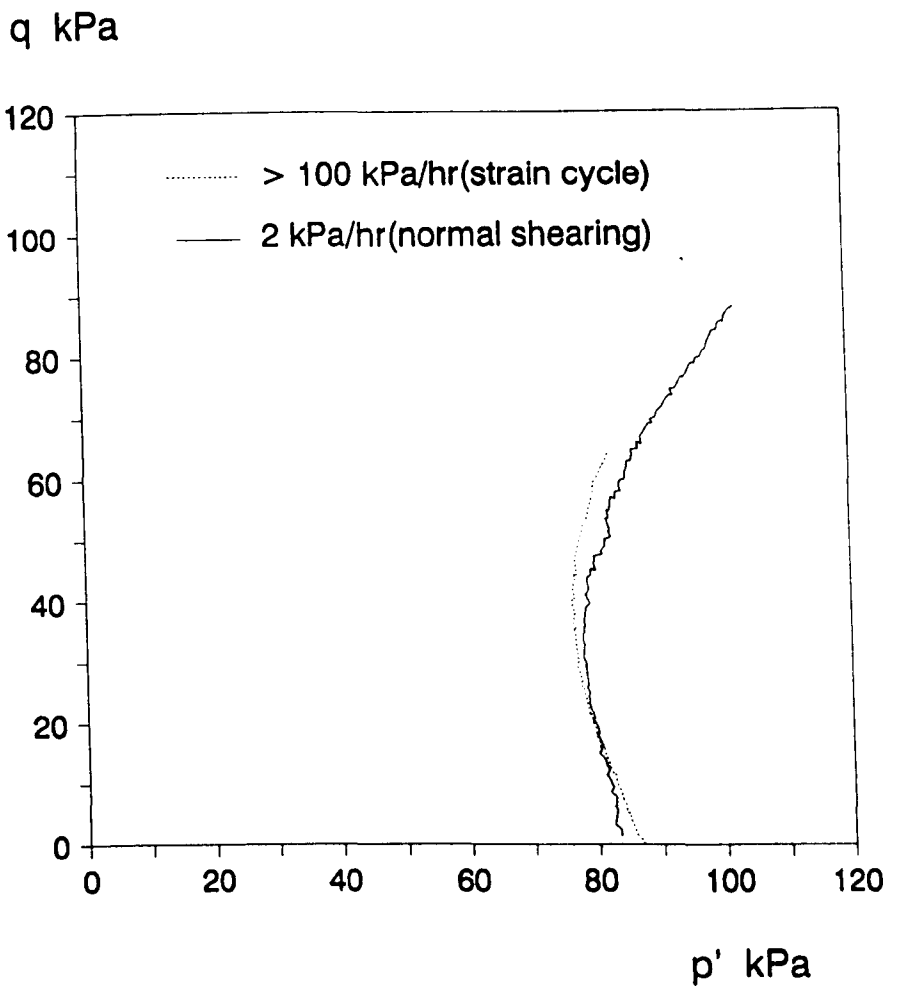

Fig 7.14 Effect of rate of shearing on the stress path of one-dimensionally overconsolidated specimens

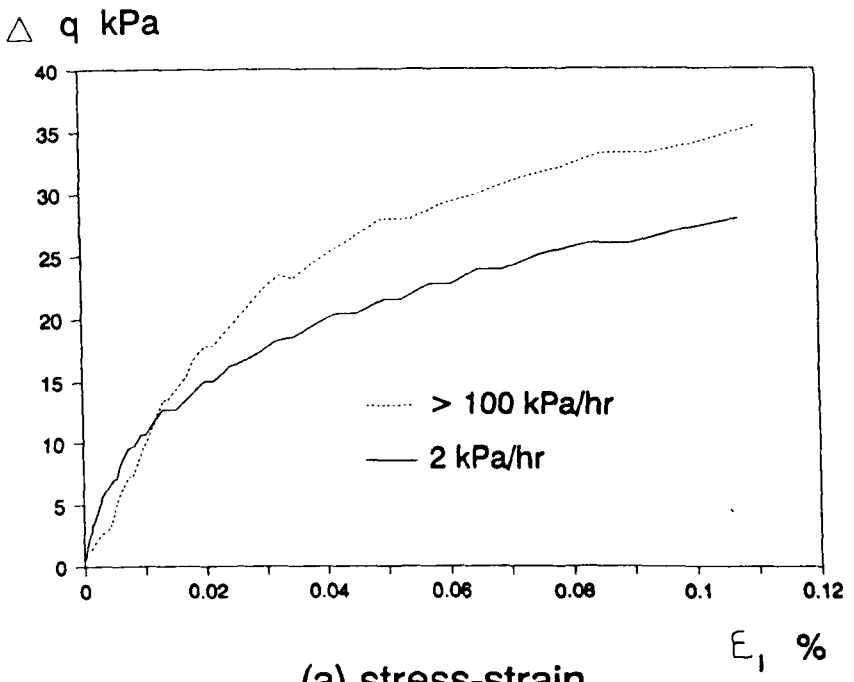

(a) stress-strain

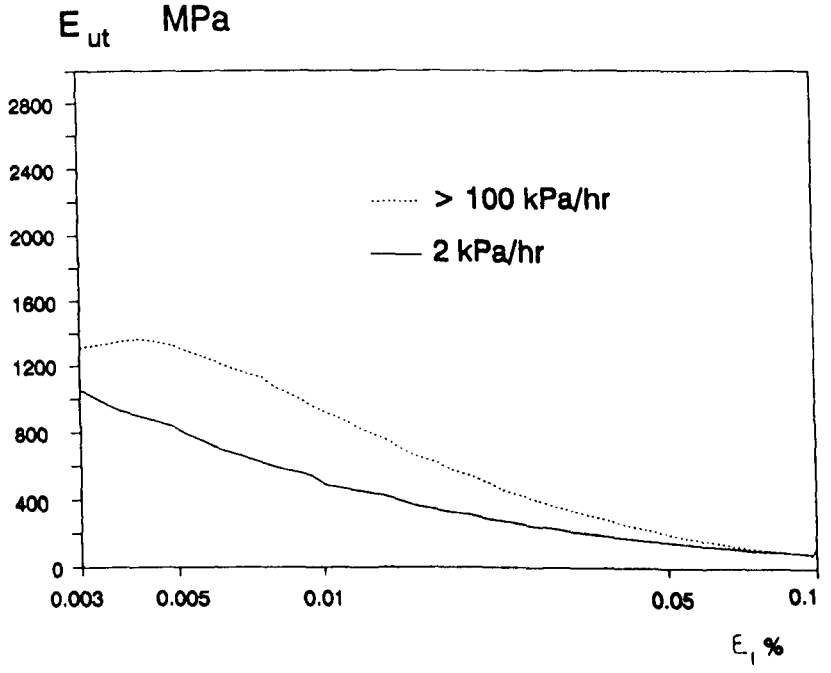

(b) stiffness-strain

Fig 7.15 Effect of rate of shearing on the deformation behaviour of one-dimensionally over-consolidated specimens

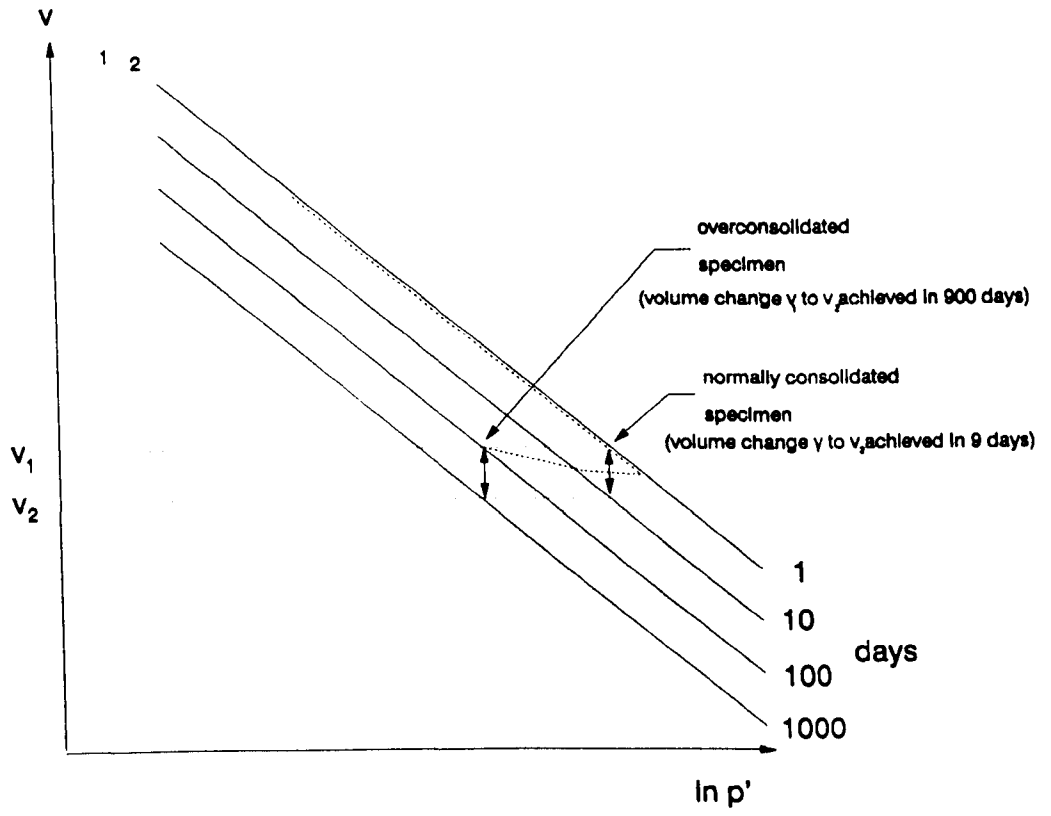

Fig 7.16 Diagrammatic comparison between creep behaviour of normally consolidated and overconsolidated soils

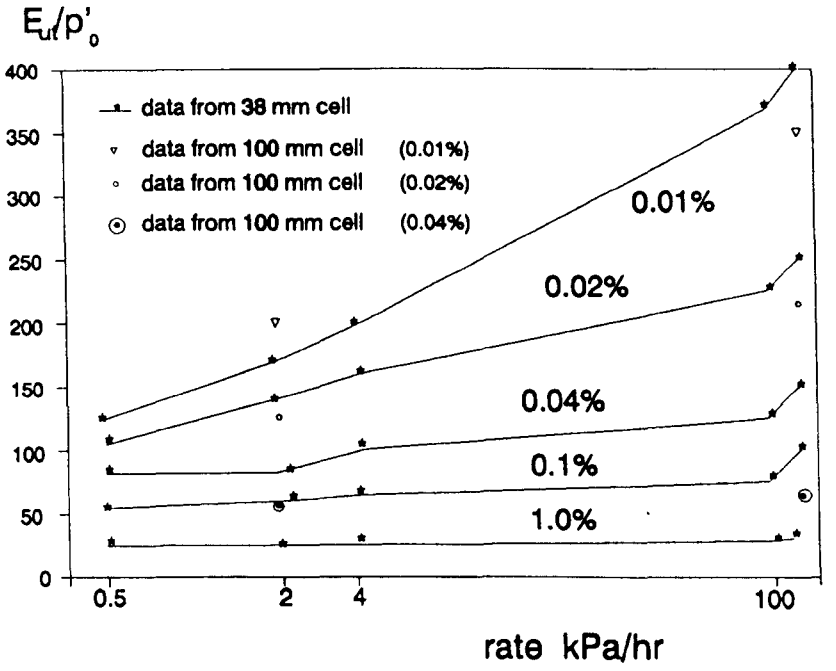

Fig 7.17 Effect of rate of shearing on normalised stiffness

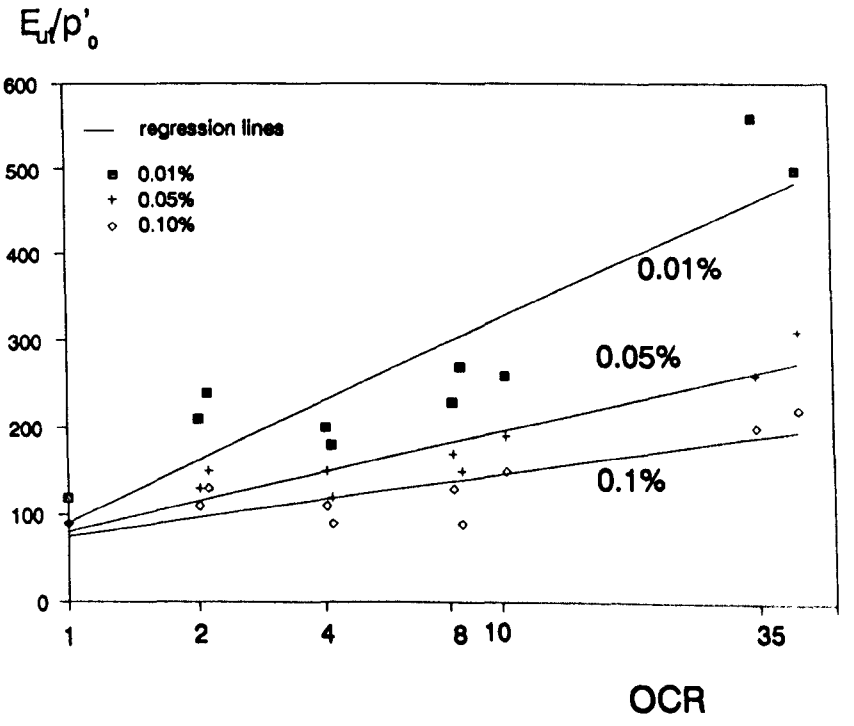

Fig 7.18 Effect of overconsolidation ratio on normalised stiffness

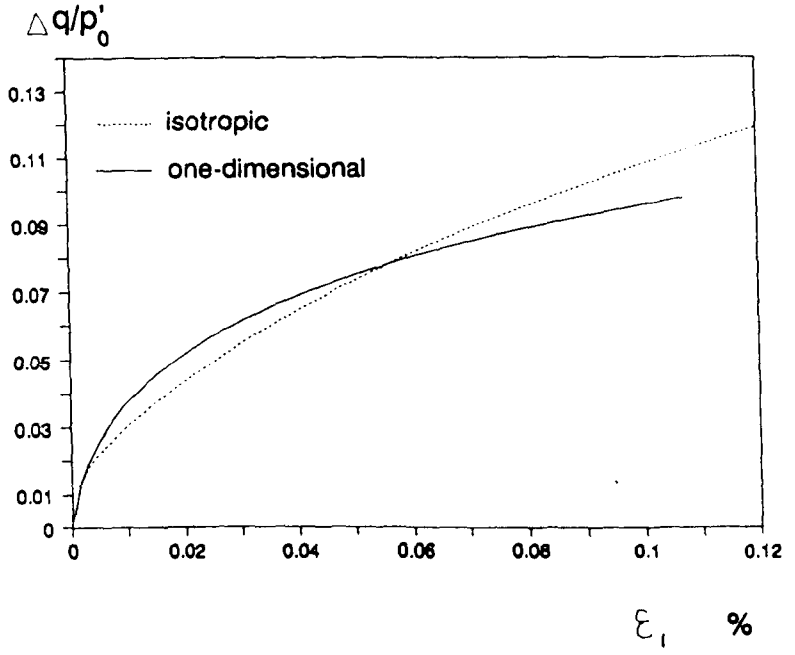

(a) stress-strain

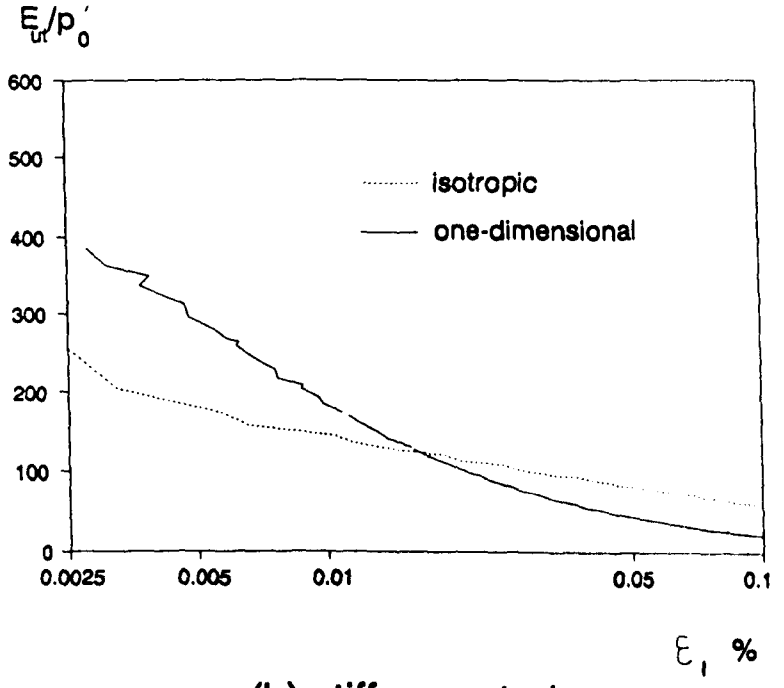

(b) stiffness-strain

Fig 7.19 Comparison of deformation behaviour of isotropically and one-dimensionally consolidated specimens (normally consolidated)

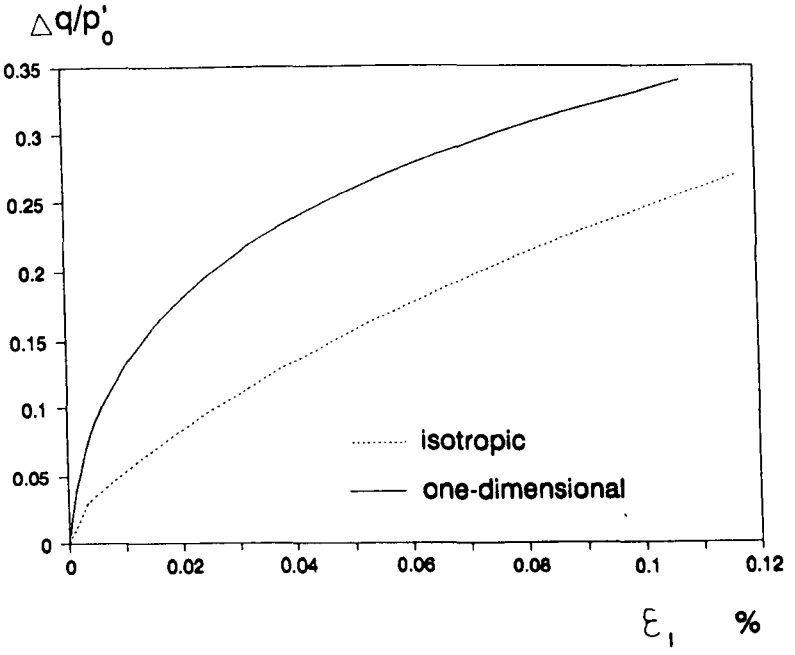

(a) stress-strain

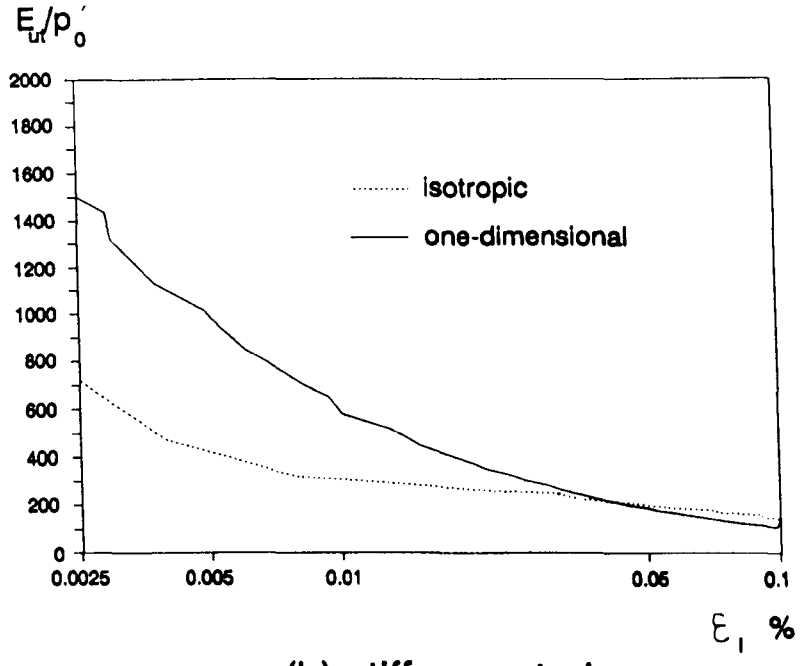

(b) stiffness-strain

Fig 7.20 Comparison of deformation behaviour of isotropically and one-dimensionally consolidated specimens (overconsolidated ; OCR=4)

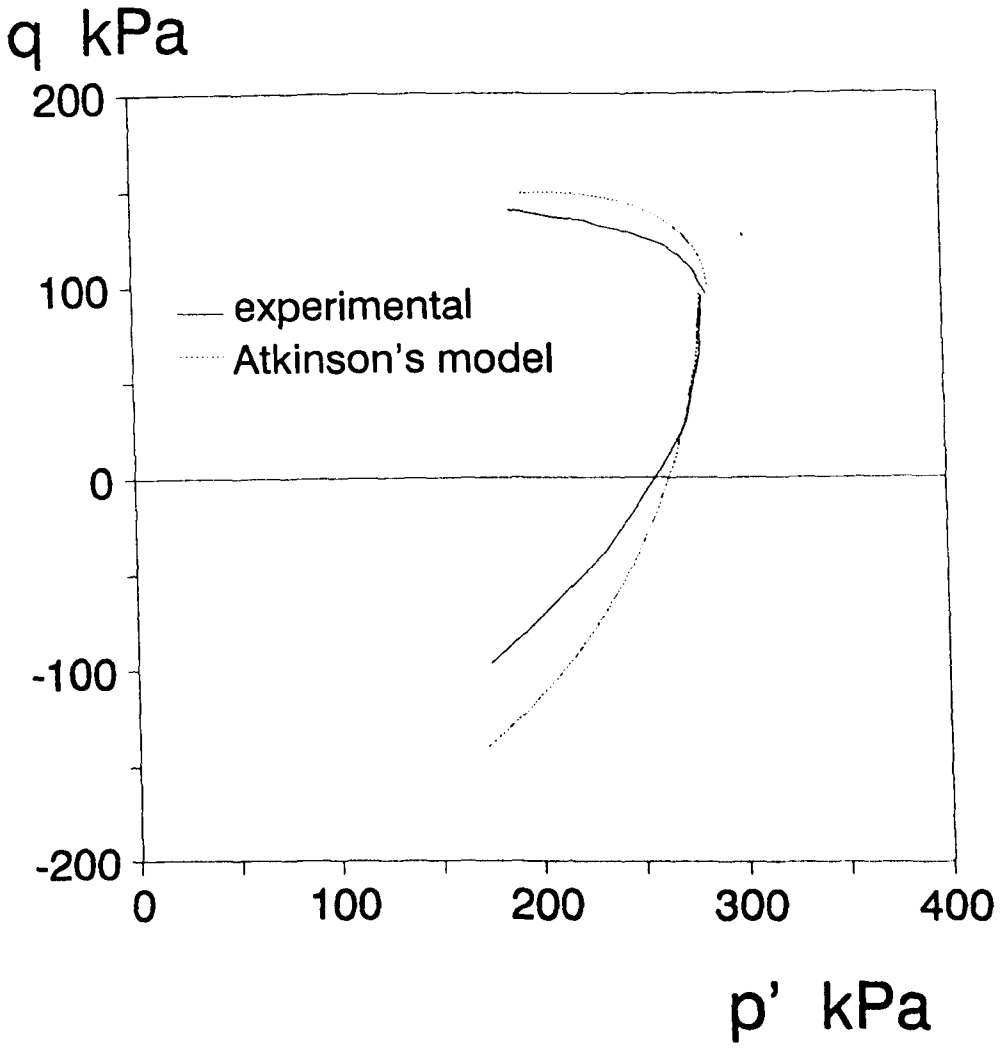

Fig 7.21 Comparison between experimental and predicted stress paths from Atkinson's model for normally one-dimensionally consolidated specimens

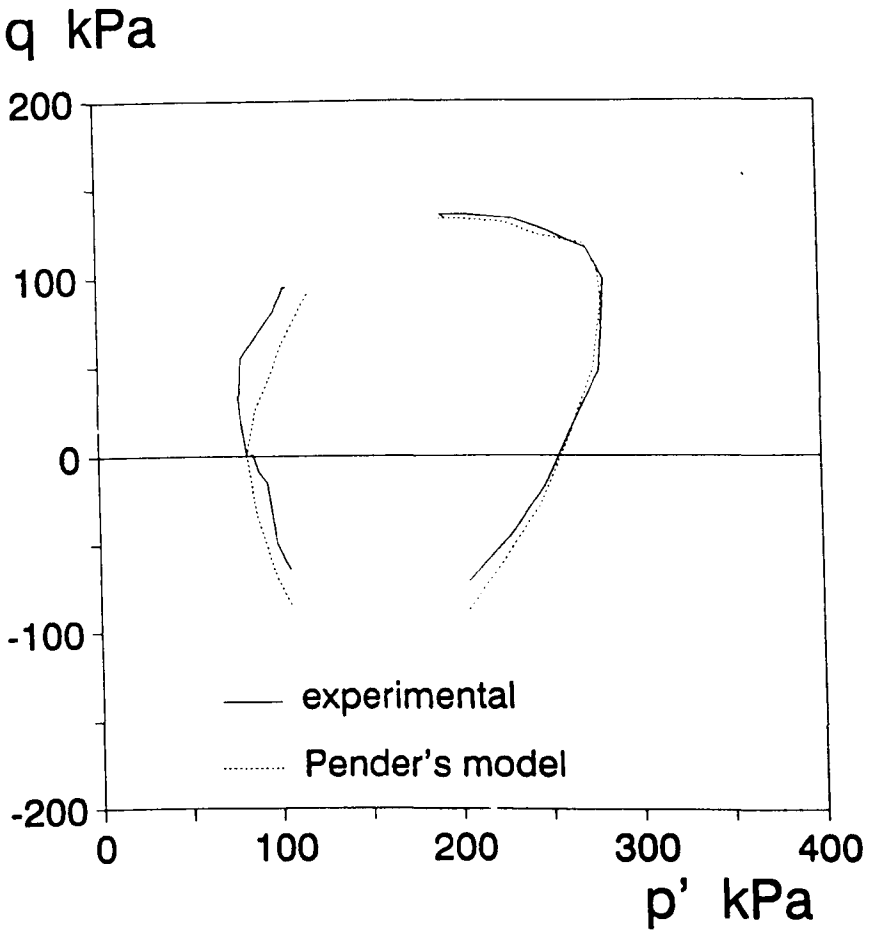

Fig 7.22 Comparison between experimental and predicted stress paths from Pender's model for one-dimensionally consolidated specimens

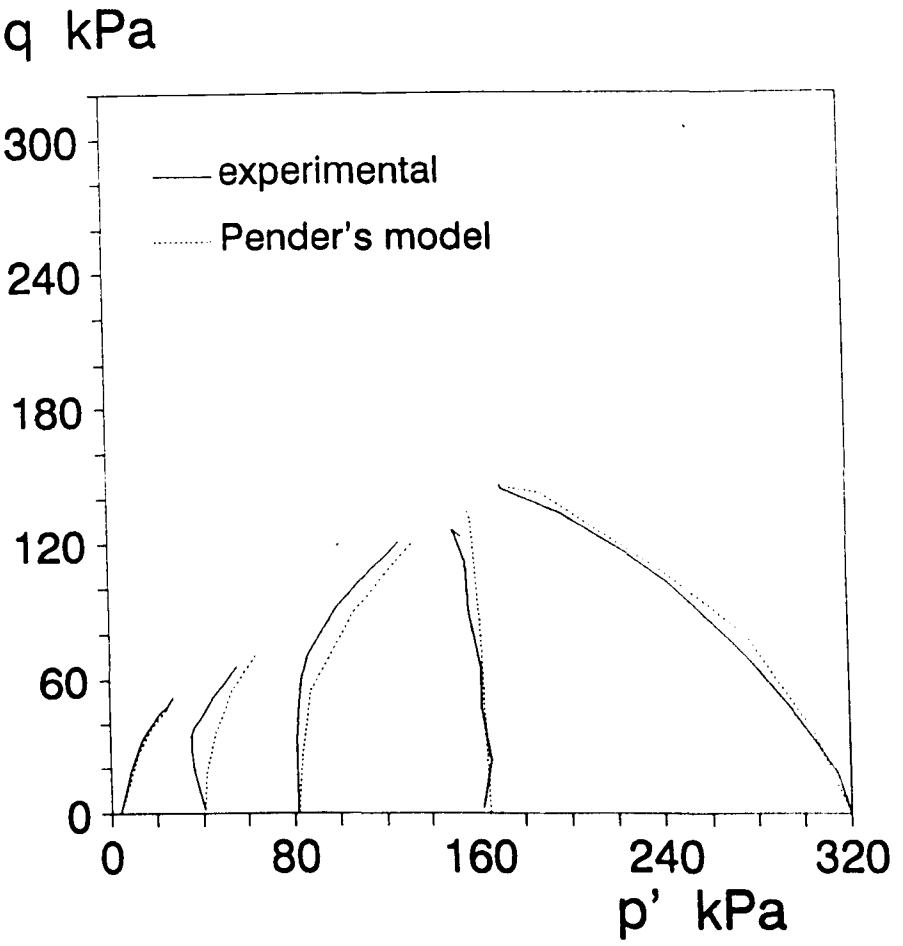

Fig 7.23 Comparison between experimental and predicted stress paths from Pender's model for isotropically consolidated specimens

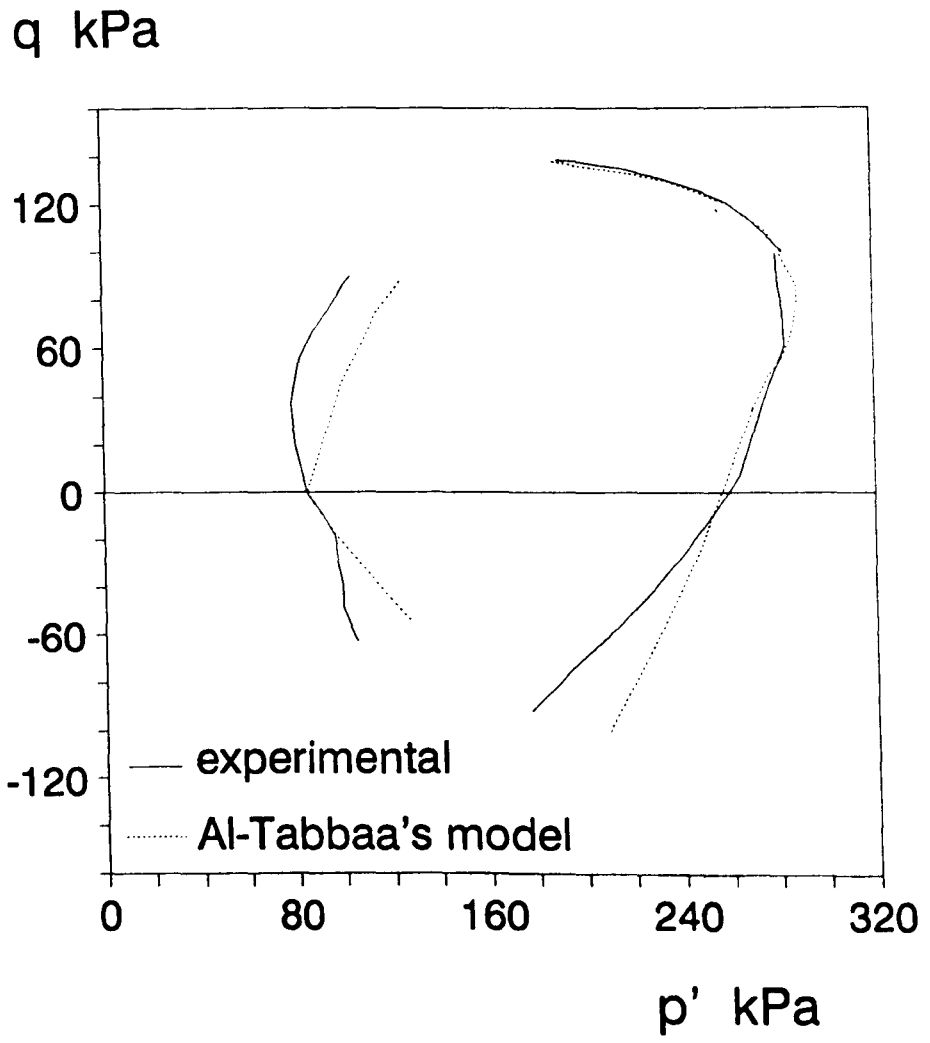

Fig 7.24 Comparison between experimental and predicted stress paths from Al-Tabbaa's model for one-dimensionally consolidated specimens

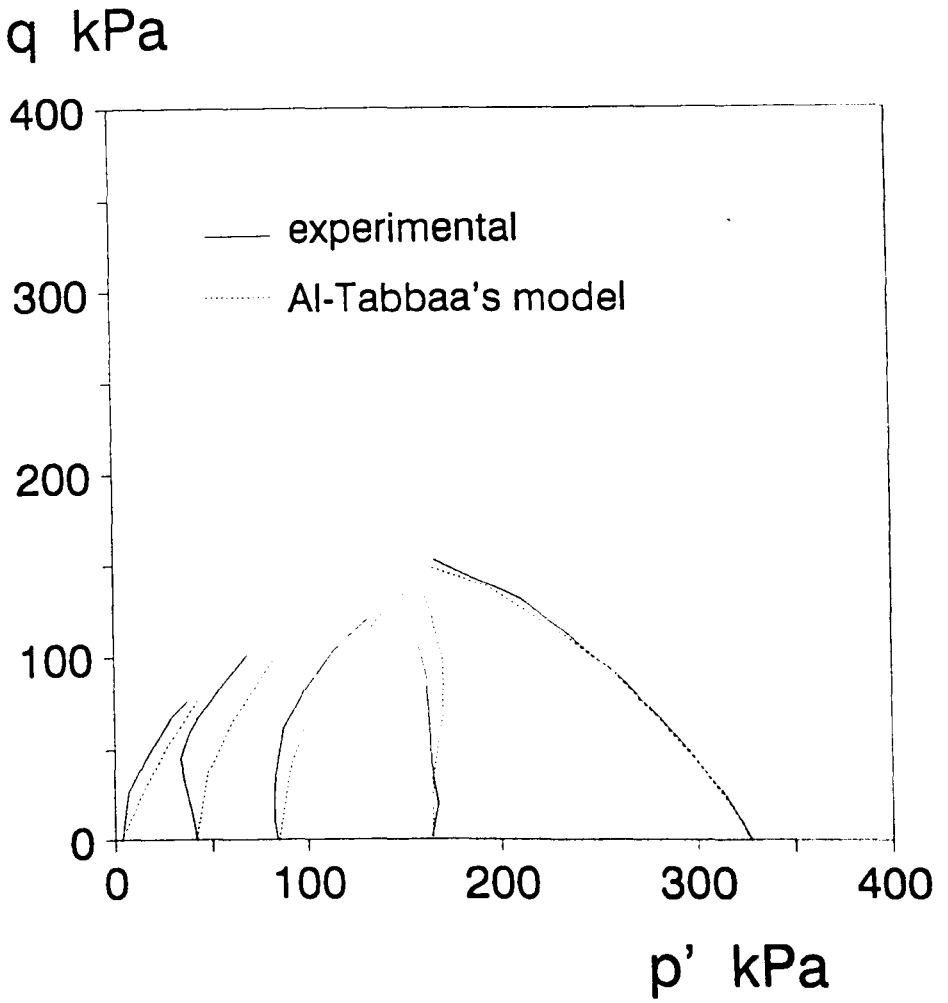

Fig 7.25 Comparison between experimental and predicted stress paths from Al-Tabbaa's model for isotropically consolidated specimens

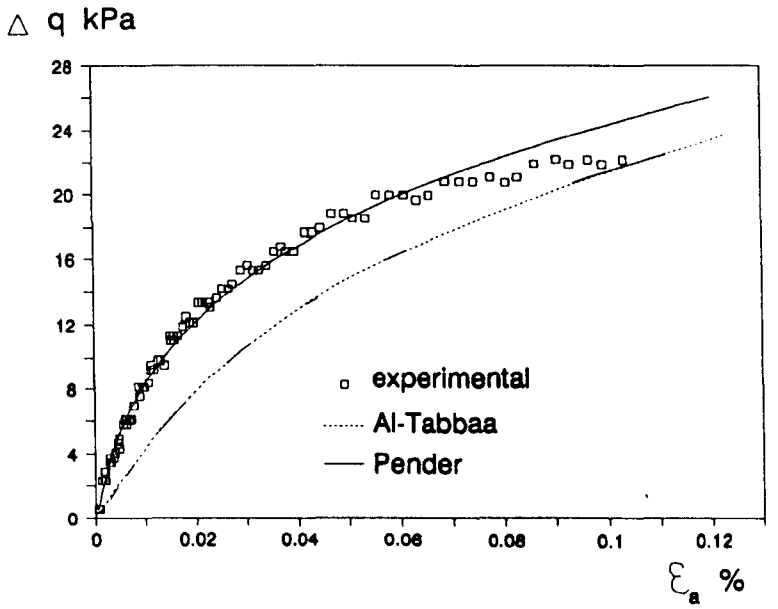

(a) stress-strain

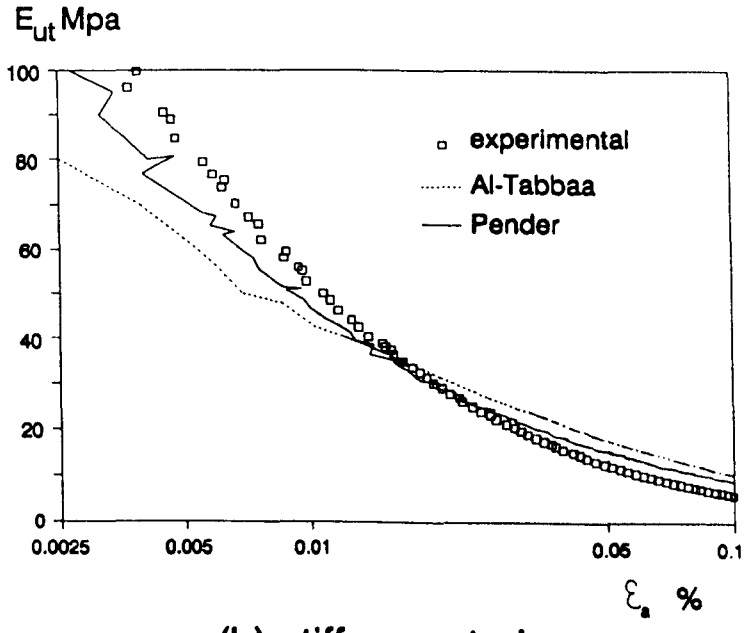

(b) stiffness-strain

Fig 7.26 Comparison between experimental and predicted deformation behaviour of one-dimensionally consolidated specimens-compression loading (OCR=1)

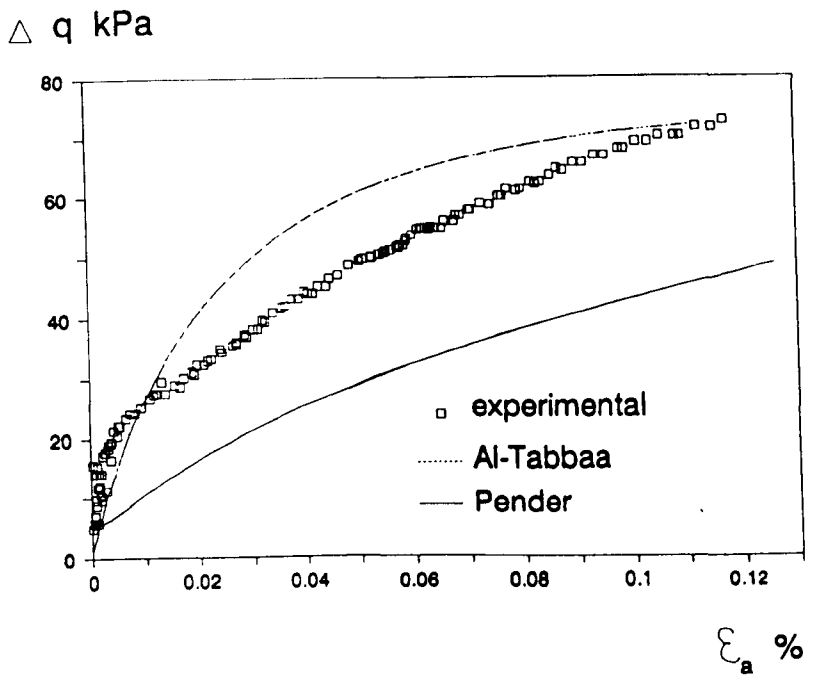

(a) stress-strain

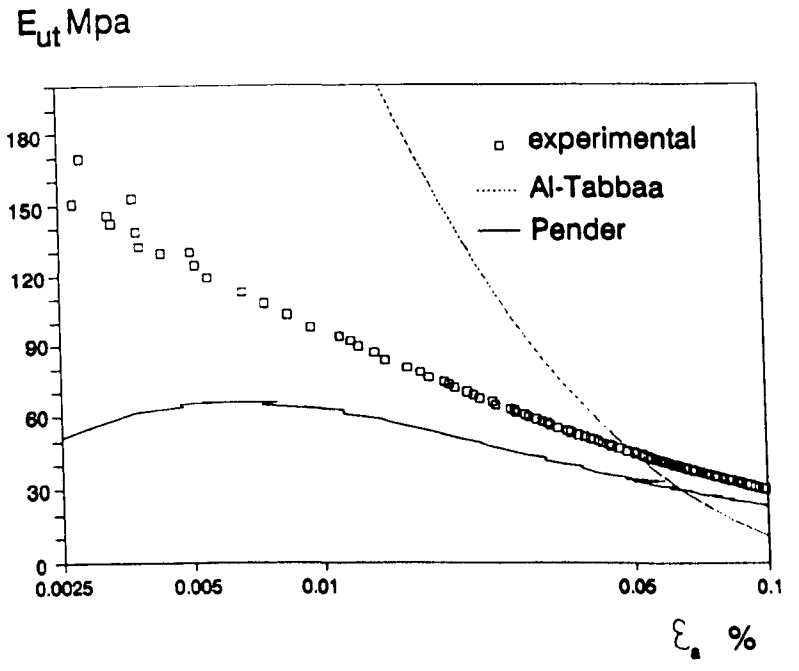

(b) stiffness-strain

Fig 7.27 Comaprison between experimental and predicted deformation behaviour of one-dimensionally consolidated specimens-extension (OCR=1)

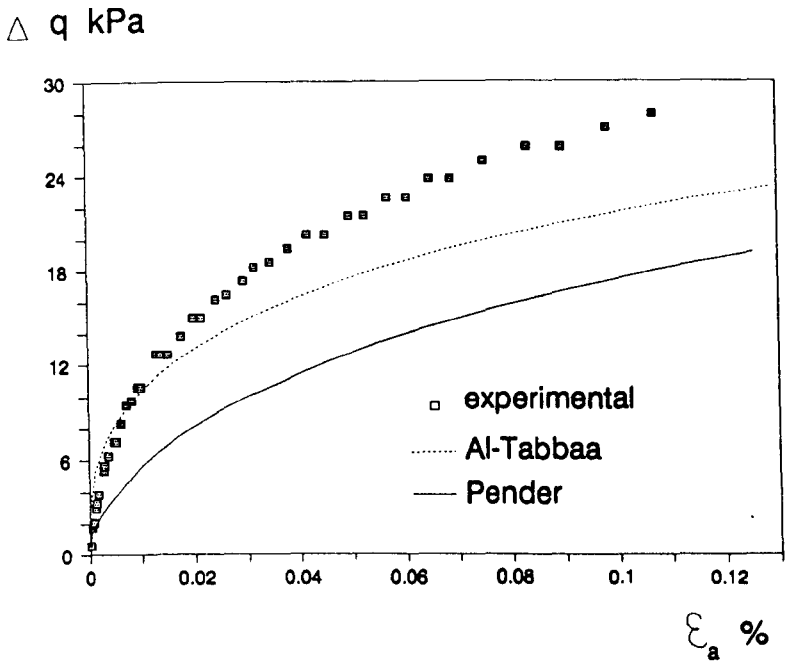

(a) stress-strain

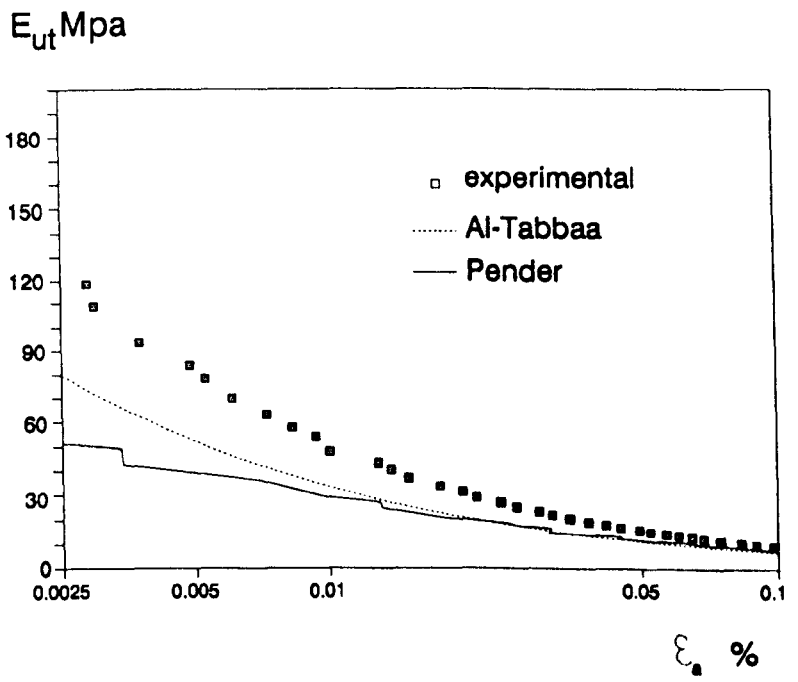

(b) stiffness-strain

Fig 7.28 Comparison between experimental and predicted deformation behaviour of one-dimensionally consolidated specimens-compression (OCR=4)

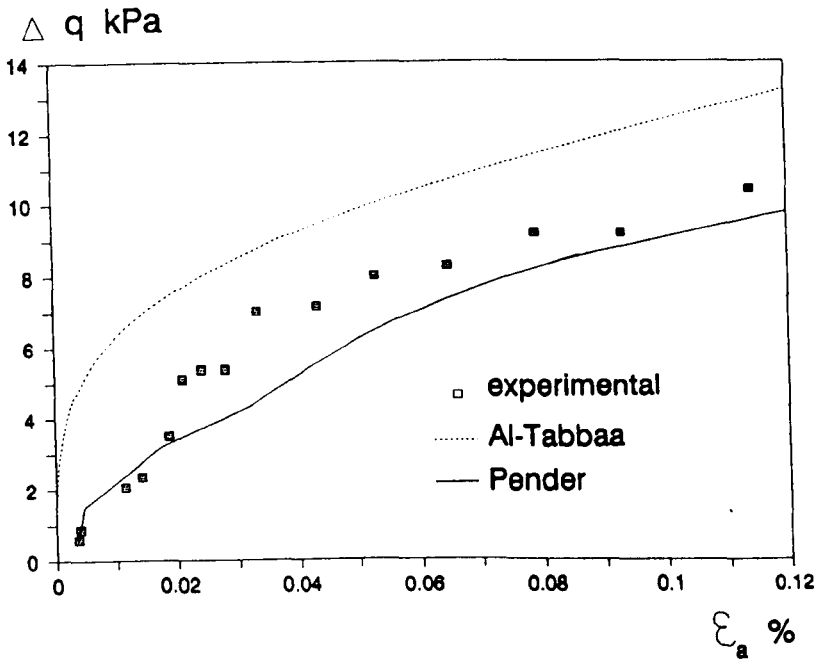

(a) stress-strain

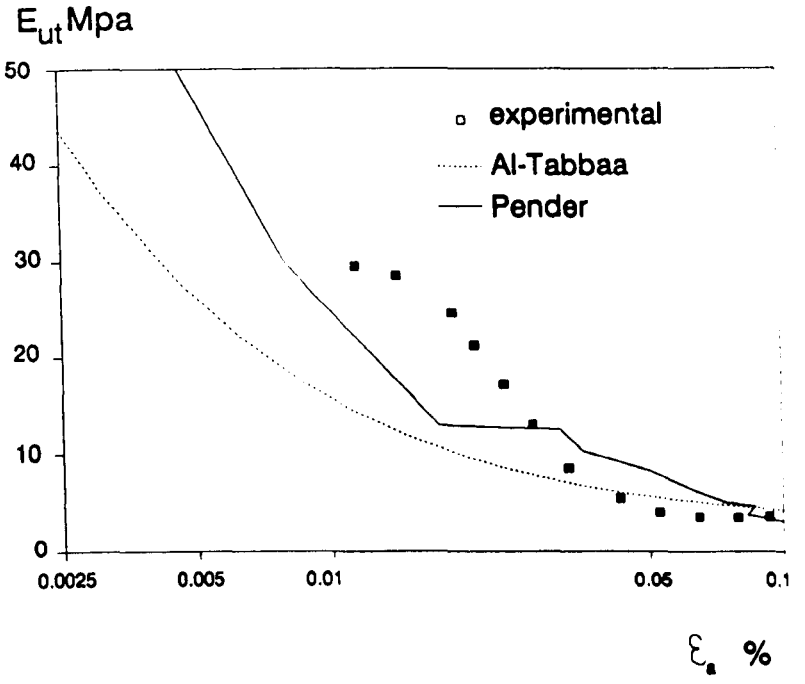

(b) stiffness-strain

Fig 7.29 Comparison between experimental and predicted deformation behaviour of one-dimensionally consolidated specimens-extension (OCR=4)

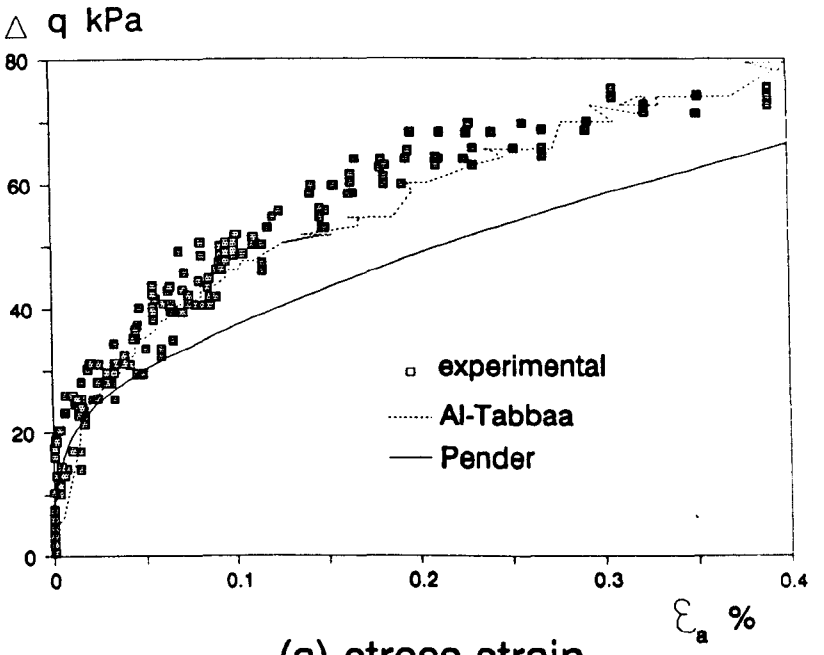

(a) stress-strain

Note : experimental points taken from more than one test

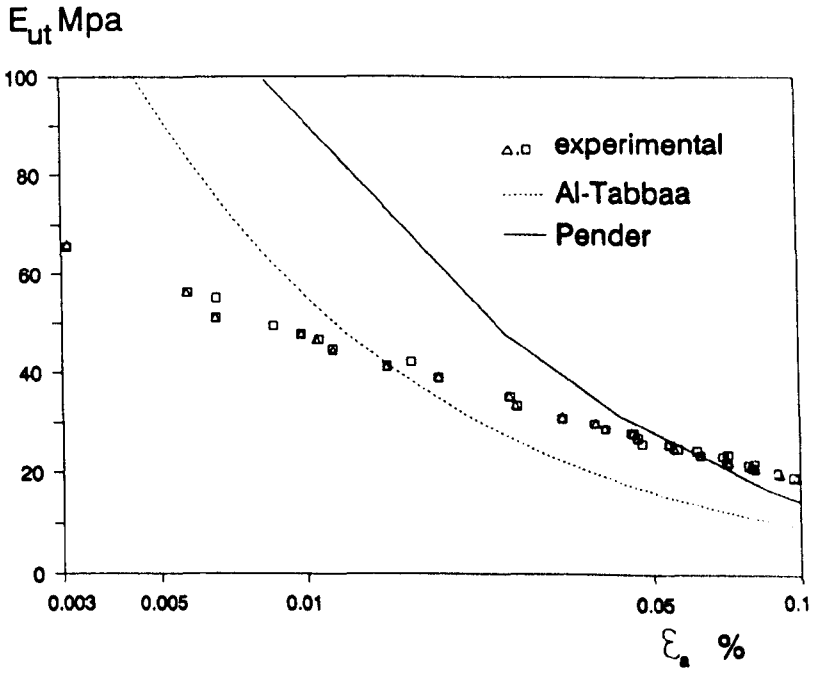

(b) stiffness-strain

Fig 7.30 Comparison between experimental and predicted deformation behaviour of isotropically consolidated specimens-compression (OCR=1)

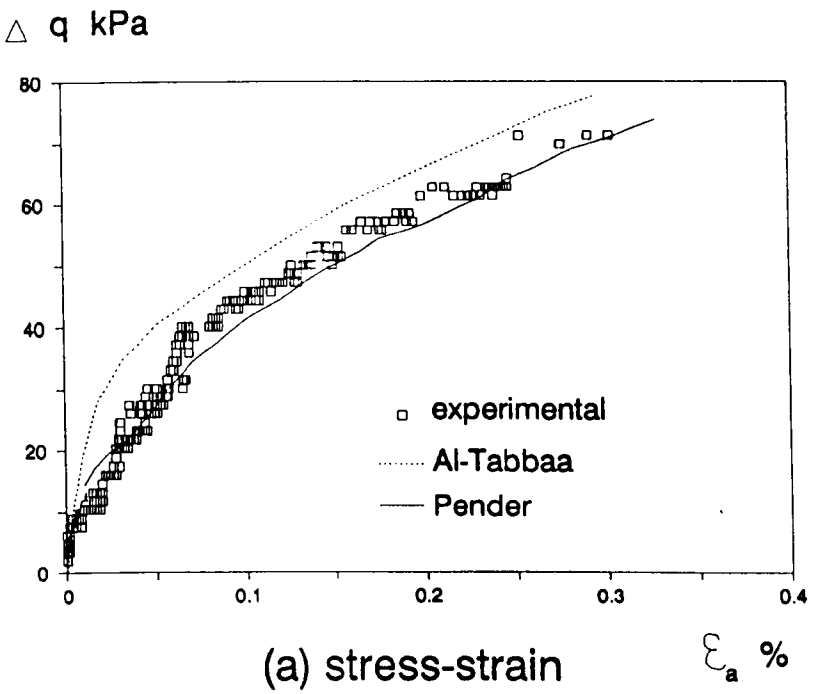

Note : experimental points taken from more than one test

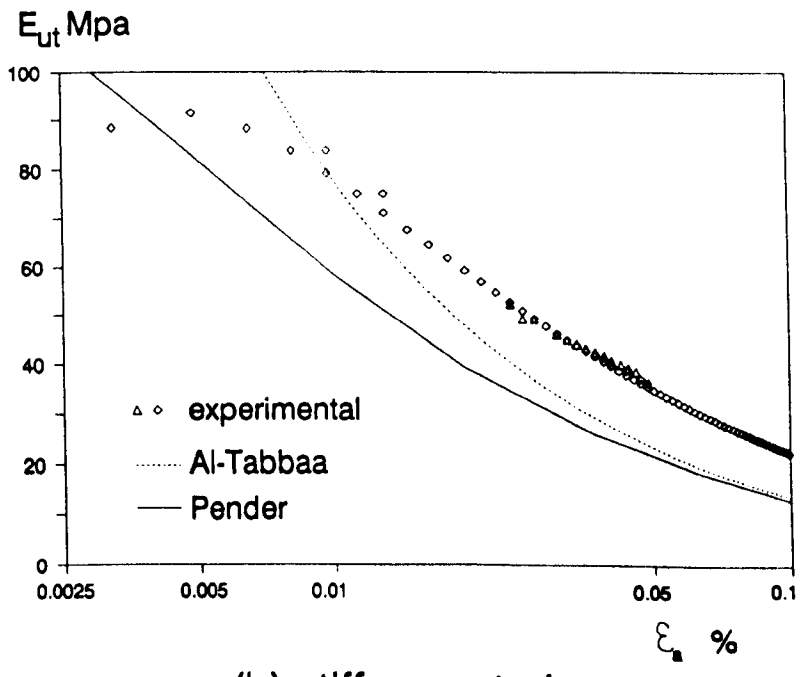

Fig 7.31 Comparison between experimental and predicted deformation behaviour of isotropically consolidated specimens-compression (OCR=2)

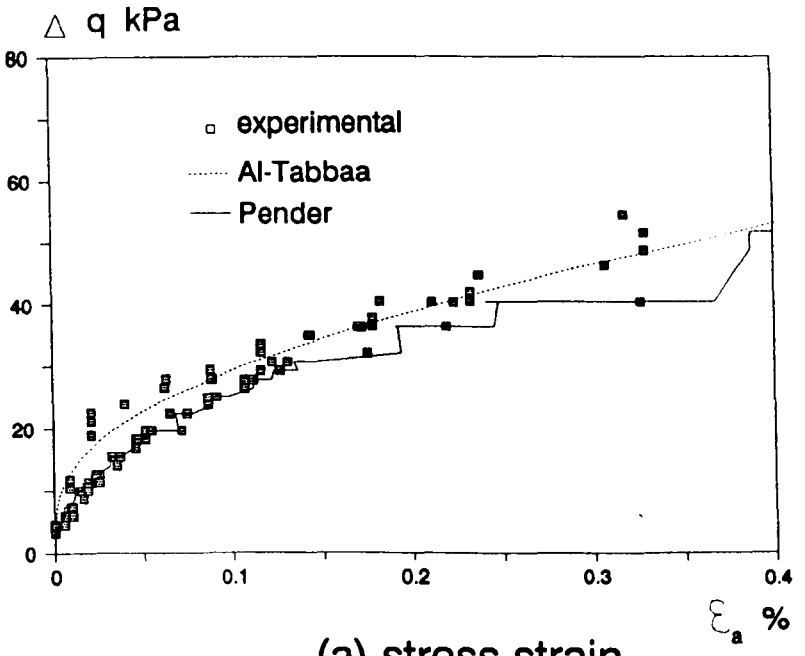

(a) stress-strain

Note : experimental points taken from more than one test

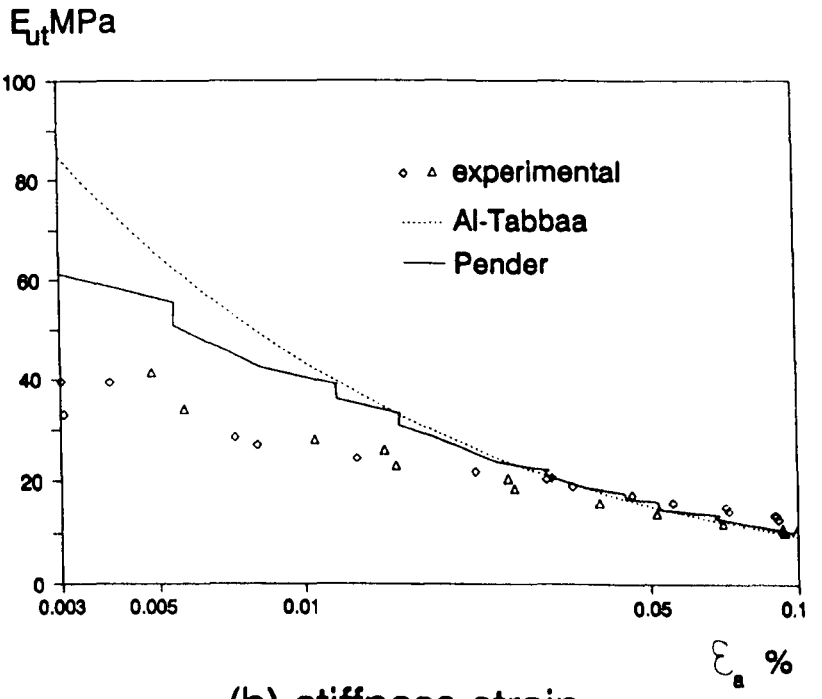

(b) stiffness-strain

Fig 7.32 Comparison between experimental and predicted deformation behaviour of isotropically consolidated specimens-compression (OCR=4)

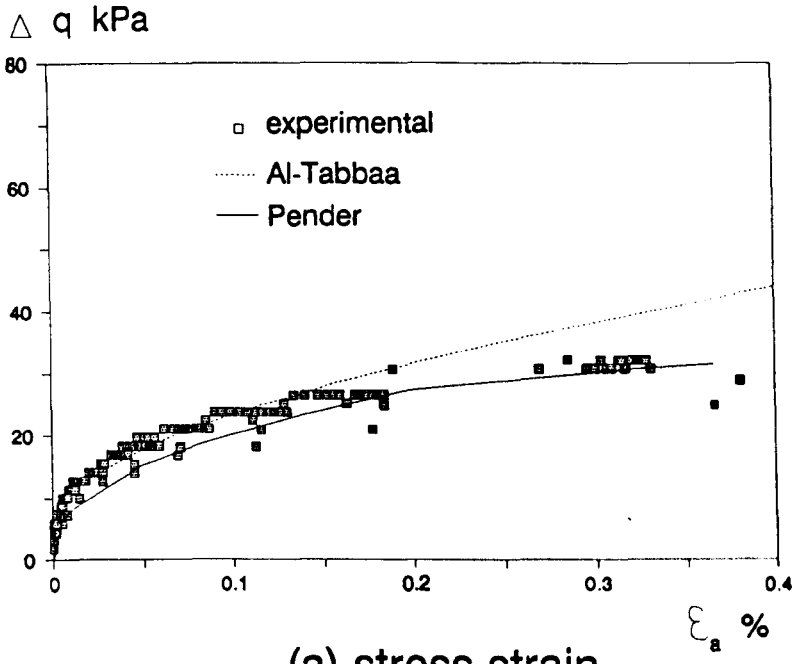

(a) stress-strain

Note : experimental points taken from more than one test

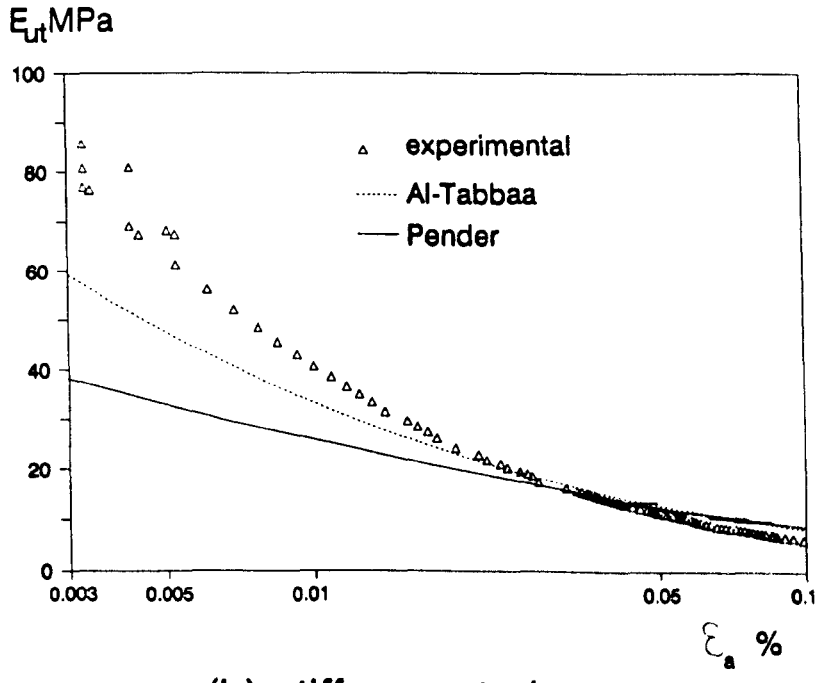

(b) stiffness-strain

Fig 7.33 Comparison between experimental and predicted deformation behaviour of isotropically consolidated specimens-compression (OCR=8)

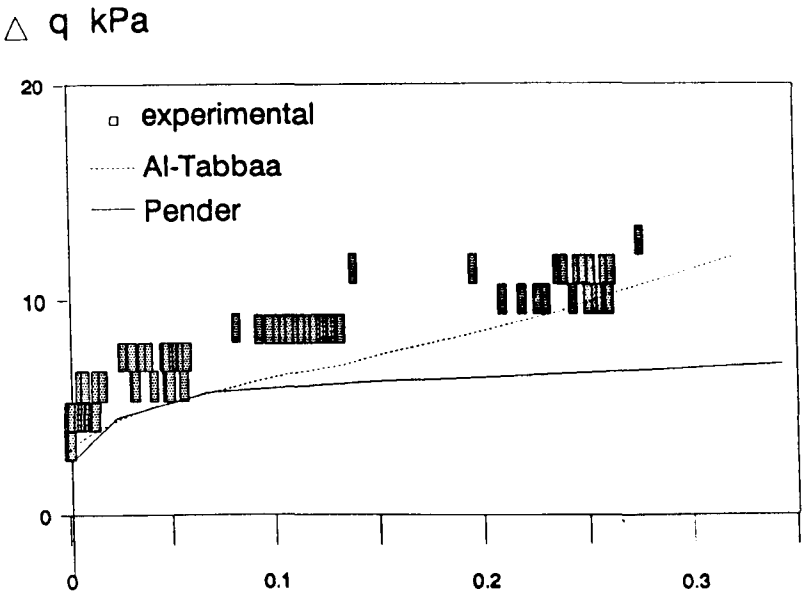

Note : experimental points taken from more than one test

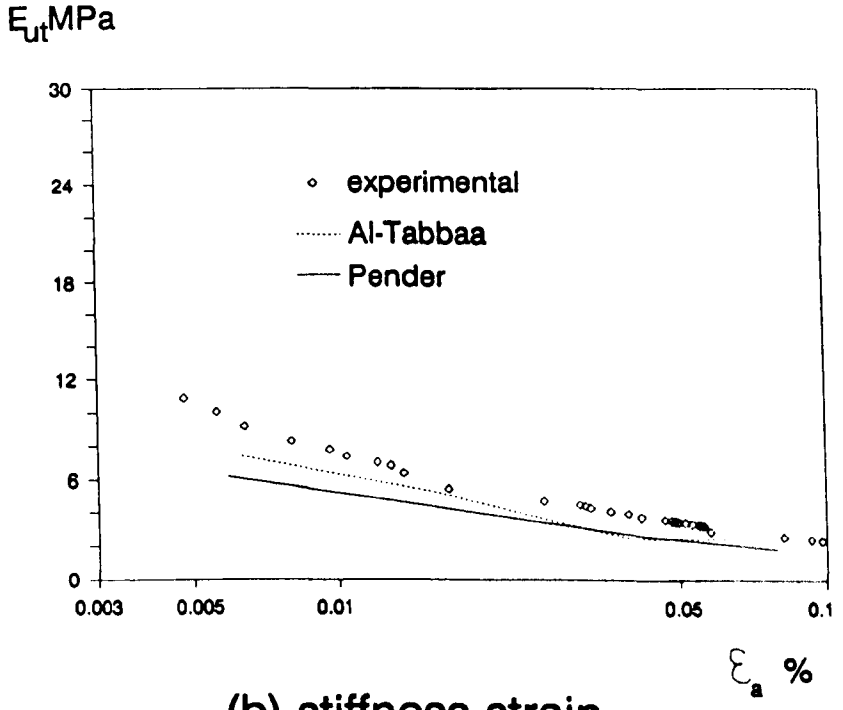

Fig 7.34 Comparison between experimental and predicted deformation behaviour of isotropically consolidated specimens-compression (OCR=45)

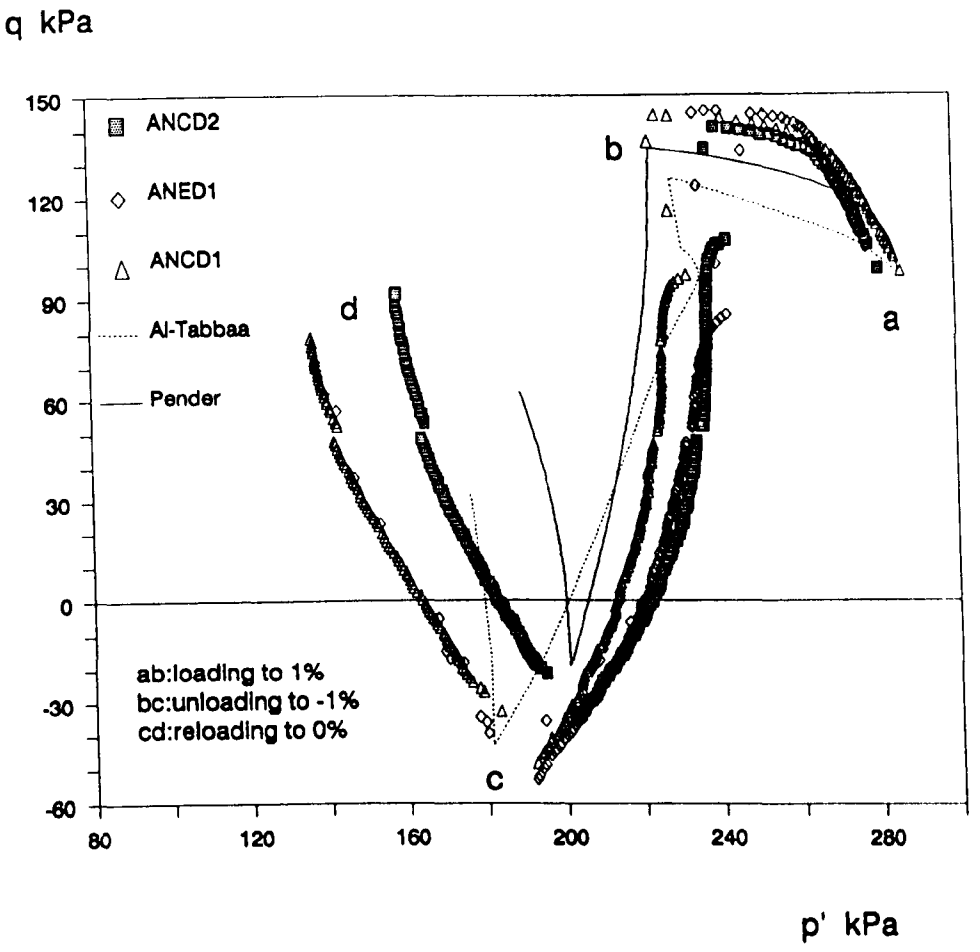

Fig 7.35 Comparison between predicted and experimental stress paths for normally consolidated specimens during strain cycles

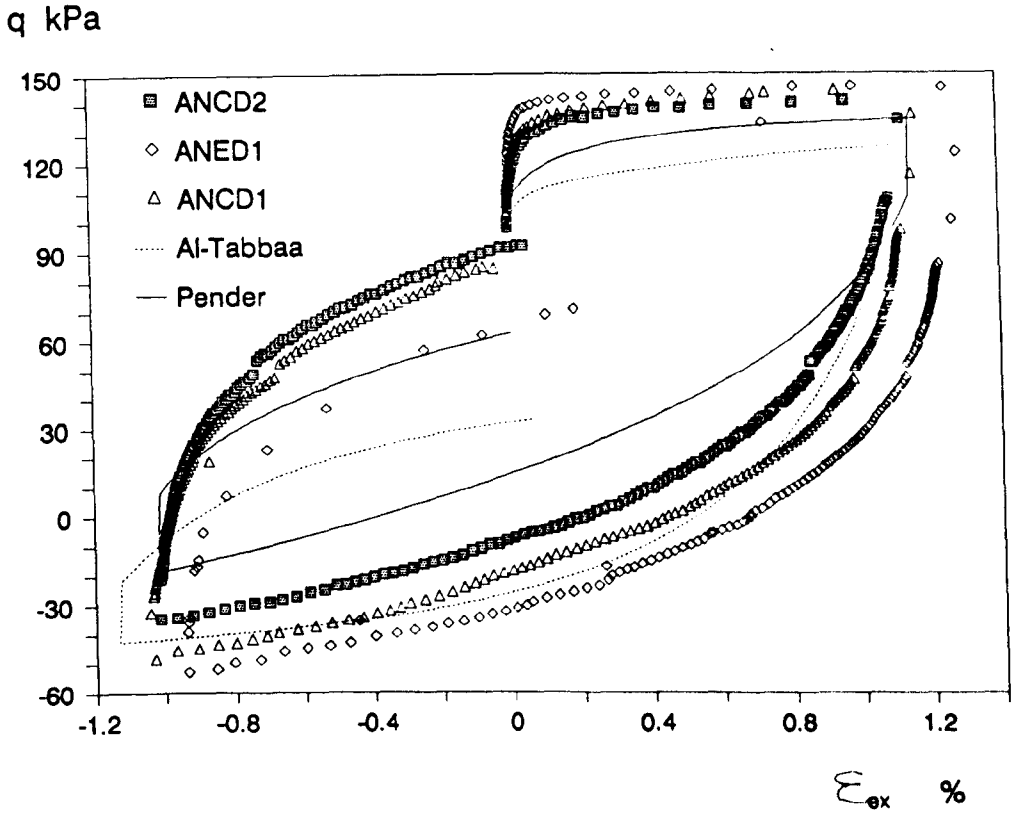

Fig 7.36 Comparison between experimental and predicted stress-strain cycles for normally consolidated specimens

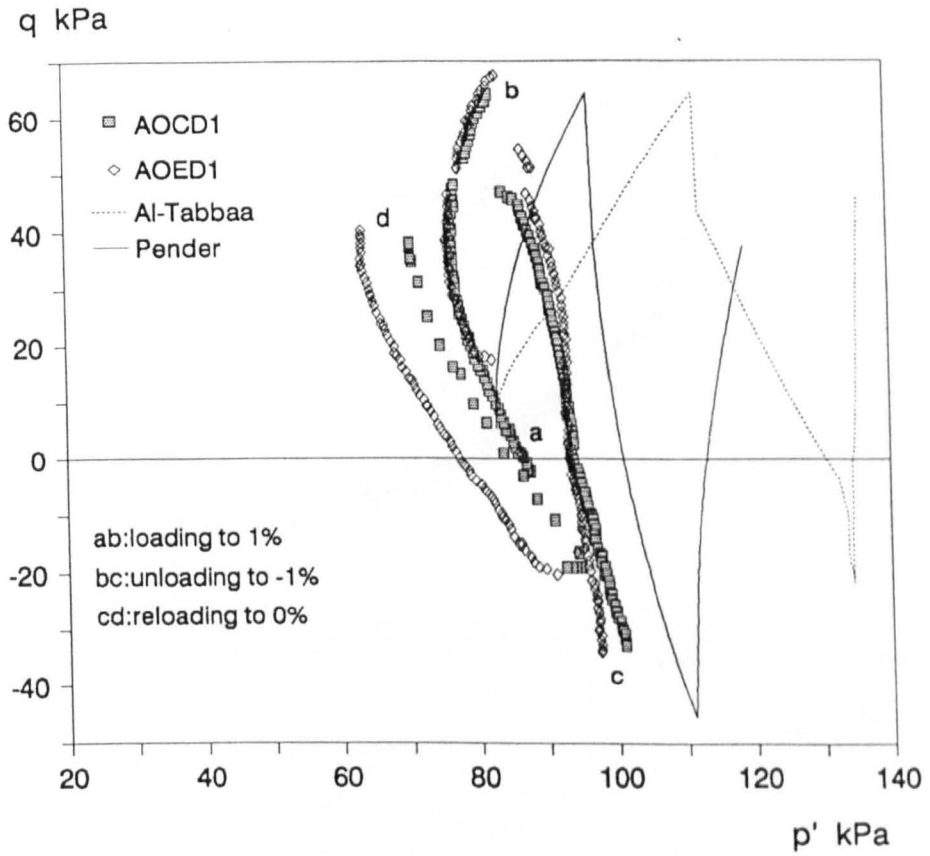

Fig 7.37 Comparison between predicted and experimental stress paths for overconsolidated specimens during strain cycles

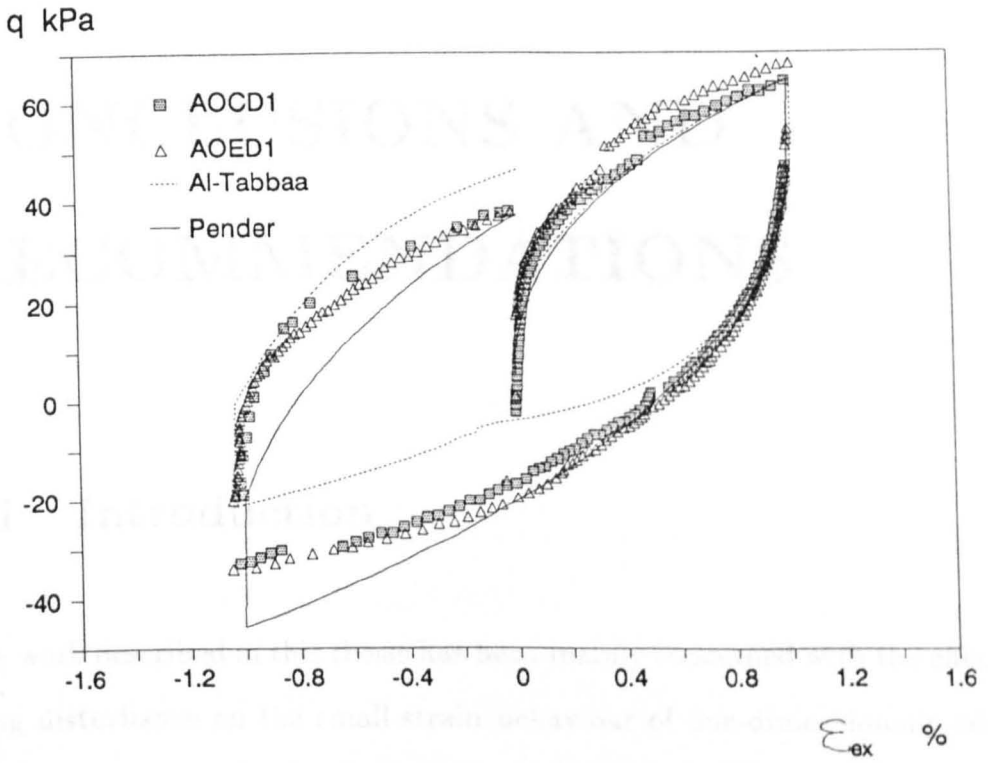

Fig 7.38 Comparison between experimental and predicted stress-strain cycles for overconsolidated specimens

Chapter 8

CONCLUSIONS AND RECOMMENDATIONS

8.1 Introduction

The work described in this thesis has been mainly concerned with the effects of sampling disturbance on the small strain behaviour of one-dimensionally consolidated kaolin. The disturbance due to tube sampling was simulated in the triaxial cell after being computed using the method put forward by Baligh (1985). The effects of two other parameters, the rate of loading and the OCR, were also examined using isotropically consolidated kaolin specimens.

Tests concerned with the effects of sampling disturbance were conducted in a specially designed and manufactured 100 mm triaxial apparatus of the Bishop and Wesley (1975) type. This equipment superseded an earlier version, used in previous studies of the small strain behaviour of clays (Yung (1987)). The rest of the tests

were carried out in an existing 38 mm Bishop and Wesley triaxial apparatus after some modification. All the tests were performed under computer control.

In this short chapter the main findings of the work are summarised and suggestions for future work are presented.

8.2 Conclusions Relating to Experimental Techniques

8.2.1 The 100 mm Apparatus

Significant improvements in data quality were achieved by comparison with the previous work of Yung (1987). This can be attributed to changes made to the bellofram area ratio of the cell, the use of a rigid top cap-load cell connection and improved instrumentation arrangements.

The proximity transducers, used for local strain measurement have better precision than the ones used by Yung. Furthermore, they are placed on adjustable mountings, which not only allow the transducers to be kept in range throughout the test but also make it possible to bring the specimens to failure without imposing any restraint and without causing any damage to the instrumentation. The collapsible targets for radial strain used by Yung are no longer necessary.

The local radial strain can now be measured along two perpendicular diameters rather than a single diameter. Thus Poisson's ratio can be evaluated more confidently.

A comparison of the results of the three methods of axial strain measurement employed in the 100 mm cell revealed that strains evaluated locally and between the end caps were in good agreement, indicating that the bedding errors at the end caps were negligible. This was possible in the present work because the specimens were initially homogeneous, with relatively flat surfaces, and were subjected to a high consolidation pressure prior to shearing. The external strain measurement suffered from larger random and systematic errors. However, in compression tests, better agreement between external and local strains was obtained after correcting the external strain for system compliance. The tests indicated that under favourable conditions, strains could be measured externally with sufficient accuracy, but this would require more accurate transducers than presently used.

8.2.2 The 38 mm Apparatus

The axial strain measurement in this cell was improved by introducing end cap strain measurement similar to that adopted in the 100 mm cell. However, the data obtained at small strains were of lower quality than those from the larger cell since the transducers used displayed larger random errors during calibration. More accurate transducers would significantly improve the quality of the measured strains.

8.2.3 Computer Programs

The provision of computer control has proved to be virtually essential for the kind of testing described in this thesis. The computer programs developed provided greater flexibilty of control than those used by Yung (1987). They allowed considerable and speedy interaction with the operator through the system of menus and the visual dis-

play of numeric and graphical output during the test. The desired stress paths were followed with sufficient accuracy, but further improvements in performance could be achieved by controlling more closely the stresses applied during one-dimensional consolidation and swelling. This would eliminate the unwanted oscillations in the stress paths from these stages.

8.2.4 Data Processing

In the present work advantage was taken of advances made in computerised data processing via commercially available software. Using the Lotus 123 spreadsheet package, macro programs were developed for polynomial curve fitting and regression analysis. This permitted an automated method of evaluating tangent stiffnesses from the stress-strain data to be developed, so that the evaluation became considerably faster and more accurate. Thus, it seems likely that data processing of this kind via computer spreadsheets will become standard practice. However, it should be noted that, the sensitivity of the interpretation to the curve fitting technique needs to be checked.

An analysis of errors present in data from the 100 mm cell showed that the percentage error in stiffness decreases rapidly with strain level but can be larger than 50 % at strains lower than 0.01 %. These errors were found to stem mainly from uncertainties in the axial strain measurement, with a lesser contribution from the errors in the deviator stress. A similar analysis revealed that at such small strains the percentage error in Poisson's ratio can be as high as 100 %. Once again, this error decreases rapidly with increasing strain. At the 0.1 % strain level the errors in stiffness and Poisson's ratio are 7% and 10% respectively.

8.3 Conclusions Relating to Test Results

8.3.1 Value of K_0 during Consolidation and Swelling

One-dimensional consolidation test results gave an average K_0 value of 0.7 which compares well with other reported experimental values for kaolin. Semi-empirical relationships proposed in the literature were found to underestimate K_0. One-dimensional swelling test results indicated that K_{0u} varies non-linearily with either OCR or ln (OCR). Comparison with proposed relationships for evaluating K_{0u} produced reasonable agreement at low OCRs (i.e. < 2); discrepancies between the experimental and proposed relationships increased at larger OCRs.

8.3.2 Critical State Parameters

The critical state parameters evaluated from the current tests are in good agreement with those reported by other researchers. Where specimens approached failure they were found to be in states close to the estimated critical state line.

8.3.3 Sampling Disturbance

The sampling disturbance was achieved by subjecting the triaxial specimens to a quick strain cycle of amplitude 1 % under undrained conditions. Normally consolidated specimens were seen to undergo a significant drop (40 to 60 %) in the mean effective pressure while overconsolidated specimens (OCR=4) exhibited much smaller reductions (< 10 %). By inspection of the stress paths in q, p' space, both normally consolidated and overconsolidated specimens appeared to approach failure

during the strain cycle. However, while the former exhibited complete flattening of the stress-strain curve at strains approaching 1 %, the latter showed persistent strain hardening. Upon re-consolidation, the average drop in the water contents of the normally consolidated specimens (1.5 %) was significantly higher than that of the overconsolidated specimens (0.12 %).

Generally, after re-consolidation to the initial stress conditions, the disturbed specimens exhibited small strain stiffnesses similar to those of the corresponding undisturbed specimens. The disturbed specimens loaded in extension showed slightly larger small strain stiffnesses than the undisturbed ones, but it is difficult to assess whether this is genuine or due to inadequate repeatability of test technique. In agreement with the results published by Baligh et al (1987), the disturbed specimens exhibited larger stiffnesses than undisturbed specimens at intermediate and large strains.

8.3.4 Rate of Shearing and Stress History Effects

Tests concerned with the effects of rate of shearing indicated that the small strain stiffness increased linearily with the logarithm of loading rate at a given strain level. The experimental relationship between stiffness and loading rate at large strain levels was found to be in agreement with those reported by other researchers. The effects of loading rate were found to be most significant in the case of normally consolidated specimens.

Tests carried out on specimens with different overconsolidation ratios supported the linear relationship between normalised stiffness at a given strain level and ln (OCR) for isotropically consolidated specimens suggested by Wroth et al

(1979). It must be appreciated that for anisotropically consolidated specimens the relationship has been reported to be non-linear.

Reasonably good agreement was found between normalised small strain stiffnesses of isotropically and one-dimensionally normally consolidated specimens. A less satisfactory agreement was noticed in the case of overconsolidated specimens. In both cases, however, the one-dimensionally consolidated specimens exhibited larger degrees of non-linearity.

8.3.5 Model Predictions

The three theoretical models, all based on critical state soil mechanics, were found to predict the general patterns of stress paths followed in the tests adequately. In the case of stress-strain curves and stiffnesses at small strains, discrepancies between predicted and experimental behaviour patterns were encountered; these were more serious for extension loading.

The general pattern of behaviour of specimens subjected to sampling disturbance (cyclic loading), in terms of both stress paths and stress-strain curves, was well captured by the models, although larger discrepancies started to appear as the strain cycle entered its final phase. Smaller predicted areas of the stress-strain loops are thought to result from the fact that the models do not account for rate of shearing effects.

8.4 Recommendations for Future Research

The described work concerned with sampling disturbance effects in clays was carried out using the latest developments in triaxial testing and computer control techniques. However, all the tests were carried out on kaolin and only a limited number of tests could be conducted in the available time. It is suggested, therefore, that a more comprehensive series of tests be carried out, not only on kaolin, but also on natural clays which also take into account the effects of ageing discussed lately by Burland (1990). This would establish the generality or otherwise of the behaviour patterns observed for kaolin.

The sampling disturbance effects were studied for only one case where the amplitude of the strain cycle was equal to 1 %. Consequently, a fuller understanding of the effect of tube sampling could be achieved by examining the behaviour of soil specimens subjected to different strain cycles corresponding to different sampler geometries. Progress might also be made through the use of theoretical models. The work described in this thesis indicates that the models predict reasonably well the general patterns of behaviour during the strain cycle.

The strain cycle simulates the minimum mechanical disturbance to a tube sample and does not reflect other disturbances due to friction along the wall of the sampler, storage or mishandling. Therefore, an experimental study which took into account such effects would provide a more representative simulation of sampling disturbance.

Tests carried out to examine the effects of OCR on small strain stiffness were mainly limited to isotropically consolidated specimens in the 38 mm cell which provides data of lower quality than the 100 mm cell. It is suggested that more

tests be performed in the 100 mm cell to quantify the relationship between normalised stiffness and OCR. It is recommended that tests involving different preconsolidation pressures and both isotropically and one-dimensionally consolidated specimens should be carried out.

To quantify the effects of ageing on the small strain behaviour of clays, tests similar to those described are required on specimens with different rest periods prior to shearing. The results of such a study could have an important bearing on triaxial testing practice.

Appendix A

Steel Ring Response to Changes in Cell Pressure

Proximity transducers are mounted on the stainless steel ring as shown in Figure 3.15. The thickness of this ring had to be large enough so that upon any change in the cell pressure, the resulting strains in it are insignificant compared to those measured on the soil specimens. The two perspex parts of the cell have an inside diameter of 330 mm. The change in tangential stress over a cross section is given by :

$$\Delta\sigma_t = \frac{\Delta\sigma_3 \times r}{t_r} \tag{A.1}$$

where $\Delta\sigma_3$, r, and t_r are the change in cell pressure, the inside radius of the steel ring ($= 0.145m$) and the thickness of the ring respectively. The change in tangential strain of the steel ring due to the change in cell pressure may be written as

$$\Delta\epsilon_t = \frac{\Delta\sigma_3 \times r}{E \times t_s} \tag{A.2}$$

where E is the Young's modulus of the stainless steel ($= 2.1 \times 10^8$) kPa. Since radial and tangential strains are equal, the change in the inside radius of the steel ring is :

$$\Delta r = \Delta \epsilon_t \times r \tag{A.3}$$

For a 100 mm specimen, the additional strain due to the change in the steel ring diameter is given by

$$\Delta \epsilon_r = \frac{\Delta r}{100} \times 100 \tag{A.4}$$

For a cell pressure change of 800 kPa, the change in specimen radial strain due to stresses on a steel ring with $t_r = 40$ mm is about $2 \times 10^{-4}\%$. This is very small compared to other errors such those resulting from the inaccuracy of the proximity transducers.

LIST Of REFERENCES

Airey, (1984). 'Clays in Circular Simple Shear Apparatus'. Ph.D. thesis, Cambridge University.

Alonso, E.E.; Onate, E. and Casanova, J.S. (1981). 'Investigation into Sampling Disturbance'. Proceedings of the International Society of Soil Mechanics and Foundation Engineering, Stockholm, Vol 2, pp 419-422.

Al-Tabbaa, A. (1987). 'Permeability and Stress-strain Response of Speswhite Kaolin'. Ph.D. thesis, Cambridge University.

Alva-Hurtato, J.E., and Selig, E.T. (1981). 'Survey of Laboratory Devices for Measuring Soil Volume Change'. Geotechnical Testing Journal, Vol. 4, pp 11-18.

Anderson, W.F., and Mickenly, D.G. (1975). 'Tests to Find the Modulus of Deformation of Till'. Proceedings of the Symposium on the Engineering Behaviour of Glacial Materials. Birmingham, pp 165-179.

Arthur, J.R., and Phillips, A.B. (1975). 'Homogeneous and Layered Sand in Triaxial Compression'. Geotechnique, Vol 25, pp 799-1815.

Atkinson, J.H. (1973). 'The Deformation of Undisturbed London Clay'. Ph.D. thesis, University of London.

Atkinson, J.H. (1981). 'Foundations and Slopes'. McGraw-Hill, London.

Atkinson, J.H. (1984). 'Some Procedures for Normalising Soil Test Results'. Geotechnical Research Centre, Report GE/84/3, The City University.

Atkinson, J.H. (1984). 'Rates of Loading in Drained and Undrained Stress Path and Triaxial Tests'. Geotechnical Engineering Research Centre, Report GE/84/3, The City University.

Atkinson, J.H., and Evans, J.S. (1985). Discussion : 'The Measurement of Soil Stiffness in The Triaxial Apparatus'. Geotechnique, Vol 35, pp 378-382.

Atkinson, J.H., Evans, J.S., and Scott, C.R. (1985). 'Development in Microcomputer Controlled Stress Path Testing Equipment for Measurement of Soil Paramaters'. Ground Engineering, Vol 18, pp 15-22.

Atkinson, J.H., and Kubba, L.M. (1981). 'Some Effects of Sampling Disturbance on Soft Clays'. Proceedings of the International Society of Soil Mechanics and Foundation Engineering, Stockholm, Vol 2, pp 423-426.

Atkinson, J.H., and Little, J.A. (1988). 'Undrained Triaxial Strength and Stress-Strain Characteristics of a Glacial Till Soil'. Canadian Geotechnical Journal, Vol. 25, pp 428-439.

Atkinson, J.H., Richardson, D. and Stallebrass, S.E. (1989). 'Effects of Recent Stress History on the Stiffness of soil'. The City University, Report No. GE/89/16.

Atkinson, J.H., Richardson, D., and Robinson, P.J. (1986). 'Compression and Extension of K_0 Normally Consolidated Clay'. The City University, Report No. GE/86/5.

Atkinson, J.H., Richardson, D., and Woods, R.I. (1986). 'Technical Note on the Determination of Tangent Stiffness Parameters from Soil Test Data'. Computer and Geotechnics, Vol 2, pp 131-140.

Balasubramanian, A.S. (1969). 'Some Factors Influencing the Stress-strain Behaviour of Clays'. Ph.D. thesis, Cambridge University.

Balasubramanian, A.S. (1976). 'Local Strains and Displacement Patterns in the Triaxial Specimens of a Saturated Clay'. Soils and Foundations, Vol 16, pp 101-114.

Baldi, G., Hight, D.W., and Thomas, G.E. (1988). 'A Reevaluation of Conventional Triaxial Test Methods'. Advanced Triaxial Testing of Soil and Rock, ASTM, STP 977, Robert T. Donaghe, Ronald C. Chaney, and Marshall L. Silver, Eds, American Society for Testing and Materials, Philadelphia, pp 219-263.

Baligh, M.M. (1985). 'Strain Path Method'. Journal of Geotechnical Engineering, ASCE, Vol 111, pp 1108-1136.

Baligh, M.M., Azzouz, A.M., and Chung-Tien Chin, S.M. (1987). 'Disturbances Due to Ideal Tube Sampling'. Journal of Geotechnical Engineering, ASCE, Vol 113, pp 739-757.

Berre, T. (1986). 'Suggested International Procedure for Triaxial Compression Tests'. Norwegian Geotechnical Institute, Internal Report 56103-30.

Bishop, A.W., and Henkel, D.J. (1962). 'The Measurement of Soil Properties in the Triaxial Cell'. E. Arnold, London.

Bjerrum, L. (1973). 'Problems of Soil Mechanics and Construction on Soft Clays'. State-of-the-Art Report, Session 4, Proceedings of the 8th International

Conference on Soil Mechanics and Foundation Engineering, Moscow, Vol 3, pp 109-159.

Bishop, A.W., and Wesley, L.D. (1975). 'A Hydraulic Triaxial Apparatus for Controlled Stress Path Testing'. Geotechnique, Vol 25, pp 657-670.

British Standards Institution (1957). 'Determination of Hardness'. BS903, Part A7.

British Standards Institution (1968). 'Specifications for Metric Gauge Blocks- Part 1 : Gauge Blocks' BS4311.

British Standards Institution (1981). 'Code of Practice for Site Investigation'. BS 5930.

Broms, B.B. (1980). 'Soil Sampling in Europe : State-of-the-Art'. Journal of Geotchnical Engineering, ASCE, Vol 106, pp 65-98.

Brooker, E.W., and Ireland, H.O. (1965). 'Earth Pressures at Rest Related to Stress History'. Canadian Geotechnical Journal, Vol. 12, pp 1-15.

Brown, P.T., and Chow, J,C-P. (1988) 'Prevention of Sample Deterioration'. Geotechnical Testing Journal, GTJODJ, Vol. 11, pp 296-300.

Brown, S.F., Austin, G., and Overy, R.F. (1980). 'An Instrumented Triaxial Cell for Cyclic Loading of Clays'. Geotechnical Testing Journal, Vol 3, pp 145-152.

Brown, S.F., and Snaith, M.S. (1974). 'The Measurement of Recoverable and Irrecoverable Deformations in the Repeated Load Triaxial Test'. Geotechnique, Vol 24, pp 255-259.

Burland, J.B. (1967). 'Deformation of Soft Clay'. Ph.D. thesis, Cambridge University

Burland, J.B. (1990). 'Rankine Lecture: On the Compressibilty and Shear Strength of Natural Clays'. Geotechnique, Vol 40, pp 329-378.

Burland, J.B., Simpson, B., and St John, H.D. (1979). 'Movements around Excavations in London Clay'. Proceedings of the 7th European Conference of Soil Mecahnics and Foundation Engineering. Brighton, Vol 1.

Burland, J.B., and Symes, M.J. (1982). 'A Simple Axial Displacement Gauge for Use in the Triaxial Apparatus'. Geotechnique, Vol 32, pp 62-65.

Castro, G. (1969). 'Liquifaction of Sands'. Harvard Soil Mechanics Series, No. 81, Harvard University, Cambridge, MA.

Clarke, B.G. and Wroth, C.P. (1985). 'Discussion on Fahey, M. and Randolph, M.F. ' Effect of disturbance on parameters derived from self boring pressuremeter tests in sand". Geotechnique, Vol 35, pp 219-222.

Clayton, C.R.I, Simons, N.E. and Matthews, M.C. (1982) 'Site Investigation'. London, Granada.

Clayton, C.R., and Khatrush, S.A. (1986). 'A New Device for Measuring Local Axial Strains on Triaxial Specimens'. Geotechnique, Vol 36, pp 595-597.

Cooling, L.F. (1949). Discussion : 'Site Investigation Including Boring and Other Methods of Sub-surface Exploration'. Jounal of the Institution of Civil Engineers, Vol 32, pp 141-142.

Costa Filho, L.M. (1980). 'A Laboratory Investigation of the Small Strain Behaviour of London Clay'. Ph.D. thesis, University of London.

Costa Filho, L.M. (1985). 'Measurement of Axial Strains in Triaxial Tests on London Clay'. ASTM, Geotechnical Testing Journal, GTJODJ, Vol 8, pp 3-13.

Dafalias, Y.F. (1987). 'An Anisotropic Critical State Clay Plasticity Model'. Proceedings of the 2nd International Conference on Constitutive Laws for Engineering Materials, Arizona, Vol 1, pp 513-522.

Daramola, O. (1978). 'The Influence of Stress History on the Deformation of Sand'. Ph.D. thesis, University of London.

El-Ruwayih, A.A. (1975). 'Stress-Strain Characteristics of Rockfill and of Clays under High Pore Water Pressure Tension'. Ph.D. thesis, University of London.

Fahey, M. and Randolph, M.F. (1985). 'Effect of Disturbance on Parameters Derived from Self-Boring Pressuremeter Tests in Sand'. Geotechnique, Vol 34, pp 81-97.

Freeser,B. (1984). 'Optographic Trace Recording: A New Method of Strain Measurement in Geotechnical Testing'. Geotechnique, Vol 34, pp 277-281.

Gens, A. (1983). 'Stress-strain and Strength Characteristics of Low Plasticity Clay'. Ph.D. thesis, University of London.

Georgiannou, V.N., Burland, J.B. and Hight, D.W. (1990). 'The Undrained Behaviour of Clayey Sands in Triaxial Compression and Extension'. Geotechnique, Vol 40, pp 431-450.

Germaine, J.T., and Ladd, C.C. (1988). 'Triaxial Testing of Saturated Cohesive Soils'. Advanced Triaxial Testing of Soil and Rock, ASTM, STP 977, Robert T. Donaghe, Ronald C. Chaney, and Marshall L. Silver, Eds, American Society for Testing and Materials, Philadelphia, pp 421-495.

Goodwin, A. (1991). 'The Behaviour of Unsaturated Soils at Low Stress Levels'. Ph.D. thesis - in preparation, University of Sheffield.

Graham, J., Crooks, J.H.A., and Bell, A.L. (1983). 'Time Effects on the Stress-Strain Behaviour of Natural Soft Clays'. Geotechnique, Vol. 33, pp 327-340.

Graham, J., and Lau, S.L-K. (1988). 'Influence of Stress-Release Disturbance, Storage, and Reconsolidation Procedures on the Shear Behaviour of Reconstituted Underwater Clay'. Geotechnique, Vol. 34, pp 279-300.

Hanzawa, H. (1977). 'Geotechnical Properties of Normally Consolidated Clay'. Iraqi Soils and Foundations, Vol 17, pp 1-15.

Hight, D.W. (1982). 'A Simple Piezometer Probe for the Routine Measurement of Pore Pressure in Triaxial Tests on Saturated Soils'. Geotechnique, Vol 32, pp 396-401.

Hight, D.W. (1983). 'Laboratory Investigation of Sea Bed Clays'. Ph.D. thesis, University of London.

Hight, D.W., Gens, A., and Jardine, R.J. (1985). 'Evaluation of Geotechnical Parameters from Triaxial Tests on Offshore Clay'. Proceedings of the International Conference on Offshore Site Investigation, Society for the Underwater Technology, pp 253-268.

Hird, C.C., and Yung, P. (1987). Discussion : 'A New Device for Measuring Local Axial Strain on Triaxial Specimens'. Geotechnique, Vol 34, pp 593-597.

Hird, C.C., and Yung, P. (1989). 'Use of Proximity Transducers for Local Strain Measurements in Triaxial Tests'. ASTM, Geotechnical Testing Journal, Vol 12, pp292-296.

Holden, J.C. (1971). 'Performance of a Device for Sealing Sample Tubes'. 4th Asian Conference, International Socity of Soil Mechanics and Foundation Engineering, Proceedings of the Specialty Session on Quality in Soil Sampling, Bangkok, pp 58-61.

Hvorslev, M.J. (1949). 'Subsurface Exploration and Sampling of Soils for Civil Engineering Purposes'. Waterwaus Experimental Station, Mississippi River Commission, U.S. Army Corps of Engineers.

Ilyas, T. (1983). 'Development and Application of Triaxial Stress Path Soils Testing' M.Eng thesis, University of Sheffield.

Jacky, J. (1948). 'Pressure in Silos'. Proceedings of the 2nd International Conference of Soil Mechanics and Foundation Engineering, London, Vol. 1.1, pp 103-107.

Jardine, R.J. (1985). 'Investigation of Pile-Soil Behaviour with Special Reference to the Foundations of Offshore Structures'. Ph.D. thesis, University of London.

Jardine, R.J., Fourie, A., Maswoswe, J., and Burland, J.B. (1985). 'Field and Laboratory Measurements of Soil Stiffness'. Proceedings of the 11th International Conference on Soil Mechanics and Foundation Engineering., San Francisco, Vol 2, pp 511-514.

Jardine, R.J., Potts, D.M., Fourie, A.B., and Burland, J.B. (1986). 'Studies of the Influence of Non-linear Stress-strain Characteristics in Soil-Structure Interaction'. Geotechnique, Vol 36, pp 377-396.

Jardine, R.J., Symes, M.J., and Burland, J.B. (1984). The measurement of Soil Stiffness in the Triaxial Apparatus'. Geotechnique, Vol 34, pp 323-340.

Jerbo, A., Nirder, B., and Sandegren, E. (1961). 'Some Interesting Geotechnical Observations on Clays from Kramfros'. Jarnvagstekinik, Vol 29, pp 89-90.

Kaye, G.W.C., and Laby, T.H. (1973). 'Tables of Physical and Chemical Constants'. Longman Book Co., London.

Kallstenius, T. (1963). 'Studies on Clay Samples Taken with Standard Piston Sampler'. Proceedings of the Swedish Geotechnical Institute, Vol 21.

Khan, M.H., and Hoag,D.H. (1979). 'A Non-contacting Transducer for Measurement of Lateral Strains'. Canadian Geotechnical Journal, Vol 16, pp 409-411.

Kirkpatrick, W.M., and Belshaw, D.J. (1976). 'On the Interpretation of the Triaxial Test'. Geotechnique, Vol 18, pp 336-350.

Kirkpatrick, W.M., Khan, A.J., and Mirza, A.A. (1986). 'The Effects of Stress Relief on Some Overconsolidated Clays'. Geotechnique, Vol 36, pp 511-525.

Kirkpatrick, W.M., and Rennie, I.A. (1975). 'Stress Relief Effects in Deep Sampling Operations'. Underwater Construction Conference, University College, Cardiff.

Knoyle, D.S. (1979). 'The Influence of Pore Water Pressure Tension on the Undrained Shear Strength of Kaolin'. Cambridge University Engineering Tripos, Research Project Part 2.

Koutsoftas, D.C. (1980). 'Undrained Behaviour of a Marine Clay'. Laboratory Shear Strength of Soils. American Society fot Testing and Materials, Special Technical Report No 740.

Lacasse, S. (1985). 'Testing of Special Soils : Ocean Floor Soils'. Panel Discussion, Session 2B, 11th Conference of the International Society of Soil Mecahnics and Foundation Engineering, San Francisco, USA.

Lacasse, S., and Berre, T. (1988). 'Triaxial Testing Methods For Soils'. Advanced Triaxial Testing of Soil and Rock, ASTM, STP 977, Robert T. Donaghe, Ronald C. Chaney, and Marshall L. Silver, Eds, American Society for Testing and Materials, Philadelphia, pp 264-289.

Ladd, C.C., and Foott, R. (1974). 'New Design Procedure for Stability on Soft Clays'. Journal of the Geaotechnical Engineering Division, ASCE, Vol 100, pp 763-786.

Lambe, J.W. (1967). 'Stress Path Method'. Journal of Soil Mechanics and Foundation Engineering Division, ASCE, Vol 90, pp 43-67.

Lambe, J.W., and Whitman, R.V. (1979). 'Soil Mechanics'. John Wiley & Sons, New York.

Lewin, P.I. (1970). 'Stress Deformation Characteristics of a Saturated Soil'. MSc thesis, University of London.

Loudon, P.A. (1967). 'Some Deformation Characteristics of Kaolin'. Ph.D. thesis, Cambridge University.

Maguire, W.M. (1975). 'The Undrained Strength and Stress Strain Behaviour of Brecciated Upper Lias Clay'. Ph.D. thesis, University of London.

Manson, S.M. (1980). 'An Investigation of the Strength and Consolidation Properties of Speswhite Kaolin'. Cambridge University Engineering Tripos, Research Project Part 2.

Marsland, A. (1971a). 'Large In-situ Tests to Measure the Properties of Stiff Fissured Clays'. Proceedings of the 1st Australian N.E. Conference on Geomechanics, Melbourne, Vol 1, pp 180-189.

Marsland, A. (1973). 'Laboratory and In-situ Measurement of the Deformation Moduli of London Clay'. Building Research Establishement., Report CP 24/73.

Mayne, P.W., and Kulhawy, F.H. (1982). 'K_0-OCR Relationships in Soil'. Journal of Geotechnical Engineering, ASCE, Vol. 108, pp 851-872.

Meyerhof, G.G., and Murdock, L.J. (1953). 'An Investigation of the Bearing Capacity of Some Bored and Driven Piles in London Clay'. Geotechnique, Vol 3.

Moore, W.M. (1966). 'Effects of Variations in Poisson's Ratio on Soil Triaxial Testing'. Highway Research Record, No. 108, pp 19-30.

Nelson, J.D., Brand, E.W., Moh, Z.C., and Mason, I.D. (1971). 'The Use of Residual Stress to Define Sample Quality'. 4th Asian Conference, International Societey of Soil Mechanics and Foundation Engineering, Proccedings og the Specialty Session on Quality in Soil Sampling, Bangkok, pp 82-87.

Okumura, T. (1971). 'The Variation of Mechanical Properties of Clay Samples Depending on its Degree of Disturbance'. 4th Asian Conference, International Societey of Soil Mechanics and Foundation Engineering, Proccedings of the Specialty Session on Quality in Soil Sampling, Bangkok, pp 73-81.

Pang, L.S. (1987). 'The Effects of Rate of Strain on the Expansion of a Cylindrical Cavity in Clay'. Ph.D. thesis, University of Sheffield.

Parry, R.H.G. (1979). Discussion : 'Design Parameters in Geotechnical Engineering'. Proceedings of the 7th European Conference on Soil Mecahnics and Foundation Engineerng, Brighton, Vol 4, pp 129-131.

Parry, R.H.G., and Nadarajah, V. (1973). 'Observations of Laboratory Prepared Lightly Overconsolidated Specimens of Kaolin'. Geotechnique, Vol. 24, pp 345-358.

Parry, R.H.G., and Wroth, C.P. (1976). 'Pore Pressures in Soft Ground'. U.S. Army Engineer Waterways Experiment Station Dept, No. S-76-3, Vicksburg, Miss.

Pender, M.J. (1977). 'A Unified Model for Soil Behaviour'. Proceedings of the 9th International Conference on Soil Mechanics and Foundation Engineering, Tokoyo, Vol 2, pp 213-222.

Pender, M.J. (1978). 'A Model for the Behaviour of Overconsolidated Soil'. Geotechnique, Vol 28, pp 1-26.

Richardson, D. (1988). 'Investigation of Threshold Effects in Soil Deformations'. Ph.D. thesis, The City University.

Roscoe, K.H., and Burland, J.B. (1968). 'On the Generalised Stress-strain Behaviour of Wet Clay'. Engineering Plasticity, Ed. J. Heyman and F.A. Leckie, Cambridge University Press, pp 535-609.

Roscoe, K., Schofield, A.N., and Thurairajah, A. (1963). 'A Critical Appreciation of Test Data for Selecting a Yield Criterion for Soils'. Proceedings of the Symposium on Laboratory Shear Testing of Soils, STP 361, American Society of Testing and Materials, Philadelphia, pp 22-53.

Sarsby, R.W., Kaleziotis, N., and Haddad, E.H. (1980). 'Bedding Error in Triaxial Tests on Granular Material'. Geotchnique, Vol 30, pp 302-309.

Sayed,M. and Hamed,S. (1988). 'Pressuremeter Tests and Disturbance Effects'. Journal of Geotechnical Engineering, ASCE, Vol 88, pp 631-637.

Schjetne, K. (1971). 'The Measurement of Pore Pressure During Sampling'. 4th Asian Conference, International Society of Soil Mechanics and Foundation Engineering, Proceedings of the Specialty Session on Quality in Soil Sampling, Bangkok, pp 12-16.

Schmidt, B. (1966). Discussion on 'Earth Pressures at Rest Related to Stress History'. Canadian Geotechnical Journal, Vol. 3, pp 239-242.

Schofield, A.N., and Wroth, J.B. (1968). 'Critical State Soil Mechanics'. McGraw-Hill, London.

Seippel, R.G. (1983). 'Transducers, Sensors and Detectors'. Reston Publications Co.

Sheeran, D.E., and Krizek, R.J. (1971). 'Preparation of Homogeneous Soil Samples by Slurry Consolidation'. Journal of Mataerials, JMLSA, Vol. 6, pp 356-373.

Sketchly, C.J., and Bransby, P.L. (1973). 'The Behaviour of an Overconsolidated Clay in Plane Strain'. Proceedings of the 8th International Conference on Soil Mechanics and Foundation Engineering, Moscow, Vol. 1, pp 377-384.

Skempton, A.W., and Henkel, D.J. (1957). 'Tests on London Clay from Deep Borings at Paddington, Victoria, and the South Bank'. Proceedings of the 4th International Conference on Soil Mechanics and Foundation Engineering, Vol 11, pp 100-106.

Skempton, A.W., and Sowa, V.A. (1963). 'The Behaviour of Saturated Clays During Sampling and Testing'. Geotechnique, Vol 13, pp 269-290.

Simpson, B., O'Riordon, N.J., and Croft, D.D. (1979).'A Computer Model for the Analysis of Ground Movements in London Clay'. Geotechnique, Vol 29, pp 149-175.

Singh, H. (1965). 'The Behaviour of Normally Consolidated and Heavily Overconsolidated Clays at Low Effective Stresses'. Ph.D. thesis, Cornell University, USA.

Stallebrass, S.E. (1990).'Modelling Small Strains for Analysis in Geotechnical Engineering'. First BGS Young Geotechnical Engineers Symposium, University of Sheffield.

St John, H.D. (1975). 'Field and Theoretical Studies of the Behaviour of Ground around Deep Excavations in London Clay'. Ph.D. thesis, Cambridge University.

Tatsuoka, F. (1981). 'A Simple Method for Automated Measurement of Volume Change in Laboratory Tests'. Soils and Foundations, Vol. 21, pp 104-105.

Taylor, J.R. (1982). 'An Introduction to Error Analysis'. University Science Books, Oxford University Press.

Taylor, D.W. (1941). 'Research on the Consolidation of Clays'. MIT Department of Civil and Santary Engineering, Serial 82.

Terzaghi, K. (1941). 'Undisturbed Clay Samples and Undisturbed Clays'. Journal of the Boston Society of Civil Engineers, Vol 28.

Thevanayagam, S. and Prapaharan, S. (1988). Discussion : 'Compression and Extension of K_0 Normally Consolidated Kaolin'. Jo. . al of Geotechnical Engineering, ASCE, Vol 115, pp 1173-1179.

Wroth, C.P. (1971). 'Some Aspects of the Elastic Behaviour of Overconsolidated Clay'. Proceedings of the Roscoe Memorial Symposium, Foulis, pp 347-361.

Wroth, C.P. (1975). 'In-Situ Measurements of Initial Stresses and Deformation Characteristics'. CUED/D - SOILS/TR 23, University of Cambridge.

Wroth, C.P., Randolph, M.F., Houlsby, G.T., and Fahey, M. (1984). 'A review of the Engineering Properties of Soils with Particular Reference to the Shear Modulus'. O.U.E.L. Report No. 1523/84, Soil Mechanics Report No. SMO49/84.

Yung, P.C.Y. (1987). 'The Measurement of the Deformation Properties of Cowden Till at Small Strains'. Ph.D. thesis, University of Sheffield.

Zienkiewicz, O.C. (1977). 'The Finite Element Method'. London, McGraw Hill.